Inferring Mantle Flow Histories from Global Continental Hiatus Surfaces

Dissertation von

Berta Vilacís Baurier

München 2025

Inferring Mantle Flow Histories from Global Continental Hiatus Surfaces

Dissertation von

Berta Vilacís Baurier

Dissertation zur Erlangung des Doktorgrades
an der Fakultät für Geowissenschaften
der Ludwig-Maximilians-Universität München

Department für Geo- und Umweltwissenschaften

vorgelegt von
Berta Vilacís Baurier

aus Taradell (Katalonien)

München, den 13 Februar 2025

Erstgutachter:	Prof. Dr. Hans-Peter Bunge Lehrstuhl für Geophysik Department für Geo- und Umweltwissenschaften Ludwig-Maximilians-Universität München Theresienstraße 41 80333 München
Zweitgutachterin:	Prof. Dr. Anke M. Friedrich Lehrstuhl für Geologie Department für Geo- und Umweltwissenschaften Ludwig-Maximilians-Universität München Luisenstrstraße 37 80333 München
Tag der mündlichen Prüfung:	28 Mai 2025

You need to catch your breath,
take a moment, fall apart, and come back.
We're gonna figure this out.

Jaqueline, The Bold Type

It's not the note you play that's the wrong note – it's the note you play afterwards that makes it right or wrong.

Miles Davis

Don't say "I'm sorry" when you have nothing to apologise for.

Someone, somewhere, sometime

Contents

List of Figures

List of Tables

Summary

Mantle convection is a fundamental process that governs the evolution of our planet. The buoyancies associated with this process induce vertical deflections at the Earth's surface (i.e., dynamic topography), and flow in the asthenosphere, which can result in changes in lateral plate motion. Mapping independent geological data sets allows us to observe and track past mantle convection processes, thereby providing constraints on mantle circulation models and expanding our knowledge of the Earth's convective system over time. It is therefore important to find and map these time-dependent observations. First, oceanic spreading rates can be extracted from magnetic anomalies on the sea floor, which gives a robust history of horizontal plate motion changes. Second, dynamic topography imprints the stratigraphic record at inter-regional scales. Subsided regions result in sedimentation, while dynamically uplifted continental regions create erosional/non-depositional environments, leading to gaps in the stratigraphic record, known as sedimentary hiatus. Consequently, mapping the distribution of hiatus surfaces over time can be utilised as an independent mantle flow indicator.

The present study utilises continental- and country-scale digital geological maps, with a temporal resolution of geological series (ranging from ten to tens of millions of years), to map the planform of convection through geological time. The resulting maps are the hiatus maps, which show the distribution of "hiatus" and "no hiatus" surfaces for all continents (except Antarctica) across eight geological series since the Upper Jurassic. They provide a proxy for the inter-regional patterns of uplift and subsidence associated with dynamic topography. The maps reveal that the distribution of hiatus surfaces significantly changes across and between continents at timescales of geological series. Their wavelengths are on the order of 10^3 km. Some inter-regional hiatus surfaces can be linked to dynamic uplift generated by the rise of a mantle plume, as they are frequently followed by flood basalt eruptions. Furthermore, these hiatus surfaces are usually followed in the next geological series by a nearby plate motion change. Other hiatus surfaces can be linked to the transport of hot material in the asthenosphere. Moreover, sea-level variations also affect the generation of hiatus surfaces on a global scale. These variations can be distinguished from regional changes induced by dynamic topography by comparing the sediment distribution across continents.

The characteristics of the hiatus maps are consistent with the presence of a mantle viscosity stratification with a weaker upper mantle and reinforce the importance of the viscosity in shaping the convective platform. The time delay between the vertical and horizontal motion of the lithosphere highlights the importance of an asthenospheric flow beneath the tectonic plates, as thermal anomalies traverse this layer and shear the base of the lithosphere. Furthermore, a change in base level of approximately 100 m, whether by a sea-level variation or a dynamic topography change, affects the inter-regional sediment distribution either globally or regionally.

The results of this thesis suggest that the occurrence of a hiatus surface, followed by a flood basalt eruption and subsequent horizontal plate motion change can be seen as characteristic of plume-induced dynamic uplift and asthenospheric flow. They imply that a key property of time-dependent geodynamic Earth models must be a difference in timescale between mantle convection itself and the resulting dynamic topography. Moreover, they highlight the importance of continental-scale compilations of geological data to map the temporal evolution of mantle flow beneath the lithosphere, which can provide powerful constraints for global geodynamic models.

Keywords: dynamic topography, sedimentary hiatus, mantle plume, asthenospheric flow, mantle convection, viscosity stratification

Acknowledgements

Where to start? This journey has been a roller coaster in every aspect of my life. I have laughed, enjoyed, and learnt a lot. I also got stressed, cried and doubted myself, but that's part of the package when jumping on the PhD train. I am not the same person than when I started, I have grown, I have know myself a bit better, and although I still do not know exactly what I want to do, what I have gained in the past five-ish years will never leave me.

I would like to start by saying thanks to my supervisor, Peter. Thank you for making time, giving me advice and guidance. Thank you for these long meetings in C419, which although they were intense, I always left it with something to think about and further explore. You are the person that has impacted the most on this journey and I am very grateful you introduced me all these years ago to mantle dynamics and its imprints on the surface of the Earth. I would also like to thank Anke for all the geology lectures and the field trips, especially the Pfingstexcursion. I am really happy I can say: I have seen and touched the rocks I always saw represented on the geological maps and, I can read and understand geological maps and stratigraphic columns (at least a bit more than before).

There are a lot of people I would like to thank, so in no particular order I would like to first thank Jens. Thank you for being so good at your job that we never had to worry about our computers and where to run our codes. I never knew that Spain is actually called Spananien until you showed me the proof! Also to Marcus, Beth, Stuart, Elisa, Bernhard, and Sara, for the immense knowledge. I always learned something when I talked with you! To Heiner, is it too late now to switch to seismology?

I would also like to acknowledge the opportunity I got to participate in the interdisciplinary UPLIFT project. Being part of it showed me another part of science, helped me to grow as a scientist, and made me expand extensively my vocabulary. I am thankful for all the discussions with colleagues from many different branches.

The geophysics department is very diverse, and in it I found some of my best friends ... Sabrina, I am so glad that after seven years, you are still my best friend and we continue experience life together. I can just hope that we perpetuate this "we've only just begun", and we always celebrate life together, no matter what :). Nicolás, I am really happy I didn't have to disentangle completely by myself the hiatus world and that led us to work together. I have learned a lot about endurance observing you overcome this challenge, I wish you the best in your bright future! Ingo, thanks for all the advice and the chatty science and non-science moments, I am awaiting to see what your future brings ;). Hamish, thanks for making me a better scientist and musician. You are a remarkable researcher and I am very grateful I could share three years working with you, the amount of things I learned are immeasurable. Dieke, you have a wonderful future in front of you, and I am sure you will reach very far, thanks for all

the Zumba times, and the long after-dinner conversations. To Roman, please do not ever lose the spark and passion you have when you talk about what you find interesting either in science, your love for Crete or food. Nils, it has been awesome to chat with you about music, exchange impressions, discuss opinions and future plannings! I want to say thank you to Eugenio and Suganth, for all the climbing sessions and the joyful and laughing moments. It was always nice to have "a double date" with you two! Isi, I am very happy we ended up being office-mates. I am delighted I got the opportunity to know you better, share happiness, not so happy things too, and enjoy the complicated days of the PhD together. Thanks for the talks behind closed doors ;) Leon, sharing an office with you is one of the coolest thing that could have happened to me. I leave here written that I truly believe you will do gracious things, and that I hope you remember me when you win the Nobel Prize in medicine for one of your fantastic and crazy projects! And thanks to everyone with whom I shared lunch or went for a casual "Beer Friday", I have so many amazing happy memories from it!

I would like to acknowledge also the awesome people I met in Stusta (Chris, Kishan, Thommy, Elisa, Roma, ...) with whom I spent the majority of my time during the COVID lockdowns. It was great to share a house with you, where there was always someone in the mood to do something in the evenings: chill in the common room, drink a beer, watch a movie or have endless discussions about the different topics that moved us. Also, to Alwin and Camilo, most of my best memories in Stusta are with you both! Although some things got cold and half broken, I always hoped you will be part of my chosen-family. You always gave me another point of view and taught me a lot about life, even with the choices we make when things go dark. To Ola, Gurki and Nici for sharing every Wednesday evening during the semester in MiCapella. But even more for the car rides to rehearsal weekends, crazy conversations, shared playlists, Disney singing nights, and movie evenings.
To Queralt also, què faria jo sense tu? You are the only person that for more than seven years I have talked and messaged almost every day. You have accompanied me in all my happy, and sad moments, the awesome and the worst situations, and you have been there with my doubts. Thank you for always listening, giving me advice and being just there, knowing I can count on you is invaluable. To Sergi, Alvaro, and Bruna, for this intermittent relationship we have, yet it feels like it was yesterday since the last time I saw you.

And finally to the people that I love the most in this world. Gabriel, I don't know what conferences have... but from conference to conference, something ignited, and I slowly found myself in a place of happiness that I did not think I deserved. Thanks for bearing, hugging me and loving me regardless of the weather. You have populated these last two years-ish of happy moments and showed me that life is not all about geodynamics and geology. I am really happy we enjoy life together and we tackle its challenges co-op style. Mama, Papa, Ignasi, el camí que he triat m'ha portat lluny de vosaltres, però tot i que no ens veiguem massa, sou una part molt important de la meva vida. Sempre m'he sentit molt acompanyada tot i la distància, em sento molt feliç de tenir-vos al costat. Us estimo molt.

Chapter 1

Introduction

The Earth's surface is affected by dynamic processes happening inside the Earth. Mantle convection, one of these dynamic processes, plays a crucial role in the dynamics of plate tectonics, the formation of mountain ranges and the development of sedimentary basins. Therefore it is important to quantify and study its effects on the Earth's surface. This section gives an overview of the fundamental and key concepts of mantle convection, its surface expression, and some of the methodologies used for observing and modelling these phenomena.

1.1 Mantle convection

Convection occurs in the Earth's mantle at geological timescales. This process is a buoyancy-driven movement of solid rock induced by the temperature difference between the heat emanating from the Earth's core and the cold surface (Davies, 1999). It is the main driver of plate tectonics and influences surface processes over geological timescales. It operates in two primary modes: the plate and the plume mode (Davies, 1988b; Davies and Richards, 1992; Davies, 1999). The plate mode is characterised by the movement of cold, dense surface material that subducts into the mantle, whereas the plume mode involves hot, buoyant upwellings originating at the core-mantle boundary (CMB). The interplay between these modes defines the spatial and temporal variability of mantle convection and its surface expressions.
The Earth's mantle behaves as a highly viscous fluid, that convects vigorously over geological timescales due to its large viscosity. Early studies (e.g., Pekeris, 1935; Morgan, 1965; McKenzie, 1977; Richards and Hager, 1984) established that mass and gravity anomalies in the mantle generate viscous stresses that deflect the surface of the Earth and the CMB. These surface deflections due to mantle convection can be calculated and observed through the geoid and the dynamic topography. The geoid is defined as the shape that the ocean surface would take under the influence of the gravity of Earth and the density anomalies in the mantle. The surface topography, also termed dynamic topography by Hager et al. (1985), is defined as the vertical motion of the plates generated due to the buoyancies within the mantle. The majority of the parameters that govern mantle convection have been inferred from second-order observations, such as the movement of the tectonic plates, seismic studies and seismic tomography, rock experiments or measurements of surface heat flow (Fowler, 2004). However, there are some parameters that still remain uncertain or unknown, for instance, the rheology of the mantle (i.e., the viscosity).

The viscosity, more specifically the radial viscosity structure, is a key parameter that controls the wavelength of mantle convection and affects its surface expression (Davies and Richards, 1992; Bunge et al., 1996).

1.2 Observations

Mantle convection cannot be directly observed or measured because of the long timescales at which it flows, and because the mantle is not accessible. However, seismic tomographic models, measurements of heat flow or the geoid are a tool to infer the present-day state of the Earth's mantle. Tomographic models (e.g., Ritsema et al., 2011; French and Romanowicz, 2015; Koelemeijer et al., 2016; Fichtner et al., 2018; Simmons et al., 2021; Cui et al., 2024) give a filtered representation of the current mantle structure, while the geoid, measured from satellite data (Pail et al., 2010), provides the distribution of the balance of those buoyancy anomalies. Yet, these observations are limited to the present-day state of the mantle.
A time dependant observation of mantle convection is the movement of the tectonic plates. The horizontal motion of the lithosphere is principally driven by the basal forces resulting from mantle convection patterns beneath the lithosphere. The movements of the plates can be extracted from the magnetic anomalies recorded in the rocks of the ocean floor for the last 200 Myrs (Seton et al., 2020) and from paleomagnetic data derived from continental rocks (Torsvik et al., 2012) for older ages. Therefore, utilising this information, plate reconstruction models are created (e.g., Gordon and Jurdy, 1986; DeMets et al., 2010; Seton et al., 2012; Müller et al., 2016; Müller et al., 2022). They provide information of the position of the continents in the past, which is crucial to create mantle circulation models. That means that this data set is imposed as a surface boundary condition, to obtain an Earth-like model.
Another time-dependent observation of mantle convection is dynamic topography. Although it is a concept that has been long known, observing it poses a significant challenge. Yet, it is a crucial geodynamic observable. Dynamic topography is expressed through surface subsidence, which is linked to mantle downwellings, and surface uplift, associated with mantle upwellings. The uplifted areas are frequently linked to mantle plumes, which are often associated with flood basalt and volcanic activity. Recent advances have determined it at present-day. Winterbourne et al. (2009b) and Hoggard et al. (2016, 2017) extracted the oceanic residual depth, removing the isostatic signal and crustal thickness anomalies from the current topography, and used it as a proxy for present-day dynamic topography. The results from Hoggard et al. (2017) showed that the present-day dynamic topography estimates for the oceans have amplitudes of approximately ± 1 km and wavelengths around 1000 km. These values contrast to the predictive models that propose amplitudes larger than ± 2 km and wavelengths of 10 000 km (e.g., Steinberger, 2007), although recent geodynamic models predict smaller wavelengths for dynamic topography (e.g., Ghelichkhan et al., 2021). Holdt et al. (2022) extended residual dynamic topography estimates to the continents, as well as, expanded the oceanic data set. They found that the power spectra of the residual dynamic topography has a peak at spherical harmonic degree 2 but still there are reasonable contributions at degree 30-40, which means contribution of wavelengths around 1000 km. The data set pertaining to the continents, was revised and updated in Stephenson et al. (2024). They utilised a database comprising seismically determined crustal thickness estimates

and laboratory-based velocity-density measurements for the continents. They calculated the continental residual topography anomalies, finding that these anomalies vary between ± 1 km to 2 km with wavelengths of 1000 km to 5000 km. It is important to note that extracting this signal from oceanic lithosphere is a simpler process than for a continental setting, because the oceanic depth decreases with the square root of the age (Fowler, 2004).

1.2.1 The geological record

Mapping of dynamic topography in a snapshot is challenging due to its similarity in length-scales to other signals, such as isostasy, and its smaller amplitudes. But, the defining feature of dynamic topography is that it changes over time, which is a motivation to turn to the geological record. The transient nature of dynamic topography gets engraved in the geological record and geological maps are a tool to map it. Negative surface deflections creates accommodation space for sediment deposition, while positive surface deflections leads to erosion or non-deposition in sedimentary environments. One of the earliest applications of geological data to infer dynamic topography variations due to mantle downwellings was pioneered by Mitrovica et al. (1989) and Burgess et al. (1997). They used the sedimentary record from the Western Interior Seaway and the cratonic interior of North America to study the subsidence of the continent due to the subduction of the Farallon slab. Shortly after, Gurnis (1998) showed that the downwelling under Australia was responsible for the Cretaceous Eromanga Sea, which was later confirmed by Harrington et al. (2019). Conversely, Bond (1978b, 1979) linked the continent-scale sediment distribution to the uplift of continental platforms. Bond (1978a) stated that Africa experienced a late Tertiary uplift relative to other continents, which agrees with the findings of Burke and Whiteman (1973). Several studies (Cox, 1989; Şengör, 2001; Rainbird and Ernst, 2001; Saunders et al., 2007b) concluded that hot mantle upwellings, also known as mantle plumes, create a dome-shaped uplift of 1 km to 2 km over a radius of 1000 km to 2000 km inducing changes in continental drainage patterns, followed by large-scale magmatism (i.e., flood basalts) after the arrival of the plume beneath the lithosphere (Rainbird and Ernst, 2001; Campbell, 2007; Saunders et al., 2007b).

Friedrich et al. (2018) and Friedrich (2019) proposed a new method to track and study the inter-regional expression of mantle convection through its dynamic topography. This approach starts by considering the principles of stratigraphy, also referred to as Steno's principle (Steno, 1669), named after the Danish scientist Nicolas Steno. They state that the sediments are deposited from oldest to youngest (principle of superposition) creating horizontal layers parallel to the Earth's surface (principle of original horizontality). These layers of sediments are laterally continuous (principle of lateral continuity) and if they are not continuous, that indicates that a younger process has affected them (principle of cross-cutting relationships), for example, erosion due to uplift. Therefore, variations from these principles in the sedimentary record may be indicative of external processes, such as dynamic uplift, affecting the distribution of the sediments. As previously mentioned, mantle convection deflects the Earth's surface, and this imprints the geological record. The non-depositional or erosional environments generated by surface uplift due to the rise of a plume create in gaps in time in the sedimentary record (Barrell, 1917). These gaps, also referred to as hiatus, populate the geological record in the

form of unconformities (e.g., Miall, 2016). The approach from Friedrich et al. and Friedrich is then based on the premise that the lack of information (i.e., sedimentary gaps) can be part of a larger signal. In other words, this approach surpasses the limitations imposed by regional lack of information, thereby providing a solution to this challenge by considering these stratigraphic gaps to be part of the positive mantle dynamic signal at the inter-regional scale.

The real process of how mantle convection affects the Earth's surface is very complicated, but Fig. 1.1 presents a conceptual model of the surface expression of a rising plume. This sketch, is a simplified version of Fig. 8 from Friedrich et al. (2018). It shows the rise of a mantle plume, accompanied by the sedimentation record of two stratigraphic columns located on top of the plume centre and in the far field. In Fig. 1.1a), the plume is located in the lower-mid mantle, far from the surface resulting in no interaction between the surface and the plume, and therefore there is uniform sedimentation in both columns. In Fig. 1.1b), the plume interacts with the surface, generating an uplift. This uplift creates a non-depositional or an erosional environment in the region of column A, while sedimentation persists in the far field, around column B. The rocks of the following geological series are only deposited in the far field, as shown in Fig. 1.1c). This results in a temporal gap in the stratigraphy of column A, i.e., a hiatus of the green geological unit. Finally, when the plume material spreads out into the asthenosphere (Fig. 1.1d), the surface subsides and sedimentation resumes everywhere. This process results in column B with the expected sedimentation, while column A has a hiatus of the green unit. The yellow sediments in the figure are a combination of volcanic and sedimentary rocks. After the

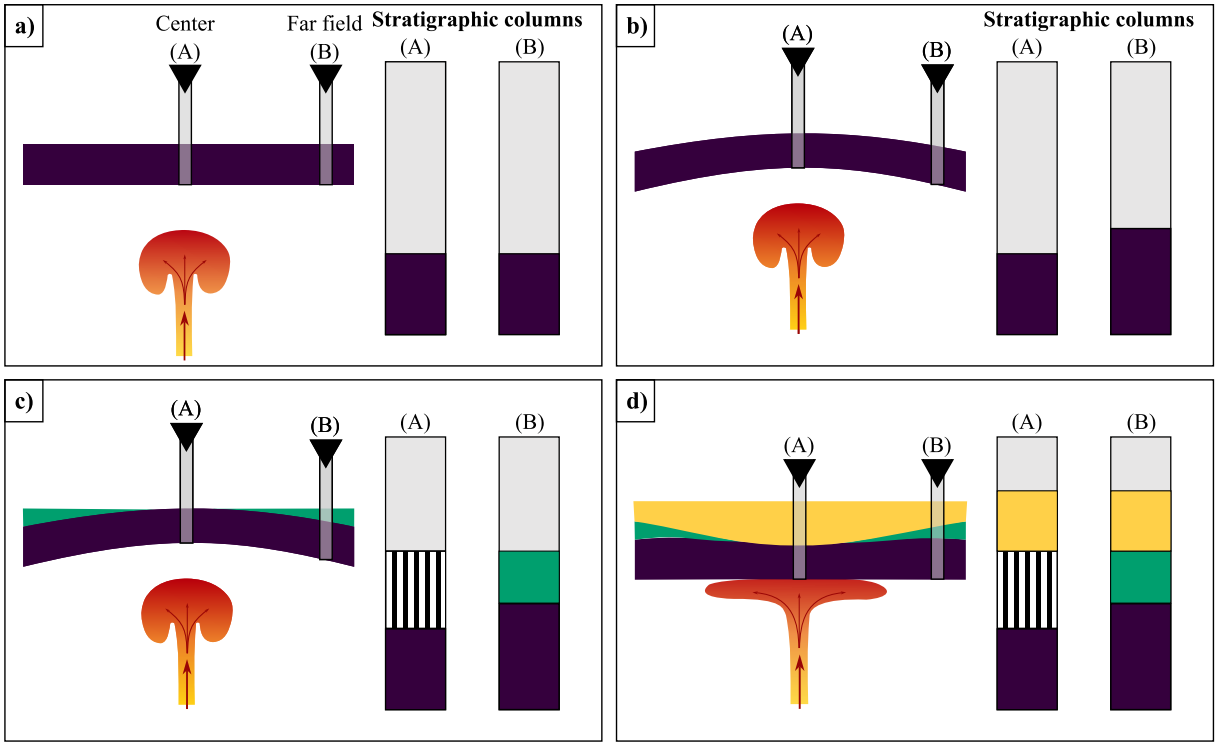

Figure 1.1: Simplified sketch representing the imprint of a rising mantle plume to the geological record. In each subfigure there is a rising plume in different stages, two stratigraphic columns located on top of the plume centre and in the far field. The two stratigraphic columns are amplified on the right. This figure is a modified version of a figure in a manuscript in preparation, and it is a simplification of Fig. 8 from Friedrich et al. (2018).

initial uplift, the plume arrives beneath the lithosphere, which is often followed by the formation of large igneous provinces at the surface (Friedrich, 2019). These igneous provinces usually persist for 1 Myrs to 2 Myrs (e.g., Saunders et al., 2007a). This process is accompanied by the subsidence of the surface. This is because the plume material spreads in the asthenosphere and the thermal anomaly no longer maintains the surface uplift. Therefore sedimentation resumes everywhere, and the volcanic rocks can inbeded with sedimentary rocks.

1.2.2 Hiatus maps

Hiatus mapping is a method to infer past mantle activity by identifying gaps in the geological record caused by erosion or non-deposition proposed by Friedrich et al. (2018); Friedrich (2019). These hiatuses, often expressed as unconformities, serve as proxies for vertical surface motions driven by mantle processes. At a continental scale, sedimentation of a geological time unit (no hiatus) is used as a proxy for subsidence, while the absence of sedimentary rocks (hiatus) is used as a proxy for uplift. This thesis outlines the methodology developed to extract hiatus maps from digital geological maps and regional studies, such as stratigraphic columns. It also presents the steps that are required to create the hiatus map: the compilation of digital geological maps and the digitisation of the stratigraphic columns. It follows by identifying absence or presence of a geological unit and the application of a spherical harmonic expansion. The resulting maps provide a unique perspective on the interactions between the lithosphere and mantle, and they offer insights into past mantle flow patterns.

Renaming of the hiatus maps

During my PhD, a number of papers were published that employed the hiatus mapping technique. Through these publications, the terminology associated with thee results of the mapping technique changed to better represent the maps; that is to say, the maps were renamed. Initially, the maps were named “Base of” maps. “Base of” was followed by the geological series at which the mapping was conducted. This nomenclature was chosen to align with the original methodology and already published manuscripts (Friedrich et al., 2018; Vibe et al., 2018; Carena et al., 2019). However, the mapping choice employed in Vibe et al. (2018) and the following manuscripts, part of this thesis, Hayek et al. (2020, 2021); Vilacís et al. (2022) differed from the aforementioned studies (Friedrich et al., 2018; Carena et al., 2019). Nevertheless, the nomenclature remained the same.
We now therefore distinguish between the two mapping approaches: the “Base of” mapping and the “hiatus/no hiatus” mapping. The “Base of” mapping follows Friedrich et al. (2018) and Carena et al. (2019), and maps the contact strictly and only at the base of a geological series. The resulting maps show the information of the type of contact this geological series has: conformable or unconformable. That means that this mapping technique shows if the geological series is in contact with the immediately preceding geological series or not (i.e., is in contact with older units). Conversely, the ”hiatus/no hiatus” mapping choice used in Hayek et al. (2020, 2021); Stotz et al. (2021b); Vilacís et al. (2022); Stotz et al. (2023, 2024); Vilacís et al. (2024) maps the presence and absence of a given geological series, i.e., the hiatus or no hiatus of a geological series. These maps are obtained by adding in the “Base of” maps, the occurrence of

immediately preceding geological series, regardless of the presence of that target series. The resulting maps show "hiatus" or "no hiatus" of a given geological series and are a proxy for the dynamic topography that occurred during that geological series.
The maps obtained from each mapping choice, transmit different information. For example, the Base of Miocene map shows where Miocene is present and if Oligocene (the immediately preceding series) is in contact with these Miocene rocks or not. Conversely, the Miocene hiatus maps shows the absence or presence of Miocene rocks. Thus, after publishing the firsts papers and participating in a few conferences, we refined the nomenclature to enhance clarity. A careful explanation between both mapping options can be found in Chapter 5 (i.e., the published manuscript Vilacís et al. (2024)) and in Vilacís et al. (In prep).

1.3 Geodynamic modelling

Geodynamic models are essential for understanding mantle convection and its surface expressions. They solve the physical principles of fluid dynamics and thermodynamics, and simulate the behaviour of the mantle over geological timescales (e.g., Bunge et al., 2002b; McNamara and Zhong, 2005a; Zhong et al., 2008; Müller et al., 2018b). The governing equations of mantle convection are the conservation of mass, momentum and energy. These equations are computationally challenging to solve particularly when utilising Earth-like parameters such as compressibility and temperature-dependent viscosity, and a realistic geometry and spatial resolution. The latter means that the modelling domain has to be a thick spherical shell with a surface resolution between grid points of 1 km to 5 km. To address the complexities inherent in these equations and parameters that govern mantle convection is often required the utilisation of considerable computational resources such as large computational clusters or a supercomputer, in conjunction with optimised algorithms and solvers (Kohl and Rüde, 2022; Mohr et al., 2023). Although these models are computationally expensive, they can be employed to refine the knowledge about the parameters that drive mantle convection, by testing them against observations.

Simple analytical solutions and informed simplifications of the governing equations facilitate the exploration of key phenomena. The theory to extract dynamic topography or the geoid for a given density structure and a viscosity profile involves solving the Stokes equation coupled with the gravitational Poisson equation in a spherical shell (Hager, 1984; Richards and Hager, 1984). The Stokes equations are the mass and momentum conservation equations for a highly viscous fluid, such as the Earth's mantle. That means that the inertial forces are not relevant in the system and thus the momentum conservation equation can be approximated as an instantaneous balance of forces. It is a balance between the body forces, the viscous forces and the pressure gradients in the mantle. The body forces term is given by the gravitational force generated by thermal buoyancies in the mantle. This force is determined using the gravitational Poisson equation, which relates the gravitational potential and the density field. The solutions of the Stokes and Poisson equations are usually represented through kernels. The kernels are defined as quantities that relate the contribution of a mass anomaly of a specific wavelength and depth, to key parameters, such as dynamic topography or the geoid. These kernels are calculated in the spectral domain, and the resulting quantity field is derived from the radial integration of the spherical harmonic component over the mantle depth (Richards and Hager,

1984; Horbach, 2020). Therefore, given a density structure, for example the present-day density structure derived from a tomographic model or the density structure from a geodynamic model, it is possible to calculate the surface deflection and the geoid generated by the buoyances of that given density structure. These kernels, and by extension mantle convection, are strongly influenced by the radial viscosity profile.
A viscosity profile that has a constant value throughout the mantle (i.e., isoviscous) has a kernel that shows significant contributions of the lower mantle anomalies in the surface topography. Conversely, a stratified viscosity profile, with a lower viscosity in the upper mantle, leads to minimal contributions to the surface topography from the anomalies located in lower mantle. In other words, a lower viscosity in the upper mantle leads to the decoupling of viscous stresses between the upper and lower mantle, resulting in contributions to the surface topography from only the anomalies located in the upper mantle (Colli et al., 2016). This suggests that in an isoviscous mantle, changes in dynamic topography are expected to be on the order of a transit time, i.e., the time required for a mantle overturn (Iaffaldano and Bunge, 2015). For the Earth, this time is estimated to be within 100 Myrs to 150 Myrs. In a stratified mantle, however, the changes in the topography are expected to be much faster, with an estimated time span of tens of millions of years. This is due to the fact that only the anomalies located in the upper mantle contribute to the deflection of the Earth's surface. It is important to understand the impacts of the viscosity profile and the density structure that is created to comprehend the results of this thesis and to infer links to mantle convection.

Another simple analytical solution to study the interaction between the lithosphere and asthenosphere is through the Couette/Poiseuille flows (Höink and Lenardic, 2008, 2010; Höink et al., 2011; Höink et al., 2012; Stotz et al., 2018). The Poiseuille flow is a flow driven by lateral pressure gradients such as plumes or slabs transiting through the asthenosphere. This flow can actively push overlying plates. The Couette flow is flow driven by the movement of tectonic plates, that generates shear stresses in the underlying mantle, i.e, in the asthenosphere. These flows are solutions of the Stokes equations for a highly viscous fluid in a channel. Combined and calculated in a spherical shell, these models, the Poiseuille-Couette models, are particularly effective in providing a framework to link mantle convection, such as the transit of plumes and slabs in the asthenosphere, to observable phenomena, such as dynamic topography and plate motion changes, see Stotz et al. (2021b, 2024) and Chapters 3 and 4. This is because this theoretical framework can explore changes in the basal forces through the Poiseuille flow, introducing a plume source or a slab sink to assess diverse scenarios that explain the observations. This approach is based on the premise that for a plate motion change to occur, it is required a change in the plate boundary torques, the basal shear stresses or both. The utilisation of this framework enables the separation of each component and facilitates the study of their individual effects.

1.4 Thesis aims and outline

This thesis builds on the fundamental concepts of mantle dynamics and stratigraphy to explore the links between mantle convection through its surface expression, i.e., the dynamic topography, using the geological record. This work aims to map and study the spatial and temporal

patterns of mantle-driven surface processes, provide time-dependent constraints on mantle viscosity, and enhance our understanding on the influence of mantle dynamics in the evolution of the lithosphere and the geological processes. Finally, it aims to provide insights into the planform of convection and constrain governing parameters of mantle convection.

This thesis is structured in four main chapters, which present the digital hiatus mapping methodology, the resulting hiatus maps, and links to mantle convection as well as surface processes. Chapter 2 introduces the digital processing of digital geological maps that result in continent-scale hiatus maps for the Atlantic Realm and Australia. It links the inter-regional patterns of unconformities to mantle flow-induced dynamic topography events. It also emphasises the importance of considering varying convection timescales in geodynamic Earth models.

Chapter 3 expands upon the relationship between the horizontal and vertical motion of the lithosphere by correlating the hiatus maps with spreading rate changes to infer active upper mantle flow in the Atlantic and Indo-Australian realms. The study reinforces the link between dynamic topography and horizontal plate motions, offering evidence of vigorous upper mantle convection.

Chapter 4 investigates plume-driven plate motion changes in the South Atlantic, demonstrating the importance of the Poiseuille flow in the asthenosphere in inducing plate motion shifts during the Paleogene. This work identifies the Tristan and Sierra Leone plumes as key torque sources driving these changes.

Chapter 5 explores the global distribution of hiatus surfaces since the Jurassic, revealing the planform of mantle convection and its time and length scales. This work highlights that a mantle viscosity stratification plays an important role in shaping the dynamic topography patterns and provides specific regional events to constrain geodynamic models. Furthermore, it separates the effects of sea-level variation in the hiatus surfaces from the regional changes induced by dynamic topography.

Chapter 2

Continent-scale Hiatus Maps for the Atlantic Realm and Australia since the Upper Jurassic and links to mantle flow induced dynamic topography

Interregional geological maps hold important information for geodynamic models. Here we use such maps to visualize major conformable and unconforma-ble contacts at interregional scales and at the level of geologic series from the Upper Jurassic onward across North and South America, Europe, Africa and Australia. We extract hiatus information from these paleogeological maps, which we plot in a paleogeographical reference frame to link the maps to the plate and plume modes of mantle convection. We assume that interregional patterns of hiatus surfaces are proxy records of continent-scale mantle-induced vertical motion of the lithosphere. We find significant differences in the distribution of hiatus across and between continents at the timescale of geologic series, that is ten to a few tens of millions of years (Myrs). This is smaller than the mantle transit time, which, as the timescale of convection, is about 100-200 Myrs. Our results imply that different timescales for convection and topography in convective support must be an integral component of time-dependent geodynamic Earth models, consistent with the presence of a weaker upper mantle relative to the lower mantle. Additional geological constraints together with interregional geological maps at the resolution of stages (1-2 Myrs), are needed to assist in future geodynamic interpretations of interregional geologic hiatus.

Published on October 7th 2020 in the Proceedings Royal Society A.
doi:10.1098/rspa.2020.0390
Correction published on June 17th 2021 in the Proceedings Royal Society A.
doi:10.1098/rspa.2021.0437

Author list: Jorge N. Hayek, Berta Vilacís, Hans-Peter Bunge, Anke M. Friedrich, Sara Carena and Yulia Vibe.

Ludwig-Maximilians-Universität München, Department of Earth and Environmental Sciences, Theresienstraße 41 and Luisenstraße 37, 80333 Munich, Germany.

Note: In this chapter I present the original article and the correction together, which means that Figs. 2.4 and 2.6 to 2.8 slightly differ from the published manuscript.

Disclaimer: This article has been previously comprised in the thesis of Jorge N. Hayek. However, it is part of my work, essential for my PhD and is the ground base for the articles I published afterwards; thus, I also included also it as part of my thesis.

2.1 Introduction

An early success in geodynamics was the quantitative description of mantle convection by a boundary-layer model of high Rayleigh number and low Reynolds number flow (Turcotte and Oxburgh, 1967). The model came into its own when mantle convection was explored explicitly in terms of the plate and plume mode (e.g., Davies, 1988b; Davies and Richards, 1992; Davies, 1999). The former is associated with the cold upper thermal boundary layer, which is the lithosphere, and the latter with the hot lower thermal boundary layer, which sources plumes.

The plate mode has since then been mapped by kinematic models of lithosphere motion for the Cenozoic (Gordon and Jurdy, 1986) and Mesozoic (e.g., Müller et al., 2016). Its temporal evolution has been linked to the generation of large-scale mantle heterogeneity through the history of subduction (Richards and Engebretson, 1992a; Lithgow-Bertelloni and Richards, 1998) and assimilated into global mantle convection simulations (Bunge et al., 1998; McNamara and Zhong, 2005b; Bower et al., 2013) to construct mantle circulation models, which from here on we will call MCM. Recently, the plume mode has been imaged by seismic tomography as localised upwellings that rise from the core-mantle boundary (CMB) to the base of the lithosphere (French and Romanowicz, 2015; Nelson and Grand, 2018; Rickers et al., 2013), and the boundary-layer nature of mantle convection is now widely recognised.
Geodynamicists also understood early on that mantle convection deflects the Earth's surface away from its isostatically compensated state (Pekeris, 1935). Termed "dynamic topography" by Hager et al. (1985) the deflections are receiving renewed attention (e.g., Braun, 2010), particularly as an agent in passive margin environments (Bunge and Glasmacher, 2018), where the proximity to a base-level allows one to gauge topographic changes better than at other places.
The boundary-layer interpretation of mantle flow makes it convenient to interpret the sedimentary expression of dynamic topography explicitly in terms of the plate and plume modes. For the plate mode, the approach was pioneered using the sedimentary record from the *Cretaceous Interior Seaway* and the cratonic interior of North America (e.g., Mitrovica et al., 1989; Burgess et al., 1997) because surface depressions induced by mantle downwellings in these regions left accommodation space to preserve a sedimentary archive. Other regions, such as the Cretaceous Eromanga Sea in Australia (Gurnis et al., 1998; Harrington et al., 2019) and a regional unconformity of Cretaceous-Eocene age in southeast Asia (Clements et al., 2011b) also record plate-mode-related vertical motion. Recently, MCMs have modelled the evolution of plate-mode-related dynamic topography since the Cretaceous (Müller et al., 2018).

It is more difficult to map the stratigraphic expression of the plume mode because the positive surface deflections create erosional/non-depositional environments, which leave time gaps in the sedimentary record. Field observations of the surface expression of the plume mode document changes in drainage patterns (e.g., Cox, 1989) and a dome-shaped uplift of 1-2 km (e.g., Şengör, 2001; Rainbird and Ernst, 2001; Saunders et al., 2007a) over a radius of 1000-2000 km. The resulting discontinuity surfaces in the sedimentary record are known as unconformities (e.g., Miall, 2016), although their wavelengths are so large and their amplitudes so little that at large distances an unconformity may locally be recorded as a disconformity. They preserve time missing (hiatus) from the geological record (Friedrich et al., 2018). To this end, an approach of hiatus-area mapping was introduced (Friedrich et al., 2018; Friedrich, 2019)

to highlight the long wavelength nature of sedimentation records as explored by Sloss (1963, 1972). It visualizes interregional-scale unconformities because, at continental scales, what is normally perceived as a lack of data (material eroded or not deposited) becomes part of the dynamic topography signal. The method has been applied to map the temporal and spatial patterns of conformable and unconformable geological contacts across Europe (Vibe et al., 2018) and Africa (Carena et al., 2019).
Continent-scale geological maps, such as the 1:5 Million International Geological Map of Europe and Adjacent Areas (IGME 5000) (Asch, 2004), are crucial databases to reveal hiatus area of geodynamic origin, that is falcogeny in the sense of Şengör (2003). They provide internally consistent compilations of geological observations, including chronostratigraphic age, lithology, and geolocalization of the strata, at the scale of thousands of kilometres. This links them naturally to continent-scale elevation changes induced by mantle flow. Here we explore interregional-scale geological maps. We identify temporal and spatial patterns of geological hiatus contacts across North and South America, Europe, Africa and Australia, under the assumption that interregional-scale conformable and unconformable contacts are proxy records of paleotopography and vertical motion. We organize our paper as follows: first, we explain our hiatus mapping method. Then we present results starting from hiatus maps for the Upper Jurassic. We find significant differences in the spatial extent of hiatus area across and between continents at the timescale of geologic series, ten to a few tens of millions of years (Myrs), which is considerably smaller than the mantle transit time (Iaffaldano and Bunge, 2015). We note that this negates the concepts of Stille (1919, 1924b) and Sloss (1972), who argued for global synchronicity cycles. Finally, we discuss our results, place them into a geodynamic context, explore their implications for dynamic Earth models, and draw conclusions.

2.2 Data compilation, preparation, and uncertainties

We mapped conformable and unconformable contacts at the resolution of geological series because this is the most frequently adopted temporal resolution among interregional geologic maps (Friedrich, 2019). We also opted to map hiatus from the Upper Jurassic onward, to remain within a timescale comparable to the mantle transit time, which is about 100-200 Myrs (Iaffaldano and Bunge, 2015). To this end, we took the digital vector maps of Europe, Australia, and North America, which describe the chronostratigraphic units within specific temporal and spatial resolutions. For South America, we compiled individual country-scale information, since only this was available at the temporal resolution of series.

Diverse Open-Access Databases summarised in Table 2.1 provide digital information from geological maps as vector files. Some maps include information from the continental shelf and other seafloor features. We did not use this information because it also includes magnetic isochron data, which is not related to the sedimentation paleoenvironment. However, oceanic pointwise information in the form of localised stratigraphic columns from the ocean drilling program can record oceanic hiatus events. For this reason, we imported offshore data from Ocean Drilling Program (ODP) (1985–2004) Legs 100-190 and Deep Sea Drilling Program (DSDP) (1968–1983) Legs 1-95. Additionally, we used Carena et al. (2019) for the Cenozoic series of Africa augmented by further information for the Upper and Lower Cretaceous.

Table 2.1 summarises our compilation of geological information.

Region		**Temporal resolution**	**Spatial resolution**	**Reference**
Australia		Series and Stages	1:1 Million	Raymond et al. (2012)
Europe		Series	1:5 Million	Asch (2004)
North America		Series and Stages	1:5 Million	Garrity and Soller (2009)
South America	Argentina	Systems	1:2.5 Million	SEGEMAR (2017)
	Bolivia	Series	1:1 Million	Claure Zapata et al. (2012)
	Brazil	Series	1: 250 000	SGB (2010)
	Chile	Stages	1:1 Million	SERNAGEOMIN (2003)
	Colombia	Stages	1:1 Million	Jorge et al. (2015)
	Ecuador	Series	1:100 000	MAGAP (2005)
	Peru	Stages	1:100 000	INGEMMET (2016)
	Uruguay	Series	1:500 000	Loureiro et al. (2016)
	Venezuela	Series	1:500 000	Hackley et al. (2004)
Africa		Series and Stages	1:5 Million*	Carena et al. (2019)
Ocean Drilling Projects		Series	-	ODP (1985–2004) DSDP (1968–1983)

Table 2.1: Geological maps used in this work with their respective spatial and temporal resolution. Compilations performed at the country level for South America (see text). * Africa hiatus information taken from Carena et al. (2019) with hiatus information added for Upper and Lower Cretaceous. Offshore data imported from ODP (1985–2004) Legs 100-190 and DSDP (1968–1983) Legs 1-95 as pointwise signal.

The geological maps published at continent and country-scale vary both in spatial and temporal resolution. Some maps are resolved at the series level. Others provide finer or coarser geological time intervals, such as combinations of series, stages, or systems, as defined in the chronostratigraphic chart (Cohen et al., 2013; updated.; Ogg et al., 2016). For instance, the map may state *Paleogene* for the units shown. Thus time resolution falls within three categories: series, series/stages/systems mix, and systems. The maps moreover use distinct naming conventions for age descriptions, including different abbreviations, languages, and aggregations of time units. To handle the diversity, we adopted a standardization procedure and harmonized the time resolution among the maps. We saturated all subseries information to the series level and brought the geological unit conventions to a standard reference. This translates languages, abbreviations, and combinations or ranges of geological units to the numerical value of geological time. For instance, a polygon defined as *Oligocene-Miocene* or *Chattian-Langhian* time has the same time range after the standardization and spans two series ($\sim$30 Myrs). For polygons with systems resolution we assigned the hiatus information to the base of the polygon's age range. For South America our procedure brought the country-specific maps to a unified continent-scale format. An exception had to be made for Argentina, where the temporal resolution was available only at the systems level.

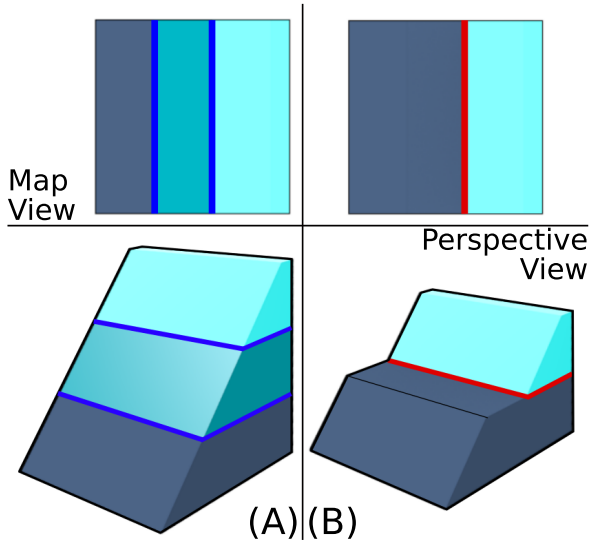

Figure 2.1: **(Left)**: Schematic map (top) and perspective view (bottom) of geological units in conformable contact (blue lines). **(Right)**: Same scheme showing an unconformable contact (red line), where the middle unit is missing, representing a gap (hiatus) in the geologic record.

Following Carena et al. (2019) we define *conformity* if a target series sits atop the one immediately preceding it in the chronostratigraphic chart, regardless of whether either series has missing stages. We define *unconformity* as the complementary state to *conformity*. This holds for any place where one or more series immediately preceding the target series are missing. The definitions apply regardless of the physical contact type between both **rock** units. Figures 2.1 and 2.2 provide a schematic illustration of hiatus and the extraction process for un/conformable contacts (Friedrich, 2019). To delimit hiatus for a given series we also include in the maps any occurrence of the immediately preceding series and categorise the signal as conformable.

Since the temporal resolution is restricted to the series level, the un/conformity represents a time span that varies for different series. For instance, unconformity at the base of the Miocene datum is at least 11 Myrs, because this is the duration of the Oligocene series. Unconformity at the base of the Paleocene datum lasts a minimum of 34 Myrs, which is the duration of the Upper Cretaceous series. We note, however, that the hiatus duration could be longer for either case. In the former, rocks of Lower and Middle Miocene and/or Upper and Middle Eocene could be missing. In the latter, rocks of Lower and Middle Paleocene and/or Lower Cretaceous could be absent.

The uncertainty of a hiatus transforms into a spatial uncertainty when plate motions are taken into account. If we take the current global root mean square (RMS) plate velocity of 5 cm/yr

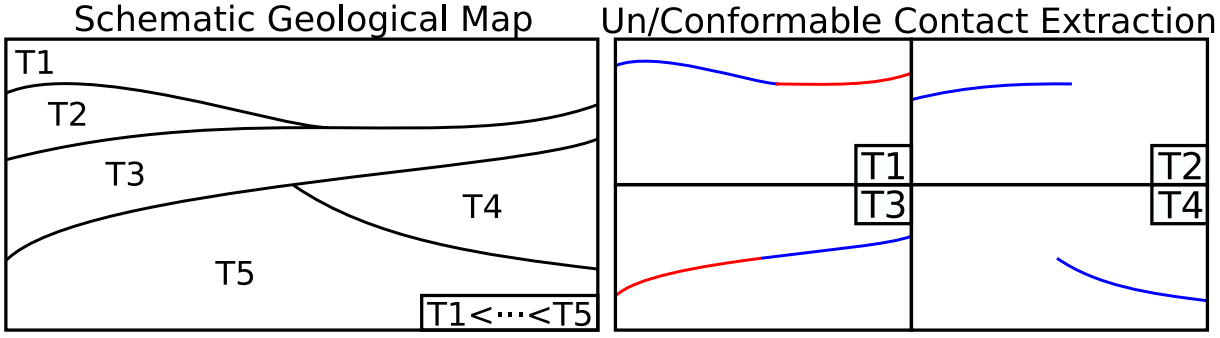

Figure 2.2: **(Left)**: Schematic geological map for five consecutive chronostratigraphic units (T1 to T5) with T1 youngest and T5 oldest. **(Right)**: Schematic showing the extraction of un/conformable contacts for a target unit. Conformable lines for the target unit are the contours of the preceding unit. Unconformable contacts contour the contact of the unit with units older than the immediately preceding one.

DeMets et al. (2010) as a representative value, temporal uncertainty for a hiatus at the series level (10-30 Myrs) translates into a minimum spatial uncertainty of 500-1500 km. Moreover, by saturating temporal resolution to the series level, we underestimate the total amount of hiatus because unconformities and hiatus at the resolution of stages may be masked at the stratigraphic resolution of series. Figure 2.3 illustrates these uncertainties.

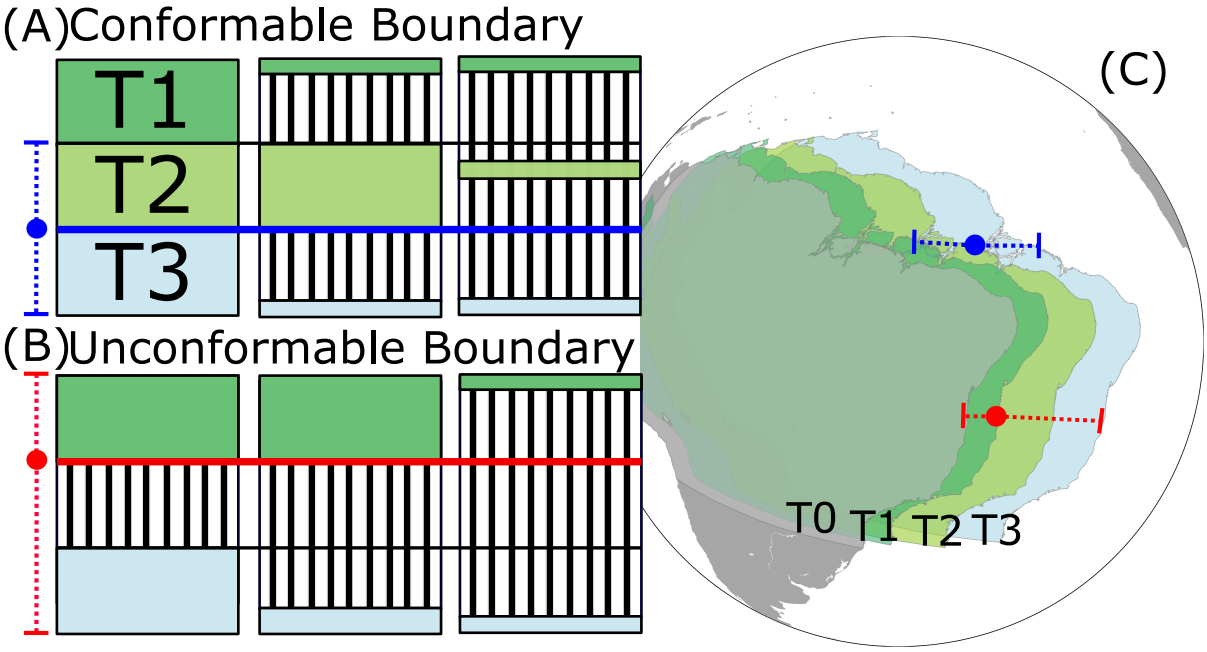

Figure 2.3: Schematic illustration of the temporal and spatial uncertainty of hiatus mapping Friedrich et al. (2018); Friedrich (2019); Vibe et al. (2018); Carena et al. (2019). **(A)** and **(B)** show conformable and unconformable contacts, respectively. **(C)** displays how temporal uncertainty translates into spatial uncertainty for the paleogeographical reconstruction representing hiatus.

2.3 Results

2.3.1 Geological Hiatus Maps

Figure 2.4 shows hiatus mapped with our method for North and South America, Europe, Africa, and Australia for eight geologic series. This yields a set of eight **Geological Hiatus Maps (GHMs)**, beginning with the Lower Cretaceous (i.e., hiatus here meaning that the Upper Jurassic is missing). We use *pyGPlates* (Müller et al., 2018a) to reconstruct each hiatus to its past tectonic setting with a global Mesozoic-Cenozoic plate motion model (Müller et al., 2016) tied to a reference frame of Indo-Atlantic hotspots (O'Neill et al., 2005; Burke and Torsvik, 2004) and present the extracted signal in a plate tectonic configuration corresponding to the base of each series. Red and blue colours depict un/conformable contacts, respectively. Blank regions indicate the absence of the considered series and its immediately preceding unit.

In the following, we describe the results for each GHM. **Base of Pleistocene** datum, Fig. 2.4(A), presents North and South America, Greenland, and Australia with predominantly unconformable contacts. Conformable contacts exist in the High Plains of North America, parts of South America, and the Australian *Nullarbor Plain*. Europe is dominated by conformable contacts. Africa

shows a mix of un/conformable contacts, with conformable contacts located in the northwest and in the Kalahari and Congo Basins. Unconformable contacts extend through the East African Highlands and the Sahara desert. **Base of Pliocene** datum, Fig. 2.4(B), exposes conformable contacts in North and South America, around the Gulf of Mexico, the *Basin and Range*, the *Rocky Mountains* front, the Brazilian Highlands and the western Amazon Basin. Australia

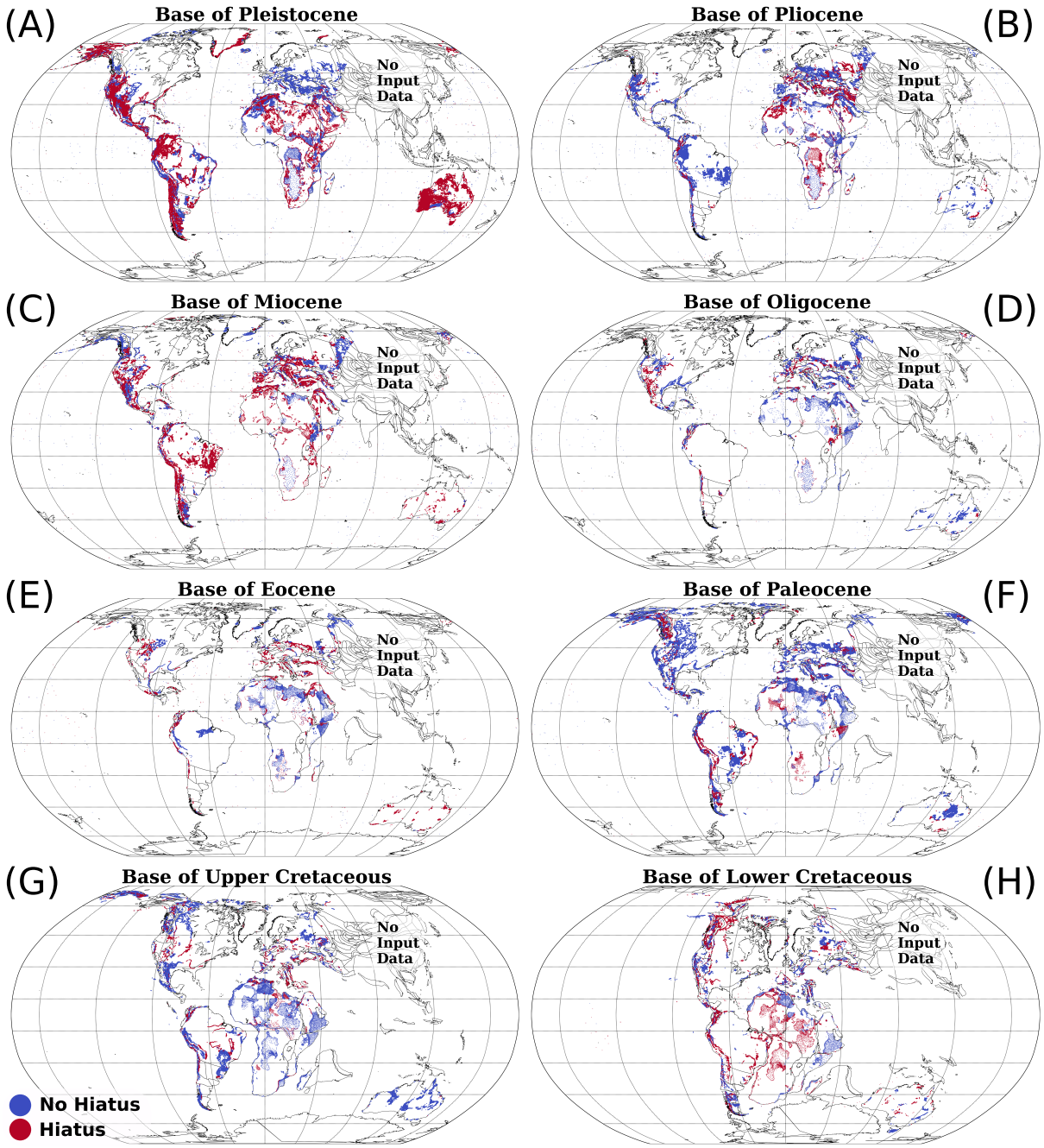

Figure 2.4: Geological Hiatus Maps (GHMs) at chronostratigraphic division of series Cohen et al. (2013; updated.) from the Base of Pleistocene datum to the Base of Lower Cretaceous datum **(A)-(H)** reconstructed paleogeographically with a global Mesozoic-Cenozoic plate motion model (Müller et al., 2016) tied to a reference frame of Indo-Atlantic hotspots (O'Neill et al., 2005) and shown in a plate tectonic configuration corresponding to the base of each series. Red/blue points represent un/conformable contacts, respectively. Blank regions indicate absence of considered series and its immediately preceding unit. See text for further information.

shows sparse conformable contacts throughout the continent and isolated unconformable contacts in the north and in the southeast. Conformable contacts cover eastern Europe and the Iberian Peninsula, while unconformable contacts prevail in western/central Europe and in tectonically active regions in the Mediterranean. Africa exhibits unconformable contacts in the Congo Basin and the Canary-Atlas region, while conformable contacts occur in the Kalahari Basin, the Afar region, and the northern edges of the continent. **Base of Miocene** datum, Fig. 2.4(C), is dominated by unconformable contacts across the continents. Unconformable contacts abound in the western part of North America, Brazil, and much of Europe, whereas isolated hiatuses exist in Australia and Africa. Conformable contacts are exposed in Greenland, western and easternmost Europe and the Kalahari Basin. **Base of Oligocene** datum, Fig. 2.4(D), exposes conformable contacts in many regions, with a striking absence of signal across South America. Unconformable contacts are mapped in the western parts of North America, the Afar region and in Europe. **Base of Eocene** datum, Fig. 2.4(E), features a mix of signals. Unconformable contacts exist in eastern Africa, Europe, and the western parts of North America adjacent to conformable contacts in the plains of Canada. South America lacks information except for conformable contacts in the eastern Amazon. Africa reveals conformable contacts in its northern parts and the Kalahari Basin, but signal is absent in the central and southern parts of the continent. Scattered unconformable contacts are mapped across Australia. **Base of Paleocene** datum, Fig. 2.4(F), reveals abundant conformable contacts across North and South America, Europe, North Africa, and Australia. Unconformable contacts are located in the northwestern part of North America and Greenland. South America exposes unconformable contacts along the Andes and the east coast of Brazil. Africa shows clusters of unconformable contacts in the Kalahari Basin, the northern Djoue Basin, and the Afar region. Unconformable contacts are mapped in southern Australia near Tasmania. **Base of Upper Cretaceous** datum, Fig. 2.4(G), is characterized by unconformable contacts, which prevail across Europe, and the western parts of North America. Conformable contacts are mapped in Canada, Mexico, Africa, the Parana region of South America, and Australia. Finally, **Base of Lower Cretaceous** datum, Fig. 2.4(H), exhibits a mix of un/conformable contacts. Most notable are unconformable contacts in Alaska and Africa as well as a lack of signal throughout much of South America. We point out that the absence of Mesozoic/Cenozoic strata across much of Scandinavia and the cratonic part of North America precludes hiatus mapping for the Mesozoic/Cenozoic series in these regions.

2.3.2 Base Hiatus Surfaces

The GHMs allow us to perform a spherical harmonics expansion of the hiatus signal to create **Base Hiatus Surface (BHS)**. We adopted *pyshtools* (Wieczorek and Meschede, 2018) with fully normalized spherical harmonic coefficients (Stacey and Davis, 2008), using a global equidistant grid of 720/1440 points in latitude/longitude for a resolution of $\approx$ 30 km between grid nodes. Numerical values of 1/-1 were assigned to un/conformable signal, respectively. Each grid node was then initialized with the nearest hiatus value that falls within a radius of 1/2 of the grid node distance. Otherwise, the grid node value was set to zero.
We performed the expansion up to spherical harmonic degree 100. However, our assumption of a geodynamic origin for interregional-scale hiatus implies the choice of a spectral window that

one should consider in the **BHS** representations. Longstanding arguments based on dynamic models of the Geoid suggest a dominant contribution to dynamic topography of spherical harmonic degree 2 (Richards and Hager, 1984). The dominance of the longest wavelength components for convectively maintained topography was challenged recently by an observational database of >2000 spot measurements of residual bathymetry in the oceanic realm (Hoggard et al., 2017). The latter suggests that contributions up to and including degree 30 are required to represent topography in convective support. Figure 2.5 illustrates the difference and reports **BHS** for the Base of Miocene datum for four cut off degrees (2, 10, 15, and 30) and a tapered Gaussian smoothing to the spectral coefficients. The taper width of 40 degrees allows the contribution of spectral components beyond the cut off. For the long-wavelength cut off at degree 2 there remains a 30% contribution of the original signal at degree 27, while the degree 30 cut off maintains 30% of the original signal up to degree 55. We report **BHS** starting with the Lower Cretaceous and assuming an intermediate cut off at degree 15 in Fig. 2.6.

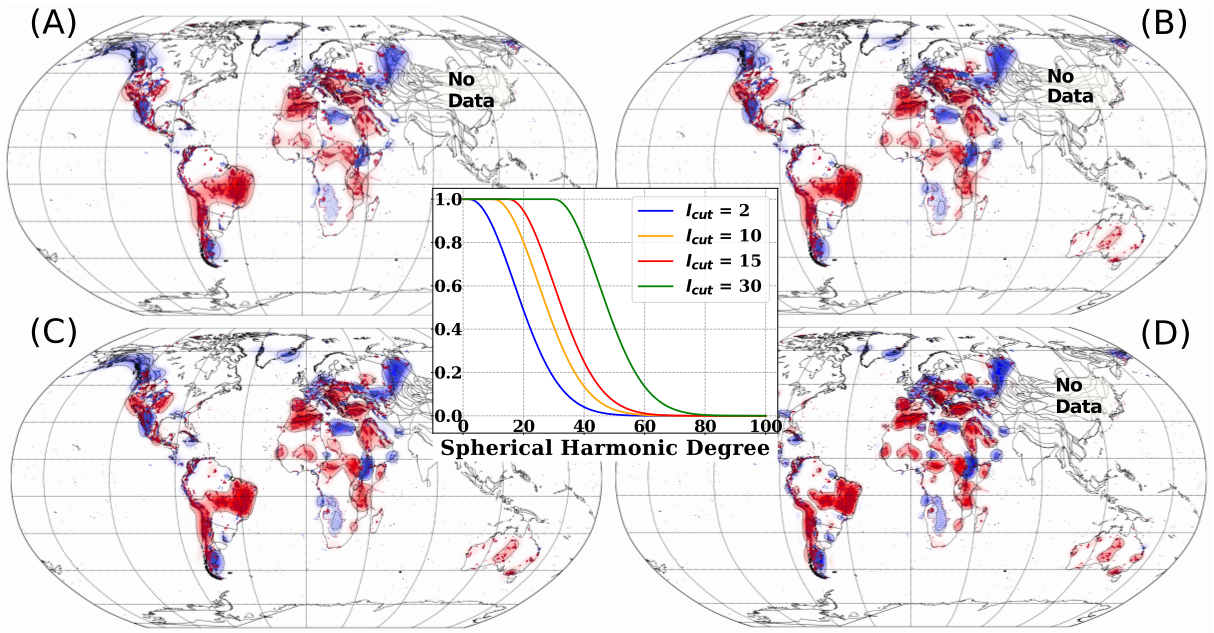

Figure 2.5: Base of Miocene Hiatus Surface (BHS) obtained by expanding the Miocene Geological Hiatus Map (GHM) (Fig. 2.4 C) in fully normalised (Stacey and Davis, 2008) spherical harmonics (SH) and convolving with a Gaussian taper at four different cut off values for degree 2 **(A)**, 10 **(B)**, 15 **(C)**, and 30 **(D)**, respectively. Red/blue areas represent un/conformable surfaces. Black dotted lines contour the SH signal at the ± 0.1 amplitude. Hiatus data from the input GHM shown as blue/red dots. Center plot: four Gaussian tapers applied in the SH expansion, see text.

The **BHS** provides information on the temporal evolution in the ratio of the area of conformal surface relative to the total area of conformal and unconformal surface. The latter can be plotted both aggregated over all continents and separate for each. The aggregated curve (Fig. 2.7) achieves a maximum in the ratio of conformable surface relative to the total area of conformable and unconformable surface at the Base of Paleocene and the Base of Upper Cretaceous (corresponding to topography of the Upper and Lower Cretaceous). There are also two prominent maxima in the ratio of the area of unconformable surface relative to the total area of conformable and unconformable surface at the Base of Miocene and the Base of Pleistocene, respectively. The curves for individual continents (Fig. 2.8) are more variable. They reveal

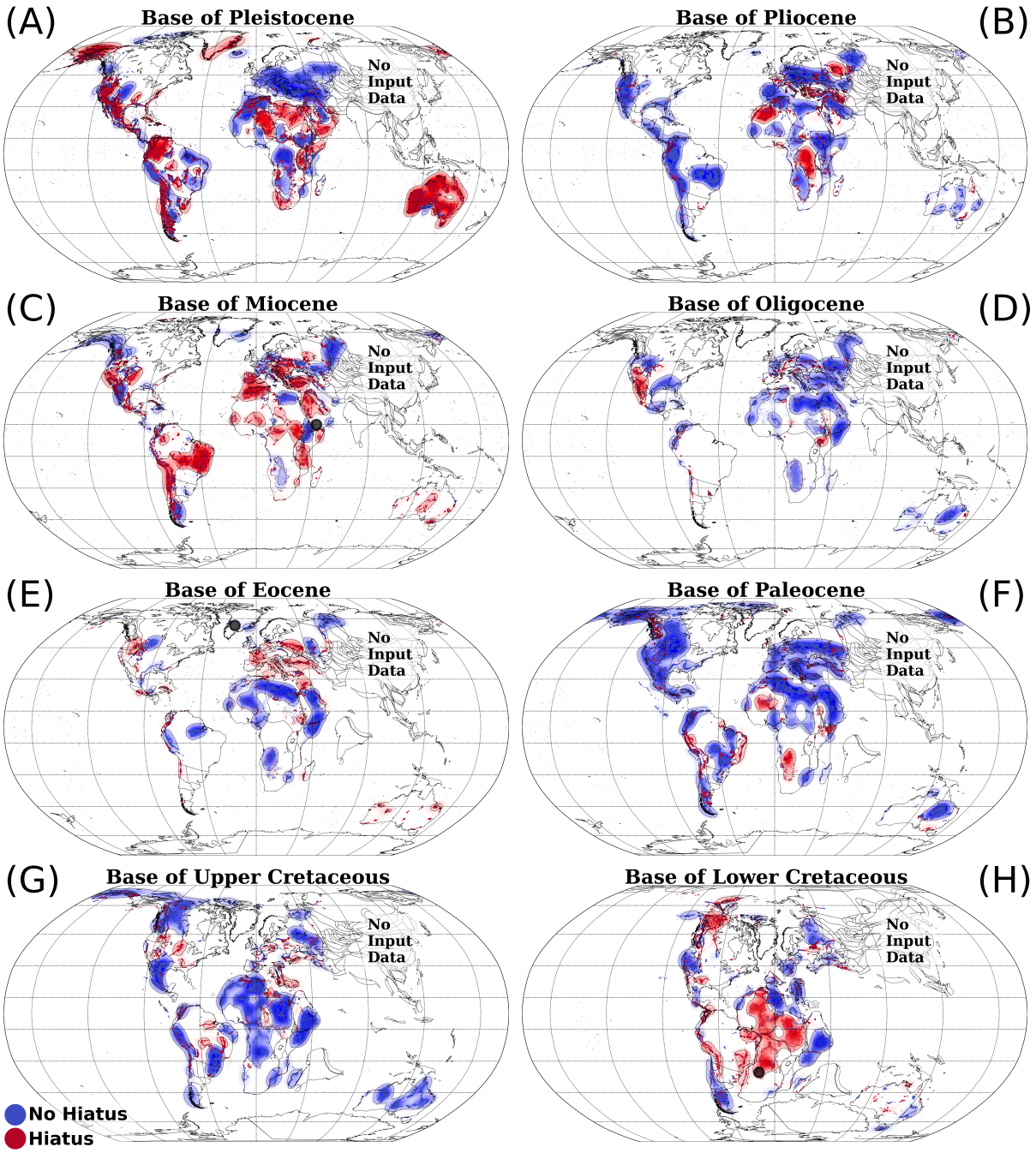

Figure 2.6: Base Hiatus Surface (BHS) obtained by expanding the Geological Hiatus Maps (GHMs) (Fig. 2.4) in fully normalized (Stacey and Davis, 2008) spherical harmonics (SH) and convolving with a Gaussian taper starting at degree 15 (compare Fig. 2.5). BHS shown at chronostratigraphic division of series (Cohen et al., 2013; updated.) from the Base of Pleistocene to the Base of Lower Cretaceous **(A)-(H)** reconstructed paleogeographically with a global Mesozoic-Cenozoic plate motion model (Müller et al., 2016) tied to a reference frame of Indo-Atlantic hotspots (O'Neill et al., 2005) and placed into a plate tectonic configuration corresponding to the base of each series. Blue/red colours represent no-/hiatus surfaces, indicative of low/high topography in the preceding series, respectively. Black dotted lines contour the SH signal at the ± 0.1 amplitude. Hiatus data from the input GHMs shown as blue/red dots. Black circles at Base of Miocene **(C)**, Base of Eocene **(E)** and Base of Lower Cretaceous **(G)** maps correspond to location of flood basalts associated with Afar, Iceland and Tristan hotspots (Courtillot et al., 2003). Blank regions indicate absence of series and its immediately preceding unit, suggesting long hiatus duration. See text for further information.

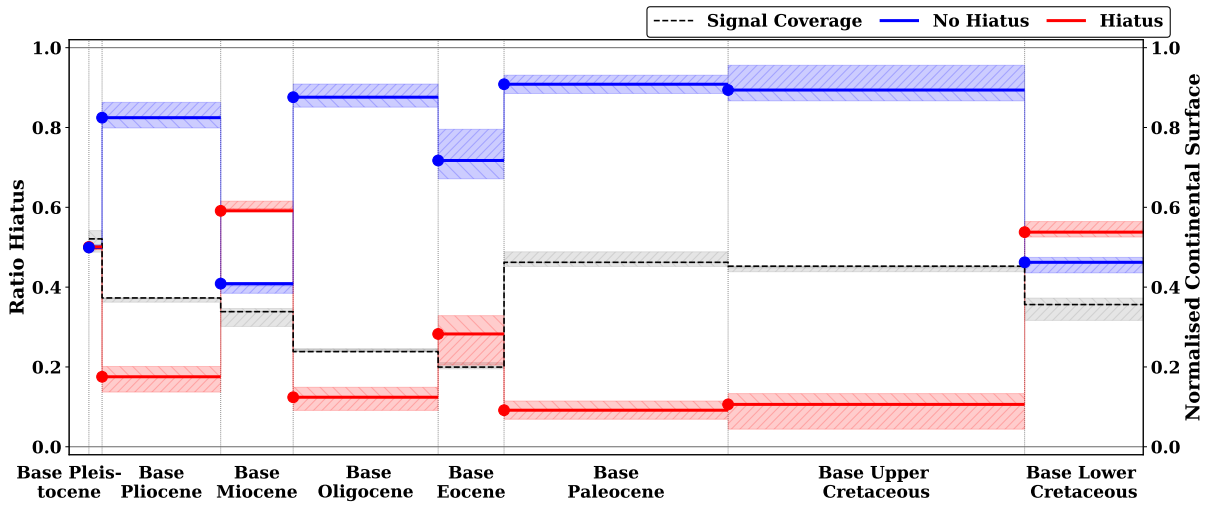

Figure 2.7: Ratio of the area of un/conformal (solid red/blue lines) surface relative to the total area of conformal and unconformal surface aggregated over North/South America, Europe, Africa and Australia from the Base of Lower Cretaceous to the Base of Pleistocene, indicative of mean relative elevation (blue=low, red=high) across the continents in the preceding series (see text). The spherical harmonics (SH) area of conformal and unconformable surface is taken within the amplitude range ($\geq$ 0.1) for a tapered cut off at degree 15 (see Fig. 2.6). The // and \\ shaded envelopes represent the ratio variations that correspond to tapered cut offs in the SH surface at degree 2 and 30, respectively (compare Fig. 2.5). A maximum in the ratio of conformable surface at the Base of Paleocene and Base of Upper Cretaceous (corresponding to mean topography in the Upper and Lower Cretaceous) relative to the total area of conformal and unconformal surface agrees with global sea-level curves (e.g., Müller et al., 2008; Rowley, 2017). Two maxima in the ratio of unconformable surface relative to the total area of conformal and unconformal surface at the Base of Miocene and the Base of Pleistocene coincide with the onset of glaciation in Antarctica (Petersen and Schrag, 2015) and the Northern Hemisphere (Maslin et al., 1996), respectively (see text). The total area (within the amplitude range ($\geq$ 0.1) for a tapered cut off at degree 15) of conformal and unconformal surface relative to the total area of the considered continents is shown by the grey curve. The grey hatched // and \\ shaded envelopes represent the ratio variations that correspond to tapered cut offs in the SH area at degree 2 and 30, respectively.

considerable differences between continents and series.

2.4 Discussion

Geodynamicists have long recognised the essential role of dynamic topography in studies of the Geoid because the mass anomalies associated with surface deflections yield gravity anomalies of comparable amplitude to the flow-inducing mantle density variations. Geoid models therefore account for dynamic topography as well as mantle density heterogeneity (e.g., Ricard et al., 1984; Richards and Hager, 1984; Forte and Peltier, 1991). However, it is difficult to separate dynamic topography from topography in isostatic support (Fishwick and Bastow, 2011; Ravenna et al., 2018; Jones et al., 2017) outside the oceanic realm (Hoggard et al., 2017). This has led some to doubt the existence of dynamic topography (Molnar et al., 2015).

The transient nature of dynamic topography suggests to overcome this difficulty by turning to geologic archives. Ahead of his time, Bond (1978b, 1979) analysed continent-scale sediment distributions to argue for substantial uplift of continental platforms. He concluded that

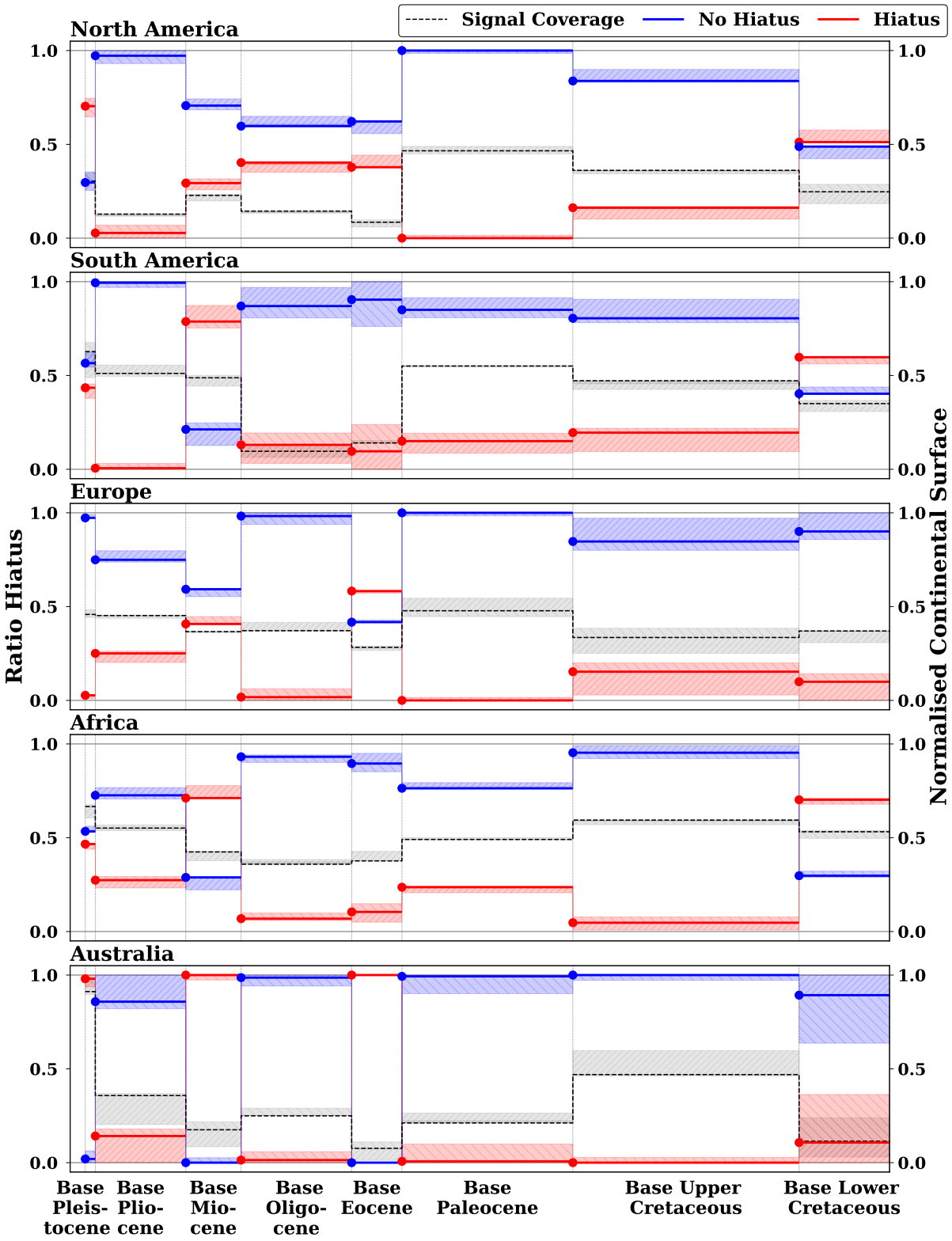

Figure 2.8: Same as Fig. 2.7, but for individual continents. The curves are more variable and reveal considerable differences between continents and series. See text for interpretation.

Africa, for instance, experienced late Tertiary uplift relative to other continents (Bond, 1978a), in agreement with Burke and Whiteman (1973). Our interregional hiatus maps also turn to sedimentary archives, in the form of interregional unconformities. But we note that the existence of such unconformities has long been known (e.g., Suess, 1883; Blackwelder, 1909; Stille, 1924b; Levorsen, 1933; Wheeler, 1958b; Belousov and Maxwell, 1962; Sloss, 1963, 1992; Vail et al., 1977; Şengör, 2003, 2016) and that some have pointed out the need of physical models for their interpretation (e.g., Burgess et al., 1997; Şengör, 2016).

Our **GHMs** locate sedimentary rocks of any origin, including volcanic effusive and pyroclastic products that, for the purpose of mapping depositional sequences, behave like sediments. Thus, to first order, the time slices in Fig. 2.4 show, where sediments were or were not deposited (or deposited and then eroded before the deposition of the next series) in the series immediately preceding the target series. Surfaces of unconformable contact (marked in red) in the **BHS** (Fig. 2.6) define regions in the series immediately preceding the target series that undergo erosion and/or non-deposition, whereas areas of conformable contact (marked in blue) identify depositional regions. At the interregional scales invoked, this serves as a proxy for either exhumation and surface uplift, or burial and subsidence. Lack of signal in the **BHS** indicates the absence of sediments in the target series and its immediately preceding series. This describes regions that may have undergone intense and/or long-lasting erosion or non-deposition and suggests intense and/or persistent exhumation and surface uplift (Friedrich et al., 2018; Friedrich, 2019; Vibe et al., 2018; Carena et al., 2019). Examples for un/conformable surfaces and for lack of signal can be identified in the **BHS**.
South America reveals a continent-scale lack of signal at the Base of Eocene and the Base of Oligocene (Fig. 2.6(D)/(E)), indicating early Tertiary uplift in the region. This coincides temporally with the onset of rapid South Atlantic spreading rates (Colli et al., 2014) and an Eocene subaerial exposure of the Rio Grande Rise at Drill Site 516 (Barker, 1983). There are also reports from thermochronological data and landscape analysis for post-rift Eocene reactivation in Brazil (Cogné et al., 2012; Japsen et al., 2012; Krob et al., 2019) and Argentina (Kollenz et al., 2017), and there is a Paleogene hiatus documented in Andean Foreland Basins (Horton, 2018). Expansion of the total unconformable area from one time slice to the next indicates the onset of relative subsidence; it means that sediments now deposit in areas that previously underwent erosion/non-deposition. A significant expansion of unconformable area in central and northern Africa occurs at the Base of the Lower Cretaceous when compared to the Base of Upper Cretaceous (Fig. 2.6(G)/(H)) and suggests that the Lower Cretaceous was a period of subsidence in Africa. An exception is the South African Plateau (SAP). It reveals a lack of signal suggestive of net high elevation. While this agrees with reports by some authors (Baby et al., 2018; Gallagher and Brown, 1999; Tinker et al., 2008) calling for a Cretaceous age of the SAP topography, others suggest more recent Oligo-Miocene or younger uplift phases (Burke and Gunnell, 2008; Carena et al., 2019). Another major expansion of unconformable area across Africa occurs at the Base of Miocene when compared with the Base of Oligocene (Fig. 2.6(C)/(D)). It implies relative subsidence in the Miocene and suggests that the Oligocene was a period of uplift in most of the continent, as noted by several authors (Bond, 1978a; Şengör, 2001; Carena et al., 2019) and reviewed very effectively by Burke and Gunnell (2008). A recent geologic/geodynamic analysis suggests that Africa may cover different dynamic topography domains owing to its large

area. Carena et al. (2019) took the presence of Upper Cretaceous to Eocene exposed marine sediments in the interior of northern Africa together with the absence of exposed Oligocene to Pleistocene marine sediments there as evidence that this region uplifted significantly after the end of the Eocene, remaining high since. Oligocene to recent sediments in northern Africa are exclusively of continental origin. Far less marine sedimentation exists in the southern half of Africa for the Cenozoic series, where it is limited to coastal regions. While none of the exposed Cenozoic sediments in the interior of southern Africa are marine, there is a complete absence of coastal marine sediments in the Oligocene and Pleistocene. From this, and from the observation that some Miocene and Pliocene marine sediments along the southern coast are now at elevations significantly above 200 m, Carena et al. (2019) inferred that southernmost Africa reached a high elevation in the Oligocene, subsided in the Miocene-Pliocene, and has been high again since the Pleistocene.
Europe features a strong expansion of unconformable area at the Base of Eocene when compared to the Base of Paleocene (Fig. 2.6(E)/(F)), indicative of relative subsidence in the Eocene. We note that the above examples of expanding unconformable area follow each in the wake of major plume events (i.e., Tristan, Lower Cretaceous; Afar, Oligocene; and Iceland, Paleocene, see Fig. 2.6).
Conformable area expansion from one time slice to the next indicates continued subsidence (Friedrich, 2019; Vibe et al., 2018; Carena et al., 2019). Prominent examples include Australia at the Base of Upper Cretaceous when compared to the Base of Lower Cretaceous (Fig. 2.6(G)/(H)), and western North America at the Base of Paleocene when compared to the Base of Upper Cretaceous (Fig. 2.6(F)/(G)). Continent-scale subsidence implied by growing conformable area in these regions has been linked to subduction at the eastern margin of Gondwana (Matthews et al., 2011; Heine et al., 2010) and to the descent of the Farallon Plate beneath western North America (Mitrovica et al., 1989; Burgess et al., 1997; Spasojevic et al., 2009).

Figures 2.7 and 2.8 show the temporal evolution in the ratio of the area of un/conformal surface relative to the total area of conformal and unconformal surface, both aggregated over all continents and separate for each. The aggregated curve (Fig. 2.7) reveals a sea-level signal. It is indicated by a maximum in the ratio of the area of conformable surface at the Base of Paleocene and the Base of Upper Cretaceous (corresponding to the Upper and Lower Cretaceous, respectively) relative to the total area of conformal and unconformal surface. The maximum agrees with global sea-level curves even when the amplitude of the latter is not well constrained (e.g., Müller et al., 2008; Rowley, 2017). There are also two prominent maxima in the ratio of the area of unconformable surface relative to the total area of conformal and unconformal surface at the Base of Miocene and the Base of Pleistocene. These coincide with the onset of glaciation in Antarctica (Petersen and Schrag, 2015) and the Northern Hemisphere (Maslin et al., 1996), respectively.
The curves for individual continents (Fig. 2.8) provide additional information: a sharp decline for North America in the ratio of conformable surface relative to the total area of conformal and unconformal surface at the Base of Eocene marks the disappearance of the *Interior Seaway* in the western part of the continent. South America displays a gradual growth with time in the ratio of conformable surface relative to the total area of conformal and unconformal surface. The lack of signal at the Base of Eocene and the Base of Oligocene, which we noticed before in the **BHS**

(Fig. 2.6(D)/(E)), is evinced in Fig. 2.8 by the drop in the grey curve reporting the ratio of the total conformal and unconformal surface relative to the total area of South America. Europe's ratio of conformable surface relative to the total area of conformal and unconformal surface sinks dramatically at the Base Eocene, in agreement with the continent-scale growth of unconformable surface and the implied Eocene subsidence that followed the arrival of the Iceland Plume. Africa incurs two increases in the ratio of unconformable surface relative to the total conformal and unconformal surface at the Base of Lower Cretaceous and the Base of Miocene, presumably reflecting Lower Cretaceous and Miocene subsidence as discussed before. Notable for Australia is the increase in the ratio of conformable surface to the total un/conformable surface at the Base of Upper Cretaceous, attributed to Australia's eastward passage over subducted oceanic lithosphere. These results are in broad agreement with the analyses of Bond (1978b, 1979) and support the notion that there are no stable continental platforms (Moucha et al., 2008b).

In our discussion we must point to the severe limitations of our method. First: GHMs strongly depend on the spatio-temporal resolution and accuracy of data compiled on geological maps. This means that the duration over which a particular hiatus area is defined depends on the temporal resolution of the input geological map, as noted before (see Fig. 2.3). Our analysis is limited to the series level. But true hiatus is likely longer than indicated by the missing series, because at any one location sedimentary successions represent only a small portion of a series. This implies large temporal uncertainties in our analysis, even when only one series is absent or when the adjacent series is not fully represented in the field. While our saturation of the time intervals to the series level is dictated by the data (i.e., the geological convention), it inevitably hides shorter duration lacunae and thereby avoids artifacts related to the Sadler effect (Sadler, 1981). This is critical, because if shorter duration lacunae are hidden, shorter duration events from lithospheric processes may be conflated with longer duration mantle-driven signals. Essentially our method favors large time intervals and hides shorter time intervals. Krob et al. (2020b) deduced an uplift duration signal of 50 Myrs for the Parana-Etendeka plume. So even at the temporal resolution of series it may be difficult to detect plume related uplift events. A similar difficulty arises when continents move laterally over different dynamic topography domains in relatively short geological time frames (Braun et al., 2014). Future stratigraphic work should therefore respond to the geodynamic need for more precise dating of hiatus. Interregional geological maps at the resolution of stages (1-2 Myrs) are needed to reduce the uncertainties and to assist in geodynamic interpretations of hiatus.
Second: GHMs on their own do not identify the lithospheric or sublithospheric causes for continental vertical motion. Models predicting continental rise under increased horizontal stress (e.g., Ziegler et al., 1995), lithospheric folding Cloetingh et al. (2002) or delamination (e.g., Levander et al., 2011; Schott and Schmeling, 1998), which act as tectonic mechanisms within the lithosphere, must be distinguished from deeper, mantle related effects, such as the influence of rising plumes or pressure-driven asthenosphere flow. Detailed biostratigraphy and geomorphological methods of slope investigation or planation surfaces (Guillocheau et al., 2018) are needed in the identification of broad scale (falcogenic) structures in the sense of Şengör (2003). It is clear that viable dynamic models of lithosphere motion must provide for a coupling of tectonic and mantle related forces (e.g., Stotz et al., 2017) to represent the behavior of the litho-

sphere as the combination of lithospheric and sublithospheric effects.
Third: GHMs are well constrained in lateral extend but not in amplitude. The latter requires independent calibration, for example, by using thermochronological data (Ehlers and Farley, 2003). A variety of inferences provide constraints on surface uplift of the lithosphere. They include studies of river profiles (e.g., Roberts and White, 2010), sediment compaction (Japsen, 2018) and provenance (Meinhold, 2010; Şengör, 2001), landform analysis (Guillocheau et al., 2018) based on planation surfaces (King, 1955), paleoaltimetry (Kohn, 2018), or the analysis of sediment budgets at the scale of continental margins (Guillocheau et al., 2012; Said et al., 2015a,b). Passive margins have been advocated as suitable locations for such studies (Bunge and Glasmacher, 2018). MacGregor (2013) summarizes episodes of margin uplift for South America and Africa, and similar inferences have been made for the Arctic (Dörr et al., 2012) and the European passive margin of the North Atlantic, summarised in the Stratagem project (Stoker and Shannon, 2005, and references therein). Inferences for an active post-rift evolution of passive margins have been collected into propositions for geodynamic models (Green et al., 2018b). Geological hiatus maps suggest to extend the studies to broader spatial scales beyond passive margins.

2.4.1 Geodynamic implications

Geodynamicists explore mantle convection in terms of the plate and plume modes. Hiatus maps reveal the plate mode as broad conformable surfaces at the Base of Upper Cretaceous in Australia (Fig. 2.6(G)) and the Base of Paleocene in western North America (Fig. 2.6(F)), as noted before. Unconformable surfaces and areas of lack of signal located away from active plate margins are instead expressions of the plume mode. Seismic evidence suggests a strong plume mode (French and Romanowicz, 2015; Nelson and Grand, 2018; Rickers et al., 2013), imaged for the upper (Schaeffer and Lebedev, 2013b; van Herwaarden et al., 2020; Colli et al., 2013) and the lower mantle as prominent regions of seismically slow velocities (e.g., Kennett et al., 1998; Ritsema et al., 2011; Simmons et al., 2009b; Hosseini et al., 2020). The geodynamic analysis of these anomalies remains under debate and permits interpretations of the lower mantle anomalies primarily by elevated temperature (Davies et al., 2012; Schuberth et al., 2009; Simmons et al., 2009b) or combinations of thermal and compositional effects (Lu et al., 2020; McNamara, 2019). The repeated appearance of continent-scale hiatus surfaces in our maps provides additional constraints. It implies significant positive mantle buoyancies presumably related to elevated temperature.
The distribution of un/conformable surface varies at the timescale of geologic series, (i.e., ten to a few tens of Myrs). This is considerably faster than the mantle transit time which, as the timescale for convection, is about 100-200 Myrs (Iaffaldano and Bunge, 2015; Butterworth et al., 2014). The difference in the convective timescale and the timescale for topography in convective support is illustrated by geodynamic kernels. They reflect the properties of dynamic Earth models and depend strongly upon the assumed rheology (see Colli et al., 2016, for a review). For internal loads (e.g., hot rising plumes or cold sinking slabs) passing through a uniform-viscosity mantle, the kernels predict a continuous evolution of the induced surface deflections. In other words, a comparable timescale for convection and convectively-maintained

topography is implied and borne out in laboratory models of isoviscous mantle flow (Griffiths et al., 1989). The presence of a weaker upper mantle relative to the lower mantle, which is consistent with inferences from geodynamics (Richards and Hager, 1984) and mineral physics modelling (Reali et al., 2019), amplifies surface deflections for loads passing through the upper mantle. This property of dynamic Earth models makes rapid changes of convectively-maintained topography geodynamically plausible.

Geological hiatus maps have implications for time-dependent geodynamic Earth models: progress has been made in understanding how to retrodict past mantle states. Early backward advection schemes (e.g., Bunge and Richards, 1992; Steinberger and O'Connell, 1997) have given way to a formal inverse problem based on adjoint equations that provide sensitivity information in a geodynamic model relative to earlier system states. Adjoint equations have been derived for incompressible (Bunge et al., 2003b; Ismail-Zadeh et al., 2004; Horbach et al., 2014), compressible (Ghelichkhan and Bunge, 2016) and thermo-chemical (Ghelichkhan and Bunge, 2018) mantle flow, and the uniqueness property of the inverse problem has been related to the tangential component of the surface velocity field of the convection model (Colli et al., 2015). Knowledge of the latter is essential to ensure convergence (Vynnytska and Bunge, 2015; Colli et al., 2020). While plate motions are a primary surface expression of mantle convection (e.g., Davies and Richards, 1992), one needs to assimilate the tangential component of the surface velocity field (i.e., a past plate motion model) to solve the inverse problem. This makes past plate motions the input of retrodictions rather than their output, and suggests linking viable tests of retrodictions to inferences of past dynamic topography so that uncertain model parameters and state estimates can be assessed (Colli et al., 2018). Put differently: the horizontal motion of the lithosphere cannot be predicted from mantle flow restorations, because reconstructions of past plate motion act as an input to the inverse problem, implying that it is not viable to construct self-consistent models of plate tectonics that are testable against the geologic record. However, mantle convection also induces vertical motion in the form of dynamic topography, as noted before. These can be inferred from a mantle flow retrodiction, because they are an output of the inverse problem. Geologic constraints on the history of convectively induced vertical motion of the lithosphere (that is the evolution of past dynamic topography) therefore are crucial observations to test the validity of the geodynamic modeling parameters assumed in mantle flow retrodictions. Our results imply that changes in convectively-maintained topography at the timescale of geologic series and over spatial scales of a few thousand kilometres must be an integral component of time-dependent geodynamic Earth models.

2.5 Conclusion

The analysis of continent-scale geological maps yields powerful information for constraining large-scale geodynamic processes and models. By providing consistent compilations of geologic observations at the scale of thousands of kilometres, continent-scale geologic maps link naturally to large-scale mantle flow induced elevation changes known as "dynamic topography" (Hager et al., 1985; Braun, 2010). While the latter is difficult to separate by geophysical or geodetic means from the current isostatic topography of our planet outside the oceanic realm (Hoggard et al., 2017), its transient nature leaves signals in sedimentary archives as conformable

and unconformable (hiatus) time boundaries traceable over hundreds to thousands of kilometres. We have applied a hiatus mapping method, introduced by Friedrich et al. (2018) and Friedrich (2019), as a first-order technique that uses a single manipulation of existing geological maps to construct hiatus surfaces at the temporal resolution of series across North and South America, Europe, Africa and Australia starting from the Upper Jurassic. We find significant differences in the spatial extent of hiatus surface across and between continents at the timescale of geologic series, ten to a few tens of millions of years (Myrs). This is considerably smaller than the mantle transit time (Iaffaldano and Bunge, 2015) and may reflect the effects of rapid lateral motion of continents over different dynamic topography domains in relatively short geological time-frames (Braun et al., 2014) as well as vigorous upper mantle flow in the asthenosphere facilitated by a viscosity reduction from the lower to the upper mantle as implied by response functions for dynamic Earth models (e.g., Richards and Hager, 1984). The recurrent appearance of continent-scale hiatus surfaces is consistent with the existence of significant positive mantle buoyancies, presumably induced by thermal effects and elevated temperature. This supports the notion of a strong plume mode in the mantle convection system. In the future it is necessary to compile interregional geological maps at the temporal resolution of stages, most of which span 1-2 Myrs in duration, to reduce uncertainty and to assist in improved geodynamic interpretations of hiatus through time-dependent geodynamic Earth models capable of retrodicting past mantle flow states.

Chapter 3

Evidence for active upper mantle flow in the Atlantic and Indo-Australian realms since the Upper Jurassic from hiatus maps and spreading rate changes

Histories of large scale horizontal and vertical lithosphere motion hold important information on mantle convection. Here we compare continent-scale hiatus maps as a proxy for mantle flow induced dynamic topography and plate motion variations in the Atlantic and Indo-Australian realms since the Upper Jurassic, finding they frequently correlate, except when plate boundary forces may play a significant role. This correlation agrees with descriptions of asthenosphere flow beneath tectonic plates in terms of Poiseuille/Couette flow, as it explicitly relates plate motion changes, induced by evolving basal shear forces, to nonisostatic vertical motion of the lithosphere. Our analysis reveals a time scale, on the order of a geological series, between the occurrence of continent-scale hiatus and plate motion changes. This is consistent with the presence of a weak upper mantle. It also shows a spatial scale for interregional hiatus, on the order of 2000-3000 km in diameter, which can be linked by fluid dynamic analysis to active upper mantle flow regions. Our results suggest to pursue future studies of large scale horizontal and vertical lithosphere motion in combination, to track the expressions of past mantle flow. Such studies would provide powerful constraints for adjoint based geodynamic inverse models of past mantle convection.

Published on May 12th 2022 in the Proceedings Royal Society A.
doi:10.1098/rspa.2021.0764

Author list: Berta Vilacís[1], Jorge N. Hayek[1], Ingo L. Stotz[1], Hans-Peter Bunge[1], Anke M. Friedrich[1], Sara Carena[1] and Stuart R. Clark[2].

[1] Ludwig-Maximilians-Universität München, Dept. of Earth and Environmental Sciences, Theresienstraße 41 and Luisenstraße 37, 80333 Munich, Germany.
[2] University of New South Wales Sydney, Minerals and Energy Resources Engineering, Kensington, NSW, 2052, Australia.

3.1 Introduction

An enduring theme in mantle flow studies is the existence of an asthenosphere (see Richards and Lenardic, 2018, for a review). The presence of this layer was advocated by Barrell (1914) to allow for isostatic movement, and by Chase (1979) to lubricate plate motion. Modern evidence for a mechanically weak layer in the uppermost mantle beneath the lithosphere comes from a variety of observations. They include studies of the geoid (e.g., Hager and Richards, 1989), post glacial rebound (e.g., Mitrovica, 1996), lake loading (e.g., Bills and May, 1987), oceanic intraplate seismicity (Wiens and Stein, 1985), ocean ridge bathymetry (Buck et al., 2009) and seismic anisotropy (Debayle et al., 2005; Schaeffer et al., 2016). Fluid dynamic investigations employing numerical and analytic modelling techniques (e.g., Bunge and Richards, 1996; Busse et al., 2006; Tackley, 1996) agree that high material mobility in the asthenosphere is essential to promote the long-wavelength character of mantle flow observed on Earth. 3-D spherical Earth models that combine an asthenosphere and a plastic yield stress to allow localised weakening of the cold upper thermal boundary layer result in a distinctly plate tectonic style of convection (Richards et al., 2001).
Morgan and colleagues (Morgan and Smith, 1992b; Morgan et al., 1995b) linked the asthenosphere to mantle plumes, proposing an asthenosphere fed actively by hot upwellings. This and their subsequent work (Yamamoto et al., 2007a,b) explored the resulting upper mantle flow in terms of a simple model, where material flux is driven horizontally by lateral pressure variations, in order to explain various observations related to ocean bathymetry, heat flow, and mantle geochemistry. A series of papers by (Höink and Lenardic, 2008, 2010; Höink et al., 2011; Höink et al., 2012) extended this approach. They formulated mantle convection models explicitly in the context of so-called Poiseuille/Couette flow (see Fig. 3.1). An important finding is that lateral pressure variations in the asthenosphere are not tied exclusively to the influx of plume material, but occur also for convection heated purely from within. Poiseuille/Couette flow is thus an intrinsic property of material flowing in a low viscosity asthenosphere channel beneath mobile tectonic plates.

Asthenosphere flow driven by high- and low-pressure regions is a powerful concept, because it connects mantle flow to geologic observations in a testable manner. In particular, it explicitly

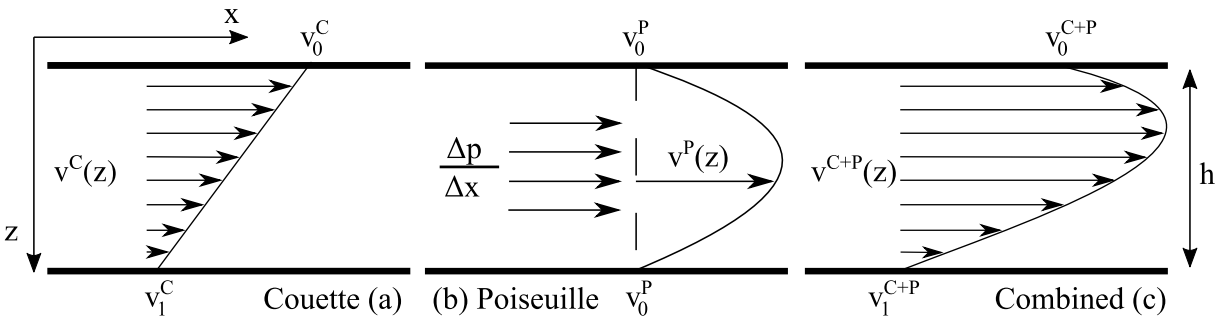

Figure 3.1: Schematic representation of **(a)** Couette flow, described a linear profile of shear driven fluid motion between two surfaces where one moves tangentially relative to the other, and seen as proxy for passive asthenosphere flow driven by motion of the overlying plate, **(b)** Poiseuille flow, described by a parabolic profile, driven by a lateral pressure gradient, and seen as proxy for active asthenosphere flow capable of driving the overlying plate, and **(c)** superposition of both.

relates temporal changes in horizontal plate motion, i.e. oceanic spreading rate variations driven by evolving basal shear stresses, to nonisostatic vertical motion of the lithosphere. The latter is a form of topography maintained dynamically by mantle convection. It was termed 'dynamic topography' by Hager et al. (1985) more than 30 years ago (e.g., Braun, 2010, for a review).
Current plate motions are well mapped (DeMets et al., 2010). But histories of plate motion are becoming better known. Initially documented for the Cenozoic (Gordon and Jurdy, 1986), global plate motion reconstructions are now available for times going back to the Mesozoic (e.g., Müller et al., 2016, for a review). Progress is also underway in mapping the magnetization of some ocean floor regions in great detail, permitting plate motion reconstructions at temporal resolutions of $\sim$1 million years (Myrs) or less (e.g., Merkouriev and DeMets, 2014; DeMets and Merkouriev, 2019) when mitigating for finite-rotation noise Iaffaldano et al. (2012). These efforts reveal that it often takes but a few Myrs for plates to change their motions. The variations may be due to changes in plate boundary forces (Iaffaldano and Bunge, 2009) and/or basal shear stresses (Colli et al., 2014). They provide important observations for geodynamic interpretations (e.g., Iaffaldano and Bunge, 2015, for a review).
Less is known about current dynamic topography, at least outside the oceanic realm (Hoggard et al., 2017). Dynamic topography for continents is difficult to map, because one needs to separate it from topography in isostatic support (Fishwick and Bastow, 2011; Ravenna et al., 2018). But histories of dynamic topography in the continents are beginning to emerge, because the transient nature of dynamic topography leaves geologic evidence in sedimentary archives (Ernst and Buchan, 2001). This approach was pioneered for regions that underwent periods of low dynamic topography, such as the *Cretaceous Interior Seaway* of North America (e.g., Mitrovica et al., 1989; Burgess et al., 1997), where the associated surface depressions created accommodation space to preserve sediments.
It is more difficult to map the stratigraphic expression of dynamic topography highs. The associated elevated topography creates erosional/non-depositional environments expressed as time gaps in the geologic record. The resulting discontinuity surfaces in sedimentary archives are known as non conformities and unconformities (see Miall, 2016, for a review). They preserve time missing (hiatus) from the geological record (Friedrich et al., 2018). To this end, an approach of hiatus-area mapping was introduced Friedrich et al. (2018) and Friedrich (2019). It visualises interregional-scale unconformities because, at continental scales, what is normally perceived as a lack of data (material eroded or not deposited) becomes part of the dynamic topography signal. The method has been applied to map the spatiotemporal patterns of conformable and unconformable geological contacts across Europe (Vibe et al., 2018), Africa (Carena et al., 2019) and the Atlantic realm and Australia since the Upper Jurassic (Hayek et al., 2020, 2021). An important finding is that significant differences exist in the spatial extent of hiatus area across and between continents at the timescale of geologic series, that is ten to a few tens of Myrs (see definition of series as a unit of chronostratigraphy in the chronostratigraphic chart (Cohen et al., 2013; updated.; Ogg et al., 2016)). This is considerably smaller than the mantle transit time, which as the convective timescale, is about 100–200 Myrs (Iaffaldano and Bunge, 2015) for Earth's mantle. The difference between the convective timescale and the timescale for topography in convective support suggests vigorous upper mantle flow, as illustrated by geodynamic kernels (see Colli et al., 2016, for a review)).

Pressure driven asthenosphere flow explicitly relates plate motion changes, induced by evolving basal shear forces, to nonisostatic vertical motion of the lithosphere, as noted before. Such correlations were reported for the South (Colli et al., 2014) and North (Vibe et al., 2018) Atlantic. Here we extend this observational geodynamic approach. We take the hiatus maps of Hayek et al. (2020, 2021), with an updated dataset for Australia following the approach of Carena et al. (2019), as proxy for mantle flow induced vertical lithosphere motion and compare them systematically to horizontal plate motion variations deduced from a past plate motion model based on the dataset of Müller et al. (2016). We organise our paper as follows: sections 2 and 3 provide brief summaries of plate motion variations and hiatus surfaces for the Atlantic and Indo-Australian realm. We study these regions to account for ocean basins with and without significant subduction activity, while our choice of the Upper Jurassic as the starting point of our analysis is motivated by geodynamic considerations on the mantle transit time, to remain within a timescale comparable to a mantle overturn (Iaffaldano and Bunge, 2015). We then compare spreading rate variations and hiatus surfaces, finding they frequently correlate, except when plate boundary forces may play a significant role. Section 5 places our results into the context of geological studies. This is followed by a discussion on geodynamic implications, where we employ Poiseuille/Couette models for scale analysis. Finally, we draw conclusions in section 6.

3.2 Oceanic Spreading Rates

Figure 3.2 presents the spreading rates of the seafloor at the time of crustal creation as a data grid from Seton et al. (2020) based on the GTS2012 (Ogg, 2012) timescale (see Clark, 2018) for a discussion of the influence of the timescale choices for the uncertainty of reconstructed spreading histories). We also superpose profiles of relative spreading rates throughout the Atlantic, the Indian and the Southern Ocean south of Australia, extracted with *pyGPlates* (Müller et al., 2018a) from the latest dataset of Müller et al. (2019), to bring out local spreading rate variations. Most of the inset spreading rate profiles are reported for the time from 80 Ma onward, whereas profiles in the oldest ocean floor regions, such as the Central Atlantic and Madagascar, are shown from earlier times onward. The Cretaceous Normal Superchron (CNS) restricts the temporal resolution of Cretaceous spreading rates to mean values (Seton et al., 2012; Müller et al., 2016), therefore we omit the report of spreading rates spanning this time period.
Overall, Fig. 3.2 reveals that rapid spreading rate variations (less than 10 Myrs) occurred throughout the oceans, with spreading rates in the South Atlantic and the Antarctica-Australia spreading centre ($\sim$6 cm/yr) being faster compared to rates in the North Atlantic ($\sim$2 cm/yr). The inset profiles from north to south for the Atlantic show distinct temporal variations. The North Atlantic rates have a noticeable peak of $\sim$4 cm/yr in the early Eocene from $\sim$55-45 Ma that follows the onset of spreading in the region. They drop to $\sim$2 cm/yr in the last 45 Ma. The South Atlantic is characterised by higher rates and larger variations. At 80 Ma, near the end of the CNS, nominal rates are $\sim$6 cm/yr. In the Paleocene, from $\sim$65-55 Ma, they drop by a factor of three to $\sim$2 cm/yr, followed by a renewed increase up to a peak of $\sim$6 cm/yr at $\sim$30 Ma. From $\sim$25 Ma onward, rates decrease to $\sim$4 cm/yr. The Central Atlantic is a superposition of trends from the south, i.e. slow rates in the Paleocene ($\sim$3 cm/yr) around 60 Ma, and from

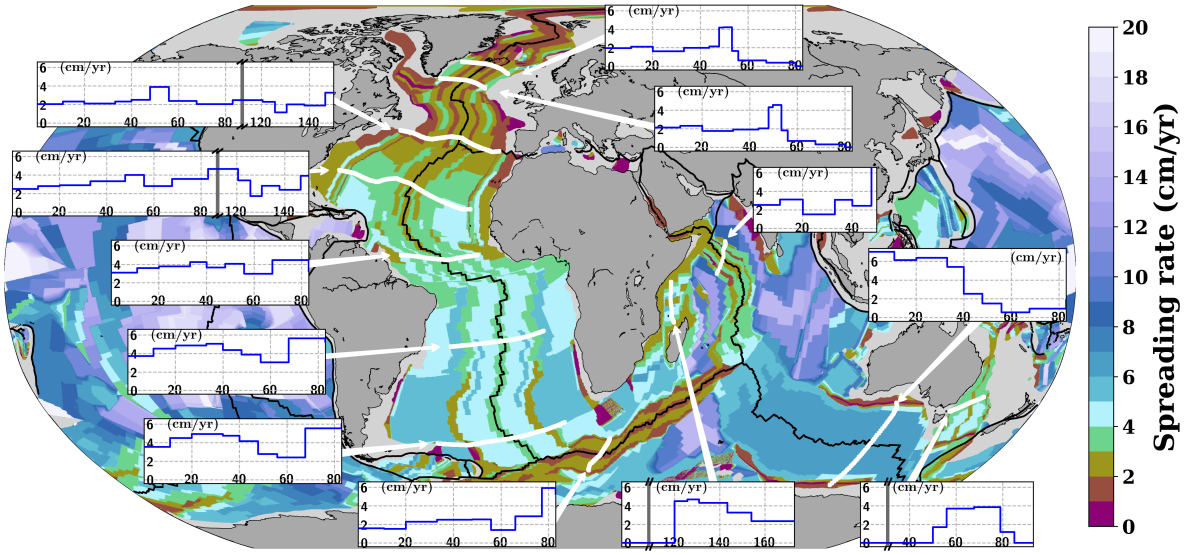

Figure 3.2: Grid of ocean floor spreading rates reproduced from Seton et al. (2020) based on GTS2012 (Ogg, 2012) timescale. Colours indicate spreading rates at time of crustal creation, revealing frequent spreading rate changes throughout the oceans. Inset figures, where y-axis is spreading rate in cm/yr and x-axis time in Ma, show rates at selected locations. Grey vertical lines in the inset plots for the Central Atlantic correspond to the Cretaceous Normal Superchron (CNS), when spreading rates are known only at mean rates across the CNS (see text). For the Indian ocean they represent omitted time. Profiles extracted from (Müller et al., 2019) database using *pyGPlates* (Müller et al., 2018a).

the north, i.e. a peak in the early Eocene at ∼50 Ma (∼4 cm/yr). The spreading rate profile between India and Africa in the Indian ocean shows two peaks of ∼3 cm/yr each. One lasts from ∼40-35 Ma, the other from ∼20-10 Ma, separated by a minimum of ∼1.5 cm/yr from ∼35-20 Ma. Prior to 45 Ma, spreading velocities are significantly higher (∼14 cm/yr). The Lord Howe Rise profile (east of Australia) shows high spreading rates (∼4 cm/yr) from ∼80-60 Ma decreasing to zero by ∼50 Ma. Conversely, spreading rates in the Southern Ocean south of Australia are near zero (∼0.5 cm/yr) from 80-60 Ma, increasing from the Paleocene onwards to spreading rates of ∼6 cm/yr.

3.3 Continental Base Hiatus Surfaces (BHS)

Figure 3.3 shows Base Hiatus Surfaces (BHS) taken from Hayek et al. (2020, 2021) for North and South America, Europe, Africa and Australia for eight geologic series beginning with the Lower Cretaceous. The resolution of geological series is chosen, because this is the most frequently adopted temporal resolution for interregional geologic maps (Friedrich, 2019). The choice of the Lower Cretaceous as the oldest stratigraphic unit represents the mantle transit time (Iaffaldano and Bunge, 2015), as noted before. We use the terms *un/conformable* and *hiatus/no hiatus* indistinguishably and follow Friedrich (2019), Carena et al. (2019) and Hayek et al. (2020). They define *hiatus/unconformable* as the state when one or more geological series in the chronostratigraphic chart Cohen et al. (2013; updated.); Ogg et al. (2016) immediately preceding the target geological series are missing, regardless of whether either geological series has missing stages. *No hiatus/conformable* is defined as the complementary state. Hiatus

is delimited for a given target geological series by any occurrence of the immediately preceding geological series. From hiatus mapped this way, Hayek et al. (2020, 2021) construct BHS

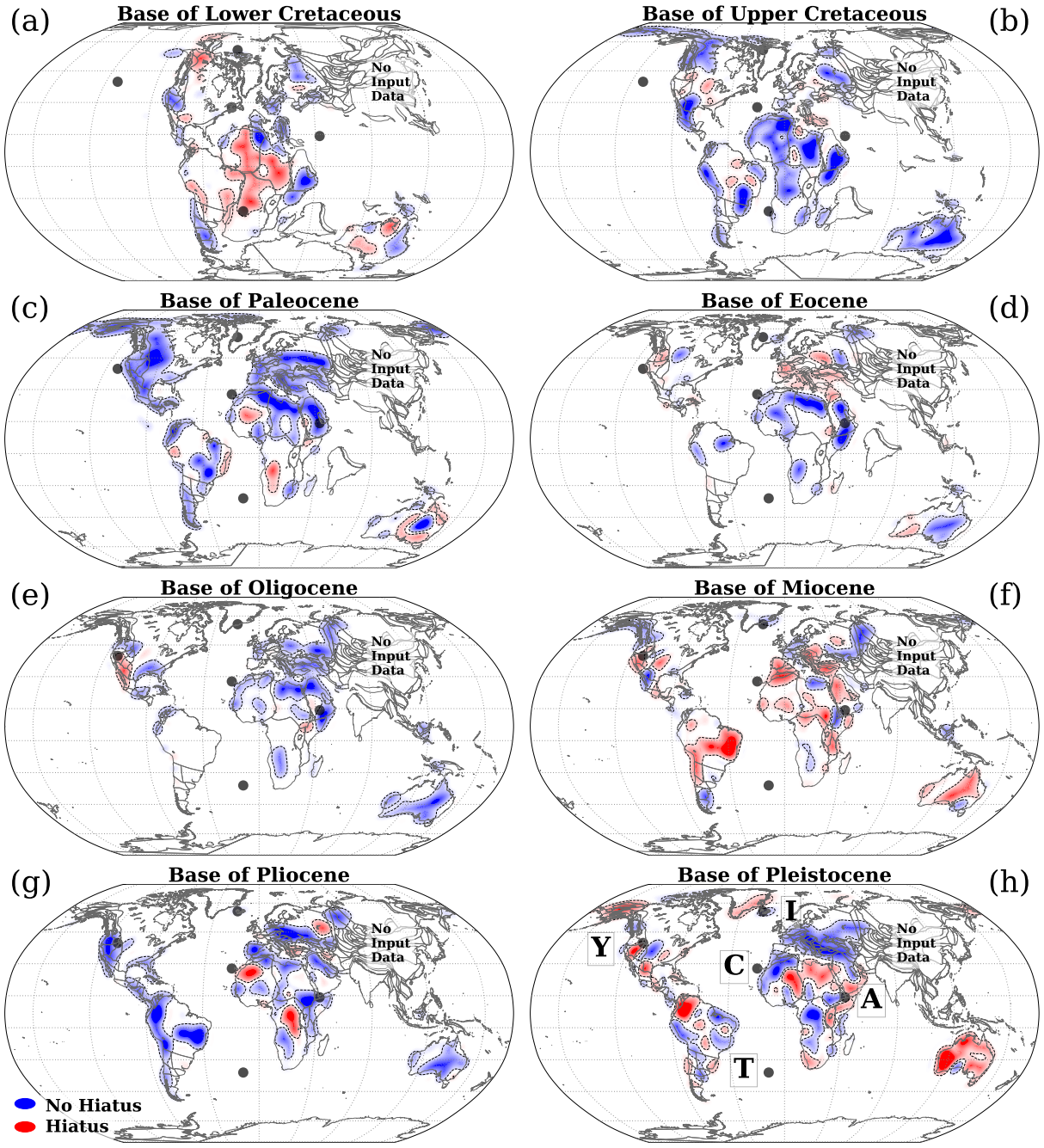

Figure 3.3: Base Hiatus Surfaces (BHS) from Hayek et al. (2020, 2021) for eight geological series from Base of Lower Cretaceous to Base of Pleistocene **(a)**-**(h)** reconstructed paleogeographically with a global Mesozoic-Cenozoic plate motion model (Müller et al., 2016) tied to a reference frame of global moving hotspot and a True Polar Wander (TPW) corrected paleomagnetic reconstruction (Torsvik et al., 2008), with the latter updated by Seton et al. (2012) (see text), and placed into a plate tectonic configuration corresponding to the base of each geological series. Red/blue colours represent the hiatus/no hiatus surfaces. Black dotted lines contour the spherical harmonics signal at the ± 0.1 amplitude. Each map serves as a proxy for paleotopography (red=high, blue=low) in the preceding series (see text). Black dots are current locations of Yellowstone (Y), Canaries (C), Afar (A), Iceland (I), Tristan (T) hotspot (Courtillot et al., 2003).

through a spherical harmonic representation (up to degree 15 and convolved with a Gaussian filter), reconstructed to their past tectonic setting with a global Mesozoic-Cenozoic plate motion model (Müller et al., 2016) tied to a global moving hotspot reference frame (Torsvik et al., 2008) from present-day to 100 Ma and a True Polar Wander (TPW) corrected paleomagnetic reconstruction (Steinberger and Torsvik, 2008) for times older than 100 Ma. The latter includes a longitudinal shift of 10° incorporated by Seton et al. (2012). The surfaces are presented in the plate configuration that corresponds to the base of each geological series.

BHS serves as a proxy for paleotopography and vertical motion of the continents, as suggested by Friedrich et al. (2018) and earlier authors (e.g., Levorsen, 1933). Red/blue colours depict un/conformable (hiatus/no hiatus) contacts, respectively, indicative of high/low topography in the preceding geological series. Blank regions reveal the absence of the target geological series and its immediately preceding unit. Such regions may have undergone intense and/or long-lasting erosion or non-deposition, indicative of intense and/or persistent exhumation and surface uplift (Friedrich et al., 2018; Friedrich, 2019; Vibe et al., 2018; Carena et al., 2019; Hayek et al., 2020, 2021). Black dots in each BHS figure mark the current location of the Yellowstone, Canaries, Afar, Iceland and Tristan hotspots (Courtillot et al., 2003). A detailed presentation of the data sources, the BHS construction, and the related uncertainties are given in Hayek et al. (2020).

Overall Fig. 3.3 reveals significant differences in hiatus distribution across and between continents at the timescale of geologic series. Described in detail in Hayek et al. (2020, 2021), we summarise the main BHS features and recall that BHS at each geological series serves as proxy for topography in the preceding geological series. **Base of Lower Cretaceous**, Fig. 3.3(a), shows hiatus surface (red) and blank regions, indicative of high topography in the Upper Jurassic, in much of North and South America, Africa and Australia. No hiatus (blue), indicative of low Upper Jurassic topography, is prominent in northernmost Africa and Europe. **Base of Upper Cretaceous**, Fig. 3.3(b), shows hiatus and blank regions in parts of Europe, North and South America. No hiatus is prominent throughout much of Africa, Australia, and South America in the Paraná region. **Base of Paleocene**, Fig. 3.3(c), reveals isolated patches of hiatus surface and blank regions along the east coast of Brazil, in Southern Africa (Karoo Basin) and Australia. No hiatus regions dominate elsewhere throughout the continents. **Base of Eocene**, Fig. 3.3(d), presents hiatus surface and blank regions prominently in two continents: Europe, and South America except the Amazon Basin. No hiatus exists in the northernmost part of Africa, the Karoo Basin, and eastern Australia. **Base of Oligocene**, Fig. 3.3(e), displays blank regions in Africa. But the foremost occurrence is in South America, where it signals an almost complete absence of Oligocene and Eocene strata throughout the continent. Limited hiatus surface exists in the western part of North America and the Afar region. Europe, northernmost Africa, the Karoo Basin and much of Australia show prominent no hiatus regions. In **Base of Miocene**, Fig. 3.3(f), hiatus surfaces dominate across the continents. Prominent examples include North and South America, parts of Europe, Australia and Africa. North America shows conformable contacts surrounding the hiatus regions near the Yellowstone hotspot location. Alaska, Patagonia and Central Europe also show conformable contacts. **Base of Pliocene**, Fig. 3.3(g), reveals minor hiatus surface and blank regions. Hiatus is located in central Africa and near the Canaries. Blank regions occur in eastern North and South America. No hiatus signals dominate

elsewhere. **Base of Pleistocene**, Fig. 3.3(h), shows North and South America and Africa with a mix of hiatus and no hiatus surfaces. Extensive hiatus surface exists in Australia, except the *Nullarbor Plain*, Alaska, the eastern margin of Greenland, and north-central Africa. No hiatus surface prevails in Europe and the Congo Basin.

Figure 3.4 shows BHS with a view centred on North America, to illuminate a continent moving towards a hotspot. Much of the eastern half of the continent reveals blank regions, reflecting the absence of Lower Cretaceous to Pleistocene series. But, in the western half of the continent, the hiatus surface changes at interregional scales while North America approaches the current location of the Yellowstone hotspot. A prominent change occurs from the **Base of Paleocene** to **Base of Eocene**, when an extensive no hiatus signal transforms to mostly blank regions and hiatus, indicative of growing topography. From the **Base of Eocene** to **Base of Miocene** hiatus signal surrounds the current location of Yellowstone, starting with hiatus to the northeast of the current plume location and leading to hiatus located in the Columbia Plateau regions and the Interior Plains, as noticed also by Friedrich et al. (2018) and Stotz et al. (2021b).

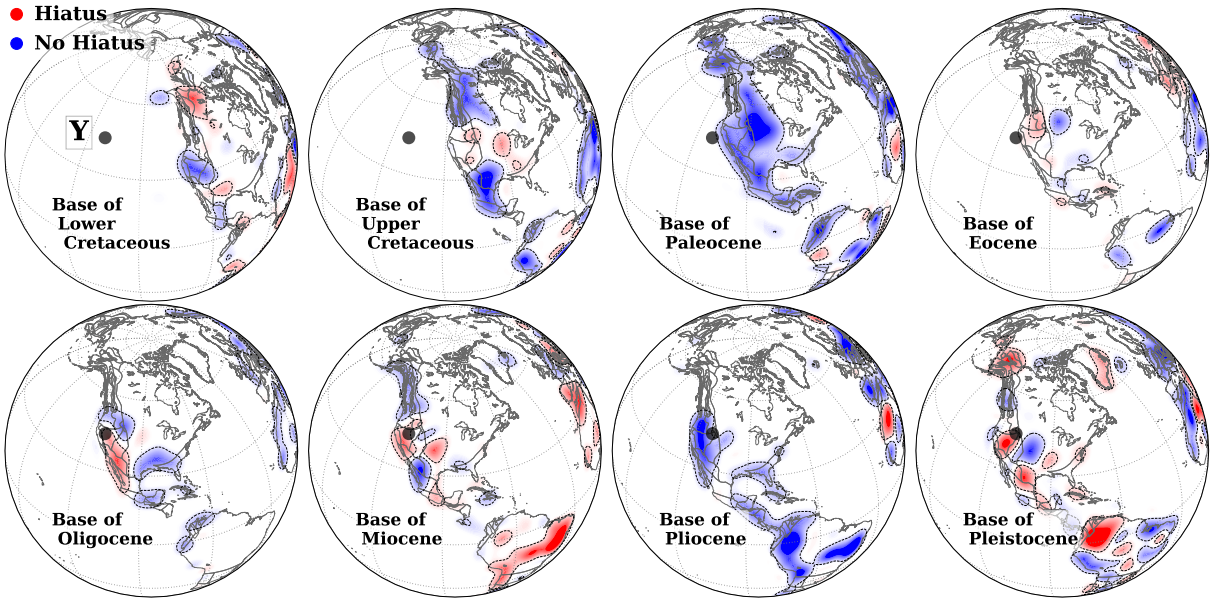

Figure 3.4: Same as Fig. 3.3, but centred on North America. Each BHS map serves as a proxy for paleotopography (red=high, blue=low) in the preceding geological series (see text). Black dot is current Yellowstone (Y) hotspot location (Courtillot et al., 2003). From the Base of Eocene to Base of Miocene hiatus signal surrounds the current location of Yellowstone.

3.4 Oceanic Spreading Rates & Continental Base Hiatus Surfaces

3.4.1 Atlantic Realm

Figure 3.5 (top row) shows BHS with a view focused on the North Atlantic/Europe. There are two periods of widespread hiatus in Europe, in the Paleocene and the Oligocene, revealed by

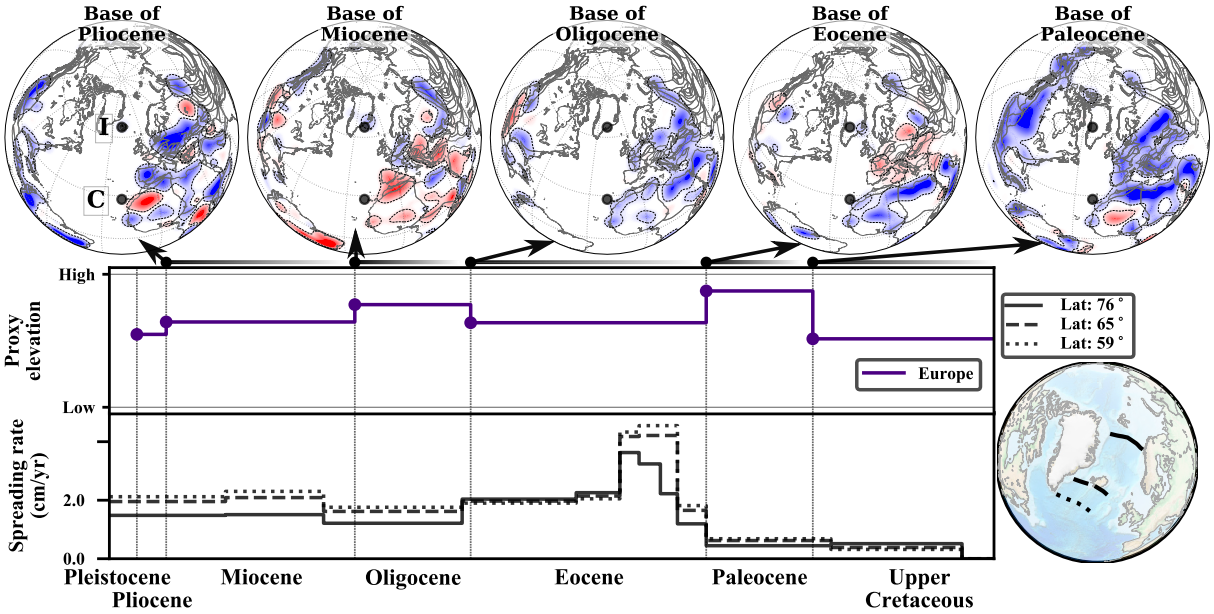

Figure 3.5: Top row shows BHS centred on the North Atlantic from Base of Pleistocene to Base of Paleocene (see Fig. 3.3 caption), with black dots showing the current hotspot locations of Iceland (I) and Canaries (C) (Courtillot et al., 2003). Middle row shows proxy elevation obtained by the sum of hiatus surfaces and blank regions (see text) for a given geological series normalised by the total area under consideration (Europe). Bottom row shows spreading rates for three transects as indicated in bottom right globe. X-axis shows the time range from Pleistocene to Mid Upper Cretaceous. The BHS show prominent hiatus surfaces at the Base of Eocene and Base of Miocene, reflected also as high proxy elevation for the Paleocene and Oligocene. The two proxy elevation peaks are followed by two periods of elevated spreading velocity in the early Eocene and early Miocene.

hiatus surface at the **Base of Eocene** and **Base of Miocene**, respectively. This is illustrated by a curve (middle row) for proxy elevation, which we construct as the sum (for a given geological series) of hiatus and blank regions, normalised by the total area (Europe) under consideration. The bottom row plots oceanic spreading rates at three transects, north to south, between Greenland and Europe from the beginning of the Upper Cretaceous onward. The spreading rate magnitude increases, as expected, with decreasing latitude and further distance of the transects from the Euler Pole. Importantly, the transects reveal two periods of higher spreading rates: a 10 Myrs peak in the early Eocene and a second increase in the early Miocene. The latter is more pronounced in the two southern profiles. These observations were noted by Vibe et al. (2018).

Figure 3.6a (top row) displays BHS with a view focused on the South Atlantic. Two periods of widespread hiatus exist for much of Africa and South America, in the Upper Jurassic and the Oligocene, revealed by hiatus surface at the **Base of Lower Cretaceous** and **Base of Miocene**. There are also two periods of prominent blank region (absence of the considered geological series and its immediately preceding unit) for both continents at the **Base of Eocene** and **Base of Oligocene**. That means the maps show neither Paleocene, nor Eocene and Oligocene strata in much of Africa and South America. In the southern half of Africa blank regions also dominate the **Base of Paleocene**. The proxy elevation curves for Africa and eastern South America, Fig. 3.6a (top part of the two middle rows) normalised to the area of Africa and eastern South America, respectively, bring this out. They show elevated Jurassic topography for both continents, followed by lower topography in the Cretaceous. The African curve increases in the

Upper Cretaceous, due to growing proxy elevation in the southern part of the continent, followed by a pronounced continent-scale Oligocene increase. The South American curve instead increases markedly in the Paleocene, and reaches an Eocene peak value. Africa is a large con-

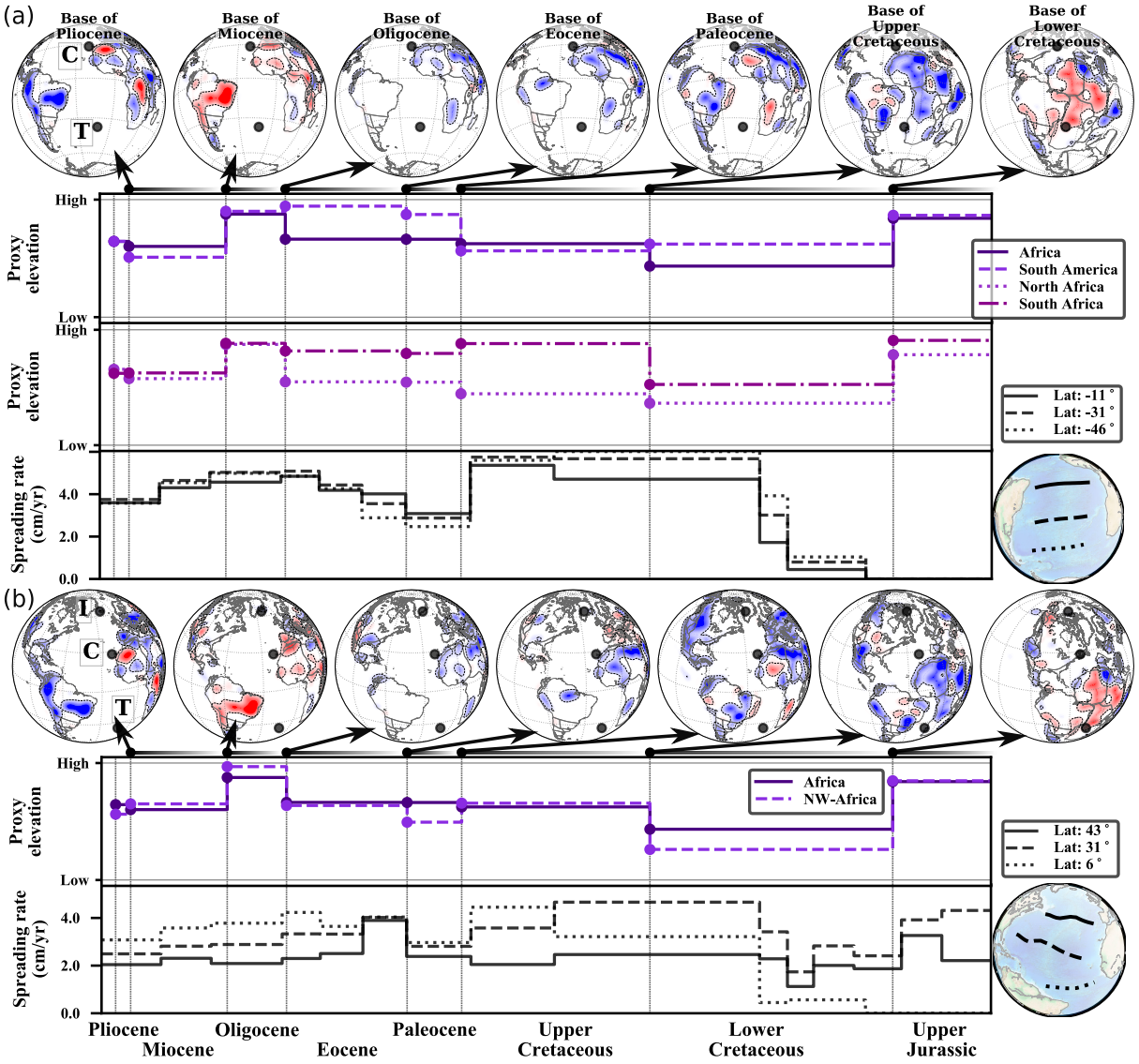

Figure 3.6: **(a)** Same as Fig. 3.5 with top row showing BHS with a view centred on the South Atlantic from Base of Pleistocene to Base of Upper Cretaceous. Black dots represent current hotspot locations of Canaries (C) and Tristan (T) (Courtillot et al., 2003). Middle rows show proxy elevation curves (see text) for Africa and South America (top) and northern and southern Africa (bottom) from Pleistocene to Lower Cretaceous (see text). Bottom row shows spreading rates for three transects as indicated in bottom right globe. Elevated Jurassic proxy elevation for Africa and South America precedes the spreading onset in the Lower Cretaceous. An increase in Upper Cretaceous African proxy elevation that owes to growing elevation in the southern part of the continent (see southern Africa proxy elevation curve) goes along with high Cretaceous spreading rates (see text). A Paleocene increase in South American proxy elevation precedes elevated Eocene spreading rates (see text). **(b)** Same as (a) for the Central Atlantic. Black dots in the BHS represent current hotspot locations of Iceland (I), Canaries (C) and Tristan (T) (Courtillot et al., 2003). Middle row shows proxy elevation curves for Africa and its northwestern portion (see text), while bottom row shows three spreading rate transects as indicated by bottom right globe. The northern/southern spreading rate profiles resemble the history of the North/South Altantic respectively (see text).

tinent, and likely responds to different dynamic topography domains due to its size (see Hayek et al., 2020, 2021; Carena et al., 2019, for a discussion). To this end, we bring out the different topographic evolution of northern and southern Africa by two proxy elevation curves (lower part of the two middle rows) that are constructed for the northern (plate IDs 714,715,503 from the Matthews et al. (2016) dataset) and southern portions (plate IDs 701,709,712,713 (Matthews et al., 2016)) of the continent, respectively. The curves show a noticeable increase of Upper Cretaceous proxy elevation for southern Africa. Figure 3.6a (bottom row) reports three spreading rate transects for the South Atlantic. Spreading rates are elevated for much of the Cretaceous and the Eocene to mid Miocene, separated by lower spreading rates in the Paleocene. These observations were noted by Colli et al. (2014). Figure 3.6b (top row) depicts BHS with a view centred on the Central Atlantic and northwest Africa. The maps show two hiatus periods, in the Jurassic and the Oligocene, indicated by hiatus surface at the **Base of Lower Cretaceous** and **Base of Miocene**. Two proxy elevation curves, constructed for all of Africa or only for its northwestern sub-region (plate ID 714 (Matthews et al., 2016)), are plotted in Fig. 3.6b (middle row). Both curves are similar. But the lower value for proxy elevation in the Lower Cretaceous and the peak in proxy elevation for the Oligocene is more pronounced in the northwestern sub-region. Figure 3.6b (bottom row) displays spreading rates for three Central Atlantic transects. They differ from each other in that the northernmost/southernmost transect resembles the spreading rate history of the North/South Atlantic, respectively. For instance, a spreading rate increase in the Lower Cretaceous relates to the South Atlantic transect, while a peak in the early Eocene resembles the spreading rates of the North Atlantic.

3.4.2 Indo-Australian Realm

Figure 3.7 (top row) shows BHS with a view focused on Australia. Extensive conformable area exists at the **Base of Upper Cretaceous**, indicative of low topography in the Lower Cretaceous. Hiatus and blank regions, apart from the Eromanga basin, dominate the **Base of Paleocene**, indicative of overall higher Upper Cretaceous topography. A distinct difference between western and eastern Australia emerges at the **Base of Eocene**, when hiatus/no hiatus surface dominates the western/eastern portion of the continent, respectively. The difference continues at the **Base of Oligocene**, with blank surface in much of northwestern Australia and no hiatus elsewhere. There is a near continent-wide hiatus surface at the **Base of Miocene**, followed by extensive no hiatus at the **Base of Pliocene**. Proxy elevation curves, Fig. 3.7 (middle row), for the entire continent or separated for eastern and western Australia (the separation corresponds to the Western Australia state border, west of 129° present-day longitude) bring these observations out. The continent as a whole experiences an overall proxy elevation increase from the Lower to the Upper Cretaceous and an Oligocene peak value. But there is a marked difference for the eastern and western Australia proxy elevation curves in the Paleocene. The former decreases, the latter increases relative to the Upper Cretaceous. We plot spreading rate transects for the Antarctic-Australia ridge and the Lord Howe Rise in the bottom row of Fig. 3.7. The Lord Howe Rise was active to the Southeast of Australia from the middle of the Upper Cretaceous onwards, with velocities of $\sim$4 cm/yr. It ceased spreading in the early Eocene, when motion initiated along the Antarctica-Australia ridge. From then on Antarctica-Australia spreading rates

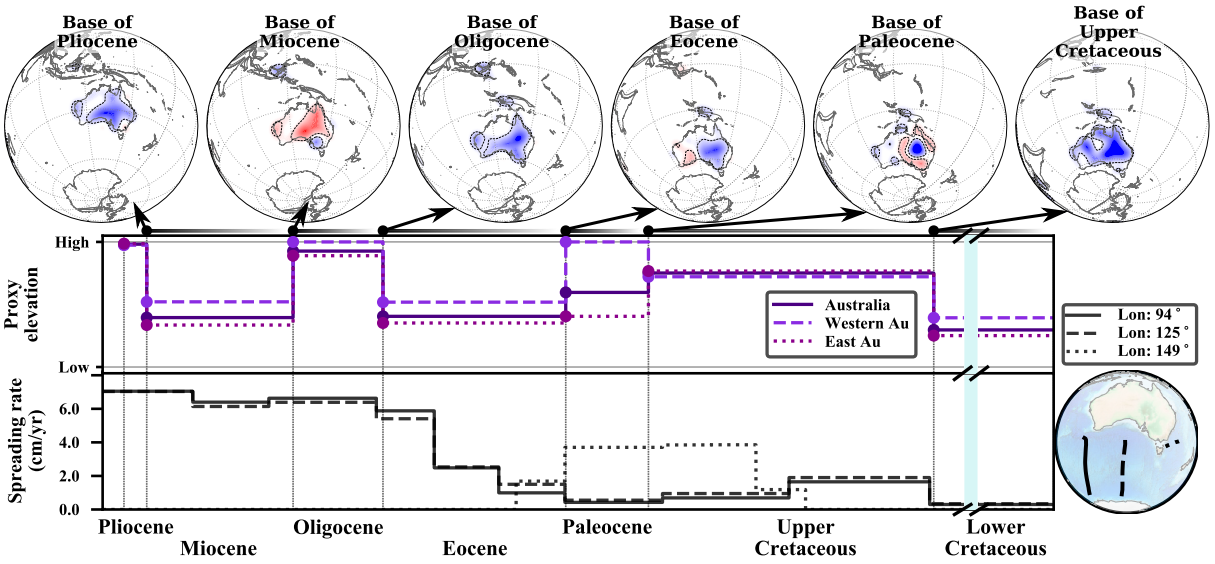

Figure 3.7: Same as Fig. 3.5 with view centred on Australia. Top row shows BHS (see text). Middle row shows proxy elevation curve for the entire continent or separated for eastern and western Australia (see text). Bottom row shows spreading rates for three transects as indicated in bottom right globe. Blue vertical line in the Lower Cretaceous represents a time-lapse omission. Elevated Upper Cretaceous proxy elevation goes along with spreading of Lord Howe Rise (dotted curve), whereas elevated western Australia proxy elevation in the Paleocene precedes rapid Eocene spreading between Antarctica and Australia (see text).

increased significantly, reaching ∼6 cm/yr by the Oligocene.

The top row of Fig. 3.8 displays BHS with a view centred on East Africa, from the **Base of Oligocene** onward. This links to the rise of the Afar plume, for which domal uplift, indicated as well in our maps, has been documented after the early Eocene (Şengör, 2001). Even though the main hiatus surface occurs at the **Base of Miocene**, there is another hiatus at the **Base of Pleistocene**. Proxy elevation curves, Fig. 3.8 (middle row), for all of Africa or its northeast subregion (plate IDs 709, 710, 712, 713, 715, 503 from the Matthews et al. (2016) dataset) bring this out. The Pliocene increase is more pronounced in the regional proxy elevation curve of East Africa compared to the curve for all of Africa. Figure 3.8 (bottom row) plots two spreading rate transects for the Carlsberg Ridge since the Upper Cretaceous. They show minor spreading rate variations from the mid-Eocene onwards.

3.5 Discussion

It is a geodynamic tenet that plates organise the flow and that they are an integral part of the convective system (see Davies and Richards, 1992, for a review). Yet the precise nature of how plate motions are caused by mantle convection remains incomplete, because the strength of plates conceals the underlying flow. The description by Morgan et al. (1995b) and Höink and Lenardic (2008, 2010); Höink et al. (2011); Höink et al. (2012) of asthenosphere flux in terms of Poiseuille/Couette flow offers a way to overcome this difficulty by mapping upper mantle flow through its topographic and viscous effects. This geodynamic perspective motivates us to compare changes of oceanic spreading rates and continental hiatus surface, by building upon

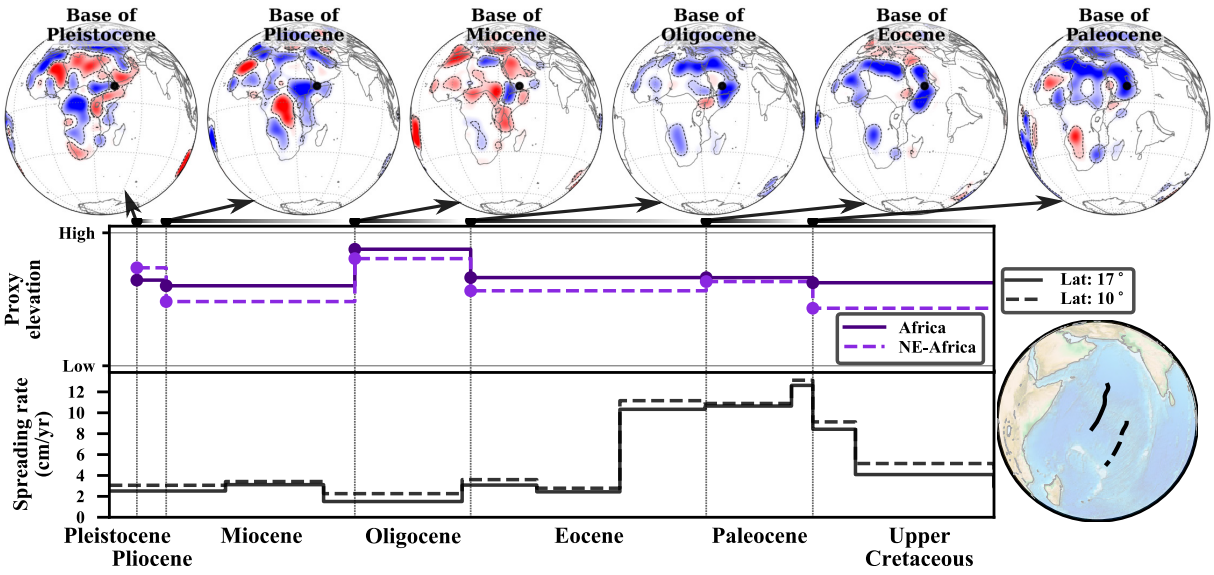

Figure 3.8: Same as Fig. 3.5 with view centred on Eastern Africa. Top row shows BHS (see text) with black dot representing the current hotspot location of Afar (A) (Courtillot et al., 2003). Middle row shows proxy elevation curve for the entire continent or its northeast subregion (see text). Bottom row shows spreading rates for two transects as indicated in bottom right globe. Growing East Africa proxy elevation in Paleocene-Oligocene and decreasing Carlsberg spreading rates, presumably reflect plate boundary forces from India-Asia Collision (see text).

earlier work and exploiting growing observational constraints on both.

A link between spreading rate variations and dynamic topography is perhaps best evinced for the North Atlantic (see Fig. 3.5), where two periods of expanding hiatus surface across Europe in the Paleocene and Oligocene precede the Eocene spreading onset and faster Miocene spreading rates, as noted by Vibe et al. (2018). The region is well suited for an observational geodynamic analysis. Its Cenozoic opening history has left well-preserved sea-floor magnetic lineations (e.g., Pitman et al., 1971; Gaina et al., 2002) and hiatus surfaces. There are also well-documented regional uplift episodes reported, for instance, for the British Isles, Greenland, Scandinavia and Central Europe (e.g., Hillis et al., 2008; Japsen et al., 2005; Riis, 1996; von Eynatten et al., 2021). Reviews of uplift and subsidence events across the region are given by various authors (Japsen and Chalmers, 2000; Stoker and Shannon, 2005; Anell et al., 2009). The region also contains prominent plume systems. They provide a geodynamically plausible mechanism to drive active upper mantle flow, as suggested by scaling analysis (Höink et al., 2011). Plume systems at the western edge of Europe include the Canaries, which experienced Oligo/Miocene uplift at the local (Meco et al., 2007) and regional scale (Sehrt et al., 2018), and the Iceland-Jan Mayen system. The broad extent of the latter was imaged seismically by Rickers et al. (2013) and Celli et al. (2021). Importantly, studies of the Iceland-Jan Mayen system reveal temporal mass flux (Poore et al., 2009) and thermal anomaly (Spice et al., 2016) variations, with peaks in the early and late Cenozoic. Our results support these accounts of temporal system variations and indicate their interregional scale, documenting early Paleogene and Neogene changes in dynamic topography and spreading rates, induced presumably through variations in pressure driven upper mantle flow.

The opening history of the South Atlantic realm, which hosts the Tristan hotspot, spans nearly

three times that of the North Atlantic, reaching back into the Mesozoic. But links between spreading rates and dynamic topography are more difficult to establish, because the early South Atlantic opening falls largely within the CNS, restricting the interpretation of Cretaceous spreading rates to mean values, and because the long duration of the Lower/Upper Cretaceous series (∼40 Myrs each) limits the temporal resolution of our geological series-based hiatus mapping during that time. The main observation is a bimodal spreading rate distribution, with Cretaceous and mid-Cenozoic peaks separated by a Paleocene low, as seen in our results and pointed out by Colli et al. (2014). This goes along with high Upper Jurassic proxy elevation for Africa and South America, and renewed proxy elevation for southern Africa in the Upper Cretaceous and for South America starting in the Paleocene. But observations beyond this first order division are beginning to emerge. For the phase preceding the South Atlantic opening, Krob et al. (2020b) use geological archives (stratigraphic and thermochronological data) and stratigraphic frameworks to document interregional-scale Upper Jurassic uplift in South America and Africa, which they link to the Paraná-Etendeka plume rise well in advance of flood basalt eruptions and the onset of seafloor spreading. For the CNS, and using a new identification of magnetic anomalies located within that time period, Granot and Dyment (2015) report accelerating rather than constant South Atlantic spreading rates, with a peak achieved in the early Campanian (∼80 Ma). This goes along with increasing Upper Cretaceous proxy elevation in southern Africa (Fig. 3.6a) and a growing consensus about the uplift history of the South African Plateau (SAP). Reports on the latter assign Upper Cretaceous ages to peak sediment flux (e.g., Guillocheau et al., 2012; Said et al., 2015b; Baby et al., 2020) around the SAP, increased kimberlite occurrence in southern Africa (Jelsma et al., 2009), and basin inversion and margin tilting along the Namibian coast (Paton et al., 2008; Dressel et al., 2016), consistent with a Late Cretaceous SAP uplift pulse inferred from thermochronological studies (Stanley et al., 2015; Green et al., 2015). No major coeval activity is indicated for the Tristan hotspot. But the ∼85 Ma eruption of the Marion hotspot (Storey et al., 1995; Torsvik et al., 1998) occurs at a geodynamically relevant distance (∼2000 km east of southern Africa) addressed in the next section. The Tertiary phase of the South Atlantic opening has accelerated spreading rates starting in the Eocene, preceded by growing South American proxy elevation (Fig. 3.6a) in the Paleocene. The interregional scale of this event is evinced by a variety of studies. They document a Paleogene hiatus in Andean Foreland Basins (Horton, 2018), regional uplift along the Argentine margin (Autin et al., 2013), and an Eocene reactivation of the South American passive margin (e.g., Japsen et al., 2012; Krob et al., 2019; Kollenz et al., 2017) deduced from landscape analysis and thermochronological data. Far field effects from plate boundary forces associated with the Andean margin (Japsen et al., 2012) have been invoked to explain these events. But most studies agree that prominent uplift of the Andes started in the mid Eocene, reaching a peak in the Oligocene, with a second uplift period in Late Miocene (Sempere et al., 2008b). It is not obvious, how increased topographic loads from the Andes would induce faster South Atlantic spreading. Instead, there are reports for anomalously young (late-stage) volcanism (≈46 Ma) on the Rio Grande Rise (RGR) and an Eocene subaerial exposure of the RGR at Drill Site 516 (Rohde et al., 2013; Barker, 1983). They point to temporal flux variations of the Tristan hotspot, similar to what is reported for Iceland. This should be considered in future geodynamic analyses of the basin. A review of Cretaceous-Cenozoic sediment supply to the South Atlantic margins and the complex

uplift and subsidence history of the region is given by MacGregor (2013).
Links between spreading rates and dynamic topography for Australia must acknowledge the onset of subduction in the Cenozoic of the Indo-Australian plate beneath Southeast Asia (e.g., Hall, 2012), so that the geodynamic setting of this region differs fundamentally from the Atlantic realm. Australia's dynamic topography history from the Jurassic onward has been reviewed by Harrington et al. (2019) and involves several key observations. Long-wavelength tilting since the late Cretaceous (e.g., Sandiford, 2007; DiCaprio et al., 2009) occurred when the continent approached the subduction systems of Southeast Asia on its northward passage. It is manifested by high Miocene subsidence rates on the Australian northwest shelf inferred from the stratigraphic architecture of carbonate platforms (Rosleff-Soerensen et al., 2016). River profile studies provide additional constraints. They report regional uplift for western and central Australia starting in the Eocene (e.g., Barnett-Moore et al., 2014; Czarnota et al., 2014) and a two-stage uplift history for the Eastern Highlands. A first stage, from 120 to 80 Ma, coincided with rifting along the eastern margin, whereas a second stage, inferred broadly for 80–10 Ma, formed the Great Escarpment (Czarnota et al., 2014). A third and long-standing observation relates to Australia's flooding record. Its maximum occurs in the Lower Cretaceous, when the Eromanga and Sutra basins in the eastern half of the continent experienced marine inundation. The discrepancy of Australia's flooding record with global sea level curves (e.g., Müller et al., 2008) was noticed early on and prompted pioneering geodynamic studies that attributed the inundation to Australia's passage over a slab associated with Gondwana subduction (e.g., Russell and Gurnis, 1994; Gurnis, 1998). Our results agree with these findings and document the interregional nature of Australia's topographic changes. They show that spreading onset of the Lord Howe Rise went along with a proxy elevation growth from the Lower to the Upper Cretaceous, although a detailed analysis is limited by the long duration of the Lower/Upper Cretaceous series. The interregional scale of this elevation change suggests the involvement of active mantle flow. Several studies have attributed Lord Howe spreading to a mantle upwelling (e.g., Storey, 1995; Spasojevic et al., 2010; Sutherland et al., 2010). Supporting evidence comes from geochemical data tracing a deep mantle (HIMU) component in Upper Cretaceous volcanics in Zealandia (Hoernle et al., 2020). Active plume-driven flow in the Upper Cretaceous at Australia's eastern edge would indeed provide a plausible link between the topographic and spreading signal at that time. In contrast, no plume activity has been invoked, to our knowledge, for Western Australia's proxy elevation growth in the Paleocene, which preceded the Eocene onset of Antarctic/Australia separation (Fig. 3.7). However, Stotz et al. (2021a) used coupled mantle circulation and tectonic models to suggest that Poiseuille flow inherited from Mesozoic mantle circulation led to the Eocene separation of Australia and Antarctica, eventually inducing subduction of the Indo-Australian plate beneath Southeast Asia and high spreading rates along the Antarctica-Australia ridge.
Links between dynamic topography and plate motion variations are perhaps least evinced in our maps for the Indian Ocean realm, because collisional forces associated with India-Eurasia convergence arguably make this ocean basin the one currently most strongly influenced by plate boundary forces. Several studies argue for significant edge forces in the region as a result of topographic loads associated with the regions orogenic plateaus (Warners-Ruckstuhl et al., 2010, 2012), amounting to $\sim$5-10 $\cdot$ 10^{12} N/m (Copley et al., 2010; Warners-Ruckstuhl et al.,

2013), sufficient to reduce India's plate motion (Copley et al., 2010). Additional complexity seemingly arises from temporal flux variations of the Reunion plume (Iaffaldano et al., 2018; Iaffaldano, 2021). Not surprisingly, our results reveal growing East Africa proxy elevation in the Paleocene-Oligocene and simultaneous decreasing Carlsberg spreading rates, which presumably reflect expanding boundary forces from India-Asia collision, and minor spreading rate variations in the late Paleogene and Neogene, at the time of the Afar plume arrival. Figure 3.9 summarises our findings and reveals the correlation between high proxy elevation and subsequent spreading rate changes with grey boxes for the studied regions from Upper Jurassic to Pliocene.

Our discussion must acknowledge the influence of eustatic contributions to the proxy elevation curves. For instance, there is an increase in the Oligocene proxy elevation curve for all regions considered, see hatched area in Fig. 3.9. In Hayek et al. (2020, 2021) we bring out the sea-level signal by plotting the temporal evolution of no-/hiatus surfaces in the BHS separately for individual continents and combined for all continents considered. This reveals two prominent continent-wide maxima in the BHS at the Base of Miocene and Base of Pleistocene corresponding to high proxy elevation curves in the Oligocene and the Pliocene, respectively. The latter coincide with the onset of glaciation in Antarctica and the Northern Hemisphere, respectively. This suggests caution in the interpretation of Oligocene and Pliocene hiatus.

Our discussion of the comparison of hiatus surfaces and past plate motion changes must emphasise the severe limitations of the input data for our hiatus mapping method. Addressed in detail by Hayek et al. (2020), we recall that the temporal resolution of interregional hiatus analysis depends on the temporal resolution of the input geological maps. At continent scale, they are currently limited to the geological series level. The limitation is aggravated because hiatus is likely longer than indicated by the missing geological series (see figure 3 in Friedrich, 2019). At any one location sedimentary successions may represent only a small portion of a geological series. This implies large temporal uncertainties in our analysis, inevitably hiding shorter duration lacunae and favouring large time intervals. The severe limitations of the input data can be alleviated with additional geologic indicators, which are beginning to yield powerful constraints on past dynamic topography. They include paleoaltimetry estimates (Kohn, 2007), studies of river profiles (e.g., Roberts and White, 2010), landforms (Guillocheau et al., 2018) and sediment provenance (Meinhold, 2010; Şengör, 2001), constraints from thermochronological (Flowers et al., 2008; Reiners and Brandon, 2006; Hodges, 2003) or paleobiological and paleoenvironmental data (Fernandes and Roberts, 2020), as well as quantifications of sediment budgets at the scale of continental margins (Guillocheau et al., 2012; Said et al., 2015a,b; Baby et al., 2020). Observational constraints on current and past dynamic topography are reviewed very effectively by Hoggard et al. (2021). Efforts to better constrain past continental vertical motion are matched by similar efforts to improve our knowledge of horizontal past plate motion. Progress is underway to map past plate velocities from sea-floor magnetic lineations at temporal resolutions of $\sim$1 Myrs or less (e.g., Merkouriev and DeMets, 2014; DeMets and Merkouriev, 2019) when mitigating for finite-rotation noise (Iaffaldano et al., 2012). In combination, these efforts should help to further constrain the recent geologic history of large scale horizontal and vertical lithosphere motion, greatly assisting in geodynamic interpretations of plate driving and resisting forces.

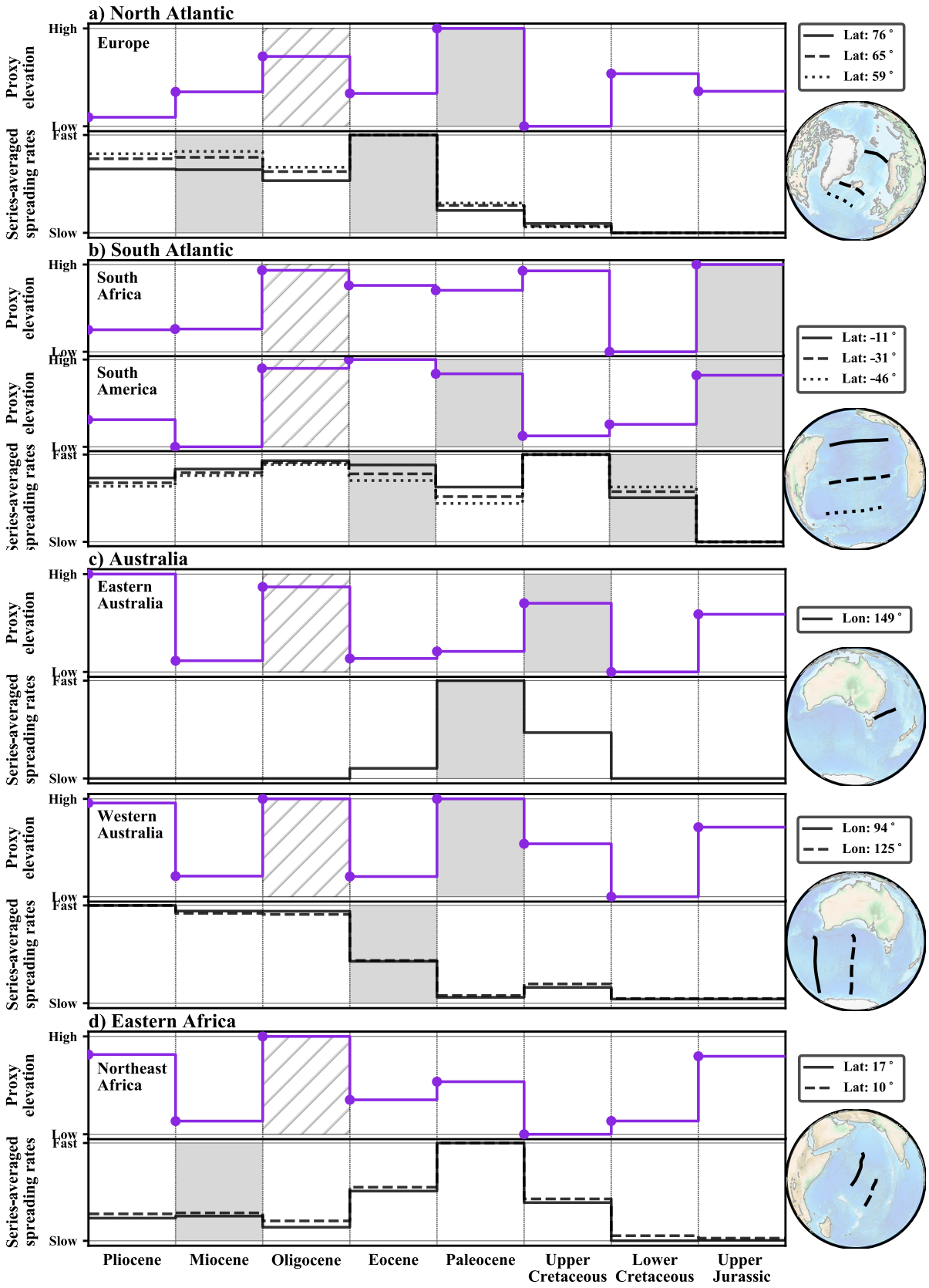

Figure 3.9: (Caption in the next page)

Figure 3.9: Summary figure showing correlation between high proxy elevation (PE) and subsequent spreading rate changes with grey boxes for studied regions from Upper Jurassic to Pliocene. PE curves (dot marks the datum) are normalised to their minimum/maximum, spreading rates are averaged over each geological series, and all series are represented with same length. **a)** North Atlantic: high Paleocene PE followed by Eocene spreading onset. **b)** South Atlantic: high Upper Jurassic South African/South American PE followed by Lower Cretaceous spreading onset. High Paleocene South American PE followed by Eocene spreading rate increase. **c)** Australia: high Upper Cretaceous Eastern Australia PE followed by peak Paleocene Lord Howe Rise spreading rates. High Western Australia Paleocene PE followed by Eocene Antarctica-Australia spreading onset. **d)** Eastern Africa: growing Paleo/Oligocene PE and simultaneous decreasing Carlsberg spreading rates presumably reflect boundary forces from India-Asia collision. High Oligocene PE (hatched box) in part reflects eustatic signal from Antarctic glaciation onset (Hayek et al., 2020, 2021). Long duration of Upper/Lower Cretaceous series combined with Cretaceous Normal Superchron mask relation between PE and spreading rate changes (e.g., high Upper Cretaceous South African PE and South Atlantic spreading rates, see text).

3.5.1 Geodynamic implications

Geodynamicists have long understood the effects of an asthenosphere on mantle flow in modulating the amplitude of dynamic topography and the horizontal flow range (e.g., Hager and Richards, 1989; Bunge and Richards, 1996). Our analysis extends these results to geologic observations and suggests a time scale, on the order of a geological series, between the occurrence of continent-scale hiatus and plate motion changes. A similar time scale comes from fluid dynamic studies reporting a delay between domal uplift and magmatism above starting plumes (e.g., Campbell and Griffiths, 1990; Farnetani and Richards, 1994). These studies are reviewed very effectively by Campbell (2007). The time scale is interpreted best through dynamic topography response functions of dynamic Earth models, because a weak upper mantle delays significant surface deflections into the final phase of material upwellings, when buoyant flow enters from the lower into the upper mantle (see Colli et al., 2016, for a review). Our analysis also suggests a spatial scale for interregional hiatus, on the order 2000-3000 km in diameter. The latter again agrees with starting plume studies, where it is attributed to plume heads flattening by lateral upper mantle flow (Campbell, 2007).

Our maps offer the opportunity to compare hiatus size with predictions from fluid dynamic models of Poiseuille/Couette flow (see Fig. 3.1), following Stotz et al. (2018). Figure 3.10 shows analytic upper mantle flow estimates, derived from the assumption of Couette flow, Poiseuille flow and the superposition of both, at the time when the Yellowstone, Canary, Afar, Iceland and Tristan plumes presumably arrived in the asthenosphere, as evinced by the onset of widespread volcanism (Courtillot et al., 2003). Couette flow (first column Fig. 3.10), induced in the underlying asthenosphere by tectonic plate motion, is computed from the reconstructions of Müller et al. (2016) tied to a global moving hotspot reference frame (Torsvik et al., 2008) from present-day to 100 Ma and a TPW corrected paleomagnetic reconstruction (Steinberger and Torsvik, 2008) for times older than 100 Ma, with the latter including a longitudinal shift of 10° incorporated by Seton et al. (2012). This flow is half the surface velocity at mid-asthenosphere depth. Poiseuille flow, induced by a plume-generated pressure gradient in the asthenosphere, is obtained from the equation

$$V_{Poiseuille} \approx \frac{D^2}{8\mu} \frac{\Delta p}{\Delta x} \tag{3.1}$$

where D is the asthenosphere thickness, and μ is its viscosity. Both values are tied together by inferences from post-glacial rebound (e.g., Paulson and Richards, 2009). We choose a thickness of 110 km and a viscosity of $5 \cdot 10^{19}$ Pa·s. $\frac{\Delta p}{\Delta x}$ is the flow inducing pressure gradient, which we estimate from values for density contrast, gravity and dynamic topographic height in $\Delta p = \rho g h$, respectively. We use a density contrast of 3300 kg/m^3 and a height of 1400 m (e.g., Hoggard et al., 2021). Δx is the distance away from the plume centre. Poiseuille flow (second column Fig. 3.10) is radially symmetric, as expected, decays away from the respective plume centres with velocities >15 cm/yr, maintains velocities ∼5 cm/yr at a distance of ∼1000 km from the plume, and decays further farther out. We note that our estimated Poiseuille flow velocities agree with inferences from geologic observations and dynamic models (Hartley et al., 2011; Weismüller et al., 2015). The combined flow (third column Fig. 3.10) is derived by adding up the Couette and Poiseuille flow as in Stotz et al. (2018). It varies geographically due to the Couette component, such that different locations experience different upper mantle flow for any given Poiseuille source. We highlight, as a proxy for active mantle flow, those areas where Poiseuille flow exceeds Couette flow by at least 0.5 cm/yr. These areas are larger under slow moving plates, as expected, and have an extent of ∼0.4-0.9·10^7 km^2, comparable to the hiatus area inferred from our maps. Our results allow us to evaluate, to first order, the ability of Poiseuille flow to initiate spreading rate changes, following Iaffaldano and Bunge (2015).

$$A_f = \frac{\Delta v_p}{\Delta v_f} A_p \tag{3.2}$$

Equation (3.2) relates the Poiseuille flow dominated area (A_f) to the area (A_p) affected by the spreading rate change. The latter is the entire plate. This relation is modulated by the ratio of the mean pressure-induced velocity change (Δv_f) to the plate velocity change, that is the spreading rate variation (Δv_p). It means that small Poiseuille flow dominated areas (A_f) can affect large plates areas (A_p), provided the mean pressure-induced velocity change(Δv_f) exceeds the plate velocity change (Δv_p). We assume a mean value Δv_f ∼5 cm/yr over a radius of ∼1500 km away from the plume centre, a Poiseuille flow dominated area $A_f \sim 10^7$ km^2, and an average plate area A_p ∼5· 10^7 km^2 for our analysis, noting that the current size of the African plate is ∼6.2· 10^7 km^2, whereas the size of the South American plate at the end of the Cretaceous, shortly before it resumed rapid spreading in the Eocene, was ∼2.5· 10^7 km^2. Our analysis shows that plume driven flow may induce spreading rate changes (Δv_p) on the order of ∼1 cm/yr for average-sized plates plates, comparable to the values reported in our study. Finally, we compute the linear force density associated with Poiseuille flow, for which we estimate plate basal shear stresses from the relationship

$$\tau = \mu \frac{\Delta v_f}{d} \tag{3.3}$$

where τ is the shear stress generated at the plate base, μ is the asthenosphere viscosity, Δv_f is the velocity difference between plate and asthenosphere flow at mid depth, and d is half the asthenosphere channel thickness. Taking an asthenosphere viscosity of $5 \cdot 10^{19}$ Pa·s, a velocity of 5 cm/yr, and a half-thickness of 55 km, as noted before, we obtain shear stresses of $\sim$ 1.5 MPa, in agreement with values reported from instantaneous and time-dependent geodynamic models (Steinberger et al., 2001; Kendall and Lithgow-Bertelloni, 2016; Bird et al., 2008; Colli

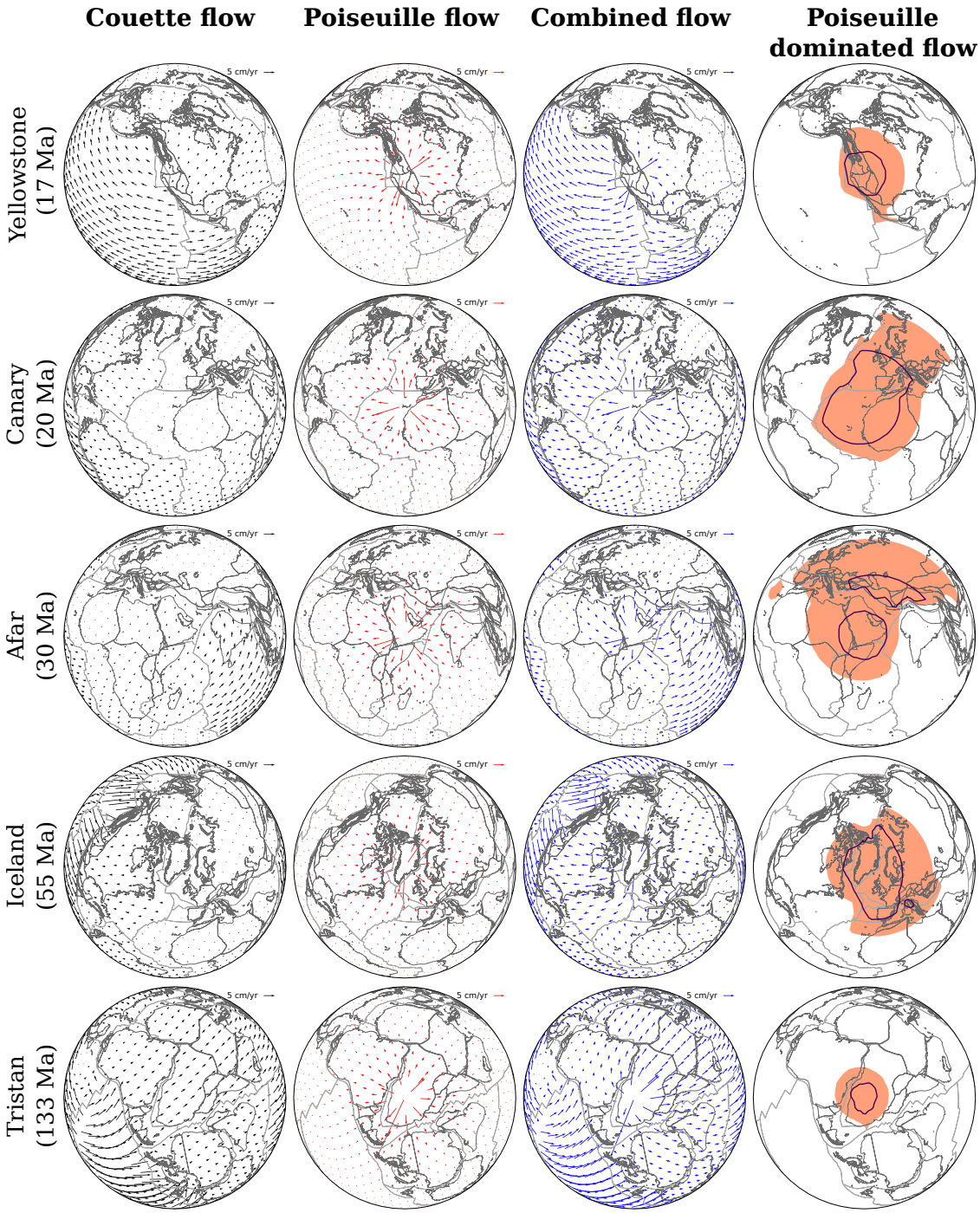

Figure 3.10: Upper mantle flow estimates based on Couette (black, first column) and Poiseuille (red, second column) models (compare Fig. 3.1), and the superposition of both (blue, third column), for a global Mesozoic-Cenozoic plate motion model (Müller et al., 2016) tied to a reference frame of global moving hotspot and TPW corrected paleomagnetic reconstruction (Torsvik et al., 2008), with the latter corrected by Seton et al. (2012) (see text), shown at mid-asthenospheric level for the time when the Yellowstone, Canary, Afar, Iceland and Tristan plumes presumably arrived in the asthenosphere (see text for details). Poiseuille dominated flow regions, as indicated by areas where Poiseuille flow exceeds Couette flow by at least 0.5 cm/yr, are shown in colour in column four. These regions are larger under slow-moving plates and comparable to the hiatus area inferred from our maps (compare Fig. 3.3, see text for details). Note the small size for the Poiseuille flow dominated region of Tristan compared to the other hotspots. Blue continuous line contours Poiseuille dominated area when the Poiseuille flow strength is reduced to half the reference value (see text).

et al., 2018; Ghelichkhan et al., 2021). The spatial coherence of Poiseuille flow evinced from our maps allows us to integrate the shear stress along flow lines. We take a distance of $\sim$1500 km, the radius achieved by Poiseuille flow dominated areas (fourth column Fig. 3.10) and obtain linear force densities of $\sim 2.25 \cdot 10^{12}$ N/m, comparable to ridge push values, which are estimated to $\sim 2 \cdot 10^{12}$ N/m (Harper, 1975, and references therein). Our estimates agree with earlier studies that have called for strong plume push forces (Westaway, 1993a), related, for instance, to the Reunion hotspot (Iaffaldano et al., 2018; Van Hinsbergen et al., 2011; Cande and Stegman, 2011). However, we point to the limitation of our analysis, having assumed for the sake of simplicity a Newtonian upper mantle. Strong evidence exists for a Non-Newtonian upper mantle rheology (Karato and Wu, 1993). This would induce more complex upper mantle flow, as indicated by recent geodynamic models (Semple and Lenardic, 2018a).

We must also acknowledge that our analysis for the sake of simplicity ignores lateral variations in asthenosphere thickness related to lithospheric thickness variations and the presence of Cratonic keels. The latter would have important effects on the flow, particularly by reducing the extent of Poiseuille flow dominated area beneath these Cratonic roots.

We close with some implications, starting with the Poiseuille flow dominated area A_f computed for the Tristan hotspot (fifth row, fourth column Fig. 3.10) at 133 Ma. The area is $\sim$3 times smaller than A_f computed for the more recent Cenozoic plume events (fourth column Fig. 3.10). Moreover, the small size contrasts with the large hiatus mapped at the Base of Lower Cretaceous, Fig. 3.3a, for Africa and South America. This result is a consequence of the large Couette flow inferred at that time for the upper mantle beneath Africa and South America from the assumed plate motion model (Müller et al., 2016). The latter is tied to a global moving hotspot reference frame (Torsvik et al., 2008) from present-day to 100 Ma and a TPW corrected paleomagnetic reconstruction (Steinberger and Torsvik, 2008) for times older than 100 Ma, which also includes a longitudinal shift of 10° incorporated by Seton et al. (2012). O'Neill et al. (2005) drew attention to the effects of absolute reference frames in past plate motion models, which may include TPW corrections and may assume fixed or moving hotspots or combinations of both. For times $<$80 Ma the reference frame differences are not discernible. But they grow further back in time. Moving hotspot reference frames have been computed from geodynamic models through so-called backward advection (e.g., Steinberger and O'Connell, 1997), which introduces uncertainties related to model parameters and starting conditions. It is possible that backward advection may mispredict Cretaceous hotspot motion, with consequences for plate motion reconstructions, and it is also possible that TPW corrections may overcompensate for the reorientation of the lithosphere-mantle system. Studies exist on absolute reference frame choices in geodynamic models (e.g., Shephard et al., 2012; Becker et al., 2015). But further investigations and the use of mantle flow retrodictions (e.g., Colli et al., 2018; Ghelichkhan et al., 2021) seem advised for improved assessments of past hotspot motion. The influence of absolute reference frame choices on the extent of Poiseuille dominated area is explored in Fig. 3.11.

Next we recall that Hayek et al. (2020, 2021) interpreted hiatus maps in terms of the plate and plume mode of mantle convection (see Davies and Richards, 1992, for a review of these convective modes). Broad conformable surfaces reveal the plate mode, while broad unconformable surfaces and areas of lack of signal express the plume mode. From the repeated appearance of continent-scale hiatus they deduced a significant role for the plume mode, which fits with

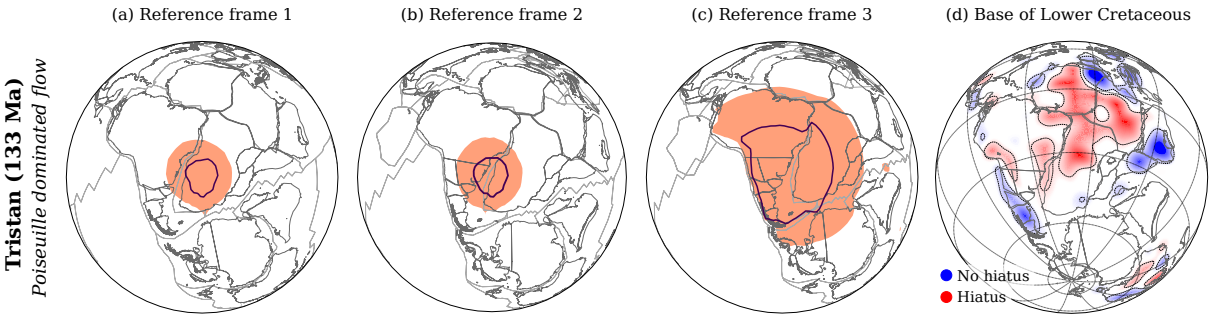

Figure 3.11: Estimates of Poiseuille flow dominated areas computed for Tristan at 133 Ma using three absolute plate motion models. **(a)** is the same as Fig. 3.10 and assumes a global Mesozoic-Cenozoic plate motion model (Müller et al., 2016). **(b)** uses an Indo-Atlantic moving hotspot reference frame (O'Neill et al., 2005) for the past 100 Myrs and a TPW corrected paleomagnetic model (Steinberger and Torsvik, 2008) for older times. **(c)** applies a reference frame of Indo-Atlantic moving hotspots (O'Neill et al., 2005) for the last 100 Myrs and of fixed African hotspots (Müller et al., 1993) for prior times. **(d)** BHS for Base of Lower Cretaceous (see Fig. 3.3). Note that the size of hiatus and blank areas throughout Africa and South America in the Base of Lower Cretaceous map compares well to the extent of the Poiseuille-dominated area in Reference Frame 3.

geodynamic studies placing the total plume heat transport into the range of 10 TW (e.g., Bunge, 2005; Simmons et al., 2009a), that is ∼20-30% of the global mantle heat budget (e.g., Davies and Davies, 2010). Our results suggest that plate motion variations should be included in this interpretation. Taking the current global RMS plate velocity of 5 cm/yr (DeMets et al., 2010) as representative and recalling that rapid plate motion variations in the range of ∼1-2 cm/yr are potentially linked to the plume mode from our analysis, we speculate that ∼20-30% of overall plate velocities could be attributed to the plume mode.

Finally we turn to plate boundary forces. Several studies emphasised their role in the Indian Ocean realm (Warners-Ruckstuhl et al., 2010, 2012; Copley et al., 2010; Warners-Ruckstuhl et al., 2013) owing to the topographic load of Tibet, as noted before. Others linked plate motion changes to Tibet's evolving topography (e.g., Gordon, 2009; Iaffaldano et al., 2011). This interpretation remains under debate (Iaffaldano, 2021). But the significant contribution of topography, which is partially controlled by external processes such climate and erosion, to plate boundary forces may go some way in helping to explain why it remains difficult even with advanced mantle convection models, capable of generating plate-like surface motions, to reproduce the recent history of plate motions (Coltice and Shephard, 2018), as this would have to be parameterised in geodynamic simulations. Global coupled models of mantle and lithosphere dynamics may offer a possibility to address these challenges (Stotz et al., 2021a).

3.6 Conclusion

We have used continent-scale hiatus maps as a proxy for mantle flow induced dynamic topography and compared them with plate motion variations in the Atlantic and Indo-Australian realms since the Jurassic, building upon earlier work and exploiting growing observational constraints on both. We find that oceanic spreading rate changes and hiatus surfaces frequently correlate, except when plate boundary forces may play a significant role. Our work is geody-

namically motivated from the description of asthenosphere flow beneath tectonic plates in terms of Poiseuille/Couette flow. This description explicitly relates plate motion changes, induced by evolving basal shear forces (Poiseuille flow), to nonisostatic vertical motion of the lithosphere. Our analysis reveals a time scale on the order of a geologic series between the occurrence of continent-scale hiatus and plate motion changes. It is best interpreted through dynamic topography response functions of dynamic Earth models, because a weak asthenosphere delays significant surface deflections into the final phase of material upwellings, when buoyant flow enters from the lower into the upper mantle. Our analysis suggests that the spatial scale of interregional hiatus, which is on the order of 2000-3000 km in diameter, should be interpreted through Poiseuille flow, where it corresponds to regions of active plume-driven upper mantle flow. We use fluid dynamic arguments to show that such active upper mantle flow can induce plate motion changes of $\sim$1-2 cm/yr, comparable to observations. Our results offer the motivation to further improve the temporal resolution of interregional geological maps, to enhance the constraints on past dynamic topography and associated paleogeography. This means such maps should be compiled more directly in relation to the relevant geodynamic processes that are revealed in the geological record. They also motivate one to pursue future studies of large scale horizontal and vertical lithosphere motion in combination, as both of them track the expressions of past mantle flow. Such studies would provide powerful constraints for geodynamic inverse models of past mantle convection that are becoming feasible through the adjoint method.

Chapter 4

Plume driven plate motion changes: New insights from the South Atlantic realm

Plate motion changes are increasingly well documented in the geologic record. Directional plate motion changes, in particular, provide powerful constrains on plate tectonic torques, because they require a change in plate boundary torques, basal shear stresses or both that can be spatially located. Over the past years a pressure driven, so-called Poiseuille, flow model for upper mantle flux in the asthenosphere has gained increasing geodynamic attention – for a number of fluid dynamic arguments. This conceptually simple model makes a powerful testable prediction: Poiseuille flow induced plate motion changes should coincide with inter regional scale mantle convection induced dynamic topography around the origin of the Poiseuille source. Here we focus on the South American plate, which undergoes two distinct directional changes in motion in the Paleogene. During this time period there is evidence for Paleocene and Eocene/Oligocene high dynamic topography in South America and Africa, which we infer by mapping geological hiatus (i.e., gaps in the stratigrafic record). This suggests a high-pressure source in the upper mantle in the South Atlantic. We apply Poiseuille/Couette flow models to show that the Sierra Leone and Tristan plumes are suitably located to provide the torque to initiate these plate motion changes. Our modelling results are entirely consistent with changes in proxy elevation in the African and South American continents at those times. Moreover, they imply that it is possible to locate torques from sources of active upper mantle flow that can explain directional plate motion changes, and identify them for the South American plate with geological features such as the Sierra Leone and Tristan plumes.

Published on February 12th 2023 in the Journal of South American Earth Sciences
doi:10.1016/j.jsames.2023.104257

Author list: Ingo L. Stotz, Berta Vilacís, Jorge N. Hayek, Sara Carena and Hans-Peter Bunge.

Ludwig-Maximilians-Universität München, Dept. of Earth and Environmental Sciences, Theresienstraße 41 and Luisenstraße 37, 80333 Munich, Germany.

4.1 Introduction

The South Atlantic pronounced bathymetric asymmetry (e.g., Winterbourne et al., 2009a) and the African anomalous topography, also know as the african superswell (e.g., Nyblade and Robinson, 1994) are well established. Africa's atypical high topography compared to other continents (e.g., Bond, 1978a; Burke and Gunnell, 2008) is the result of successive periods of burial and exhumation in late Tertiary rather than a prolonged exposure (Burke and Whiteman, 1973). It's complex elevation history is stored in the sedimentary data, crustal landforms, river incision histories and offshore sedimentation studies (e.g., Partridge and Maud, 1987; Roberts and White, 2010; Guillocheau et al., 2012; Dressel et al., 2015; Carena et al., 2019). Altogether these data suggest multiple regional uplift/exhumation and subsidence/burial episodes in the Cenozoic. The repeated retreats and advances of its paleocoastlines in the Cretaceous/Cenozoic are an evidence of the time changes in continental elevation (Fig. 4.1). For example, most of northwestern Africa basins experienced marine inundations in the Cretaceous, while it remained mostly above sea level in the Cenozoic. More unusual is the intra-continental evolution of South America since the Cretaceous. For instance, its been argued that its topography owes to moving out of a dynamic topography high beneath south Africa (e.g., Behn et al., 2004; Flament et al., 2014). But recent studies on the principle of hiatus mapping shows that South America has experienced several uplift and subsidence periods throughout the Cenozoic (i.e., Hayek et al., 2020; Vilacís et al., 2022), which is also reflected in its paleocoastlines (Fig. 4.1B). For example, the Eocene coastline in Patagonia extended several hundreds of kilometres off-shore

A) Present-day features of the South Atlantic **B)** Paleo coast lines of the South Atlantic

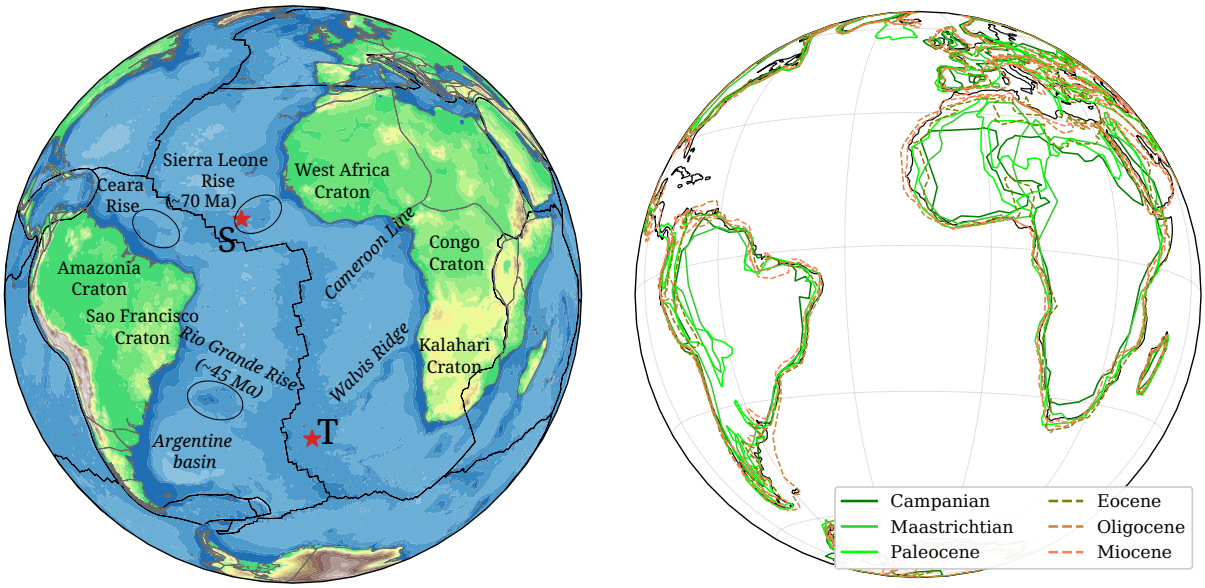

Figure 4.1: Past and present-day geological features of the South Atlantic. A) Topographic map and key geological features in South America, Africa and the South Atlantic ocean basin. Red stars show present-day location of the Sierra Leone and Tristan plumes and the age of their activity (45, 70 Ma) are marked on the map. Black lines are the present-day plate boundaries. B) Paleocoastlines of South America and Africa after Heine et al. (2015, and references therein). Note the significant outward extend of the Patagonian shoreline in the Oligocene.

onto the Argentine basin. Additionally, northeast Brazil experienced several episodes of burial and exhumation in the Cenozoic (Japsen et al., 2012). In fact, most passive continental margins experienced repeated episodes of uplift and subsidence (see Bunge and Glasmacher, 2018, for a review).

Histories of large-scale vertical motion of the continents (i.e., past dynamic topography) are documented in geological archives, because its transient nature leaves an imprint in the sedimentary records. The long wavelength nature of these deflections was recognized early on in the sedimentary record through unconformities and missing sections (e.g., Stille, 1924a). For instance, the Cretaceous Interior Seaway of North America owes to mantle convection induced surface depression resulted in a large inland sea that extended from the Arctic Ocean to the Gulf of Mexico (e.g., Mitrovica et al., 1989; Burgess et al., 1997). Friedrich et al. (2018) and Friedrich (2019) developed a stratigraphic framework revealing continent-scale erosion/non-deposition environments, which serves as a proxy for past dynamic topography. Their analysis of interregional unconformities on geological maps could be used to trace the plume rises within the mantle (e.g., Krob et al., 2020a). Plumes originate at the core mantle boundary and rise up through the mantle towards the lithosphere base, generating a continuously evolving surface response known as dynamic topography (e.g., Hager et al., 1985; Colli et al., 2016). The temperature and buoyancy distribution at the core mantle boundary is most likely due to the mantle circulation history (e.g., Bunge et al., 2002a). Hence, in their ascent, mantle plumes uplift the lithosphere leaving a distinct mark in the sedimentary record and, in turn, this record can be used to trace past movement of mantle plumes (e.g., Rainbird and Ernst, 2001; Vibe et al., 2018; Friedrich et al., 2018; Carena et al., 2019; Hayek et al., 2020). Upon their arrival at the lithosphere base they trigger pressure driven upper mantle flow (Morgan and Smith, 1992a; Morgan et al., 1995a), which generates horizontal shear stresses significant enough to drive plate motion changes (e.g., Harper, 1990; van Hinsbergen et al., 2011; Cande and Stegman, 2011; Stotz et al., 2021b).

The most prominent sources of buoyant material in the South Atlantic realm during the Cenozoic are the Sierra Leone and Tristan hotspots (Fig. 4.1A). This is manifested by the formation of the Ceara and Sierra Leone rises in the Paleocene (e.g., Hekinian et al., 1978; Schilling et al., 1994, and ODP sites 354, 366, 367 and leg 108). Similarly, there are reports of subareal exposure and increased magmatic activity in the Rio Grange Rise magmatic system during the Eocene time (Drill Site 516 Barker, 1983). These events are indicative of two periods of vigorous active upper mantle flow underneath the South Atlantic basin in the Paleocene and Eocene times. Often vertical plate motions are followed by a change in horizontal plate motions (e.g., Vilacís et al., 2022). Nevertheless, South American plate motion history has been commonly associated to the orogeny of the Andes (e.g., Iaffaldano et al., 2006). Observations point out active tectonism along the Andes in the Paleocene times (i.e., K-T event) (e.g., Steinmann et al., 1929; Sempere et al., 1994; Orts and Ramos, 2006; Charrier et al., 2007), although no definitive evidence supports a high elevated Andes. Most studies, however, agree on two main phases of uplif in the Andes; starting by mid Eocene/ Oligocene (Incaic) and later in the Neogene (Quechua) (Cornejo et al., 2003; Mpodozis et al., 2005; Horton, 2018). But it remains ambiguous how the Andes could drive a velocity increase of the South American plate.

Horizontal and vertical lithosphere motion are often studied in isolation. However, Colli

et al. (2014) did a simple torque balance calculation to analyse the mechanisms that can explain the changes in velocity magnitude of the South American plate. They found that those changes were coeval with vertical motions in the surrounding continents, indicative of temporal changes of the pressure-driven flow in the asthenosphere. The latter is a mechanically-weak layer beneath the lithosphere (see Richards and Lenardic, 2018, for a review). The results of Stotz et al. (2021a,b) are in line with a growing recognition that it is useful to describe asthenosphere flow in the context of Poiseuille/Couette flow. The former is initiated by lateral pressure gradients, while the latter is driven by movements of overlying tectonic plates, with the relative importance of Couette to Poiseuille flow depending upon the degree to which plates locally inhibit or drive underlying asthenosphere flow. In a series of papers by Höink and Lenardic (2008, 2010) and Höink et al. (2011); Höink et al. (2012) explored Poiseuille/Couette flow in mantle convection models. Notable findings of these and other studies are that Poiseuille flow within the asthenosphere increases lithosphere/asthenosphere coupling (Höink et al., 2012), results in depth variations of asthenosphere shear (Natarov and Conrad, 2012), yields rapid horizontal asthenosphere flow velocities of $\sim$10 cm/yr in global geodynamic models (Weismüller et al., 2015), and thus provides active driving shear beneath the lithosphere. Importantly Poiseuille/Couette flow connects mantle flow to geologic observables in a testable manner, because it links temporal changes of horizontal and vertical plate motions to upper mantle flow variations in a dynamically viable way. It thus motivates us to explore horizontal and vertical plate motion changes together.

Here we exploit the South Atlantic's well-known spreading record, geologic history and dynamic topography evolution to explore plume effects from the Tristan and Sierra Leone hotspots quantitatively. First, we estimate the motion of the South American plate w.r.t. the South Atlantic hotspots. Next, we investigate these observations in the context of Poiseuille and Couette flow. We find that the two most distinct plate motion changes experienced by the South America plate are consistent with the plume activity in the region.

4.2 Paleogene South American plate kinematics relative to hotspots

We estimated Paleogene South American absolute (i.e., w.r.t. hotspots) plate motion based on recently published finite rotations by Müller et al. (1999) and Maher et al. (2015). The latter provides high temporal resolution and noise mitigated finite rotations via Redback open-source software (see Iaffaldano et al., 2014, for further details). First, we combine finite rotations of South America w.r.t. Africa (Müller et al., 1999) and with Africa w.r.t. the South Atlantic hotspots based on the study by Maher et al. (2015). Next, we use such finite rotations to calculate stage Euler vectors that describe the motion of the South American plate relative to the hotspots from $\sim$70 Ma to $\sim$20 Ma (Fig. 4.2). The stage angular velocity displays an increase of velocity from $\sim$70 Ma to $\sim$52 Ma, within the uncertainty level. The angular velocity, then, decreases and remains stable from $\sim$46 Ma to $\sim$19 Ma. The stage Euler pole (Fig. 4.2B) displays an intriguing path of paleolocations of the pole of rotation. First, it migrates in the Paleocene closer to the South American plate along the midocean ridge, but in the Eocene/Oligoce times

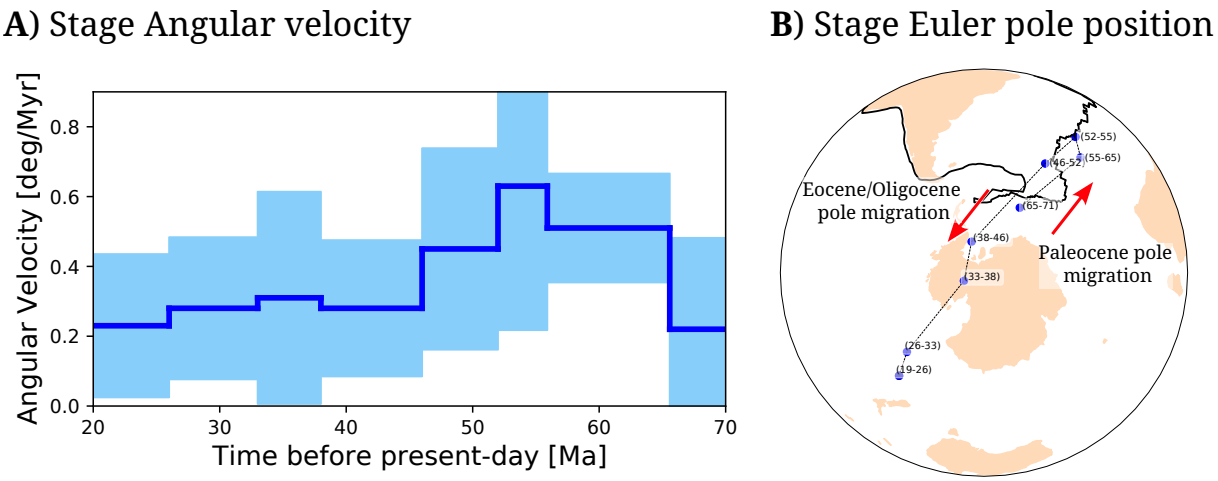

Figure 4.2: Stage Euler vectors of the South American plate relative to hotspots. A) Magnitude of the angular velocity of the South American plate (blue), where the lightblue color area shows the 68% confidence range. Note the velocity increase between 70 and 50 Ma. B) Geographical position of the Euler vector pole of the South American plate. Red arrows highlight two distinct periods of Euler pole migration; first, it migrates in the Paleocene closer to the South American plate along the mid-ocean ridge and, then it persistently moves away from South America and across Antarctica in the Eocene/Oligocene times.

and beginning from ∼52 Ma it persistently moves away from South America and across Antarctica – as described with red arrows in Fig. 4.2B.

Figure 4.3a-h shows time stages of surface velocity of South America w.r.t hotspots and with solid-line the average direction of motion at the geometrical center of the plate at each stage. The latter allows one to highlight the main direction of motion of the South American plate at each time period. In the earliest stage between ∼70 Ma and ∼65 Ma (i.e., Maastrichtian) the South American plate is slowly moving westward. Next, in the Paleocene (∼65 - ∼52 Ma) the South American plate increases its velocity and experiences a counter-clockwise (ccw) rotation and moves predominantly south-westward (Fig. 4.3a-d). Then, in the late Eocene/Oligocene (∼46 - ∼19 Ma) the South American plate undergoes a clockwise (cw) rotation and changes its direction from south- to north-westward (Fig. 4.3e-h).

4.3 South America and Africa's stratigraphic record

We use a recently derived inventory of Base Hiatus Surfaces (BHS) collected by Hayek et al. (2020) and Carena et al. (2019), where they mapped conformable and unconformable contacts at the temporal resolution of geological series (Cohen et al., 2013; updated.) for the Atlantic realm (i.e., North America, Europe, Africa and South America) and Australia. The BHS are provided as spherical harmonic representation of no-/hiatus scattered contacts convolved in a Gaussian filter with a cut off at degree 15. They serve as a proxy for paleotopography, as introduced by Friedrich et al. (2018). Figure 4.4 (top row) shows the BHS for the South American and African continents from Base of late Cretaceous to Base of Pliocene, representative of the time periods from Paleocene to Miocene. Red/blue colours depict hiatus/no-hiatus contacts, respectively, indicative of high/low topography in the preceding series. Blank regions reveal the absence

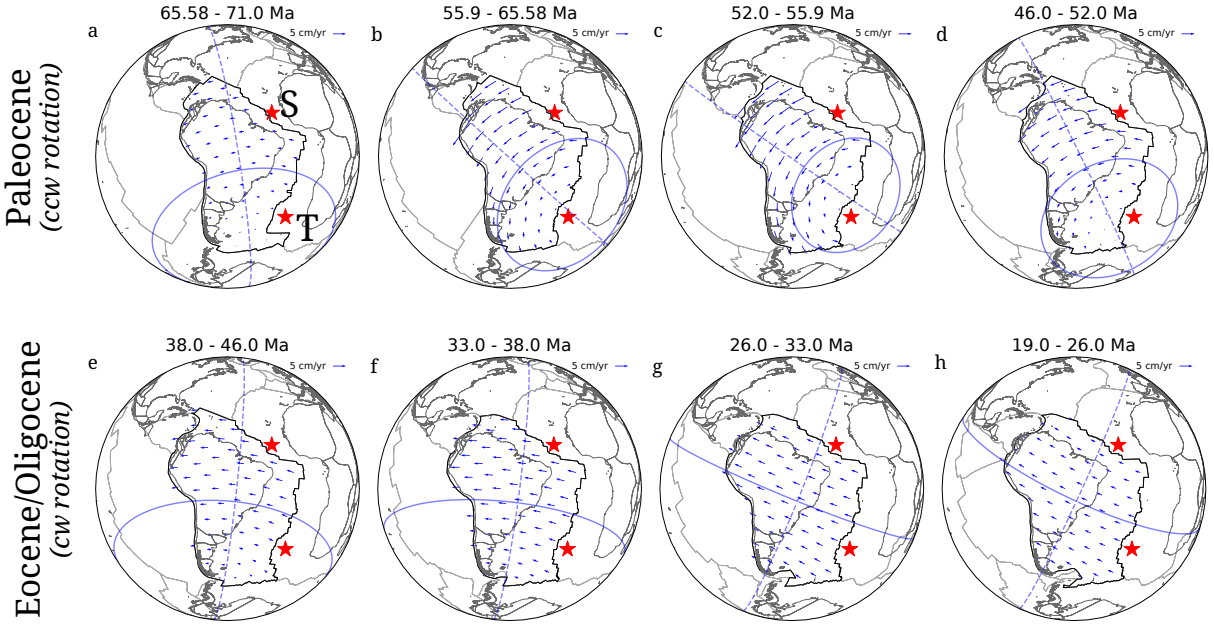

Figure 4.3: Plate kinematic evolution of the South American plate relative to hotspots. Red stars show the location of Sierra Leone and Tristan hotspots and solid line blue line highlights the average direction of motion of South America. The paleocoastlines are in black, plate boundaries in gray and the outline of the South American plate in black bold line. (a–d) Stage surface velocity showing a counter-clockwise (ccw) rotation of South America plate motion in the Paleocene (e–h) Stage surface velocity showing a clockwise (cw) rotation of South America plate motion in the Eocene/Oligocene.

of the target series and its preceding unit. Such regions may have undergone intense and/or long-lasting erosion or non-deposition, suggestive of intense and/or persistent exhumation and surface uplift. Recent examples of continent scale hiatus mapping for Europe, Africa and North America are given in Vibe et al. (2018), Carena et al. (2019) and Stotz et al. (2021b).

Figure 4.4 (top row) Base of Paleocene displays hiatus areas in the northern coastal areas of South America and in the West African and Kalahari cratons. At Base of Eocene and Base of Oligocene blank areas are the most prominent feature in South America, while Africa is characterized by no-hiatus surfaces to the north and blank regions to the south of the continent. This means the maps show neither Paleocene, Eocene nor Oligocene strata in much of Africa and South America. There is one period of widespread hiatus in Africa and South America at Base of Miocene, indicative of high topography in Oligocene. Base of Pliocene displays mostly no-hiatus surfaces in South America, while a mixture of hiatus/no-hiatus surfaces across Africa.
We computed proxy elevation curves for Africa and South America (Fig. 4.4, bottom row), which we construct as the sum (for a given geological series) of hiatus and blank regions, normalised by the continental area of Africa and South America, respectively. The proxy elevation curves elevation curves display two distinct changes since the late Cretaceous. The oldest one is recorded in the South American continent with a marked increase in elevation between late Cretaceous to Paleocene (i.e., Base of Paleocene). Then the African continent displays a younger rise of proxy elevation between Eocene to Oligocene (i.e., Base of Oligocene).

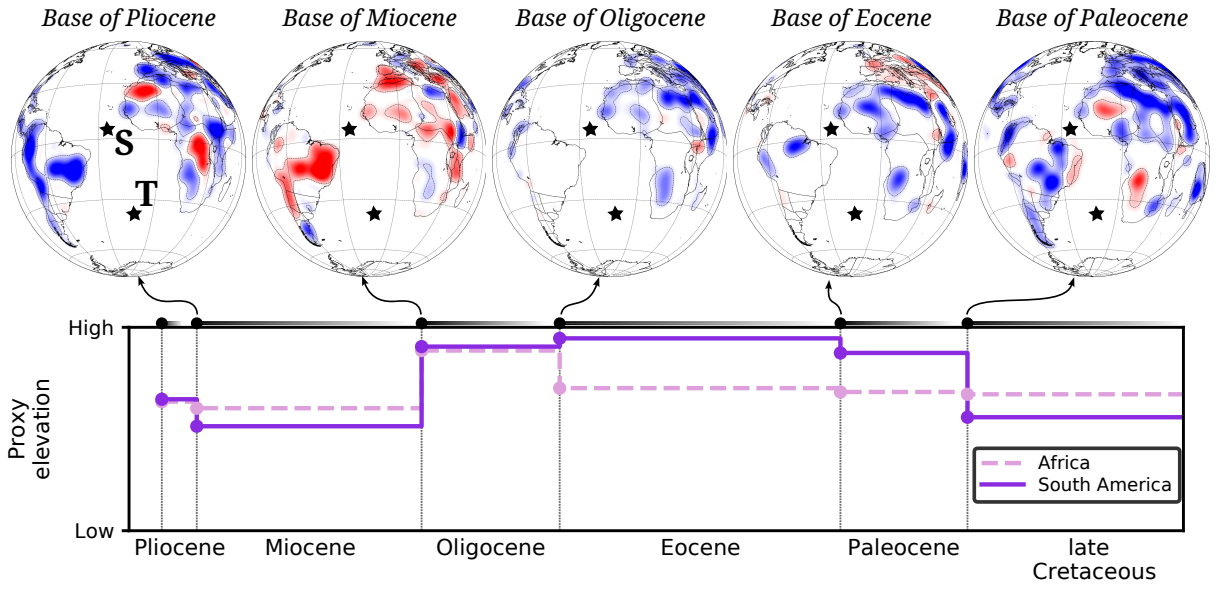

Figure 4.4: Top row shows BHS centred on the South Atlantic from Base of Paleocene to Base of Pleistocene, with black stars showing the current hotspot locations of Sierra Leone (S) and Tristan (T). Red/blue areas are indicative high/low elevation. Blank areas signal prolonged erosion and are also indicative of high elevation. Bottom row shows proxy elevation obtained by the sum of hiatus and blank surfaces for a given geological series normalised by the total area under consideration (i.e., South America and Africa, respectively). Two distinct increases in the proxy elevation stand out in the Paleocene and Eocene/Oligocene in South American and African, respectively.

4.4 Plume push torque upon the South American plate

There are growing constraints on a time-dependent plume driven Poiseuille flow in the upper mantle, as indicated by numerous studies that attempt to estimate plume strength histories. They include records of magmatic flux variations (e.g., Spice et al., 2016; Parnell-Turner et al., 2014), past denudation and uplift events derived from provenance analysis (e.g., Hartley et al., 2011; Barker, 1983; Şengör, 2001; Saunders et al., 2007a), and recently compiled hiatus maps (Vibe et al., 2018; Carena et al., 2019; Hayek et al., 2020, and this study).

Here we explore the role that the Sierra Leone and Tristan plumes have on the Paleogene South America plate motion changes. To do so, we estimate the direction of motion of the South American plate in the Paleocene and Eocene/Oligocene driven by upper mantle basal shear torques generated by the Sierra Leone and Tristan plumes alone, or in combination with the Couette flow. Figure 4.5 shows simple analytical estimates of upper mantle flow beneath South America derived from the assumption of Couette, Poiseuille flows and the superposition of both. To achieve this, first, we calculated the Couette flow at late Cretaceous (i.e., Maastrichtian) time induced by the rigid motion of the South American plate in the underlying asthenosphere – the latter is obtained from the kinematic reconstructions based on the finite rotations from Maher et al. (2015) and Müller et al. (1999). We assume the Couette flow is half the surface velocity at mid-asthenosphere depth and induced by the motion of the overlying South American plate (Fig. 4.5a). In the next step, we estimate the Poiseuille flow generated by the arrival of the

Sierra Leone and Tristan plumes in the asthenosphere following the equation,

$$V_{plume} = \frac{D^2}{8\mu}\frac{\Delta p}{\Delta x} \tag{4.1}$$

where, D is the asthenosphere thickness and μ its viscosity. The two values are tied together by inferences from post-glacial rebound (e.g., Paulson and Richards, 2009). Thus we choose a thickness of 110 km and a viscosity of $5 \cdot 10^{19}$ Pa·s. The expression $\frac{\Delta p}{\Delta x}$ is the pressure gradient, which we estimate from density contrast, gravity and topographic height in the following relationship $\Delta p = \rho g h$. We use a density contrast of 3300 kg/m^3 and a topographic height of 1400 m. The latter is in agreement with observational estimates of dynamic topography (e.g., Hoggard et al., 2017) and theoretical considerations of geodynamic response functions (e.g., Hager et al., 1985; Colli et al., 2016). Δx is the distance away from the plume center. The Sierra Leone plume driven Poiseuille flow (Fig. 4.5b) spreads away radially from the plume center, achieves velocities of ∼20 cm/yr and extends throughout much of the upper mantle beneath the South America and northwest Africa. The combined flow beneath the South American plate is obtained by summing up the Couette and Poiseuille flow and is shown in Fig. 4.5c. In Fig. 4.5e-g we repeat the same process for the Tristan plume.

Next we estimate the torque associated with the asthenosphere flows described in Fig. 4.5b/c,

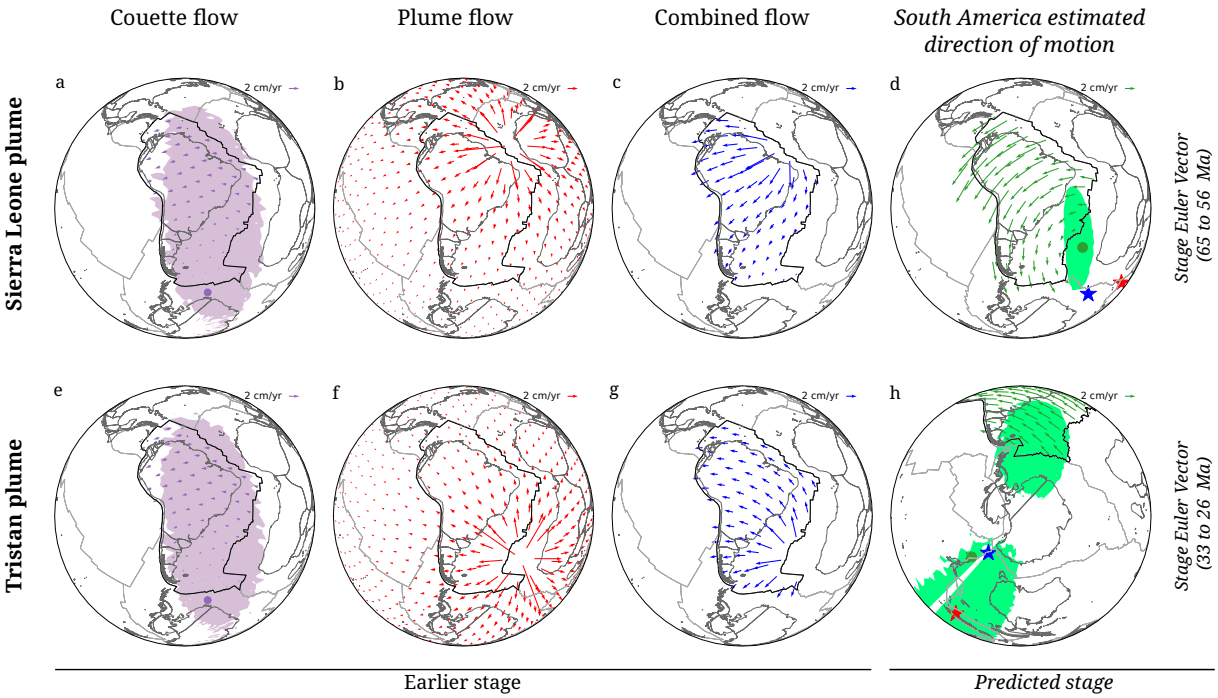

Figure 4.5: Computed asthenosphere flow beneath the South American plate at two time periods derived from either Couette (a, e) or Poiseuille (b, f) flow, or a combination of both (c, g) – for a Poiseuille source associated with the Sierra Leone (top row) or Tristan (bottom row) plumes, shown in a reference frame relative to the hotspots (Müller et al., 1999; Maher et al., 2015). (a, e) also show the uncertainty of the kinematic reconstruction with a purple area. The right most column (d, h) shows Euler poles of the predicted motion of South America as a result of plume push only (red star), or a combination of plume push and Couette flow (blue star) against the observed South American plate motion w.r.t hotspots (green and lighth green areas). Note that the location of the Euler pole that describes the combined flow (Couette and Poiseuille) is located close to observations (green areas).

i.e., Poiseuille flow only or in combination with the Couette flow – in the case of the Sierra Leone plume. To do so, we calculate the shear stress at the lithosphere base: $\tau = \frac{\mu}{D'}\vec{v}_{as}$ where $D' = D/2$ and the asthenosphere flow velocity is composed of $\vec{v}_{as} = \vec{v}_c^{t_{-1}}(\vec{r}) + \vec{v}_p^{t_0}(\vec{r})$. The time t_0 represents the current time, while t_{-1} represents the time of the previous stage. In particular, the Couette flow ($\vec{v}_c^{t_{-1}}$) arises from the motion of the South American plate in the previous time stage, while the Poiseuille $v_p^{t_0}$ comes from the flow generated by the Sierra Leone plume at the present stage (i.e., predicted stage). We then integrate the cross product of the basal shear stresses over the area of the South American plate with $\vec{r}$ (i.e., the position of each grid point to the center of Earth) to obtain a basal shear torque M_B, as stated in the following equation,

$$\vec{M}_B = \int_A \vec{r} \times \frac{\mu}{D'}\vec{v}_{as}(\vec{r})dA \tag{4.2}$$

$$\vec{M}_B^{t_0} = \int_A \vec{r} \times \frac{\mu}{D'}[\vec{v}_c^{t_{-1}}(\vec{r}) + \vec{v}_p^{t_0}(\vec{r})]dA \tag{4.3}$$

This formulation brings out the direction of the torque (i.e., Euler pole location). In Fig. 4.5d we display with red and blue stars the direction of the South American plate if it was driven by asthenosphere basal shear torque from a flow due to the Sierra Leone plume or combined with Couette flow, respectively. We also display the position of the reconstructed Euler pole with 68% uncertainty level from the kinematic reconstruction of South America. Figure 4.5d shows that the asthenospheric basal shear torque underneath South America predicts a south-westward motion of the plate, well in agreement with the observations – see the proximity of the red and blue stars to them in Fig. 4.5d. In other words, the Sierra Leone plume to the northeast of South America is suitably located to provide a torque capable of driving the South American plate north-westwards in the Paleocene – as summarized in Fig. 4.5a-d.

We perform the same analytical torque calculation for the Tristan plume in the Eocene/Oligocene time (Fig. 4.5e-h). In Fig. 4.5h we display with red and blue stars the direction of the South American plate if it was driven by asthenosphere basal shear torque from a flow due to the Tristan plume or combined with Couette flow, respectively. The asthenospheric basal shear torque underneath South America predicts a north-westward motion of the plate, in agreement with the observations as shown by the location of the red and blue stars in Fig. 4.5h. The Tristan plume Poiseuille flow alone and in combination with the Couette flow are capable of producing a asthenosphere flow that would drive the South American plate motion change from south- to north-westwards.

4.5 Discussion

Convection in the Earth's mantle provides the necessary torques to drive plate motions (e.g., Davies and Richards, 1992). However, the precise nature of the interaction between tectonic plates and mantle flow remains somewhat incomplete. This is because the strength of plates conseals a presumably complex flow field – making it challenging to get a glance even on the recent Cenozoic. However, the description by Morgan et al. (1995a), Höink and Lenardic (2008, 2010), Höink et al. (2011); Höink et al. (2012) of mantle convection explicitly in terms

of Poiseuille and Couette flow provides a chance to overcome this difficulty. It provides, essentially, a simple theoretical framework that connects dynamic topography observations to plate motion changes.

Previous studies by Colli et al. (2014), Vibe et al. (2018) and Vilacís et al. (2022) have reported cases in which non-isostatic vertical motions of the lithosphere were followed by plate motion changes. This is consistent with the notion that mantle plumes can generate significant basal shear stresses to drive plate motion changes via plume push torque (e.g., Westaway, 1993b). In fact, recent work has shown that the Yellowstone plume provides a dynamically viable mechanism to drive Neogene North America plate motions (Stotz et al., 2021b). Thus making explicit the link between plume induced vertical plate motions and horizontal plate motion changes.

The motion of South America w.r.t hotspots features two distinct directional changes in plate motion in the Paleogene, which can be explored explicitly in terms of the torques required to the explain them. First a Paleocene counter-clockwise rotation of motion which is consistent with a torque acting to the northeast of the South America plate. The Sierra Leone plume is suitably located to provide this torque and to drive the South America plate south-westwards (Fig. 4.5a-d). The Sierra Leone plume was particularly active in the Paleocene times when it formed the The Ceara and Sierra Leone rises (e.g., Basile et al., 2020). ODP and DSDP sites 13, 354, 366, 661 and 667 report Paleocene unusual thermal exhumation and prolonged periods of hiatus of the Sierra Leone Rise and Ceara Rise. In other words, they are presumably supported by sublithospheric forces related to a strong Poiseuille flow regime from the Sierra Leone hotspot. These events to the northeast of South America are consistent with the hiatus occurrence along the north and east coasts of Brazil and in northwestern Africa in the Upper Cretaceous (Fig. 4.4) and an increase in the proxy elevation of South America at the base of Paleocene. Previous studies have argued for recent activity of the Sierra Leone hotspot in uplift and exhumation along a transpressive transform fault at the mid-ocean ridge, rather to a change in the so-call far-field stress regime (i.e., Maia et al., 2016).

The South America plate motion history w.r.t hotspots holds a second directional changes in plate motion in the Eocene/Oligocene. A clockwise rotation of motion which is consistent with a torque acting to the southeast of the South America plate. The Tristan plume is suitably located to provide this torque and to drive the South America plate north-westwards (Fig. 4.5e-h). The subaereal exposure and increased magmatic activity of the Rio Grange Rise magmatic system happened during the Eocene time (i.e., 45 Ma) (Drill Site 516 Barker, 1983; Rohde et al., 2013). This is indicative of a second pulse of the Tristan plume, which has been active since at least the opening of the South Atlantic $\sim$133 Ma. Our hiatus maps also supports this finding and is evidenced by the blank regions in South America at the base of Eocene (Fig. 4.4). These observations are indicate of two periods of vigorous active upper mantle flow underneath the South Atlantic basin in Paleocene and Eocene/Oligocene times. These observations are in agreement with current understanding on plume flow, in that plume flux is not a continuous but can vary significally over time (e.g., Spice et al., 2016; Parnell-Turner et al., 2014).

We draw attention to the shortcommings of our analysis. Hiatus maps are well constrained in lateral extent but they lack the amplitude of paleo elevation. The latter requires independent data of surface uplift – i.e., thermochronological data (e.g., Ehlers and Farley, 2003), analysis of

river profiles (e.g., Roberts and White, 2010) or provenance and compaction studies (Meinhold, 2010; Japsen, 2018). Hiatus maps are currently restricted in temporal resolving power to the geological series level of compiled continental scale geological maps (time scales to ten to a few tens of Myrs). This contrasts with the finer temporal resolution of the spreading rates in the South Atlantic on the order of a few Myrs. The extent of hiatus surface can also respond to other potential mechanism, such as eustatic contributions. For instance the increase of hiatus at Base of Miocene (Fig. 4.4) is coincidental with the onset of glaciation in Antarctica, and suggests that the Base of Miocene hiatus surface in South America and Africa could be due in part to sea level changes.

We also point out the shortcomings of our Poiseuille/Couette analytical flow models. The nature of our upper mantle flow calculations (Poiseuille/Couette flow) is highly simplyfied, but has the advantage that it involves a minimum number of input parameters aimed at understanding asthenosphere flow conceptually and isolating the effects of key model parameters. The latter are often masked by the considerable computational complexities of modern geodynamic numerical models. For example, we chose a constant channel thickness that may ignore the dynamic influence of continental roots (e.g., Sleep et al., 2002; Conrad and Lithgow-Bertelloni, 2006). We also assume a Newtonian rheology. Strong evidence exists for a non-Newtonian upper mantle rheology (e.g., Karato and Wu, 1993; Karato, 2010), which would induce a more complex upper mantle flow (i.e., Semple and Lenardic, 2018b). Hoewever, for instance, a reduction in viscosity due to high temperature of plume material will strengthen our results by increasing the plume flow velocity.

Traditionally, South America plate motion changes have been attributed to variations in plate boundary torques (e.g., Iaffaldano et al., 2006) – that is the Andean orogeny. Most models of the orogenic history of the Andes describe three main phases (Steinmann et al., 1929): Peruvian during Late Cretaceous, Incaic in middle Eocene (or Oligocene, according to (Sempere et al., 1990)), and Quechua since late Miocene. In latest Cretaceous and early Paleocene, a time also referred to as the K-T Orogeny (Charrier et al., 2007), tectonic activity has been documented in the Central Andes (Sempere et al., 1994; Cornejo et al., 2003; Mpodozis et al., 2005; Orts and Ramos, 2006). The results of Colli et al. (2014), however, suggest that an active asthenosphere flow is also required to explain the motion of the South American plate. Our observationally-driven approach supports these findings based on two observations; (i) it shows that the Paleocene and Eocene/Oligocene South American plate motion changes were preceded by the occurrence of a high proxy elevation in African and South America, and (ii) that the Sierra Leone and Tristan plumes were suitably located to account for the directional plate motion change. Instead, an increase in Mountain building torque at the Central Andes in the Paleocene would make the South American plate to rotate clockwise and reduce its angular velocity. This is contrary to the kinematic reconstructions (Figs. 4.2 and 4.3). Thus the observations discard the K-T orogeny in the Andes as a plausible Paleocene plate tectonic driver. A corollary is that the tectonic activity in the Andes at that time could have been driven/initiated by the Sierra Leone plume. Similarly the second pulse of Tristan plume activity in the Eocene could be responsible for the Incaic Andean orogeny – a well documented uplift phase in the Central Andes that started in middle Eocene, reaching a peak in the Oligocene, with a second uplift period by late Miocene (Sempere et al., 1990; Gillis et al., 2006; Sempere et al., 2008a).

4.6 Conclusion

Plate motion changes are increasingly well documented in the geologic record and, the directional information of plate motion changes is one of the most powerful constrains of locating the torques required to drive them. Several key geological and geophysical observations point out that the two plate motion changes experienced by the South American plate in the Paleogene were largely driven by plume push torques from the Sierra Leone and Tristan plumes. Our observationally driven approach supports these findings based on two key observations; first, it shows that the South American plate motion changes were proceeded by the occurrence of high proxy elevation in the South American and African continents. Second, the Sierra Leona and Tristan plumes are suitably located to provide the torques to initiate these directional plate motion changes – as evindenced by the formation of the Ceara and Sierra Leone Rise in the Paleocene and the subaereal exposure of the Rio Grande Rise in the Eocene.

Our analytical calculations demonstrate the link between these two independent observations. Notably, our analysis of asthenosphere flow in terms of Poiseuille and Couette models explicitly relates horizontal plate motion changes induced by plume basal shear stresses to non-isostatic vertical motion of the lithosphere in the context of a geodynamically plausible model. Hence it provides a conceptual framework to map time variable asthenosphere flow from geological and geophysical observations. Our results also suggest to think out of the traditional view of plate tectonics. A torque arising from the Andes would not be suitably located to explain the Paleogene South American plate motion changes. Hence, directional information in plate motion changes are a powerfull constrain to better undertand the torques that drive plate tectonics, in addition to just looking at velocity changes.

Chapter 5

Dynamic topography and the planform of mantle convection since the Jurassic inferred from Global Continental Hiatus Maps

The planform is a defining feature of mantle convection. It can be gleaned from the stratigraphic record by mapping the continent-scale distribution of hiatus and no hiatus surfaces serving as a proxy for high and low dynamic topography. We carry this out for all continents apart from Antarctica for eight geological series since the Upper Jurassic, showing that: (1) the planform as indicated by our maps contains wavelengths on the order of 1000 km, smaller than the convective scales implied by the geoid. (2) The planform changes on timescales of geological series (10–20 Myrs), smaller than the mantle transit time. (3) Flood basalt eruptions are frequently preceded by hiatus surfaces. (4) Some hiatus surfaces are not linked to any known plume, potentially reflecting the lateral transport of material in the asthenosphere. Our results reveal the importance of mantle viscosity stratification in shaping the convective planform and the resulting dynamic topography. Geodynamic Earth models should aim to reproduce the global characteristics of our maps, as well as specific regional events identified in this work. Finally, we separate the effects of sea-level variation from regional changes in base level induced by dynamic topography by contrasting the stratigraphic evolution of different regions.

Article published on November 20th 2024 in the Proceedings Royal Society A.
doi:10.1098/rspa.2024.0311

Author list: Berta Vilacís[1], Hamish Brown[1], Hans-Peter Bunge[1], Sara Carena[1], Jorge N. Hayek[1], Ingo L. Stotz[1], Zhirui R. Wang[2] and Anke M. Friedrich[1].

[1] Ludwig-Maximilians-Universität München, Dept. of Earth and Environmental Sciences, Theresienstraße 41 and Luisenstraße 37, 80333 Munich, Germany.
[2] Unversity of Copenhagen, Dept. of Geosciences and Natural Resource Management, Øster Voldgade 10, 1350 København K.

Note: Figures have been updated to include the Artic region, however this part of the data set was not included in the article. The addition of this data doesn't change the results.

5.1 Introduction

The planform, i.e. the geometry in the horizontal plane of hot upwellings and cold downwellings, is a fundamental property of convecting fluids. Hence it attracted considerable attention in early studies of mantle convection, which tried to understand the flow geometry of Earth's mantle through the use of laboratory experiments (Chen and Whitehead, 1968) and their comparison to theoretical predictions (Busse and Whitehead, 1971). The subsequent arrival of 3-D computer models made it possible to study mantle convection planforms with numerical simulations, allowing one to explore effects of heating mode (Houseman, 1988; Travis et al., 1990), temperature dependent viscosity (Weinstein and Christensen, 1991), and depth-dependent rheology (Bunge and Richards, 1996). The latter in particular cannot be investigated with laboratory experiments, and it revealed the profound influence of a low viscosity upper mantle in promoting long-wavelength flow, which is a defining feature of mantle convection.
These theoretical studies shed important light on the development of mantle flow geometries. Geodynamicists, however, also believed that the strength of plates conceals the underlying flow, so that the geometry of plate tectonics would primarily reflect the mechanical properties of the solid lithosphere rather than those of the fluid mantle beneath (e.g., Davies, 1988a).

Surface deflections of the lithosphere inferred from bathymetry and geoid variations offered an early observational glimpse of the mantle convection planform beneath the lithosphere of the Pacific Ocean (McKenzie et al., 1980). Such surface deflections were later understood to be a fundamental expression of the convective stresses associated with mantle flow. They give rise to a form of topography that is maintained dynamically by the mantle, which was termed "dynamic topography" by Hager et al. (1985) more than 30 years ago. Histories of subduction offered a further glimpse of the evolving mantle convection planform (e.g., Richards and Engebretson, 1992b), albeit limited to cold downwellings. Plate reconstruction models, derived from surface (e.g., Müller et al., 2016) and more recently also from subsurface information (e.g., Wu et al., 2016; Chen et al., 2019) now provide us with maps of past plate subduction for at least the past 200 million years, bringing the locations of mantle downwellings into focus. Locations of hot mantle upwellings are by comparison more difficult to infer, except when they pierce through the lithosphere and result in volcanic tracks and massive eruptions known as "Flood Basalts" (e.g., Duncan and Richards, 1991).
While the strength of the lithosphere thus plays an important role in mantle planform studies, it is becoming increasingly clear that dynamic topography variations induced by evolving mantle flow offer a powerful way to track the mantle convection planform beneath plates, through the associated response in sedimentary systems recorded in continent-scale stratigraphy. The approach was pioneered for negative surface depressions induced by mantle downwellings using the sedimentary record from the Western Interior Seaway and the cratonic interior of North America (e.g., Mitrovica et al., 1989; Burgess et al., 1997). The Cretaceous Eromanga Sea in Australia is another prominent example for negative surface depressions induced by mantle downwellings (Gurnis, 1998; Harrington et al., 2019).

Hot mantle upwellings induce positive surface deflections. Their stratigraphic expression is given by erosional/non-depositional environments that leave time gaps in the sedimentary record. Field observations of the surface expression of mantle upwellings document changes

in drainage patterns (e.g., Cox, 1989) and a dome-shaped uplift of 1–2 km (e.g., Şengör, 2001; Saunders et al., 2007b) over a radius of 1000–2000 km. The resulting discontinuity surfaces in the sedimentary record are known as unconformities (e.g., Miall, 2016). To this end, we introduced an approach of hiatus-area mapping (Friedrich et al., 2018; Friedrich, 2019) to highlight the long-wavelength nature of sedimentation records as explored by Sloss (1963, 1972). This mapping visualises inter-regional scale unconformities because, at continental scales, what is normally perceived as a lack of data (material eroded or not deposited) becomes part of the dynamic topography signal. We have used this method to map the temporal and spatial patterns of conformable and unconformable geological contacts across Europe (Vibe et al., 2018), Africa (Carena et al., 2019), the Atlantic realm, and Australia (Hayek et al., 2020, 2021; Vilacís et al., 2022). Here we extend this effort to include Asia, subsurface information in the form of stratigraphic columns, and data from the continental shelf regions.

We organise our paper as follows: Section 5.2 describes the data set and the mapping method, Section 5.3 describes the hiatus/no hiatus surfaces, summarises the main events for the Indo-Atlantic realm and extends the description for Asia. We then introduce the concept of geological uncertainty and give a proxy for vertical motion globally and for each studied region together with their geological uncertainty. Section 5.4 gives a spectral analysis of the surfaces, involving both power spectra and the two-time correlation functions to identify spatial and temporal scales. In Section 5.5 we discuss the main geodynamic implications of the hiatus surfaces, summarise key hiatus/no hiatus surfaces and give an overview of limitations and uncertainty including the effects of sea level. We draw conclusions in Section 5.6.

5.2 Dataset and mapping

In our earlier studies, Hayek et al. (2020, 2021) and Vilacís et al. (2022), we have made use of the available continental-scale digital geological maps for North America, Europe, and Australia; and country-scale maps for South America. The maps were collected at the temporal resolution of a geological series, as this is the most frequently adopted temporal resolution for inter-regional geological maps (Friedrich, 2019). For Africa, continent-scale digital geological maps at the resolution of geological series are not available. Therefore, Carena et al. (2019) compiled and manually mapped a dataset for the continent using regional geological maps, stratigraphic studies, and online databases with surface and subsurface information. In this study we extend the data set to include Asia and Oceania. Digital geological maps of these regions at the relevant temporal and spatial resolution are not available either, and so we follow the approach of Carena et al. (2019) when mapping Asia and Oceania. We additionally include new data pertaining to the regions covered in our previous studies. These include the shelf regions of digital geological maps and subsurface information such as stratigraphic columns and drill cores for North and South America, the North Atlantic, and Europe. We use different approaches to map the spatial extent of subsurface information depending on the information available. Drill cores are represented as a point on the map using the coordinates provided by the corresponding report. Stratigraphic columns that summarise a political region are represented as a point located centrally in the area that they represent. Finally, for columns that summarise the chronostratigraphy of a sedimentary basin, we fill the area covered by the basin

(CGG-Robertson, 2022) with points using the Golden Spiral method (i.e. the Fibonacci spiral) with a distance of ≈50 km between each point. Table A.1 provides an extensive list of the data sources used in this study.

In Fig. 5.1 we summarise the basic geodynamic concepts related to dynamic topography and the mapping technique utilised to extract its imprint on the stratigraphic record. Figure 5.1a) shows a sketch of the up-/downwards deflection of the Earth's surface due to hot and cold anomalies transiting through the mantle. Dynamic uplift induces erosional and non-depositional environments, while dynamic subsidence provides new accommodation space for deposition. Figure 5.1b) shows a simplified mantle viscosity profile with a viscosity contrast between the upper and lower mantle of two orders of magnitude, together with the so-called surface topography kernel (Colli et al., 2016). The kernel shows the surface dynamic topography induced by a unit density anomaly as a function of depth and spherical harmonic degree (wavelength). From the kernel, it is evident that the contribution of a unit anomaly with spherical harmonic degree 5 or larger (wavelengths smaller than ∼6000 km) is limited to the upper mantle. This is due to the viscosity contrast between the lower and upper mantle, which reduces their coupling and damps the transmission of lower mantle stresses to the surface (Richards and Hager, 1984).

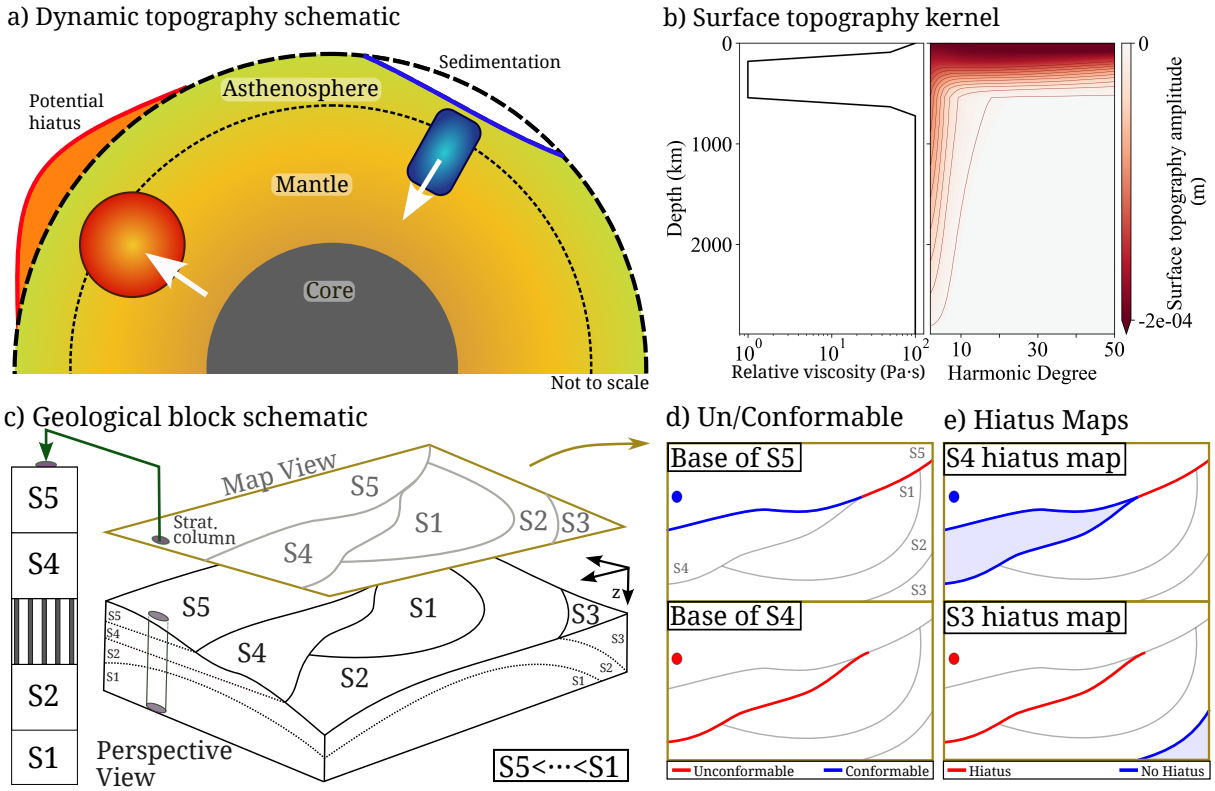

Figure 5.1: a) Sketch showing up-/downwards deflection of the Earth's surface induced by hot/cold anomalies transiting through the mantle. b) Layered viscosity profile and its surface topography kernel as a function of depth and spherical harmonic degree (Colli et al., 2016). Note that contributions of anomalies with spherical harmonic degree 5 or larger (wavelengths smaller than ∼6000 km) are limited to the upper mantle. c) Map and perspective view of a schematic geological setting containing five sedimentary units S1–S5 with S1 being the oldest and S5 the youngest. In the left corner of the schematic we include the location of a stratigraphic column, with the column shown in a standard format on the left (note the absence of S3). d) and e) depict the mapping technique used for extracting un/conformable and hiatus/no hiatus from the digital geological maps and the stratigraphic column in map view (see text).

This differs from the case of an isoviscous mantle, in which anomalies in the lower mantle have a higher contribution (see Colli et al., 2016).

In Fig. 5.1c) we present the map and perspective view of a generic schematic geological setting containing five sedimentary units S1 to S5, with S1 representing the oldest time unit and S5 the youngest. The perspective view (bottom row) shows the topography of the site and the distribution of layers in the subsurface. The map view (top row) shows how this geological setting would be represented in a map. In the left corner, a stratigraphic column that crosses the layers S5, S4, S2, and S1 is sketched, showing an absence of layer S3. The column is enlarged in a standard format on the right of the sketch. This figure is an idealised representation of a geological setting. It illustrates theoretically how different stages of a domal uplift and a later erosive episode (e.g., river incision) might be reflected in geological maps and stratigraphic columns. The hypothetical geological history of the region starts with the deposition of layer S1. During the geological series S2, the region was uplifted, creating the exposure of S1 in the centre and sedimentation of S2 around it. The uplift peaked during S3, resulting in sedimentation of this layer only in the corner on the right of the sketch. During and after the collapse of the central dome, the layers S4 and S5 were presumably deposited everywhere. Finally, a later erosion event due to a tilt of the region or a surface process such as a river incision exposed the layers S3, S2 and S1 on the right side, creating the final topography that we observe. Overall this illustrates how large-scale topographic changes may be imprinted on the geological record, and affect subsequently the location of hiatus/no hiatus surfaces.

Figure 5.1d) shows the mapping of un/conformable contacts at the Base of series S5 and S4. Following the methodology introduced by Friedrich (2019) and further used by Carena et al. (2019), we define *unconformable* as the state when a geological series in the chronostratigraphic chart (Cohen et al., 2013; updated.; Ogg et al., 2016) is not underlain by the preceding geological series, but rather overlies a gap in the stratigraphic record. *Conformable* is defined as the complementary state, in which a geological series is in contact with the immediately preceding geological series. Applying this approach to the Base of S5 in Fig. 5.1d), we map the conformable contact between S5 and S4 in blue and unconformable contacts between S5 and both S1 and S2 in red. The stratigraphic column is mapped as a blue point, showing the conformable contact between the two consecutive layers S5 and S4. Below this, at the Base of S4, unconformable contacts are extracted from the geological map between S4 and both S1 and S2, while an unconformable contact between S4 and S2 is mapped from the stratigraphic column. This indicates the absence of S3 beneath S4, reflecting the peak of uplift during S3. In Fig. 5.1e) we extend the mapping technique from Fig. 5.1d) to map hiatus and no hiatus areas. We do so by adding the available information about the distribution of a given geological series. This delimits the extent of hiatus during a geological series and allows us to obtain a more complete picture of the uplift/subsidence history during the time span considered. We define a *no hiatus* as the presence of a given geological unit, as introduced by Hayek et al. (2020), and a *hiatus* as an unconformable contact. This mapping technique is shown in Fig. 5.1e) for layers S4 and S3. The S4 hiatus map shows the same un/conformable contacts as the Base of S5 in Fig. 5.1d), with the additional constraint of the contour of layer S4, which delimits the spatial extent of where S4 is absent. This map gives us an indication of where the layer S4 is present in blue, and where it is absent in red. We stress that the mapping was carried out regardless of the rock

type. For instance, volcanic and sedimentary rocks are mapped equivalently, which leads to volcanic rocks being part of the no hiatus signal. This choice was made in order to standardise the input data, as not all of the compiled sources provide a lithological description of the rock units. Further details are discussed by Hayek et al. (2020).

Figure 5.2 shows the full data set of un/conformable points for eight geological series from the Base of Lower Cretaceous until the Base of Pleistocene, using the mapping technique shown in Fig. 5.1d). This time span was chosen as it corresponds approximately to a single mantle transit time (Iaffaldano and Bunge, 2015), the time span over which one would expect large-scale changes in the buoyancy field and therefore mantle-flow-induced changes in topography.

5.3 Global Continental Hiatus Surfaces

Figure 5.3 shows the hiatus/no hiatus surfaces for all continents except Antarctica. As we have done in our previous work, and shown in Fig. 5.1e), we add the occurrence of the previous layer as a no hiatus to the un/conformable points in Fig. 5.2 , in order to delimit the hiatus surface of a given series. We then fit a spherical harmonic expansion to these points in order to create smooth surfaces through the data. The binary nature of our data set means that it contains sharp edges. As such, fitting a finite spherical harmonic expansion to it leads to edge artefacts (Gibbs phenomenon). We counteract this by introducing a Gaussian taper, that has a cutoff at degree 15, and gradually decreases the spectral contribution from degrees 15–60, after which it reaches zero. This results in the global *Continental Hiatus Surfaces*. Further details of the construction, limitations and uncertainties of the hiatus maps can be found in Hayek et al. (2020). The surfaces are reconstructed to their appropriate paleolocations using a global Phanerozoic plate motion model derived from a paleomagnetic reference frame (Merdith et al., 2021) that is optimised to constrain mantle flow models using a set of ”tectonic rules”, as stated in Müller et al. (2022). They are mapped at the plate configuration that corresponds to the younger boundary of a given geological series. The current location of the Ascension, Juan Fernandez, Caroline, Samoa, Yellowstone, Canaries, Afar, Balleny, Iceland, Réunion, Sierra Leone, Marion, Galapagos, Louisville, Tristan, Kerguellen, and Cape Verde hotspots (Courtillot et al., 2003) are included as stars in Fig. 5.3. We emphasise that the hiatus/no hiatus surfaces within each geological series serve as a proxy for the topography and vertical motion of the continents, as suggested by Friedrich et al. (2018) and earlier authors (e.g., Levorsen, 1933). Red/blue colours indicate hiatus/no hiatus surfaces respectively, and serve as a proxy for high/low dynamic topography during a given geological series. Following our mapping technique (Fig. 5.1e), blank regions reveal the absence of a series and the series which immediately follows. This can reveal regions with long-standing sedimentary hiatuses, particularly if maps show consistent blank regions in consecutive time windows. Note that the amplitude of the coloured areas only represents the distribution of the raw points, and is not related to the amplitude of topography.
Here we briefly summarise the main features for America, Africa, Europe, and Australia, while a more extensive description is provided in Hayek et al. (2020). Overall, we observe significant differences in hiatus distribution across and between continents at the timescale of at least geological series. The **Upper Jurassic** hiatus map (Fig. 5.3a) shows an inter-regional hiatus

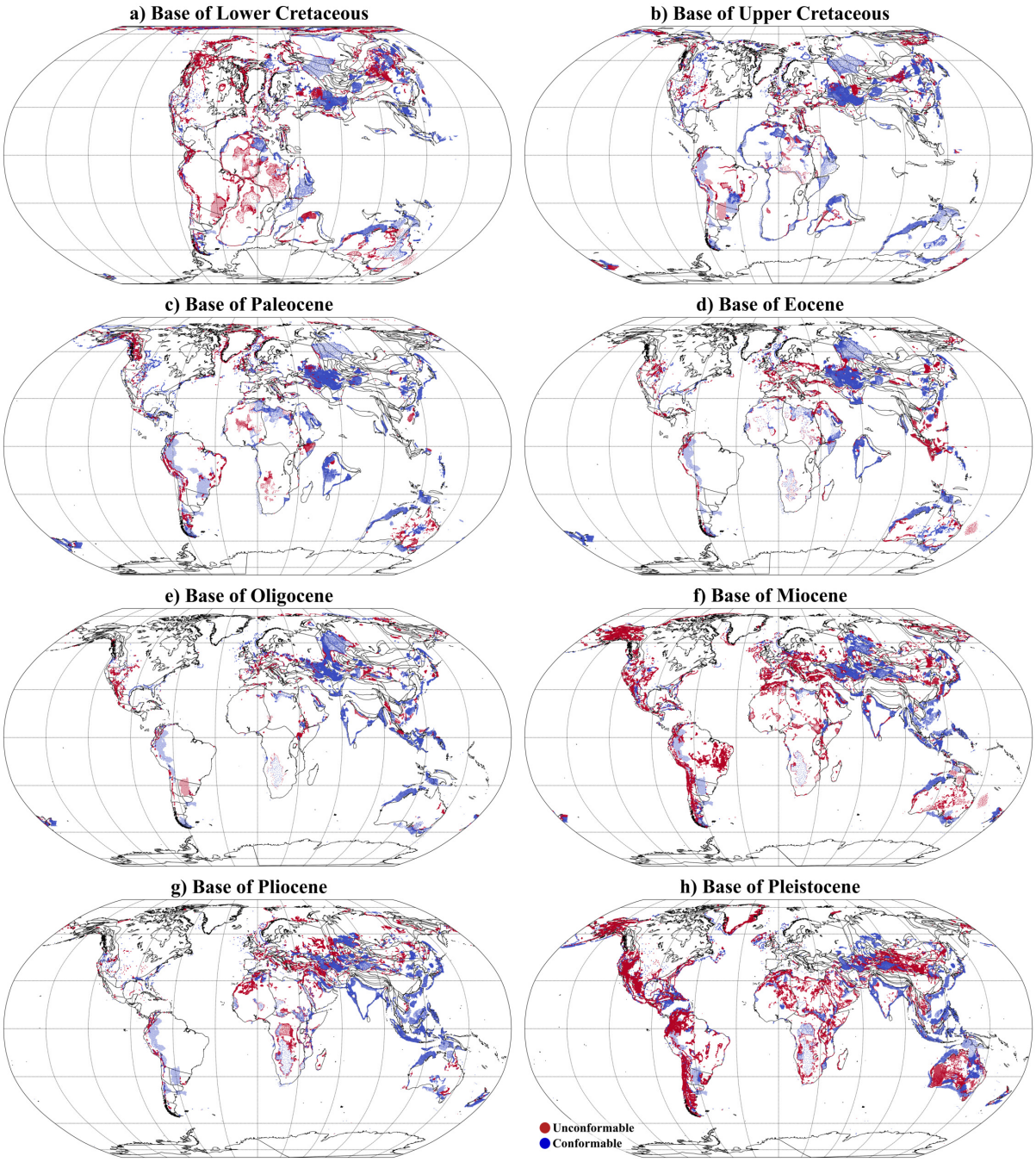

Figure 5.2: Un/conformable points at the chronostratigraphic division of geological series (Cohen et al., 2013; updated.) from the Base of Lower Cretaceous datum (a) to the Base of Pleistocene datum (h). Points are reconstructed paleogeographically using a global Phanerozoic plate motion model with a paleomagnetic reference frame optimised for mantle flow models (Müller et al., 2022) in a plate tectonic configuration corresponding to the base of each series. Red/blue points represent un/conformable contacts. See text for further information.

in western Gondwana, indicating high topography of the region during this time. In contrast, the **Lower Cretaceous** map (Fig. 5.3b) shows sedimentation of this series almost globally. In North America this coincides with the development of the Western Interior Seaway (Mitrovica et al., 1989; Burgess et al., 1997). During the **Upper Cretaceous** (Fig. 5.3c), while sedimentation continued in most of the continents, significant sedimentary hiatuses are present in eastern

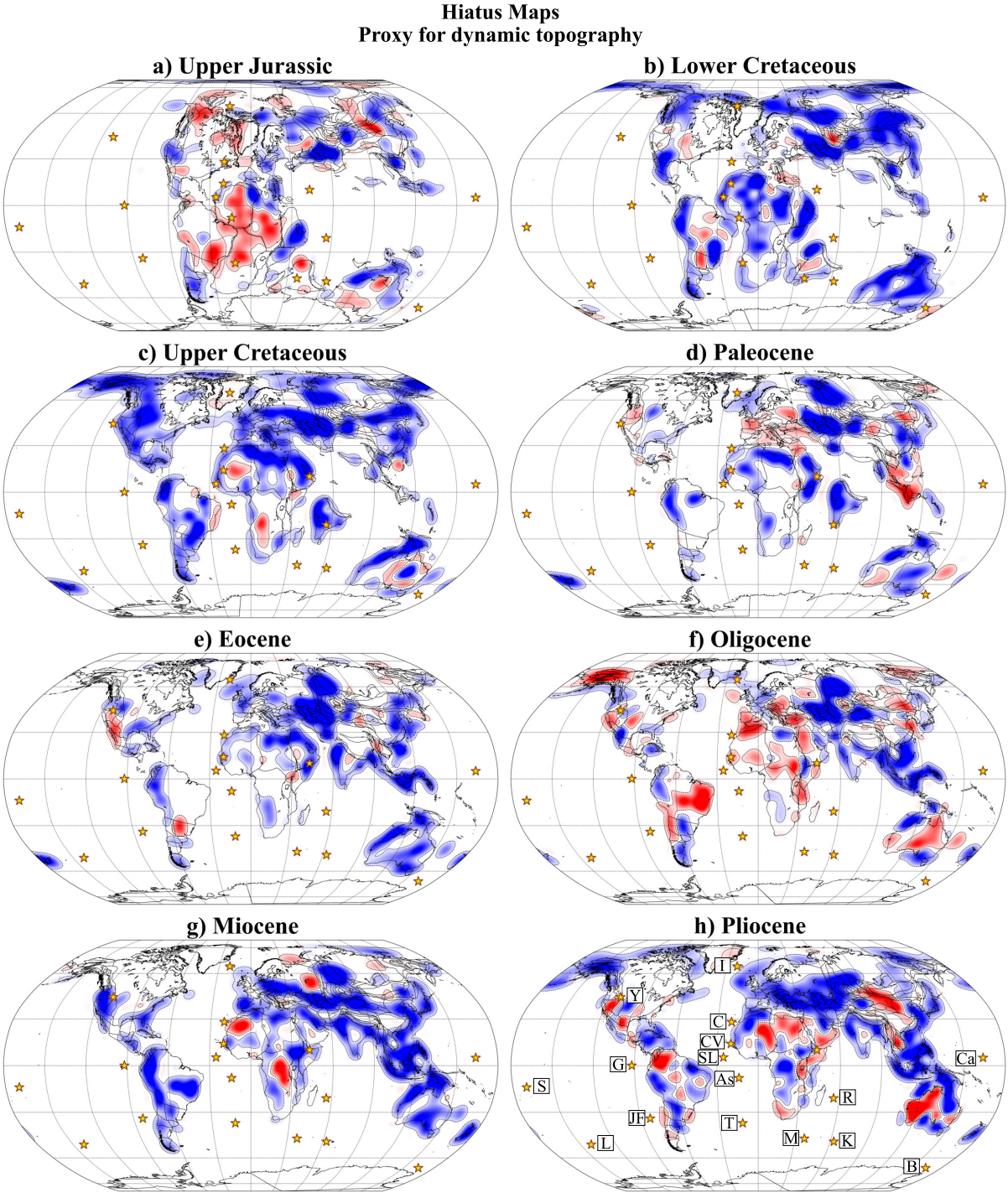

Figure 5.3: Hiatus maps extended from Hayek et al. (2020, 2021) for eight geological series spanning from the Upper Jurassic to the Pliocene. The maps are reconstructed back in time using a global Phanerozoic plate motion model based on a paleomagnetic reference frame optimised for mantle flow models (Müller et al., 2022). They are displayed at the plate configuration corresponding to the younger boundary of the given series. Red/blue colours represent the hiatus/no hiatus surfaces. Black dotted lines contour the spherical harmonic signal at ± 0.075 amplitude. Each map serves as a proxy for dynamic topography (red=high, blue=low) during a given series (see text). Yellow stars mark the current locations of the Ascension (As), Juan Fernandez (JF), Caroline (Ca), Samoa (S), Yellowstone (Y), Canaries (C), Afar (A), Balleny (B), Iceland (I), Reunion (R), Sierra Leone (SL), Marion (M), Galapagos (G), Louisville (L), Tristan (T), Kerguellen (K) and Cape Verde (CV) hotspots (Courtillot et al., 2003).

Australia (surrounding the Eromanga basin), Northwestern Africa, and South Africa. The **Paleocene** hiatus map (Fig. 5.3d) shows a region of high elevation in Europe and Western Australia. In Europe, we have added chronostratigraphic columns located on the continental shelf in the North Atlantic. Note that they show no hiatus surfaces compared to the hiatus surface in the continent. However, in the Paleocene, most of the stratigraphic columns have volcanic rocks (see Fig. 7.7 from Hopper et al. (2014a)), which are inter-bedded with hiatus or sedimentation. Furthermore, the lithostratigraphy of the columns shows a shift in the Upper Cretaceous to the Paleocene/Eocene from limestone/chalk to mudstone, or mudstone to sandstone. This change indicates a change in the sedimentary environment from deep/shallow marine sediments to shallower marine or terrestrial sediments, consistent with the suggested inter-regional uplift during this time. The **Eocene** hiatus map (Fig. 5.3e) shows mainly sedimentation in Europe, central Asia, northernmost Africa, the Karoo Basin, and Australia. Hiatus surfaces are localised in western North America and the Afar region. The latter hiatus surface has been extensively studied and linked to the arrival of the Afar plume by Şengör (2001). In the **Oligocene** hiatus map (Fig. 5.3f), most continents show an absence of Oligocene rocks over large regions. Focussing first on the European-North African region, the map indicates high topography in Iberia and northern Africa while Iceland and northern Europe show lower elevation. The lower elevation in northern Europe coincides with the lowest flux of the Iceland plume (Poore et al., 2009) and the high elevation in south-west Europe coincides with a regional uplift in the Oligo/Miocene (Meco et al., 2007) which precedes the formation of the Canary archipelago (Troll and Carracedo, 2016). South America also shows a widespread hiatus during the Oligocene. Note that this region shows blank surfaces in the preceding two maps, indicating a widespread absence of Paleocene, Eocene, and Oligocene rocks. Others have noted this long-standing hiatus (Wong, 1994; Horton, 2018). In particular, the on-shore basins of the southern Brazilian margin registered a hiatus of the Maastrichtian (youngest stage of the Upper Cretaceous) and the Paleocene (Contreras et al., 2010). Gerster et al. (2011) reports that the Colorado Basin, on the northern shore of Argentina, has a stratigraphic gap from the mid-Paleocene until the mid-Eocene. Furthermore, the Austral-Magallanes basin in southern Argentina preserves a Paleocene hiatus that extends into the Eocene towards the northern part of the basin (Cuitiña et al., 2019; Gallardo Jara et al., 2021). In some basins, the hiatus lasts for $\sim$20 Myrs, however, it is not resolved in our maps because of the temporal resolution of geological series that we use. The **Miocene** hiatus map (Fig. 5.3g) shows most of the continents covered with rocks of this age. In Africa, hiatuses are present in the eastern Congo Basin and the northwest of the continent. The latter hiatus can be linked to the long-term uplift of the Canaries during the Miocene–Pliocene (Sehrt et al., 2018) and the late Miocene uplift of the Atlas mountains (Babault et al., 2008; Lanari et al., 2023). Finally, during the **Pliocene** (Fig. 5.3h) there are scattered surfaces of hiatus and no hiatus throughout America, Africa, and Australia. Europe has widespread low elevation.

5.3.1 Asia

Here we describe the newly added hiatus/no hiatus surfaces for Asia. Figure 5.4 shows the hiatus maps with a view centred on the continent. The Upper Jurassic (Fig. 5.4a) shows a continuous no hiatus signal in Southeast Asia that extends into the Lower Cretaceous, which one

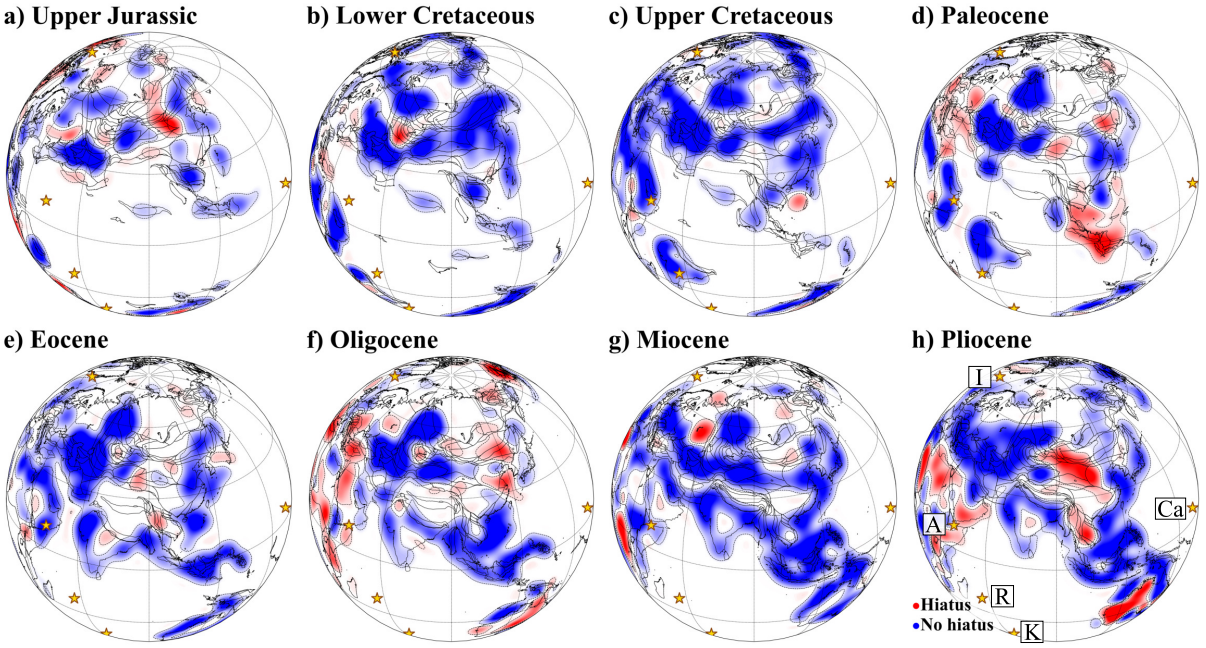

Figure 5.4: Same as Fig. 5.3 with the Hiatus Maps centred in Asia. Note the absence of sedimentation during the Upper Cretaceous and Paleocene in Southeast Asia, as noted previously by Clements et al. (2011a), and the hiatus surface in the Oligocene in East Asia previously linked to the motion of hot-asthenospheric flow from the Pacific to the Asian domain Brown et al. (2022) (see text).

would expect due to its proximity to the subducting Meso- and Neo-Tethys slabs during this time (e.g., Müller et al., 2016). In contrast, during the Upper Cretaceous, sediments are completely absent from Southeast Asia, as indicated by the large blank area during this series (Fig. 5.4c). The next map shows a hiatus during the Paleocene. This means that the uplift event could have spanned back into the Upper Cretaceous, or occurred during the Paleocene and removed the entire preceding series. This inter-regional hiatus event spans an area of $\sim 5.6 \times 10^6\,\mathrm{km}^2$ (Clements et al., 2011a), which has previously garnered attention in the literature due to its likely link to mantle dynamics (Clements et al., 2011a). Following this, Southeast Asia entered a phase of widespread subsidence and extensional basin development during the Eocene–early Miocene (Pubellier and Morley, 2014). While not highlighted when mapping is carried out at the temporal resolution of geological series, as we have done, the onset of sedimentation shows a gradual northward progression over a distance of $\sim$3500 km at the resolution of geological stages during the Eocene–Oligocene. The earliest onset of sedimentation occurs during the early Eocene in East Java (coincident with the cessation of spreading of the now-extinct Wharton Ridge) and the latest onset of sedimentation in the Gulf of Malaysia and the onshore basins of Thailand during the early Oligocene (Pubellier and Morley, 2014). Southeast Asia shows evidence of continued inter-regional subsidence during the Neogene, with a general transition from terrestrial, lacustrine, and fluvial sedimentation during the Oligocene and Eocene to predominantly marine sedimentation during the Miocene and Pliocene (Clements et al., 2011a).

In the east Asian region (defined here to include eastern China, the Korean Peninsula and Japan, see Fig. 5.6 b), inter-regional Cretaceous sedimentation (e.g., Xi et al., 2019) coincides with the final stages of subduction of the Izanagi plate along the east Asian margin (e.g., Müller et al., 2016). This period of low topography could therefore be linked to dynamic subsidence

induced by the subducting Izanagi slab. Following this, during the Paleocene (Fig. 5.4d), the subduction of the Izanagi plate ends with the subduction of the Izanagi-Pacific ridge from ∼65–55 Ma. The Paleocene and following Eocene (Fig. 5.4d–e) are characterised by widespread extension on the east Asian margin, highlighted by the development of extensional basins such as the East China Sea Shelf Basin (Wang et al., 2019) and the Bohai Bay Basin (Qi and Yang, 2010). Thus the no hiatus signals observed in East Asia during this time are dominated by syn-rift sedimentation in such basins, which likely masks any underlying dynamic topography signal. During the Oligocene (Fig. 5.4 f) a widespread hiatus is observed in eastern China. This has been previously linked to an influx of hot asthenospheric material through the Izanagi-Pacific slab window during the early Cenozoic (Brown et al., 2022). Finally, during the Miocene and Pliocene (Fig. 5.4g–h), a large-scale transition to sedimentation occurred in East Asia, with typically thick (∼1–4 km) sedimentary successions (e.g., Wang et al., 2019; Qi and Yang, 2010). This transition from inter-regional hiatus to sedimentation during the Miocene, without additional rifting to generate this new accommodation space, is indicative of dynamic subsidence. This may potentially be due to the influence of the Pacific slab during the late Cenozoic.

5.3.2 Geological uncertainty

The hiatus maps contain blank continental regions during each time window. This can occur when an area is covered by recent sediments, meaning that underlying units are not exposed in a geological map. Subsurface information (e.g. borehole data) could be used to augment the lack of surface data in such regions. In other cases, blank regions are mapped when neither a series nor the following series are present, such that a contact to be mapped at the boundary of these series does not exist. This may be the case when much older rocks (i.e. Early Mesozoic, Precambrian, etc.) are exposed at the surface (e.g. eastern North America), or for hiatuses of extended duration which are bounded by later sedimentation (e.g. eastern South America from the Paleocene–Oligocene). These hiatuses of significant duration (i.e. $\gtrsim$20 Ma) may represent periods of long-lasting and/or intense non-deposition or erosion, indicative of intense and/or persistent surface uplift and exhumation (Friedrich et al., 2018; Friedrich, 2019). It is also possible that they underwent repeated deposition and subsequent erosion, leading to a single long-standing hiatus (e.g., Green et al., 2018a, 2022; Lovell, 2023). Here we follow Carena et al. (2019) and quantify maximum bounds of uncertainty by assigning two end-member cases to the blank areas: the sedimentary rocks were never deposited during their geological series (hiatus) or they were deposited (no hiatus) and eroded later on. The latter case is also known as lacuna, as defined by Wheeler (1958a, 1964). In other words, we fill the blank areas of the continents and continental shelf with either one of these end-member scenarios (hiatus or no hiatus). Figure 5.5 presents an example of the resulting end-member uncertainty maps when considering blank areas with a hiatus/no hiatus signal for the Miocene hiatus map.

5.3.3 Global and regional hiatus curves

In Fig. 5.6, we present hiatus ratio curves both globally and regionally. This ratio is calculated as the hiatus area relative to the combined hiatus and no hiatus areas of the target region, as previously carried out by Hayek et al. (2020). We observe that the ratios are typically lower

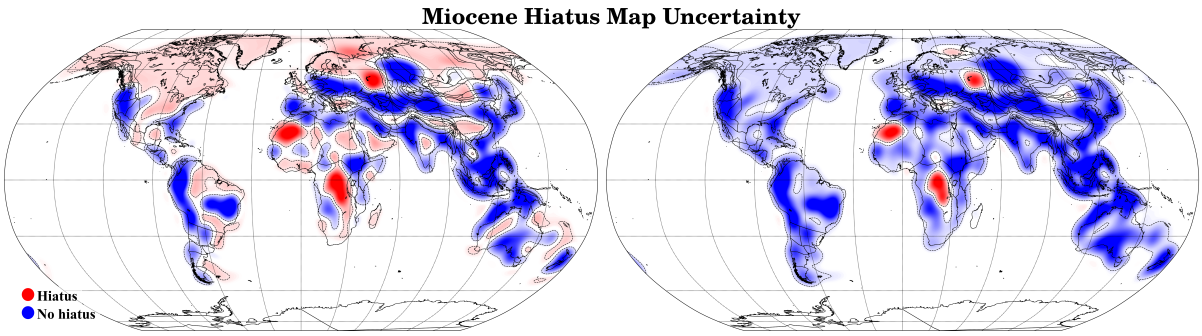

Figure 5.5: Two end-member scenarios of the Miocene hiatus map. Right: blank surfaces are hiatus, e.g. Miocene was never deposited. Left: blank surfaces are no hiatus, e.g. Miocene was deposited and later eroded (see text).

than 60% due to the prevalence of no hiatus areas in most of the maps (see Fig. 5.3). We also include (in shaded grey) the uncertainty range on the hiatus ratio curves, which are obtained when considering the blank surfaces as either hiatus or no hiatus, as explained above. Note that the uncertainty below the curve is smaller than the uncertainty above it, for instance in the global curve (Fig. 5.6a). This is because the no hiatus surfaces usually dominate most of the maps, and so filling the blank regions with the same signal has a smaller effect on the overall hiatus ratio. The ratio of hiatus to no hiatus exhibits significant changes in both time and space, even within the extreme uncertainty bounds defined before.

In the **Global curve** (Fig. 5.6a) the Oligocene and Pliocene show an anomalously high distribution of hiatus, with close to 40 % of the mapped area covered by hiatus surfaces. We note that these two geological series coincide with well-known sea-level drops due to the glaciation of the southern (De Lira Mota et al., 2023) and northern (Haug and Tiedemann, 1998) hemispheres, as previously discussed by Hayek et al. (2020), and suggest a eustatic component in the signal. In addition to the influence of glaciations, we can also observe very low hiatus ratios in the Upper and Lower Cretaceous. This widespread distribution of no hiatus surfaces coincides with the maximum peak of various sea-level curves (Müller et al., 2008; Rowley, 2017), even though their amplitude are not well constrained. The Upper Jurassic also has an anomalously high hiatus ratio, which is likely due to the inter-regional uplift in western Gondwana that has been related to the rise of the Tristan plume (Renne et al., 1992; Krob et al., 2020b; Vilacís et al., 2022).

To separate the effects of sea level from the dynamic topography, we also plot the continental regions individually. Figure 5.6b) shows a division of the continents mainly using the regionalisation of plate IDs defined in the static polygons provided by Matthews et al. (2016). Additionally we separate Oceania into two regions, Western Australia and East Oceania, and Asia into Central, East, and Southeast Asia. Figure 5.6c)–m) show the hiatus ratio for each study region, together with the associated uncertainty. Note that each curve reflects a unique regional dynamic evolution. In **North America** (Fig. 5.6c) we observe a pattern attributed to the development and disappearance of the Western Interior Seaway during the Cretaceous (low hiatus ratio) and its disappearance in the Paleocene (increase in hiatus ratio). Note that the North American curve has significant uncertainties during all geological series due to the large extent of blank regions. These include eastern North America, where rocks which predate the

study period are exposed at the surface due to glacial erosion events during the Phanerozoic, and Greenland, which only contains data in the coastal regions. **Europe** (Fig. 5.6d) shows a high hiatus ratio during the Paleocene, which precedes the arrival of the Iceland plume, and is followed by a drop in elevation during the Eocene. **South America** (Fig. 5.6e) shows subsi-

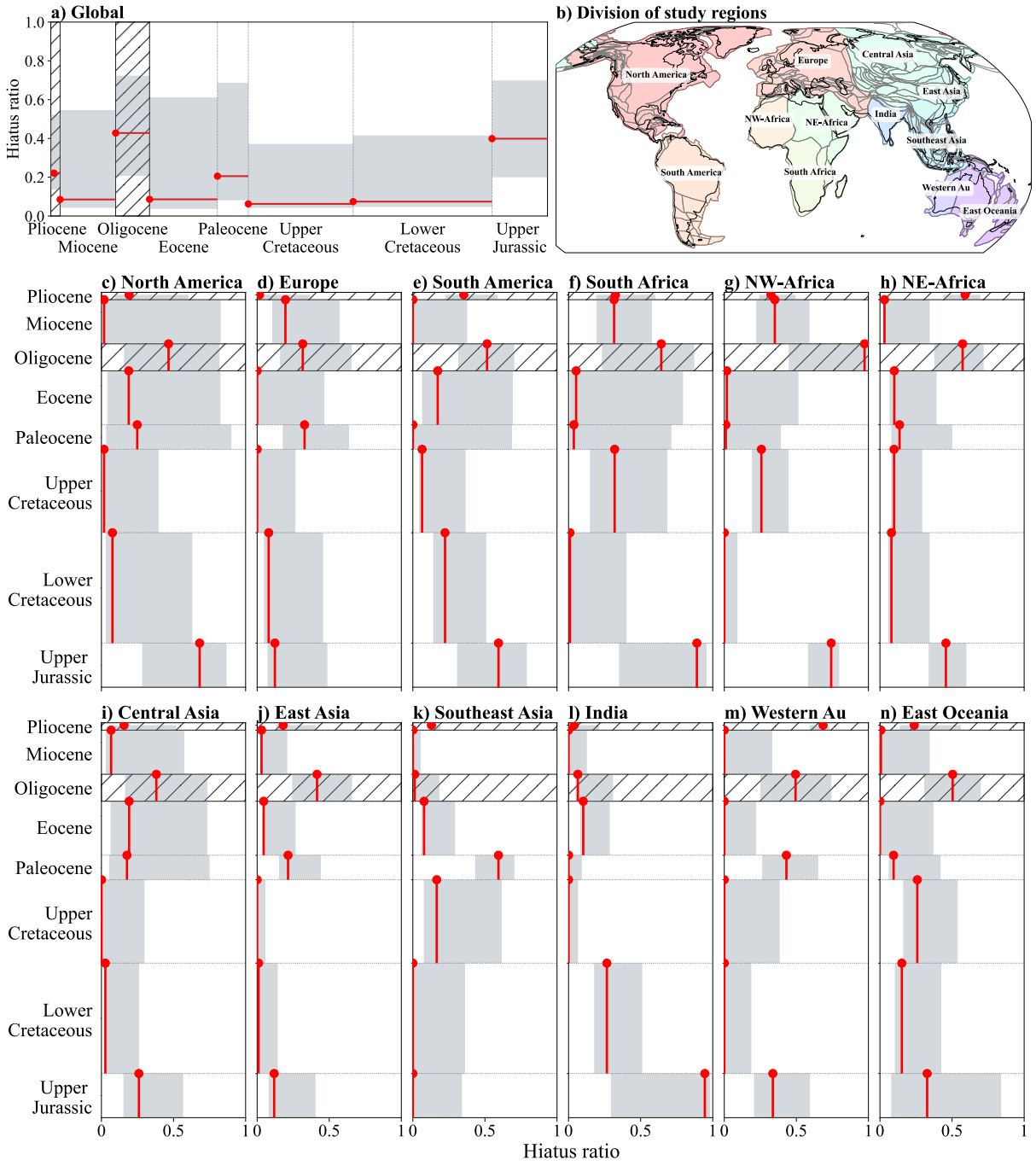

Figure 5.6: Global (a) and regional (c–n) hiatus ratios. The red line marks the hiatus ratio throughout the series considered, while red dots mark the datum. Shaded grey areas show the uncertainties of the hiatus ratio when considering blank areas as hiatus or no hiatus. A graphical example of the two possible end-member maps is shown in Fig. 5.5. The Pliocene and the Oligocene are hatched, indicating the glaciation of the northern and southern hemispheres respectively. Panel b) shows the division of the study regions by colour following the Plate ID and the static polygons from (Matthews et al., 2016) and their interaction with plume domains (see text).

dence during the Upper Cretaceous, following a topographic high in the Upper Jurassic. In the early Cenozoic, its elevation increases again, culminating with a peak in the Oligocene. Note that during the Paleocene and Eocene, the uncertainties cover more than 60 % of the area of the plot, reflecting the large coverage of blank areas. **South Africa** (Fig. 5.6f) shows high hiatus ratio in the Upper Cretaceous. In the Paleocene and the Eocene, the hiatus ratios are small, but similarly to South America, the uncertainty is substantially large due to the presence of blank regions and could indicate that the continent had a higher elevation, consistent with numerous studies that have suggested high Upper Cretaceous elevation in this region (Said et al., 2015b; Baby et al., 2020). **NW-Africa** (Fig. 5.6g) shows a high hiatus ratio in the Upper Cretaceous with a small uncertainty range, and in the Oligocene shows the highest hiatus ratio of all the regions with an uncertainty expanding to ∼50 % of the range. In contrast, **NE-Africa** (Fig. 5.6h) has only small variations in the hiatus ratio and its uncertainty through the studied time span, with a notably high hiatus ratio during the Oligocene. **Central Asia** (Fig. 5.6i) shows a low hiatus ratio during the Cretaceous and Cenozoic. In the Paleogene, the region shows an increase of hiatus ratio, which coincides with reports of uplift during the Oligocene in the West Siberian Basin (Vibe et al., 2018a). This region includes the Siberian Craton, where Precambrian rocks are exposed at the surface. As discussed previously, this leads to a blank region in the maps, resulting in large uncertainties. **East Asia** (Fig. 5.6j) primarily shows deposition during the study period, except during the Paleocene and Oligocene, when a higher hiatus ratio is recorded. **Southeast Asia** (Fig. 5.6k) has two series that stand out: the Paleocene and the Upper Cretaceous. The Upper Cretaceous maps is largely blank, which together with the hiatus surface in the following Paleocene indicates an absence of both Paleocene and Upper Cretaceous sediments. We note that this is opposite to the trend in the global sea-level curve during the Upper Cretaceous. **India** (Fig. 5.6l) shows a decrease in hiatus ratio from a topographic high in the Upper Jurassic to a minimum in the Upper Cretaceous. It does not change significantly during the Cenozoic. We note that the Upper Cretaceous rocks mapped in India are primarily volcanic and are therefore mapped as no hiatus during this series, as explained in the methods section. **Western Australia** (Fig. 5.6m) shows a pronounced increase in hiatus ratio during the Paleocene (Stotz et al., 2024). **East Oceania** (Fig. 5.6n) shows an increase in hiatus ratio from the Lower to the Upper Cretaceous, reflecting the retreat of the Eromanga Sea, which has been previously discussed in the literature (Gurnis, 1998; Harrington et al., 2019). As with most of the study regions, the Oligocene shows a high hiatus ratio.

5.4 Spectral analysis

Our spherical harmonic representation of the hiatus surfaces allows us to perform a spectral analysis. This enables us to quantitatively study the wavelengths and temporal changes of the structures present in our maps. The power spectrum ($S(l)$) is a measure of the strength of each spherical harmonic degree, and is expressed as

$$S(l) = \sum_{m=-l}^{l} |f_l^m|^2, \tag{5.1}$$

where l and m represent the spherical harmonic degree and order respectively, and f_f^m are the fully normalised spherical harmonic coefficients (Stacey and Davis, 2008).

Figure 5.7 shows the power spectrum of each hiatus map (black curves) and the uncertainty as given by the two end-member cases (see example in Fig. 5.5). Shaded red/blue regions represent the power spectrum of the expansion when blank surfaces are considered as hiatus/no hiatus. Recall that at degree 15, we apply a Gaussian filter that reduces the contributions of degrees ≥ 15, and it is therefore expected that the amplitudes in the power spectrum decrease above this point. For this reason, we mainly focus our analysis on degrees ≤ 15. Overall we see that each curve has distinct features and that longer wavelengths (degrees 1-8) tend to have higher contributions than shorter wavelengths. We note that the power spectra for geological series with higher hiatus ratios (Upper Jurassic, Paleocene, Oligocene, Pliocene) have distinct characteristics. The spectrum is flatter between degrees 1 and 15, with minor amplitude variations of ~ 0.02, and with a peak usually located between degrees 6–8. In contrast, the geological series dominated by sedimentation have higher contributions from the lowest spherical harmonics degrees. Their maximum peak is at degree 1 for the Upper/Lower Cretaceous and the Eocene, and at degree 2 for the Miocene. Furthermore, the contribution of higher degrees (5–15) reduces overall by a factor of ~ 5, except for the Lower Cretaceous. The blue and red curves show

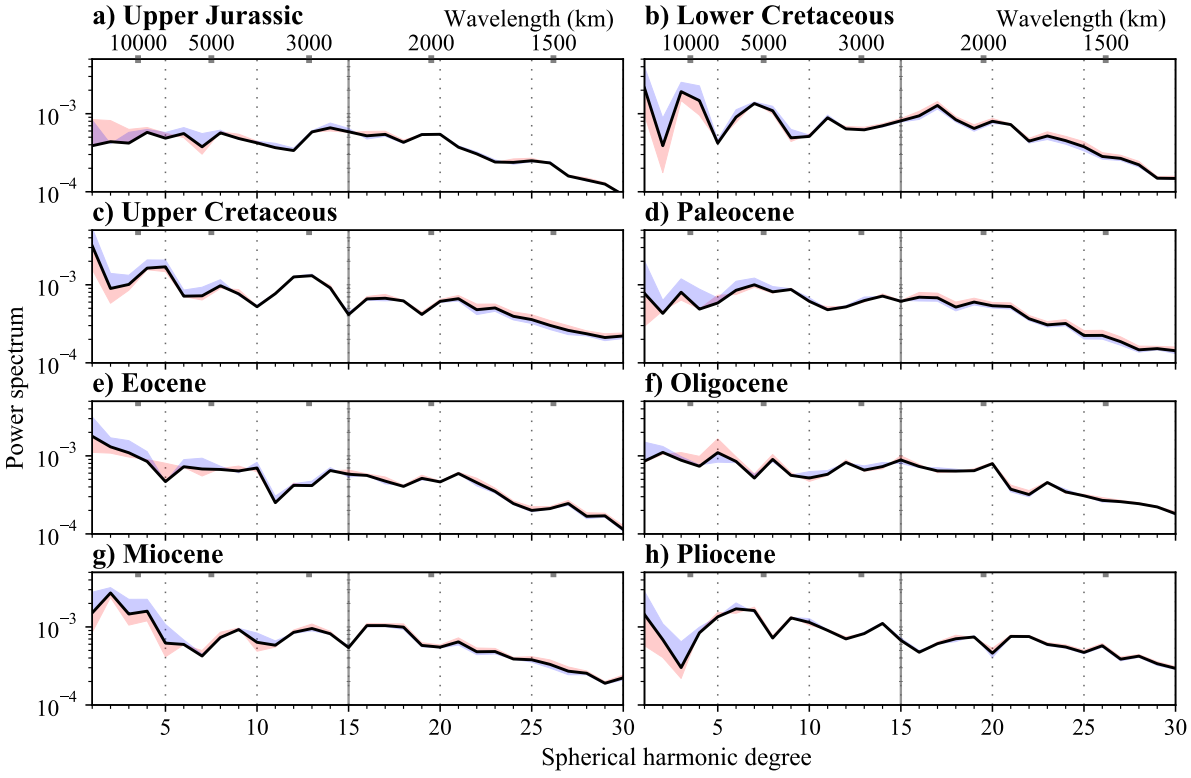

Figure 5.7: Power spectra for each geological series, obtained from the spherical harmonic expansion that generates each hiatus map. Shaded red/blue curves are the uncertainty curves generated when considering blank surfaces as hiatus/no hiatus signals. The vertical line at degree 15 indicates the start cutoff of the Gaussian filter. We identify a first group (Lower/Upper Cretaceous, Eocene and Miocene) with higher contributions from degrees 1 or 2 and a reduction for higher degrees. We distinguish these from the others (Upper Jurassic, Paleocene, Oligocene, and Pliocene) which have a flatter spectrum and minor amplitude variations (see text).

that the coverage of the blank regions with a hiatus/no hiatus largely affects the lower spherical harmonic degrees ($l \leq 10$). If we treat blank areas as no hiatus, the contribution from degrees 1–5 tends to increase. If treated as hiatus, we generally see a decrease in the contribution from degrees 1–4, with the exception of the Upper Jurassic. The red curve (blank areas treated as hiatus) in the Upper Jurassic shows a higher contribution from degrees 1–5 compared to the blue curve, placing the peak of the spectrum at degree 2. Of the geological series considered, the Upper Jurassic has the largest coherent hiatus surface. We interpret this as the latest stages of the rise of the Tristan plume, which were sampled by a large continental landmass (western Gondwana), as observed in Fig. 5.3a).

In addition to considering the spectrum of each map individually, we compare the changes between the maps over time using the two-time correlation function. This correlation compares two time steps in the spectral domain and is defined as the coefficient covariance divided by the product of the respective variances. It is therefore calculated as

$$R(t_1,t_2) = \frac{\sum\limits_{m,l} f^m_{t_1,l} f^m_{t_2,l}}{\sqrt{\sum\limits_{m,l} |f^m_{t_1,l}|^2 \sum\limits_{m,l} |f^m_{t_2,l}|^2}}, \tag{5.2}$$

where l and m represent the spherical harmonic degree and order, t_1 and t_2 the two geological series, $f_{t_1,l}$ and $f_{t_2,l}$ the fully normalised spherical harmonic coefficients (Stacey and Davis, 2008) at times t_1 and t_2 respectively, and $\sum_{m,l} = \sum_{l=0}^{l_{max}} \sum_{m=-l}^{l}$ with l_{max} being the maximum harmonic degree of the expansion. The value of the two-time correlation is normalised to between $+1$ and -1. A value of $+1$ corresponds to a perfect fit between the fields, 0 indicates no correlation, and -1 indicates a perfect anti-correlation. This correlation only measures similarities in shape and is not sensitive to amplitudes.

Figure 5.8 shows the two-time correlation between the different hiatus maps. These are calculated both at the present-day location of the continents (Fig. 5.8a) and with the continents reconstructed to their past configuration (Fig. 5.8b). The former is a representation of temporal changes within the continents. The latter is a representation of the dynamic topography changes, and thus the planform changes in the underlying mantle, as sampled by the continents over time. Both plots show values of $+1$ along the diagonal as this represents the correlation of a map with itself. The correlation decreases strongly away from the diagonal, with a maximum value of only $\sim$0.65, highlighting the change of the maps on the timescale of geological series. Panel a) displays darker colours compared to Panel b) showing a higher correlation between the signals when the continents are assumed fixed than when they are moving. This is expected. Our field is only mapped in the continents, and when they are moving there is an intrinsic decorrelation.

5.5 Discussion

Over the past several years, we have published a series of papers that make use of stratigraphic data sets in order to extract and infer past changes in dynamic topography, a key surface expression of mantle convection. Following the methodology introduced by Friedrich et al. (2018); Friedrich (2019), we began by mapping hiatus surfaces at the continental scale in Europe (Vibe

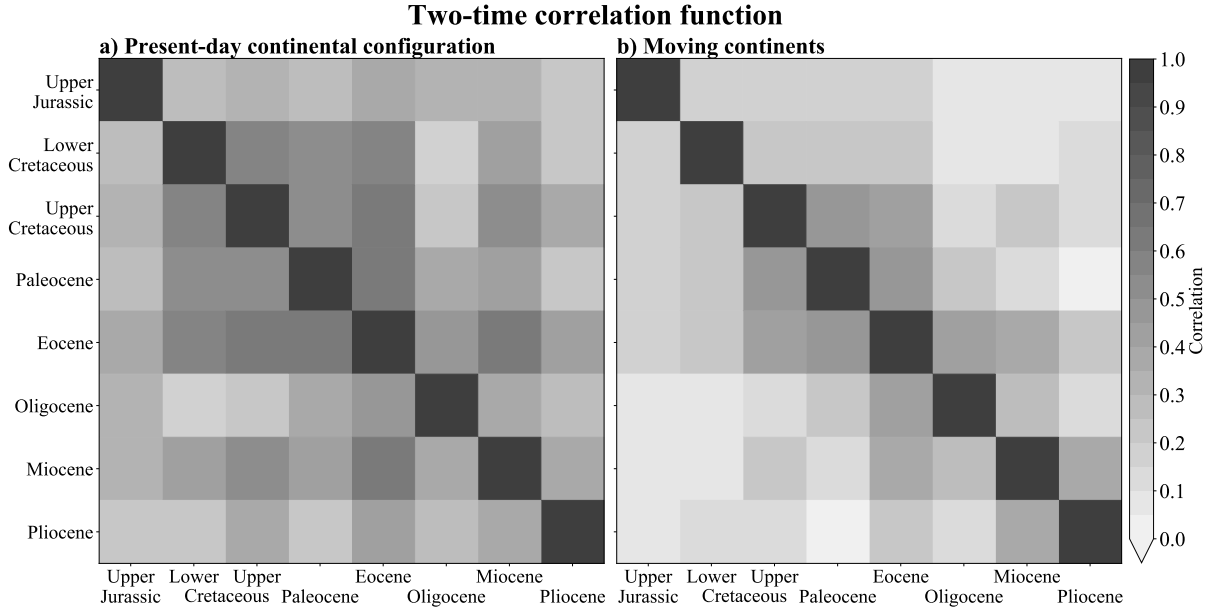

Figure 5.8: Two-time correlation function compares the spectral changes of two time series. $+1$ corresponds to a perfect fit between the fields, 0 no correlation and -1 a perfect anti-correlation. The correlation is a measure of similarities in shape and wavelength and is not sensitive to amplitudes. Panel a) shows the correlation calculated when the continents remain static at present-day location, whereas Panel b) shows the calculation when the continents are reconstructed to their paleolocations (see text). Note that the maximum value (away from the diagonal, where maps are correlated with themselves) is $\sim$0.65 and worsens when the continents are moving.

et al., 2018) and Africa (Carena et al., 2019). We then applied the method to the Atlantic Realm and Australia (Hayek et al., 2020, 2021; Vilacís et al., 2022; Stotz et al., 2024). Finally, in this work, we have included Asia, data from the continental shelf, and additional subsurface information. As in our previous studies, we have chosen to consider eight geological series spanning back to the Upper Jurassic, because this time span corresponds approximately to one transit time of the Earth's mantle (Iaffaldano and Bunge, 2015). This, in turn, corresponds to the timescale one would expect for mantle-flow-induced changes in topography. Extracting the hiatus/no hiatus surfaces at inter-regional scales provides us with a proxy for dynamic topography during a given geological series. Mapping this topography over time therefore allows us to track the temporal changes in the dynamic topography field. Hiatus maps therefore provide us with a powerful tool with which to observe the planform of mantle convection and investigate its spatial and temporal evolution within the Earth.

We observe that each map in Fig. 5.3 has a different hiatus/no hiatus distribution, indicating that the temporal evolution of dynamic topography is at least on the timescale of geological series. This is highlighted in Fig. 5.8, in which we find that the maps decorrelate over the timescale of a single series, whether or not lateral continental motion is considered. This timescale is much smaller than the mantle transit time (Iaffaldano and Bunge, 2015). This can be understood geodynamically through the so-called dynamic topography kernels (see Fig. 5.1b and Colli et al. (2016)). The kernels show that in the presence of a viscosity increase with depth, density anomalies produce significant surface deformations only in the upper mantle. Our maps therefore indicate that radial viscosity stratification exerts a strong control not only on the plan-

form of mantle convection (Bunge et al., 1996), but also on the temporal changes as viewed through our maps. This means, for instance, that the geological imprint of rising plumes may not be recorded until the latest stages of their transit through the mantle. It also means that detailed geological studies on the uplift history induced by mantle plumes allow for further constraints on the mantle viscosity structure (Şengör, 2001; Krob et al., 2020b).
We also observe that the maps have significant power at spherical harmonic degrees $\geq$2, expressed by the power spectrum curves (Fig. 5.7), meaning that the spectrum is flatter than one would expect from studies of the geoid. We recall that the geoid is sensitive to density anomalies as well as dynamic topography, which was understood early on by geodynamicists (Richards and Hager, 1984). Geoid undulations have the maximum contribution at degree 2 and a power loss between degrees 2–30 of four orders of magnitude (Pail et al., 2010). The flatter spectra of the hiatus maps is consistent with the present-day residual topography studies of Hoggard et al. (2016, 2017) and Holdt et al. (2022). These studies find that dynamic topography has significant contributions from spherical harmonic degrees up to $l \simeq 30$, which is equivalent to wavelengths of $\sim$1500 km. Furthermore, recent seismic tomographic models also find increasingly shorter wavelength anomalies in the upper mantle (e.g., Schaeffer and Lebedev, 2013a; Fichtner et al., 2018). The simultaneous presence of short-wavelength features in residual topography maps, hiatus maps, and upper mantle tomographic models is consistent with a surface dynamic topography field which is strongly influenced by asthenospheric temperature anomalies Hoggard et al. (2017).
We note that residual topography studies analyse the present-day state of the Earth, while the hiatus maps are indicative of dynamic topography at earlier times. However, if we assume that the temporal variation of dynamic topography since the Pliocene is small (Austermann et al., 2017), we can compare the Pliocene hiatus map, our most recent map, to the present-day residual topography map compiled by Holdt et al. (2022). Both maps are shown in Fig. 5.9 with the oceans removed from the map of Holdt et al. for a more direct comparison. Generally speaking, the polarity of the signals coincide. That is, regions of hiatus/no hiatus match to high/lower residual topography. A comparison of the power spectra (Fig. 5.9c) also shows similarities in their shape, with significant power up to degree 30. This is encouraging given that both maps are obtained from entirely different data sets.

Several well-known plumes can be linked to hiatus surfaces in our maps. This is perhaps most apparent in the Upper Jurassic, when we observe a hiatus surface in western Gondwana that precedes the arrival of the Tristan plume, and is followed by the eruption of the Paraná-Endeka flood basalts during the Lower Cretaceous (Renne et al., 1992). During the Cenozoic, we find a widespread absence of Paleocene rocks in Europe preceding the arrival of the Iceland plume (Saunders et al., 2007b; Parnell-Turner et al., 2014). In eastern Africa, an absence of Eocene rocks preceding the arrival of the Afar plume (Şengör, 2001). Finally, we observe hiatus surfaces and blank regions in Iberia and North Africa during the Oligocene preceding the formation of the Canaries archipelago (Meco et al., 2007; Troll and Carracedo, 2016; Sehrt et al., 2018). The absence of sedimentation prior to flood basalt eruptions can be seen as a characteristic expression of the latest stages of a plume rise (Şengör, 2001). In our maps, we observe that the hiatus lasts for at least a geological series, translating into a high hiatus ratio (see Fig. 5.6) and potentially allowing one to derive geological constraints on the mantle

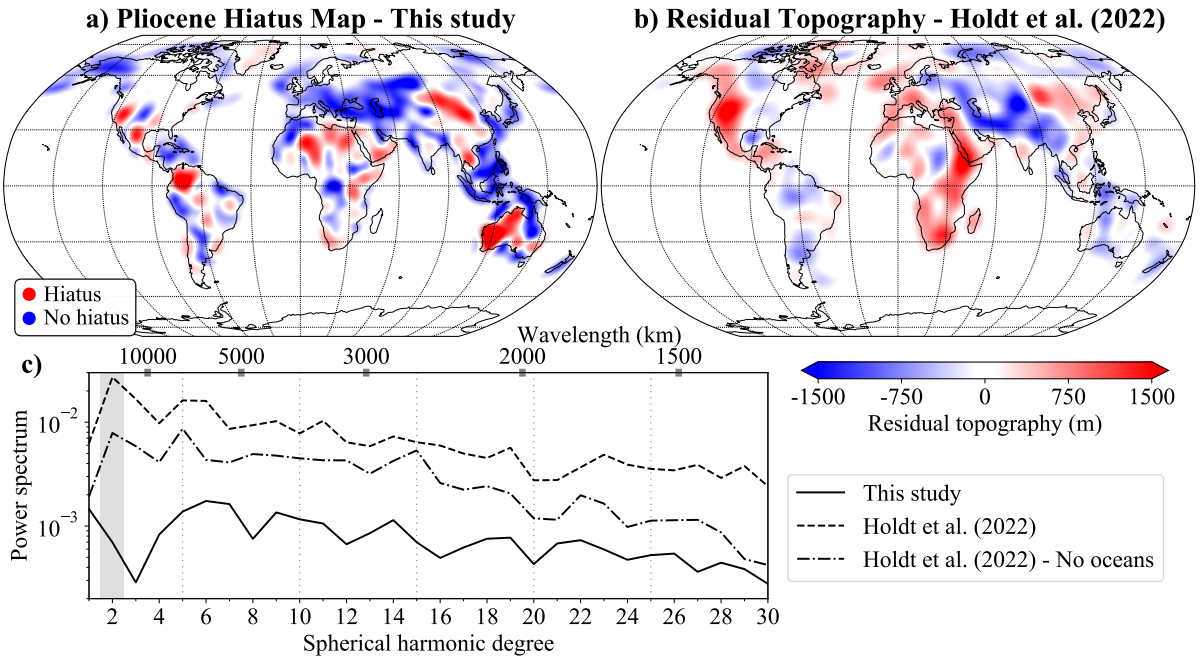

Figure 5.9: a) Pliocene hiatus map at present-day configuration with red/blue indicating hiatus/no hiatus of the Pliocene. b) Present-day residual topography from Holdt et al. (2022) without the oceans; red/blue indicates the amplitude of residual topography. c) Power spectrum of the Pliocene hiatus map and the global and (filtered) continental residual topography from Holdt et al.. Grey band in the power spectrum symbolises the maximum power spherical harmonic degree of the geoid. Note the flatter spectra of the hiatus map consistent with the recent residual topography study at present-day.

viscosity structure, as noted before. In addition to the planform of convection associated with rising plumes, we observe the long-lasting and long-wavelength features of subduction zones and their associated no hiatus signals. Clear examples include the subduction zone in South America during the Cretaceous and the Cenozoic, and the subduction zone on the East Asian margin throughout the Cretaceous and much of the Cenozoic.

We also observe some inter-regional sedimentary hiatuses which are not associated with any known plume or flood basalt eruption. For example, the maps show a hiatus surface in Western Africa during the Upper Cretaceous. This uplift was not followed by an eruption of flood basalts, but we speculate that this could still indicate the presence of a mantle plume that did not rupture the lithosphere. This would have fed the asthenosphere with hot material and induced minor volcanism in the surrounding regions. A similar mechanism was proposed by Oyarzun et al. (1997) for the Cape Verde-Canary plume system. Our maps show several other hiatus surfaces which occur far from plume arrival locations: the hiatus in Southeast Asia during the Upper Cretaceous–Paleocene (Clements et al., 2011a), the hiatus in East Asia during the Oligocene (Brown et al., 2022), and the hiatus in South America from the Paleocene–Oligocene (Wong, 1994; Horton, 2018). We posit that these events could be explained by the lateral transport of plume-sourced thermal anomalies in the asthenosphere, as implied by a Couette/Poiseuille model of asthenospheric flow (Höink and Lenardic, 2008, 2010; Höink et al., 2011; Höink et al., 2012). Geological (White and Lovell, 1997; Hartley et al., 2011; Colli et al., 2014; Parnell-Turner et al., 2014; Chen et al., 2021) and theoretical (Weismüller et al., 2015) estimates suggest asthenospheric flow velocities of 15–20 cm year^{-1}. This could allow for the transfer of buoyant,

plume-derived asthenospheric material over thousands of kilometres during the time span of a geological series. It is therefore plausible that the Paleocene–Oligocene hiatus in South America was caused by lateral flow from the Tristan plume (Colli et al., 2013; Vilacís et al., 2022; Stotz et al., 2023). In East and Southeast Asia, ridge subduction and the associated opening of slab windows allows for the lateral transfer of asthenospheric material from adjacent upwelling-dominated regions (e.g. the Tethys and Pacific domains). The Oligocene hiatus in East Asia has been linked explicitly to asthenospheric flow through the Izanagi-Pacific slab window (Brown et al., 2022), and a similar mechanism could be responsible for the hiatus in Southeast Asia during the Upper Cretaceous–Paleocene.

In summary, our maps highlight the influence of radial viscosity stratification on the planform of mantle convection in a number of different ways (Davies and Richards, 1992; Bunge and Richards, 1996; Lenardic et al., 2020; Hayek et al., 2020). Plume signals are largely damped until they reach the upper mantle (Colli et al., 2016, and Fig. 5.1b)). As a result, the characteristic plume stratigraphic signature of inter-regional hiatus followed by flood basalt eruption (Friedrich et al., 2018) presents itself on far shorter timescales than the mantle transit time, as reflected in our maps for several well-known plumes. A weak upper mantle relative to the lower mantle also plays a crucial role in generating sheet-like downwellings (slabs) (Bunge and Richards, 1996; Bunge et al., 1997; Richards et al., 2001; Richards and Lenardic, 2018; Cathles et al., 2023), which are reflected in our maps as continuous, long-wavelength no hiatus signals. Moreover, channelised flow within the asthenosphere allows for the long-distance transport of plume-sourced thermal anomalies, inducing inter-regional hiatus surfaces far from plumes (Oyarzun et al., 1997; Clements et al., 2011a; Vilacís et al., 2022; Brown et al., 2022), and flattening the spectra of both the hiatus (Fig. 5.7) and residual topography maps (Hoggard et al., 2016, 2017; Holdt et al., 2022, and Fig. 5.9). All in all, the maps therefore provide a window into the planform of mantle convection, and a powerful new constraint on models which seek to reconstruct past mantle dynamics.

5.5.1 The influence of sea-level variations

Any discussion of hiatus surfaces must also consider the effect of sea-level changes, which, at least on regional scales, are indistinguishable from dynamic topographic changes (i.e. variations in base level). In the global hiatus ratio curve (Fig. 5.6a) the Oligocene and Pliocene show an anomalously high distribution of hiatus. This high ratio occurs also in every regional curve except Southeast Asia and India in the Oligocene, and Europe and India in the Pliocene. The global curve also shows low hiatus ratios in the Upper and Lower Cretaceous. A reduction in hiatus ratio is present in all regional curves during the Lower Cretaceous. This also occurs in all curves during the Upper Cretaceous except for South Africa, Northwest Africa, Southeast Asia, and East Oceania. As noted before (Hayek et al., 2020), the two peaks in hiatus ratio during the Oligocene and Pliocene coincide with well-known sea-level drops due to the glaciation of the southern (De Lira Mota et al., 2023) and northern (Haug and Tiedemann, 1998) hemispheres, while the Cretaceous low hiatus ratio coincides with the maximum peak of various sea-level curves (Müller et al., 2008; Rowley, 2017). This highlights the importance of adopting a global perspective, in which sediment distribution is compared across continents when

inferring sea-level changes. Studies of individual regions (e.g., the North American flooding record (Tasistro-Hart and Macdonald, 2023)) instead could be affected by dynamic topography, because there is no such thing as a stable platform (Moucha et al., 2008a). We note that a global eustatic signal can be superimposed on regional dynamic topography changes. For instance, the Cretaceous subsidence of North America due to the subduction of the Farallon plate is well-known (Mitrovica et al., 1989; Burgess et al., 1997), and a link between the Oligocene hiatus in East Asia and mantle dynamics has recently been proposed (Brown et al., 2022), providing examples where the eustatic and the dynamic topography signal reinforce each other. Our regional curves also provide examples for sea-level variations and dynamic topography changes with opposing effects. For instance, the increase in hiatus ratio during the Upper Cretaceous in South Africa and Southeast Asia reflects uplift events for these regions that have been noted before (Baby et al., 2020; Clements et al., 2011a). Finally, our maps indicate that the late Eocene–early Oligocene sea-level drop of $\sim$80 m (Miller et al., 2020; De Lira Mota et al., 2023) resulted in extended global hiatus surfaces. This is interesting because it suggests that a change in base level on the order of $\sim$100 m induced either by eustasy or dynamic topography can produce a continent scale sedimentation signal.

5.5.2 Key hiatus/no hiatus surfaces

We assembled the hiatus/no hiatus data set with a geodynamic purpose. Mantle circulation models (MCMs) are now widely used in global geodynamics (e.g., Bunge et al., 2002b; McNamara and Zhong, 2005a; Zhong et al., 2008; Müller et al., 2018b). These models assimilate plate motion histories (e.g., Müller et al., 2016) to simulate the evolution of past mantle flow, meaning that the horizontal component of the surface velocity is used as an input. At the same time, MCMs make predictions of past dynamic topography, meaning that the latter is an output of the models. Global hiatus maps therefore lend themselves as an observational tool to test the specific parameter assumptions adopted in any given MCM.
From the hiatus maps, we identify several key events which MCMs should aim to reproduce. Listed in chronological order they are:

(1) The extensive hiatus surface in western Gondwana during the Upper Jurassic, linked to the arrival of the Tristan plume. Previous studies (Krob et al., 2020b) have already related this uplift to the latest stages of the rise of this plume.

(2) The development of the Western Interior Seaway in North America during the Cretaceous, linked to the lithosphere's response to the subducting the Farallon slab (Mitrovica et al., 1989; Burgess et al., 1997).

(3) The hiatus surface in South Africa during the Upper Cretaceous, which coincides with increased sedimentation rate along the continental margin (Said et al., 2015b; Baby et al., 2020). We have speculated earlier (Vilacís et al., 2022) that this uplift could be induced by the arrival of the Marion plume (Storey et al., 1995).

(4) The absence of Upper Cretaceous and Paleocene sediments in Southeast Asia. This event has been linked by Clements et al. (2011a) to dynamic rebound. It could also be related to the transport of hot asthenospheric material (Brown et al., 2022) from an adjacent domain, either from the Tethys side due to the subduction of the Wharton Ridge (Whittaker et al.,

2007), or from the Pacific side due to gaps in subduction which could have existed during the late Mesozoic (Lin et al., 2022).

(5) The high proxy elevation in Europe during the Paleocene, likely related to the arrival of the Iceland plume at the Paleocene-Eocene boundary (Saunders et al., 2007b; Parnell-Turner et al., 2014; Vibe et al., 2018).

(6) The near-continental scale absence of sediments in South America from the Paleocene–Oligocene. Multiple studies have noted this long-standing hiatus (Wong, 1994; Gerster et al., 2011; Horton, 2018; Cuitiña et al., 2019), which also coincides with anomalous volcanism in the Rio Grande Rise (RGR) and the early Eocene subaerial exposure of the RGR at Drill Site 516 (Barker, 1983).

(7) The lack of Oligocene sediments throughout much of Africa (Burke and Gunnell, 2008). Carena et al. (2019) showed that this cannot simply be a result of the concurrent Oligocene sea-level drop.

(8) The extensive hiatus in East Asia during the late Eocene–Oligocene. This event has been linked to hot asthenospheric flow between the Pacific and Asian domains during the subduction of the Izanagi-Pacific ridge (Brown et al., 2022). However, the high degree of uncertainty of tectonic reconstructions in this region (e.g., Wu et al., 2016) means that the precise combination of subduction and asthenospheric flow remains poorly known.

Geodynamicists have already attempted to reproduce some of these events. For instance, Conrad and Gurnis (2003) used a backward mantle flow model to reconstruct the uplift history of Africa during the Cenozoic and late Mesozoic. Colli et al. (2018) employed the adjoint method (Bunge et al., 2003a) to model the dynamic topography history in the Atlantic Realm. Ghelichkhan et al. (2021) have attempted to reproduce a variety of different uplift and subsidence events during the Cenozoic, also using global adjoint simulations. We note that Liu et al. (2008), using a regional adjoint model, had previously tried to model the uplift history of western North America. However, their use of a "stress guide", an artificial viscosity barrier in the upper mantle that affects the form of the surface topography kernel and largely decouples the modelled uplift history from the modelled flow history, makes their results difficult to interpret.

5.5.3 Limitations and uncertainties

Our hiatus mapping approach entails a number of uncertainties which we have extensively discussed in Hayek et al. (2020). The maps have limited data coverage and include non-standardised geological maps (e.g. different languages and age/naming conventions). In this work, we tried to alleviate the lack of data coverage by including subsurface (e.g. drill cores and stratigraphic columns) and shelf information. This expanded the observational data set and reduced the extent of blank surfaces, especially when younger sediments cover an area and thus the older rocks are not mapped at the surface. For example, in North America, the COSUNA dataset (Childs, 1985, a compilation of stratigraphic studies that covers the geology of the United States) helped to constrain the blank areas along the east coast and the west of the country. We also extended our mapping to include data in the continental shelf extracted from geological maps, IODP cores, and chronostratigraphic columns. In the North Atlantic, for instance, we have included a combination of data contained in the geological map of Europe

(Asch, 2004) and the stratigraphic columns compiled by (Hopper et al., 2014b). We note that this introduces an inherent bias towards sedimentation: the interpretation of sedimentation in the continents and the continental shelf differ due to their differing elevation. Even in the case of an uplift, the continental shelf might remain covered by sediments. On the other hand, when a hiatus is recorded on the shelf, it indicates a significant uplift event, and is therefore relevant to map. Future work could consider additional information such as paleoaltimetry estimates (Kohn, 2007), studies of river profiles (e.g., Roberts and White, 2010), landforms (Guillocheau et al., 2018) and sediment provenance (Şengör, 2001; Meinhold, 2010), constraints from thermochronology (Ehlers and Farley, 2003; Flowers et al., 2008; Reiners and Brandon, 2006; Hodges, 2003), paleobiological and paleoenvironmental data (Fernandes and Roberts, 2020), and quantifications of sediment budgets at the scale of continental margins (Guillocheau et al., 2012; Said et al., 2015a,b). Studies of deep-sea carbonate (Dutkiewicz et al., 2018), carbonate compensation depths (Dutkiewicz and Müller, 2021), and deep-sea hiatuses (Dutkiewicz and Müller, 2022) can provide constraints on the distribution of seafloor sediments through time and the processes that have driven them.

In this work, we had to resort to a mixture of digital and manual data extraction. For example, data was mapped manually for Africa or Asia, because there are no digital geological maps available at the temporal resolution of geological series. Hence we relied on standard map reading and the use of additional resources wherever available (see Table 1 in the supplementary material). It is crucial that future geological maps are made available in digital form at continental-scale and temporal resolution of geological stages, as advocated by Friedrich (2019).

In our previous work, we quantified uncertainties by varying the cut-off degree of the spherical harmonic expansion. Here we followed the approach from Carena et al. (2019) and introduced a hiatus/no hiatus signal in the blank regions (see Fig. 5.5), as explained in Section 5.3.2. This choice represents two end-member cases, and provides us with maximum bounds on the uncertainty. This is particularly evident for South America from the Paleocene–Oligocene, where it could be argued that a late uplift in the Oligocene eroded the previous geological series (Eocene and Paleocene), or that the paleotopography was high from the Paleocene onwards.

We reconstructed the hiatus surfaces to their paleolocations using the plate tectonic model from Müller et al. (2022). This is a Phanerozoic plate motion model based on a paleomagnetic reference frame optimised to constrain mantle flow models with a set of "tectonic rules" (see Müller et al., 2022, for further information). However, the choice of reference frame is an open question. Other choices include the Indo-Atlantic (O'Neill et al., 2005) and global moving hotspot (Steinberger and Torsvik, 2008) reference frames, or a combination of global moving hotspots and True Polar Wander (Torsvik et al., 2008). Merdith et al. (2021) provides a summary of the reference frames used by each plate tectonic model from the EarthByte group in the last decade. MCMs yield different flow histories based on the choice of reference frame (Shephard et al., 2012), and thus a comparison between the hiatus maps and MCM outputs should eventually account for this.

5.6 Conclusions

Planforms are a defining feature of convecting fluids. Here we show that the planform of mantle convection can be tracked through the dynamic topography that it induces. The dynamic topography in turn is revealed through its effect on the evolution of continent-scale stratigraphy, which can be extracted by mapping inter-regional hiatus and no hiatus surfaces over geological time. In this work, we have carried out this mapping for all continents apart from Antarctica since the Upper Jurassic. We chose this timescale due to geodynamic considerations, as this corresponds to a single mantle transit time. The hiatus surfaces are reflective of dynamic uplift events, while no hiatus surfaces reflect dynamic subsidence. We have found that the hiatus surfaces change on the timescales of geological series, meaning that the underlying dynamic topography and therefore the planform of convection changes at least on timescales of 10–20 Myrs. Future mapping on the timescale of geological stages may reveal changes at a finer temporal resolution. The spatial scale of these events (wavelengths on the order of 10^3 km) is significantly smaller than the lengthscales of dynamic topography implied by the geoid. We also find that known flood basalt eruptions are frequently preceded by hiatus surfaces, as expected. Some hiatus surfaces, however, are not linked to any known plume. These may reflect lateral transport in the asthenosphere. Several characteristics of our maps (e.g. rapid time variations and small spatial scales, as noted above) reflect the dominant influence of radial viscosity stratification on the planform of convection. We propose that MCMs and adjoint geodynamic models should aim to reproduce these global characteristics, as well as specific regional events. To this end, we have identified a set of eight prominent events which should eventually be reproduced in global geodynamic models. By covering all continents apart from Antarctica, we have been able to disentangle the effect of sea-level variations from regional changes in base level induced by dynamic topography. Sea-level effects can be extracted from our maps as global increases/decreases in hiatus ratio. They are seen most prominently during the Cretaceous and the Oligocene, reflecting a sea-level high-stand in the former and the onset of Antarctic glaciation in the latter. This means that geodynamicists should take additional care when interpreting dynamic topographic events during these times.

Chapter 6

Conclusions and Outlook

The main objective of this thesis is to utilise the geological record to infer the spatial and temporal patterns of dynamic topography. This work further develops the hiatus mapping methodology and applies it to all the continents with a combination of digital and manual processing. The outcome of this research is eight hiatus maps that cover all continents and the continental shelves (except Antarctica), separated temporally in geological series since the Upper Jurassic. Each hiatus map represents the accumulation of processes that occur during a given geological series and can be considered as a proxy for the vertical motion that the area has undergone (i.e., dynamic topography). Thus, the convective system is mapped over time. The resulting maps facilitate the observation of mantle convection patterns and the inference of links between specific hiatus surfaces, mantle convection processes, and changes in the horizontal motion of the lithosphere.

The main observation is that each hiatus maps systematically differs, showing changes in the hiatus surface patterns at timescales of geological series (approximately between 10 Myrs to 20 Myrs in the Cenozoic). The timescale of these dynamic topography changes is significantly shorter than the mantle transit time, which would be the first-order expectation for the timing of mantle flow-induced changes in topography. This rapid change indicates and corroborates the findings that the mantle is not isoviscous (i.e., constant radial viscosity), but has a radial viscous stratification, with the upper mantle being weaker (less viscous) than the lower mantle. Consequently, the geological imprint of rising mantle plumes may not be recorded until the final stages of their transit through the mantle. Furthermore, the maps show that the hiatus surfaces have wavelengths between 2000 km to 3000 km in diameter. These wavelengths are significantly shorter than those inferred from the geoid and coincide with the wavelengths inferred from present-day residual topography studies.

The hiatus maps regularly show a widespread absence of sedimentary rocks at the continental scale before the arrival of a mantle plume beneath the lithosphere. This hiatus surface appears a geological series before the flood basalt eruption associated with a mantle plume. There are several hiatus surfaces within the maps, which can be associated with well-known plumes. The most prominent instance is observed in western Gondwana, with a hiatus surface in the Upper Jurassic, indicating an uplift of the region, that precedes the arrival of the Tristan plume. This uplift is followed by the eruption of the Paraná-Endeka flood basalts during the Lower Cretaceous. Another example is the widespread hiatus of Paleocene rocks in Europe,

which precedes the arrival of the Iceland plume and subsequent flood basalt eruptions during the Paleocene-Eocene transition. For further examples, see Chapters 2 and 5. The hiatus maps show that these hiatus surfaces persist across a geological series prior to the onset of extensive volcanism. It may be possible that this temporal span could be reduced by creating hiatus maps at the resolution of geological stages, thereby providing additional constraints on the radial viscosity structure of the Earth's mantle.

In addition, the present study demonstrates that the vertical and horizontal motion of the lithosphere are related, showing a frequent correlation between the appearance of a hiatus surfaces and a subsequent plate motion change. However, we find that this is not the case in locations where plate boundary forces might play a significant role, e.g., in the Indian Realm. This work utilises the theoretical framework of Couette/Poiseuille flow in the asthenosphere to relate these two observations. We observe that there is a time delay on the order of a geological series between the occurrence of a continent-scale hiatus and a plate motion change. This time delay can be explained because the uplift induced by the rising plume, occurs only during the latest stages of the ascent, when the plume is in the upper mantle, but not yet in the asthenosphere. Conversely, the basal shear stresses inducing plate motion changes are only generated when the plume material reaches the asthenosphere. In summary, the uplift occurs before the plume material shears the base of the lithosphere, resulting in a time delay between these observations. For example, the hiatus surface during the Upper Jurassic in Western Gondwana, associated with the uplift of the Tristan plume, is followed by the initiation of seafloor spreading in the South Atlantic. Similarly, the hiatus during the Paleocene in Europe is followed by an increase in spreading rates in the North Atlantic during the early Eocene. Furthermore, in the case study of the South Atlantic realm (Chapter 4), we show that the South American plate experiences two plate motion changes in the Paleogene (comprising the Paleocene, Eocene and Oligocene). These changes can be attributed to the Sierra Leone plume and one of the pulses of the Tristan plume. These tectonic events are preceded by a general absence of Paleocene, Eocene and Oligocene sediments in South America and Southern Africa. They also coincide with the early Eocene subaereal exposure of the Rio Grande Rise.

The asthenosphere plays another important role in influencing the hiatus maps. There are inter-regional hiatuses that are not associated with subsequent flood basalt eruptions and occur far from plume arrival locations. These hiatuses can be created by plume material spreading laterally in the asthenosphere for 1000s of kilometres. For example, there is a hiatus surface in Western Africa during the Upper Cretaceous, a hiatus in South America from the Paleocene to the Oligocene or an Oligocene hiatus in East Asia. None of these hiatus occurrences were followed by a flood basalt eruption. In consequence, they could either indicate the presence of a mantle plume that didn't break the lithosphere, or the lateral transport of hot material within the asthenosphere, as implied by a Couette/Poiseuille model of asthenospheric flow.

Global sea-level changes also need to be considered for the interpretation of the hiatus maps, as their imprint on the geological record is indistinguishable from dynamic topography changes (i.e. variations in base level) on the regional scale. Accordingly, the hiatus maps always showed an anomalously high distribution of hiatus in the the Oligocene and Pliocene, which coincide with well-known global sea-level drops to the glaciation of the southern and northern hemispheres, respectively. Contrarily, we also observed globally low amounts of hiatus in the Upper

and Lower Cretaceous, in agreement with the maximum peak of various sea-level curves. This shows the importance of adopting a global perspective, in which sediment distribution is compared across continents when inferring sea-level changes. Moreover, individual regions can be affected at the same time by dynamic topography and global eustatic changes. These can be superimposed or have opposing effects. For instance, while global sea-level changes strongly influence hiatus formation in the Oligocene and Pliocene, the hiatus patterns observed in the Oligocene in East Asia are more consistent with dynamic topography effects. Furthermore, the sea-level drop in the Oligocene, which was on the order of $\sim$100 m, shows that a change in base level of this magnitude, either by eustacy or dynamic topography, can produce a continental scale sedimentation signal. This effect has to be considered when comparing the hiatus maps to other data sets or models that do not have sea-level variations included.

The results of this dissertation provide new insights into the wavelengths of dynamic topography and the timescales at which it changes. They highlight the importance of the viscosity stratification in shaping mantle convection and its planform. They also emphasise the necessity of a weak asthenosphere to facilitate transportation of hot plume material over long distances and induce plate motion changes while shearing the base of the lithosphere. Detailed geological studies of specific mantle plumes, and the uplift history they induce, would provide additional constraints on the structure of mantle viscosity. These results also suggest that the characteristic expression of the rise of a mantle plume can be seen as the absence of sediments at continental scale within 10 Myrs to 20 Myrs before the flood basalt eruption followed by a plate motion change.

The hiatus maps provide, for the first time, a proxy for observing time-dependent dynamic topography patterns at the geological series time resolution. They can be employed to test and further constrain mantle circulation models and the model parameters of the Earth that remain unclear. These maps can be used in conjunction with other observations such as the geoid or the present-day dynamic topography. Furthermore, it is important to consider the influence of sea-level variations when studying observations that are sensitive to this effect. Finally, it is recommended that future geodynamic Earth models aim to replicate first the global characteristics of the hiatus maps and then specific regional events that can be inferred from them, as a way to further develop our understanding of the Earth's convective system.

Appendix A

Data sources

The following are the extended data references used in Vilacís et al. (2024) to cover Asia and Oceania with the hiatus mapping, and to expand the coverage of previously mapped regions.

Region		Type	Source
North America		Correlation charts	COSUNA (Childs, 1985) Alberta Geological Survey (2019) McAlpine (1990) Core Labs (2014) Saskatchewan (2022) Nicolas (2020)
South America	Andean Basins	Journal article	Horton (2018)
	Falkland Plateau	Journal article	Stanca et al. (2022)
	Colorado Basin	Journal article	Gerster et al. (2011)
	Brazil Basins	Journal articles	Milani et al. (2007) Batezelli and Ladeira (2016)
	Austral-Magallanes	Journal article	Cuitiña et al. (2019)
	Tierra del Fuego	Journal article	Gallardo Jara et al. (2019)
North Atlantic		Correlation chart Journal article	Hopper et al. (2014a,b) Gregersen et al. (2019)
Europe	United Kingdom	Correlation charts	Waters et al. (2007a,b)
	Germany	Correlation chart	Menning and Hendrich (2016)
	Poland	Journal article	Wagner (2008)
	France	Journal articles	Sissingh (2006) Callec et al. (2006)
	Iberian Peninsula	Journal articles	De Vicente et al. (2011) Do Couto et al. (2016)
Asia and Europe		Geological map	Tingdong (1997)
Asia	Eastern Russia	Online resources Journal articles	The Geotraverse Project (2001–2016) Lindquist (2000)

Region		Type	Source
	West Siberian Basin	Journal article	Vibe et al. (2018a)
	SE Russia and NE China	Journal article	Kirillova (2003); Cao et al. (2013)
			Petit and Déverchère (2006)
	Pakistan	Geological map	Bahr et al. (1964)
		Journal article	Asghar et al. (2021)
	India	Geological map	Geological Survey of India (1993)
		Journal articles	Hansen et al. (2005)
			Prasad and Pundir (2019)
			Asim et al. (2014)
		Book chapters	Bastia and Radhakrishna (2012)
			Valdiya (2016)
		Online database	Government of India (2021)
	Central Asia	Geological map	Hwang et al. (2008)
		Journal articles	Abdullayev et al. (2017)
			Smith-Rouch (2006)
			Ulmishek (2004, 2001a,b,c)
			Abreu and Nummedal (2007)
			Shi et al. (2016)
			Sepehr and Cosgrove (2004)
			Rahimpour-Bonab et al. (2007)
			Aubekerov et al. (2010)
			Rabbani (2008)
			Jaireth et al. (2008)
		Book chapter	Lucas et al. (2000)
	China offshore basins	Book chapter	Wang et al. (2014)
		Journal article	Chang et al. (2018)
	China onshore basins	Journal articles	An et al. (2018)
			Xi et al. (2019); Cao (2018)
			Zhu et al. (2020a,b)
			Cheng et al. (2018)
			Graham et al. (2005)
			Li et al. (2016)
			Suo et al. (2020)
			Zheng (2015)
			Song et al. (2018)
			Jiaodong et al. (2012)
			Meng et al. (2003)
			Yan et al. (2007)
	Taiwan and South China Sea	Journal articles	Deng et al. (2020)
			Savva et al. (2014)
			Fang et al. (2017)
			Lin et al. (2003, 2021)

Region		Type	Source
			Teng et al. (1991)
			Ho (1986); Huang et al. (2020)
	East China Sea	Journal articles	Wang et al. (2019)
			Yang et al. (2016)
	South, East and	Geologic map	Ghose et al. (1990)
	Southeast Asia	Journal articles	Wang et al. (2020)
			Zhou et al. (2019)
			Yang et al. (2020)
			Panggabean and Heryanto (2009)
			Doust and Noble (2008)
			Clements et al. (2011a)
			Cottam et al. (2011)
			De Smet and Barber (2005)
			Rigg and Hall (2011)
		Online resources	CCOP (2002)
	Japan	Geological map	GS Japan (1982)
		Journal article	Taira et al. (1982)
		Book chapters	Takano (2017)
			Takashima et al. (2017)
	Sea of Japan	Drilling log	Ingle (1992)
		Journal article	Kano et al. (2007)
	Malaysia	Geological map	GGS Malaysia (1996)
			Tate et al. (2008)
	Thailand	Geological map	GSD Thailand (1999)
		Journal article	Charusiri and Pum-Im (2021)
Papua New Guinea		Journal articles	Marlow et al. (1988)
			Carman (1992)
Australia		Compilation of data	Stotz et al. (2024)
New Zealand		Journal articles	Rotzien et al. (2014)
			Strogen et al. (2017)
			Bland et al. (2015)
			Haque et al. (2016)
			Uruski et al. (2003)
		Thesis	Samuel (2010)
		Geological map	New Zealand GS (1972)
Arctic		Geological map	Harrison et al. (2011)
World - Sedimentary Basins		Online resource	CGG-Robertson (2022)

Table A.1: List of data sources used to extend the data set, where *GS* stands for Geological Survey. The column Type refers to the source used, as in Carena *et al.* Carena et al. (2019).

Bibliography

Abdullayev, N. A., Kadirov, F., and Guliyev, I. S. Subsidence history and basin-fill evolution in the South Caspian Basin from geophysical mapping, flexural backstripping, forward lithospheric modelling and gravity modelling. *Geological Society, London, Special Publications*, 427(1):175–196, 2017. doi:10.1144/SP427.5.

Abreu, V. and Nummedal, D. Miocene to Quaternary sequence stratigraphy of the South and Central Caspian Basins. In Yilmaz, P. O. and Isaksen, G. H., editors, *Oil and gas of the Greater Caspian Area*, pages 65–86. American Association of Petroleum Geologists, 01 2007. ISBN 9781629810348. doi:10.1306/1205845St553000. Volume 55.

Alberta Geological Survey. Alberta Table of Formations, 2019. Alberta Energy Regulator, Last accessed 2021, `https://ags.aer.ca/publications/Table_of_Formations_2019.html`.

An, K., Lin, X., Wu, L., Cheng, X., Chen, H., Ding, W., Zhang, F., Gong, J., Yang, R., Zhu, K., Li, C., Zhang, Y., and Gao, S. Reorganization of sediment dispersal in the Jiuxi Basin at $\sim$ 17 *Ma* and its implications for uplift of the NE Tibetan Plateau. *Palaeogeography, Palaeoclimatology, Palaeoecology*, 511:558–576, 2018. ISSN 0031-0182. doi:10.1016/j.palaeo.2018.09.022.

Anell, I., Thybom, H., and Artemieva, I. M. Cenozoic uplift and subsidence in the north atlantic region: Geological evidence revisited. *Tectonophysics*, 474(1):78–105, 2009. ISSN 0040-1951. doi:10.1016/j.tecto.2009.04.006. TOPO-EUROPE: The Geoscience of coupled deep Earth-surface processes.

Asch, K. IGME 5000. 1:5 million international geological map of Europe and adjacent areas. *BGR (Hannover)*, 2004.

Asghar, H., Mughal, M. S., Khan, M. S., Abbas, S., Hanif, M., Hussain, G., Ali, M., Ali, K., and Hussain, A. Biostratigraphic investigation and depositional model of the Late Thanetian Ranikot and the Ypresian Laki formations in the subsurface of the Southern Indus Basin, Pakistan. *Arabian Journal of Geosciences*, 14(13):1264, 2021. doi:10.1007/s12517-021-07530-4.

Asim, S., Kahn, N., Qureshi, S. N., Hussain, F., and Bablani, S. A. Study of a stratigraphic trap of Paleocene/Late Cretaceous age with the help of seismic data in Sulaiman Foredeep and Kirthar Foredeep area (Central & Southern Indus Basin, Pakistan). *International Journal of Geosciences*, 5(10):1049–1061, 2014. doi:10.4236/ijg.2014.510090.

Aubekerov, B. Z., Koshkin, V., Renato, S., A., N. S., and Jean-Marc, D. Prehistorical and historical stages of development of Lake Balkhash. In Watanabe, M. and Kubota, J., editors, *Reconceptualizing cultural and environmental change in Central Asia: An historical per-*

spective on the future. Proceedings of the International Workshop (Kyoto, Japan 1-2 February 2009), pages 49–76. Kyoto-Research Institute for Humanity and Nature, Kyoto, Japan, 2010. Ili Project.

Austermann, J., Mitrovica, J. X., Huybers, P., and Rovere, A. Detection of a dynamic topography signal in last interglacial sea-level records. *Science Advances*, 3(7):e1700457, 2017. doi:10.1126/sciadv.1700457.

Autin, J., Scheck-Wenderoth, M., Loegering, M. J., Anka, Z., Vallejo, E., Rodriguez, J. F., Dominguez, F., Marchal, D., Reichert, C., di Primio, R., and Götze, H. J. Colorado Basin 3D structure and evolution, Argentine passive margin. *Tectonophysics*, 604:264–279, 2013. ISSN 00401951. doi:10.1016/j.tecto.2013.05.019.

Babault, J., Teixell, A., Arboleya, M. L., and Charroud, M. A late cenozoic age for long-wavelength surface uplift of the atlas mountains of morocco. *Terra Nova*, 20(2):102–107, 2008. doi:10.1111/j.1365-3121.2008.00794.x.

Baby, G., Guillocheau, F., Boulogne, C., Robin, C., and Dall'Asta, M. Uplift history of a transform continental margin revealed by the stratigraphic record: The case of the Agulhas transform margin along the Southern African Plateau. *Tectonophysics*, 731:104–130, 2018. doi:10.1016/j.tecto.2018.03.014.

Baby, G., Guillocheau, F., Braun, J., Robin, C., and Dall'Asta, M. Solid sedimentation rates history of the Southern African continental margins: Implications for the uplift history of the South African Plateau. *Terra Nova*, 32(1):53–65, 2020. ISSN 13653121. doi:10.1111/ter.12435.

Bahr, M. A., Jackson, R. O., and Pakistan. Geological map of Pakistan. University of Pakistan, Rawalpindi, 1964. scale 1:2 M, 1 map.

Barker, P. F. Tectonic evolution and subsidence history of the Rio Grande Rise. In Barker, P. F., Carlson, R. L., and Johnson, D. A., editors, *1983 Initial Reports of the Deep Sea Drilling Project*, volume 72, pages 953–976. US Government Printing Office, Washington DC, USA, 1983. doi:10.2973/dsdp.proc.72.151.1983.

Barnett-Moore, N., Flament, N., Heine, C., Butterworth, N., and Müller, R. D. Cenozoic uplift of south Western Australia as constrained by river profiles. *Tectonophysics*, 622:186–197, 2014. ISSN 00401951. doi:10.1016/j.tecto.2014.03.010.

Barrell, J. The strength of the Earth's crust. *The Journal of Geology*, 22(7):655–683, 1914. doi:10.1086/622181.

Barrell, J. Rhythms and the measurements of geologic time. *GSA Bulletin*, 28(1):745–904, 01 1917. ISSN 0016-7606. doi:10.1130/GSAB-28-745.

Basile, C., Girault, I., Paquette, J.-L., Agranier, A., Loncke, L., Heuret, A., and Poetisi, E. The Jurassic magmatism of the Demerara Plateau (offshore French Guiana) as a remnant of the Sierra Leone hotspot during the Atlantic rifting. *Scientific Reports*, 10:7486, 05 2020. doi:10.1038/s41598-020-64333-5.

Bastia, R. and Radhakrishna, M. Chapter 5 - Sedimentary basins along the East Coast of India: Subsurface geology, depositional history, and petroleum systems. In Bastia, R. and Radhakrishna, M., editors, *Basin Evolution and Petroleum Prospectivity of the Continental Margins of India*, volume 59 of *Developments in Petroleum Science*, pages 161–267. El-

sevier, 2012. doi:10.1016/B978-0-444-53604-4.00005-3. https://www.sciencedirect.com/science/article/pii/B9780444536044000053.

Batezelli, A. and Ladeira, F. S. B. Stratigraphic framework and evolution of the Cretaceous continental sequences of the Bauru, Sanfranciscana, and Parecis basins, Brazil. *Journal of South American Earth Sciences*, 65:1–24, 2016. ISSN 0895-9811. doi:10.1016/j.jsames.2015.11.005.

Becker, T. W., Schaeffer, A. J., Lebedev, S., and Conrad, C. P. Toward a generalized plate motion reference frame. *Geophysical Research Letters*, 42(May):3188–3196, 2015. ISSN 19448007. doi:10.1002/2015GL063695.

Behn, M. D., Conrad, C. P., and Silver, P. G. Detection of upper mantle flow associated with the African Superplume. *Earth and Planetary Science Letters*, 224:259–274, 2004. doi:10.1016/j.epsl.2004.05.026.

Belousov, V. V. and Maxwell, J. C. *Basic problems in geotectonics*. McGraw-Hill, New York, USA, 1962.

Bills, B. G. and May, G. M. Lake bonneville: Constraints on lithospheric thickness and upper mantle viscosity from isostatic warping of bonneville, provo, and gilbert stage shorelines. *Journal of Geophysical Research: Solid Earth*, 92(B11):11493–11508, 1987. doi:https://doi.org/10.1029/JB092iB11p11493.

Bird, P., Liu, Z., and Rucker, W. K. Stresses that drive the plates from below: Definitions, computational path, model optimization, and error analytsis. *Journal of Geophysical Research*, 113(B11):B11406, nov 2008. ISSN 0148-0227. doi:10.1029/2007JB005460.

Blackwelder, E. The valuation of unconformities. *The Journal of Geology*, 17(3):289–299, 1909. doi:10.1130/0016-7606(1963)74[93:SITCIO]2.0.CO;2.

Bland, K. J., Uruski, C. I., and Isaac, M. J. Pegasus Basin, eastern New Zealand: A stratigraphic record of subsidence and subduction, ancient and modern. *New Zealand Journal of Geology and Geophysics*, 58(4):319–343, 2015. doi:10.1080/00288306.2015.1076862.

Bond, G. C. Evidence for late Tertiary uplift of Africa relative to North America, South America, Australia and Europe. *The Journal of Geology*, 86(1):47–65, 1978a. doi:10.1086/649655.

Bond, G. C. Speculations on real sea-level changes and vertical motions of continents at selected times in the Cretaceous and Tertiary Periods. *Geology*, 6(4):247–250, 1978b. doi:10.1130/0091-7613(1978)6<247:SORSCA>2.0.CO;2.

Bond, G. C. Evidence for some uplifts of large magnitude in continental platforms. *Tectonophysics*, 61(1-3):285–305, 1979. doi:10.1016/0040-1951(79)90302-0.

Bower, D. J., Gurnis, M., and Seton, M. Lower mantle structure from paleogeographically constrained dynamic Earth models. *Geochemistry, Geophysics, Geosystems*, 14(1):44–63, 2013. ISSN 15252027. doi:10.1029/2012GC004267.

Braun, J. The many surface expressions of mantle dynamics. *Nature Geoscience*, 3(12):825–833, 2010. doi:10.1038/ngeo1020.

Braun, J., Guillocheau, F., Robin, C., Baby, G., and Jelsma, H. Rapid erosion of the southern african plateau as it climbs over a mantle superswell. *Journal of Geophysical Research: Solid Earth*, 119(7):6093–6112, 2014. doi:10.1002/2014JB010998.

Brown, H., Colli, L., and Bunge, H.-P. Asthenospheric flow through the Izanagi-Pacific slab window and its influence on dynamic topography and intraplate volcanism in East Asia. *Frontiers in Earth Science*, 10:10:889907, 2022. ISSN 2296-6463. doi:10.3389/feart.2022.889907.

Buck, W. R., Small, C., and Ryan, W. B. F. Constraints on asthenospheric flow from the depths of oceanic spreading centers: The East Pacific Rise and the Australian-Antarctic Discordance. *Geochemistry, Geophysics, Geosystems*, 10(9):Q09007, 2009. ISSN 15252027. doi:10.1029/2009GC002373.

Bunge, H.-P., Richards, M. A., and Baumgardner, J. R. Mantle-circulation models with sequential data assimilation: Inferring present-day mantle structure from plate-motion histories. *Phil. Trans. Roy. Soc. A*, 360(1800):2545–2567, 2002a. doi:10.1098/rsta.2002.1080.

Bunge, H.-P. Low plume excess temperature and high core heat flux inferred from non-adiabatic geotherms in internally heated mantle circulation models. *Physics of the Earth and Planetary Interiors*, 153(1-3):3–10, 2005. ISSN 0031-9201. doi:10.1016/j.pepi.2005.03.017.

Bunge, H.-P. and Glasmacher, U. A. Models and observations of vertical motion (MoveOn) associated with rifting to passive margins: Preface. *Gondwana Research*, 53:1–8, 2018. doi:10.1016/j.gr.2017.07.005.

Bunge, H.-P. and Richards, M. A. The backward-problem of plate tectonics and mantle convection, (abstract). *Eos Transactions AGU*, 73(14):281, 1992. Spring Meeting suppl.

Bunge, H.-P. and Richards, M. A. The origin of large scale structure in mantle convection: Effects of plate motions and viscosity stratification. *Geophysical Research Letters*, 23(21): 2987–2990, 1996. doi:10.1029/96GL02522.

Bunge, H.-P., Richards, M. A., and Baumgardner, J. R. Effect of depth-dependent viscosity on the planform of mantle convection. *Nature*, 379(6564):436–438, 1996. doi:10.1038/379436a0.

Bunge, H.-P., Richards, M. A., and Baumgardner, J. R. A sensitivity study of three-dimensional spherical mantle convection at 10^8 Rayleigh number: Effects of depth-dependent viscosity, heating mode, and an endothermic phase change. *Journal of Geophysical Research: Solid Earth*, 102(B6):11991–12007, 1997. doi:10.1029/96JB03806.

Bunge, H.-P., Richards, M. A., Lithgow-Bertelloni, C., Baumgardner, J. R., Grand, S. P., and Romanowicz, B. A. Time scales and heterogeneous structure in geodynamic Earth models. *Science*, 280(5360):91–95, apr 1998. doi:10.1126/science.280.5360.91.

Bunge, H.-P., Richards, M. A., and Baumgardner, J. R. Mantle–circulation models with sequential data assimilation: inferring present–day mantle structure from plate–motion histories. *Philosophical Transactions of the Royal Society of London. Series A: Mathematical, Physical and Engineering Sciences*, 360(1800):2545–2567, 2002b. doi:10.1098/rsta.2002.1080.

Bunge, H.-P., Hagelberg, C. R., and Travis, B. J. Mantle circulation models with variational data assimilation: Inferring past mantle flow and structure from plate motion histories and seismic tomography. *Geophysical Journal International*, 152(2):280–301, 02 2003a. doi:10.1046/j.1365-246X.2003.01823.x.

Bunge, H.-P., Hagelberg, C. R., and Travis, B. J. Mantle circulation models with variational data assimilation: Inferring past mantle flow and structure from plate motion histories and

seismic tomography. *Geophysical Journal International*, 152(2):280–301, feb 2003b. ISSN 0956540X. doi:10.1046/j.1365-246X.2003.01823.x.

Burgess, P. M., Gurnis, M., and Moresi, L. Formation of sequences in the cratonic interior of North America by interaction between mantle, eustatic, and stratigraphic processes. *Geological Society of America Bulletin*, 109(12):1515–1535, 1997. doi:10.1130/0016-7606(1997)109<1515:FOSITC>2.3.CO;2.

Burke, K. and Gunnell, Y. *The African erosion surface: A continental-scale synthesis of geomorphology, tectonics, and environmental change over the past 180 million years*, volume 201. Geological Society of America, Boulder, Colorado, USA, 2008. doi:10.1130/2008.1201.

Burke, K. and Torsvik, T. H. Derivation of Large Igneous Provinces of the past 200 million years from long-term heterogeneities in the deep mantle. *Earth and Planetary Science Letters*, 227 (3):531–538, 2004. doi:10.1016/j.epsl.2004.09.015.

Burke, K. and Whiteman, A. J. Uplift, rifting and break-up of Africa. In Tarling, D. H. and Runcorn, S. K., editors, *Implications of Continental Drift to the Earth Sciences,*. Academic Press, London & New York, 1973.

Busse, F. H. and Whitehead, J. A. Instabilities of convection rolls in a high Prandtl number fluid. *Journal of Fluid Mechanics*, 47(2):305–320, 1971. doi:10.1017/S0022112071001071.

Busse, F. H., Richards, M. A., and Lenardic, A. A simple model of high Prandtl and high Rayleigh number convection bounded by thin low-viscosity layers. *Geophysical Journal International*, 164(1):160–167, jan 2006. ISSN 0956540X. doi:10.1111/j.1365-246X.2005.02836.x.

Butterworth, N. P., Talsma, A. S., Müller, R. D., Seton, M., Bunge, H.-P., Schuberth, B. S. A., Shephard, G. E., and Heine, C. Geological, tomographic, kinematic and geodynamic constraints on the dynamics of sinking slabs. *Journal of Geodynamics*, 73:1–13, jan 2014. ISSN 0264-3707. doi:10.1016/J.JOG.2013.10.006.

Callec, Y., Janjou, D., Baudin, T., Luquet, C., Pellé, J.-M., and Laville, P. *Echelle des Temps Geologiques*. Bureau de recherches géologiques et minières (BRGM), 2006.

Campbell, I. H. Testing the plume theory. *Chemical Geology*, 241(3-4):153–176, jul 2007. ISSN 00092541. doi:10.1016/j.chemgeo.2007.01.024.

Campbell, I. H. and Griffiths, R. W. Implications of mantle plume structure for the evolution of flood basalts. *Earth and Planetary Science Letters*, 99(1-2):79–93, 1990. doi:10.1016/0012-821X(90)90072-6.

Cande, S. C. and Stegman, D. R. Indian and African plate motions driven by the push force of the Réunion plume head. *Nature*, 475(7354):47–52, 2011. doi:10.1038/nature10174.

Cao, C. R., Kirillova, G. L., Cao, H. S., Sorokin, A. P., Kaplun, V. B., Qu, Y., and Zhang, Y. J. Structure and evolution of the Sunwu-Jiayin basin in NE China and its relation to the Zeya-Bureya basin in the Far East of Russia. *Russian Journal of Pacific Geology*, 7(6):431–440, 2013. doi:10.1134/S1819714013060055.

Cao, K. Cretaceous terrestrial deposits in China. *China Geology*, 1:402–414, 2018. ISSN 2096-5192. doi:10.31035/cg2018045.

Carena, S., Bunge, H.-P., and Friedrich, A. M. Analysis of geological hiatus surfaces across Africa in the Cenozoic and implications for the timescales of convectively-maintained topography. *Canadian Journal of Earth Sciences*, 56(12):1333–1346, mar 2019. ISSN 0008-4077. doi:10.1139/cjes-2018-0329.

Carman, G. New paleogeographic maps for the Coral Sea and Darai Megasequences, Papua New Guinea, enhanced by geological icons. In *AAPG International Conference*, volume 76, Sydney, NSW, Australia, 01 1992. doi:10.1306/F4C8F96C-1712-11D7-8645000102C1865D. Article #91015, August 2-5.

Cathles, L., Fjeldskar, W., Lenardic, A., Romanowicz, B., Seales, J., and Richards, M. Influence of the asthenosphere on Earth dynamics and evolution. *Scientific Reports*, 13(1):13367, 2023. doi:10.1038/s41598-023-39973-y.

CCOP. CCOP Exploration Promotion Forum. Coordinating Committee for Geoscience Programs in East and South East Asia, 2002. Online resource, Last accessed 08.12.2022, `http://www.ccop.or.th/epf/`.

Celli, N. L., Lebedev, S., Schaeffer, A. J., and Gaina, C. The tilted Iceland Plume and its effect on the North Atlantic evolution and magmatism. *Earth and Planetary Science Letters*, 569: 117048, 2021. ISSN 0012821X. doi:10.1016/j.epsl.2021.117048.

CGG-Robertson. Living atlas sedimentary basins of the world: Sedimentary basins of the world, 2022. Last accessed 10.12.2022, `https://www.arcgis.com/home/item.html?id=a15e179c3b6a45ef94107353c2f64fc1`.

Chang, J., Qiu, N., Zhao, X., Shen, F., Liu, N., and Xu, W. Mesozoic and Cenozoic tectonothermal reconstruction of the western bohai bay basin (east china) with implications for hydrocarbon generation and migration. *Journal of Asian Earth Sciences*, 160:380–395, 2018. ISSN 1367-9120. doi:10.1016/j.jseaes.2017.09.008.

Charrier, R., Pinto, L., and Rodriguez, M. P. Tectonostratigraphic evolution of the Andean Orogen in Chile. *The Geology of Chile, The Geological Society of London*, pages 221–114, 2007. doi:10.1144/GOCH.3.

Charusiri, P. and Pum-Im, S. Cenozoic tectonic evolution of major sedimentary basins in Central, Northern, and the Gulf of Thailand. *Bulletin of Earth Sciences of Thailand*, 2(1 & 2):40–62, Nov. 2021. Retrieved from `https://ph01.tci-thaijo.org/index.php/bestjournal/article/view/246467`.

Chase, C. G. Asthenospheric counterflow: A kinematic model. *Geophysical Journal International*, 56(1):1–18, 1979. ISSN 0016-8009. doi:10.1111/j.1365-246X.1979.tb04764.x.

Chen, M. M. and Whitehead, J. A. Evolution of two-dimensional periodic Rayleigh convection cells of arbitrary wave-numbers. *Journal of Fluid Mechanics*, 31(1):1–15, 1968. doi:10.1017/S0022112068000017.

Chen, Y.-W., Wu, J., and Suppe, J. Southward propagation of Nazca subduction along the Andes. *Nature*, 565(7740):441–447, 2019. doi:10.1038/s41586-018-0860-1.

Chen, Y.-W., Colli, L., Bird, D. E., Wu, J., and Zhu, H. Caribbean plate tilted and actively dragged eastwards by low-viscosity asthenospheric flow. *Nature Communications*, 12(1): 1603, 2021. doi:10.1038/s41467-021-21723-1.

Cheng, X., Zhang, D., Jolivet, M., Yu, X., Du, W., Liu, R., and Guo, Z. Ceno-

zoic structural inversion from transtension to transpression in Yingxiong Range, western Qaidam Basin: New insights into strike-slip superimposition controlled by Altyn Tagh and Eastern Kunlun Faults. *Tectonophysics*, 723:229–241, 2018. ISSN 0040-1951. doi:doi.org/10.1016/j.tecto.2017.12.019.

Childs, O. E. Correlation of stratigraphic units of North America—COSUNA. *AAPG Bulletin*, 69(2):173–180, 02 1985. ISSN 0149-1423. doi:10.1306/AD461C73-16F7-11D7-8645000102C1865D.

Clark, S. R. Uncertainty in the breakup, spreading history, and velocity variations of Gondwana. *Gondwana Research*, 53:189–196, 2018. ISSN 1342937X. doi:10.1016/j.gr.2017.04.029.

Claure Zapata, M., Lema Patiño, R., Riera Kilibarda, C., and Suarez Soruco, R. Mapa geológico de Bolivia, 2000, 2012. SERGEOMIN, Servicio Geológico Minero. La Paz, Bolivia, `https://geo.gob.bo/geonetwork/srv/en/catalog.search{#}/metadata/9d4640bf-522a-4949-9a14-4838685c5a2c`.

Clements, B., Burgess, P. M., Hall, R., and Cottam, M. A. Subsidence and uplift by slab-related mantle dynamics: A driving mechanism for the Late Cretaceous and Cenozoic evolution of continental SE Asia? *Geological Society, London, Special Publications*, 355(1):37–51, 2011a. doi:10.1144/SP355.3.

Clements, B., Burgess, P. M., Hall, R., and Cottam, M. A. Subsidence and uplift by slab-related mantle dynamics: a driving mechanism for the Late Cretaceous and Cenozoic evolution of continental SE Asia? *Geological Society, London, Special Publications*, 355(1): 37–51, 2011b. ISSN 0305-8719. doi:10.1144/SP355.3.

Cloetingh, S., Burov, E., Beekman, F., Andeweg, B., Andriessen, P., Garcia-Castellanos, D., de Vicente, G., and Vegas, R. Lithospheric folding in Iberia. *Tectonics*, 21(5):5–1–5–26, Sep-Oct 2002. ISSN 0278-7407. doi:10.1029/2001TC901031.

Cogné, N., Gallagher, K., Cobbold, P. R., Riccomini, C., and Gautheron, C. Post-breakup tectonics in southeast brazil from thermochronological data and combined inverse-forward thermal history modeling. *Journal of Geophysical Research: Solid Earth*, 117(B11):B11413, 2012. doi:10.1029/2012JB009340.

Cohen, K. M., Finney, S., Gibbard, P. L., and Fan, J.-X. The ICS International Chronostratigraphic Chart. *Episodes*, 36(3):199–204, 2013; updated. doi:10.18814/epiiugs/2013/v36i3/002. Version 2018/08.

Colli, L., Fichtner, A., and Bunge, H.-P. Full waveform tomography of the upper mantle in the South Atlantic region: Imaging a westward fluxing shallow asthenosphere? *Tectonophysics*, 604:26–40, 2013. doi:10.1016/j.tecto.2013.06.015.

Colli, L., Stotz, I., Bunge, H.-P., Smethurst, M., Clark, S. R., Iaffaldano, G., Tassara, A., Guillocheau, F., and Bianchi, M. C. Rapid South Atlantic spreading changes and coeval vertical motion in surrounding continents: Evidence for temporal changes of pressure-driven upper mantle flow. *Tectonics*, 33(7):1304–1321, jul 2014. ISSN 02787407. doi:10.1002/2014TC003612.

Colli, L., Bunge, H.-P., and Schuberth, B. S. A. On retrodictions of global mantle flow with assimilated surface velocities. *Geophysical Research Letters*, 42(20):8341–8348, 2015. doi:10.1002/2015GL066001.

Colli, L., Ghelichkhan, S., and Bunge, H.-P. On the ratio of dynamic topography and gravity anomalies in a dynamic Earth. *Geophysical Research Letters*, 43(6):2510–2516, 2016. doi:10.1002/2016GL067929.

Colli, L., Ghelichkhan, S., Bunge, H.-P., and Oeser, J. Retrodictions of Mid Paleogene mantle flow and dynamic topography in the Atlantic region from compressible high resolution adjoint mantle convection models: Sensitivity to deep mantle viscosity and tomographic input model. *Gondwana Research*, 53:252–272, 2018. doi:10.1016/j.gr.2017.04.027.

Colli, L., Bunge, H.-P., and Oeser, J. Impact of model inconsistencies on reconstructions of past mantle flow obtained using the adjoint method. *Geophysical Journal International*, 221 (1):617–639, 2020. doi:10.1093/gji/ggaa023.

Coltice, N. and Shephard, G. E. Tectonic predictions with mantle convection models. *Geophysical Journal International*, 213(1):16–29, APR 2018. ISSN 0956-540X. doi:10.1093/gji/ggx531.

Conrad, C. P. and Gurnis, M. Seismic tomography, surface uplift, and the breakup of Gondwanaland: Integrating mantle convection backwards in time. *Geochemistry, Geophysics, Geosystems*, 4(3):1031, 2003. doi:10.1029/2001GC000299.

Conrad, C. P. and Lithgow-Bertelloni, C. Influence of continental roots and asthenosphere on plate-mantle coupling. *Geophysical Research Letters*, 33(5), 2006. doi:https://doi.org/10.1029/2005GL025621.

Contreras, J., Zühlke, R., Bowman, S., and Bechstädt, T. Seismic stratigraphy and subsidence analysis of the southern Brazilian margin (Campos, Santos and Pelotas Basins). *Marine and Petroleum Geology*, 27(9):1952–1980, 2010. ISSN 0264-8172. doi:10.1016/j.marpetgeo.2010.06.007.

Copley, A., Avouac, J. P., and Royer, J. Y. India-Asia collision and the Cenozoic slowdown of the Indian plate: Implications for the forces driving plate motions. *Journal of Geophysical Research: Solid Earth*, 115(3):B03410, 2010. ISSN 21699356. doi:10.1029/2009JB006634.

Core Labs. Stratigraphic Correlation Chart. Online resource, 2014. Core Laboratories Geological Sciences Department, Last accessed 2021, `https://landman.ca/files/docs/CORELAB.pdf`.

Cornejo, P., Matthews, S., and Perez de Arce, C. The K-T compressive deformation event in northern Chile 24-27 S. *10 Geological Congress in Concepcion Chile*, 2003.

Cottam, M. A., Hall, R., Forster, M. A., and Boudagher-Fadel, M. K. Basement character and basin formation in Gorontalo Bay, Sulawesi, Indonesia: New observations from the Togian Islands. *Geological Society, London, Special Publications*, 355(1):177–202, 2011. doi:10.1144/SP355.9.

Courtillot, V., Davaille, A., Besse, J., and Stock, J. Three distinct types of hotspots in the Earth's mantle. *Earth and Planetary Science Letters*, 205(3-4):295–308, 2003. doi:10.1016/S0012-821X(02)01048-8.

Cox, K. The role of mantle plumes in the development of continental drainage patterns. *Nature*, 342(6252):873, 1989.

Şengör, A. M. C. Elevation as indicator of mantle-plume activity. In Ernst, R. E. and Buchan, K. L., editors, *Mantle plumes: Their identification through time*, volume 352, pages 183–245.

Geological Society of America, 2001. ISBN 9780813723525. doi:10.1130/0-8137-2352-3.183.

Şengör, A. M. C. *The large wavelength deformations of the Lithosphere: Materials for a history of the evolution of thought from the earliest times to plate tectonics*. Geological Society of America, Memoir no. 196, 2003. doi:10.1130/978-0-8137-1196-7-196.0.1.

Şengör, A. M. C. What is the use of the history of geology to a practicing geologist? The propaedeutical case of stratigraphy. *The Journal of Geology*, 124(6):643–698, 2016. doi:10.1086/688609.

Cui, C., Lei, W., Liu, Q., Peter, D., Bozdağ, E., Tromp, J., Hill, J., Podhorszki, N., and Pugmire, D. GLAD-M35: A joint P and S global tomographic model with uncertainty quantification. *Geophys. J. Int.*, 239(1):478–502, August 2024. ISSN 1365-246X. doi:10.1093/gji/ggae270.

Cuitiña, J. I., Varela, A. N., Ghiglione, M. C., Richiano, S., and Poiré, D. G. The Austral-Magallanes Basin (Southern Patagonia): A synthesis of its stratigrahy and evolution. *Latin American Journal of Sedimentology and Basin Analysis*, 26(2):155–166, 2019.

Czarnota, K., Roberts, G. G., White, N. J., and Fishwick, S. Spatial and temporal patterns of Australian dynamic topography from River Profile Modeling. *Journal of Geophysical Research: Solid Earth*, 119:1384–1424, 2014. doi:10.1002/2013jb010436.

Davies, D. R., Goes, S., Davies, J. H., Schuberth, B. S. A., Bunge, H.-P., and Ritsema, J. Reconciling dynamic and seismic models of Earth's lower mantle: The dominant role of thermal heterogeneity. *Earth and Planetary Science Letters*, 353:253–269, 2012. doi:10.1016/j.epsl.2012.08.016.

Davies, G. F. Role of the lithosphere in mantle convection. *Journal of Geophysical Research: Solid Earth*, 93(B9):10451–10466, 1988a. doi:10.1029/JB093iB09p10451.

Davies, G. F. Ocean bathymetry and mantle convection: 1. Large-scale flow and hotspots. *Journal of Geophysical Research*, 93(B9):10467–10480, sep 1988b. ISSN 01480227. doi:10.1029/jb093ib09p10467.

Davies, G. F. *Dynamic Earth: Plates, plumes and mantle convection*. Cambridge University Press, Cambridge, United Kingdom, 1999. doi:10.1017/CBO9780511605802.

Davies, G. F. and Richards, M. A. Mantle convection. *The Journal of Geology*, 100(2):151–206, 1992. doi:10.1086/629582.

Davies, J. H. and Davies, D. R. Earth's surface heat flux. *Solid Earth*, 1(1):5–24, 2010. ISSN 1869-9529. doi:10.5194/se-1-5-2010.

De Lira Mota, M. A., Dunkley Jones, T., Sulaiman, N., Edgar, K. M., Yamaguchi, T., Leng, M. J., Adloff, M., Greene, S. E., Norris, R., Warren, B., Duffy, G., Farrant, J., Murayama, M., Hall, J., and Bendle, J. Multi-proxy evidence for sea level fall at the onset of the Eocene–Oligocene transition. *Nature Communications*, 14(1):4748, 2023. doi:10.1038/s41467-023-39806-6.

De Smet, M. E. M. and Barber, A. J. *Chapter 7: Tertiary stratigraphy*, volume 31 (1), pages 86–97. Geological Society, London, Memoirs, London, UK, 2005. doi:10.1144/GSL.MEM.2005.031.01.07.

De Vicente, G., Cloetingh, S., Van Wees, J., and Cunha, P. Tectonic classification of Ceno-

zoic Iberian foreland basins. *Tectonophysics*, 502(1):38–61, 2011. ISSN 0040-1951. doi:10.1016/j.tecto.2011.02.007. TOPO-EUROPE II - From Iberia to the Carpathians and analogues.

Debayle, E., Kennett, B., and Priestley, K. Global azimuthal seismic anisotropy and the unique plate-motion deformation of Australia. *Nature*, 433(7025):509–512, feb 2005. ISSN 1476-4687. doi:10.1038/nature03247.

Deep Sea Drilling Program (DSDP). Deep Sea Drilling Project, 1968–1983. Legs 1–96, Sites 1–624, `https://iodp.tamu.edu/scienceops/maps.html`.

DeMets, C. and Merkouriev, S. High-resolution reconstructions of South America plate motion relative to Africa, Antarctica and North America: 34 Ma to present. *Geophysical Journal International*, 217(3):1821–1853, JUN 2019. ISSN 0956-540X. doi:10.1093/gji/ggz087.

DeMets, C., Gordon, R. G., and Argus, D. F. Geologically current plate motions. *Geophysical Journal International*, 181(1):1–80, 2010.

Deng, H., Ren, J., Pang, X., Rey, P. F., McClay, K. R., Watkinson, I. M., Zheng, J., and Luo, P. South China Sea documents the transition from wide continental rift to continental break up. *Nature Communications*, 11(1):4583, 2020. doi:10.1038/s41467-020-18448-y.

DiCaprio, L., Gurnis, M., and Müller, R. D. Long-wavelength tilting of the Australian continent since the Late Cretaceous. *Earth and Planetary Science Letters*, 278(3-4):175–185, 2009. ISSN 0012821X. doi:10.1016/j.epsl.2008.11.030.

Do Couto, D., Gorini, C., Jolivet, L., Lebret, N., Augier, R., Gumiaux, C., d'Acremont, E., Ammar, A., Jabour, H., and Auxietre, J.-L. Tectonic and stratigraphic evolution of the western Alboran Sea Basin in the last 25 Myrs. *Tectonophysics*, 677-678:280–311, 2016. ISSN 0040-1951. doi:10.1016/j.tecto.2016.03.020.

Dörr, N., Lisker, F., Clift, P. D., Carter, A., Gee, D. G., Tebenkov, A. M., and Spiegel, C. Late Mesozoic–Cenozoic exhumation history of northern Svalbard and its regional significance: Constraints from apatite fission track analysis. *Tectonophysics*, 514:81–92, 2012. doi:10.1016/j.tecto.2011.10.007.

Doust, H. and Noble, R. A. Petroleum systems of Indonesia. *Marine and Petroleum Geology*, 25(2):103–129, 2008. ISSN 0264-8172. doi:10.1016/j.marpetgeo.2007.05.007.

Dressel, I., Scheck-Wenderoth, M., Cacace, M., Lewerenz, B., Götze, H.-J., and Reichert, C. Reconstruction of the southwestern African continental margin by backward modeling. *Marine and Petroleum Geology*, 67:544–555, 2015. ISSN 0264-8172. doi:10.1016/j.marpetgeo.2015.06.006.

Dressel, I., Cacace, M., and Scheck-Wenderoth, M. Coupled thermo-mechanical 3D subsidence analysis along the SW African passive continental margin. *Arabian Journal of Geosciences*, 9(5):1–21, 2016. ISSN 18667538. doi:10.1007/s12517-016-2407-9.

Duncan, R. A. and Richards, M. A. Hotspots, mantle plumes, flood basalts, and true polar wander. *Reviews of Geophysics*, 29(1):31–50, 1991. doi:10.1029/90RG02372.

Dutkiewicz, A. and Müller, R. D. The carbonate compensation depth in the South Atlantic Ocean since the Late Cretaceous. *Geology*, 49(7):873–878, 04 2021. doi:10.1130/G48404.1.

Dutkiewicz, A. and Müller, R. D. Deep-sea hiatuses track the vigor of Cenozoic ocean bottom

currents. *Geology*, 50(6):710–715, 03 2022. ISSN 0091-7613. doi:10.1130/G49810.1.

Dutkiewicz, A., Müller, R. D., Cannon, J., Vaughan, S., and Zahirovic, S. Sequestration and subduction of deep-sea carbonate in the global ocean since the Early Cretaceous. *Geology*, 47(1):91–94, 12 2018. ISSN 0091-7613. doi:10.1130/G45424.1.

Ehlers, T. A. and Farley, K. A. Apatite (U–Th)/He thermochronometry: Methods and applications to problems in tectonic and surface processes. *Earth and Planetary Science Letters*, 206(1-2):1–14, 2003. doi:10.1016/S0012-821X(02)01069-5.

Ernst, R. E. and Buchan, K. L., editors. *Mantle plumes: Their identification through time*, volume 352. Geological Society of America, Boulder, Colorado, USA, 01 2001. ISBN 9780813723525. doi:10.1130/SPE352.

Fang, P., Ding, W., Fang, Y., Zhao, Z., and Feng, Z. Cenozoic tectonic subsidence in the southern continental margin, South China Sea. *Frontiers of Earth Science*, 11(2):427–441, 2017. doi:10.1007/s11707-016-0594-z.

Farnetani, C. G. and Richards, M. A. Numerical investigations of the mantle plume initiation model for flood basalt events. *Journal of Geophysical Research*, 99(B7):13813–13833, 1994. ISSN 01480227. doi:10.1029/94jb00649.

Fernandes, V. M. and Roberts, G. G. Cretaceous to recent net continental uplift from paleobiological data: Insights into sub-plate support. *GSA Bulletin*, 133(5-6):1217–1236, 2020. doi:10.1130/b35739.1.

Fichtner, A., van Herwaarden, D.-P., Afanasiev, M., Simutė, S., Krischer, L., Çubuk Sabuncu, Y., Taymaz, T., Colli, L., Saygin, E., Villaseñor, A., Trampert, J., Cupillard, P., Bunge, H.-P., and Igel, H. The collaborative seismic earth model: Generation 1. *Geophysical Research Letters*, 45(9):4007–4016, 2018. doi:10.1029/2018GL077338.

Fishwick, S. and Bastow, I. D. Towards a better understanding of African topography: A review of passive-source seismic studies of the African crust and upper mantle. *Geological Society, London, Special Publications*, 357(1):343–371, 2011. ISSN 0305-8719. doi:10.1144/SP357.19.

Flament, N., Gurnis, M., Williams, S., Seton, M., Skogseid, J., Heine, C., and Dietmar Müller, R. Topographic asymmetry of the South Atlantic from global models of mantle flow and lithospheric stretching. *Earth and Planetary Science Letters*, 387:107–119, 2014. ISSN 0012-821X. doi:10.1016/j.epsl.2013.11.017.

Flowers, R., Wernicke, B., and Farley, K. Unroofing, incision, and uplift history of the southwestern Colorado Plateau from apatite (U-Th)/He thermochronometry. *GSA Bulletin*, 120 (5-6):571–587, 05 2008. ISSN 0016-7606. doi:10.1130/B26231.1.

Forte, A. M. and Peltier, R. Viscous flow models of global geophysical observables: 1. forward problems. *Journal of Geophysical Research: Solid Earth*, 96(B12):20131–20159, 1991. doi:10.1029/91JB01709.

Fowler, C. M. R. *The Solid Earth: An introduction to global geophysics*. Cambridge University Press, 2 edition, 2004. doi:10.1017/CBO9780511819643.

French, S. W. and Romanowicz, B. A. Broad plumes rooted at the base of the Earth's mantle beneath major hotspots. *Nature*, 525(7567):95–99, 2015. doi:10.1038/nature14876.

Friedrich, A. M. Palaeogeological hiatus surface mapping: A tool to visualize vertical motion of the continents. *Geological Magazine*, 156(2):308–319, 2019. doi:10.1017/S0016756818000560.

Friedrich, A. M., Bunge, H.-P., Rieger, S. M., Colli, L., Ghelichkhan, S., and Nerlich, R. Stratigraphic framework for the plume mode of mantle convection and the analysis of interregional unconformities on geological maps. *Gondwana Research*, 53:159–188, jan 2018. ISSN 1342-937X. doi:10.1016/j.gr.2017.06.003.

Gaina, C., Roest, W., and Müller, D. R. Late cretaceous-cenozoic deformation of northeast asia. *Earth and Planetary Science Letters*, 197(3-4):273–286, 2002. ISSN 0012-821X. doi:10.1016/S0012-821X(02)00499-5.

Gallagher, K. and Brown, R. Denudation and uplift at passive margins: The record on the Atlantic Margin of southern Africa. *Philosophical Transactions of the Royal Society of London. Series A: Mathematical, Physical and Engineering Sciences*, 357(1753):835–859, 1999. doi:10.1098/rsta.1999.0354.

Gallardo Jara, R. E., Ghiglione, M. C., and Galliani, L. R. Tectonic evolution of the Southern Austral-Magallanes Basin in Tierra del Fuego. *Latin American Journal of Sedimentology and Basin Analysis*, 26(2):127–154, 2019.

Gallardo Jara, R. E., Ghiglione, M. C., and Rojas Galliani, L. Tectonic evolution of the Southern Austral-Magallanes Basin in Tierra Del Fuego. *Latin American Journal of Sedimentology and Basin Analysis*, 26(2):127–154, 03 2021.

Garrity, C. P. and Soller, D. R. Database of the Geologic Map of North America: Adapted from the map by J.C. Reed, Jr. and others (2005). Technical report, United States Geological Survey (USGS), 2009. `http://pubs.er.usgs.gov/publication/ds424`.

General Geological Survey of Malaysia. Geological Map of Sarawak, 1996. scale 1:750 k, revised edition.

Geological Survey Division of Thailand. Geological map of Thailand, 1999. Department of Mineral Resources, scale 1:1 M, 2 sheets, (2542 Buddhist Era).

Geological Survey of India. Geological map of India, 1993. scale 1:5 M, 2 sheets, Hyderabad, India.

Geological Survey of Japan. Geological map of Japan, 1982. AIST, scale 1:1 M, 6 sheets.

Gerster, R., Welsink, H., Ansa, A., and Raggio, F. Cuenca de Colorado. In *VIII Congreso de Exploración y Desarrollo de Hidrocarburos Simposio Cuencas Argentinas: Visión Actual*, pages 65–80, 2011.

Ghelichkhan, S., Bunge, H.-P., and Oeser, J. Global mantle flow retrodictions for the early Cenozoic using an adjoint method: Evolving dynamic topographies, deep mantle structures, flow trajectories and sublithospheric stresses. *Geophysical Journal International*, 226(2): 1432–1460, 2021. doi:10.1093/gji/ggab108.

Ghelichkhan, S. and Bunge, H.-P. The compressible adjoint equations in geodynamics: Derivation and numerical assessment. *GEM-International Journal on Geomathematics*, 7(1):1–30, 2016. doi:10.1007/s13137-016-0080-5.

Ghelichkhan, S. and Bunge, H.-P. The adjoint equations for thermochemical compressible

mantle convection: Derivation and verification by twin experiments. *Proceedings of the Royal Society A*, 474(2220):20180329, 2018. doi:10.1098/rspa.2018.0329.

Ghose, G., Chatterjee, D., and Banerjee, J. Geological map of South and East Asia. Commission for the Geological Map of the World/UNESCO, third edition, 1990. scale 1:5 M, 6 sheets.

Gillis, R. J., Horton, B. K., and Grove, M. Thermochronology, geochronology, and upper crustal structure of the Cordillera Real: Implications for Cenozoic exhumation of the central Andean plateau. *Tectonics*, 25(6), DEC 21 2006. ISSN 0278-7407. doi:10.1029/2005TC001887.

Gordon, R. G. Lithospheric deformation in the equatorial Indian Ocean: Timing and Tibet. *Geology*, 37(3):287–288, 2009. ISSN 00917613. doi:10.1130/focus032009.1.

Gordon, R. G. and Jurdy, D. M. Cenozoic global plate motions. *Journal of Geophysical Research: Solid Earth*, 91(B12):12389–12406, 1986.

Government of India. National Data Repository of India. Directorate General of Hydrocarbons, Ministry of Petroleum and Natural Gas, 2021. Online database, Last accessed 08.12.2022.

Graham, S. A., Chamberlain, C. P., Yue, Y., Ritts, B. D., Hanson, A. D., Horton, T. W., Waldbauer, J. R., Poage, M. A., and Feng, X. Stable isotope records of Cenozoic climate and topography, Tibetan plateau and Tarim basin. *American Journal of Science*, 305(2):101–118, 2005. ISSN 0002-9599. doi:10.2475/ajs.305.2.101.

Granot, R. and Dyment, J. The Cretaceous opening of the South Atlantic Ocean. *Earth and Planetary Science Letters*, 414:156–163, 2015. ISSN 0012821X. doi:10.1016/j.epsl.2015.01.015.

Green, P., Duddy, I., and Japsen, P. Episodic kilometre-scale burial and exhumation and the importance of missing section. *Earth-Science Reviews*, 234:104226, 2022. ISSN 0012-8252. doi:10.1016/j.earscirev.2022.104226.

Green, P. F., Duddy, I. R., Japsen, P., Bonow, J. M., and Malan, J. A. Post-breakup burial and exhumation of the southern margin of Africa. *Basin Research*, 29(1):96–127, 2015. ISSN 13652117. doi:10.1111/bre.12167.

Green, P. F., Japsen, P., Chalmers, J. A., Bonow, J. M., and Duddy, I. R. Post-breakup burial and exhumation of passive continental margins: Seven propositions to inform geodynamic models. *Gondwana Research*, 53:58–81, 2018a. ISSN 1342-937X. doi:10.1016/j.gr.2017.03.007.

Green, P. F., Japsen, P., Chalmers, J. A., Bonow, J. M., and Duddy, I. R. Post-breakup burial and exhumation of passive continental margins: Seven propositions to inform geodynamic models. *Gondwana Research*, 53:58–81, 2018b. doi:10.1016/j.gr.2017.03.007.

Gregersen, U., Knutz, P., Nøhr-Hansen, H., Sheldon, E., and Hopper, J. R. Tectonostratigraphy and evolution of the West Greenland continental margin. *Bulletin of the Geological Society of Denmark*, 67:1–21, 02 2019. ISSN 2245-707. doi:10.37570/bgsd-2019-67-01.

Griffiths, R. W., Gurnis, M., and Eitelberg, G. Holographic measurements of surface topography in laboratory models of mantle hotspots. *Geophysical Journal International*, 96(3):477–495, 1989. doi:10.1111/j.1365-246X.1989.tb06009.x.

Guillocheau, F., Rouby, D., Robin, C., Helm, C., Rolland, N., Le Carlier de Veslud, C., and Braun, J. Quantification and causes of the terrigeneous sediment budget at the scale of a continental margin: A new method applied to the Namibia-South Africa margin. *Basin Research*,

24(1):3–30, 2012. doi:10.1111/j.1365-2117.2011.00511.x.

Guillocheau, F., Simon, B., Baby, G., Bessin, P., Robin, C., and Dauteuil, O. Planation surfaces as a record of mantle dynamics: The case example of Africa. *Gondwana Research*, 53:82–98, 2018. doi:10.1016/j.gr.2017.05.015.

Gurnis, M. Cretaceous Vertical Motion of Australia and the AustralianAntarctic Discordance. *Science*, 279(5356):1499–1504, 1998. ISSN 00368075. doi:10.1126/science.279.5356.1499.

Gurnis, M., Müller, R. D., and Moresi, L. Cretaceous vertical motion of australia and the australian-antarctic discordance. *Science*, 279(5356):1499–1504, 1998. ISSN 0036-8075. doi:10.1126/science.279.5356.1499.

Hackley, P., Urbani, F., Karlsen, A. W., and Garrity, C. P. Geological shaded relief map of Venezuela. *USGS Open File Report*, 2005:1–2, 2004.

Hager, B. H. Subducted slabs and the geoid: Constraints on mantle rheology and flow. *Journal of Geophysical Research: Solid Earth*, 89(B7):6003–6015, 1984. doi:10.1029/JB089iB07p06003.

Hager, B. H. and Richards, M. A. Long-wavelength variations in earth's geoid: Physical models and dynamical implications. *Philosophical Transactions of the Royal Society of London. Series A, Mathematical and Physical Sciences*, 328(1599):309–327, 1989. doi:10.1098/rsta.1989.0038.

Hager, B. H., Clayton, R. W., Richards, M. A., Comer, R. P., and Dziewonski, A. M. Lower mantle heterogeneity, dynamic topography and the geoid. *Nature*, 313:541–545, feb 1985. doi:10.1038/313541a0.

Hall, R. Late Jurassic-Cenozoic reconstructions of the Indonesian region and the Indian Ocean. *Tectonophysics*, 570-571:1–41, 2012. ISSN 00401951. doi:10.1016/j.tecto.2012.04.021.

Hansen, H., Mohabey, D., Lojen, S., Toft, P., and Sarkar, A. Orbital cycles and stable carbon isotopes of sediments associated with Deccan volcanic suite, India: Implications for the stratigraphic correlation and Cretaceous/Tertiary boundary. *Gondwana Geological Magazine*, 8: 5–28, 2005.

Haque, A. E., Islam, M. A., and Ragab Shalaby, M. Structural modeling of the Maui gas field, Taranaki Basin, New Zealand. *Petroleum Exploration and Development*, 43(6):965–975, 2016. ISSN 1876-3804. doi:10.1016/S1876-3804(16)30114-8.

Harper, J. F. On the driving forces of plate tectonics. *Geophysical Journal International*, 40(3): 465–474, 03 1975. ISSN 0956-540X. doi:10.1111/j.1365-246X.1975.tb04143.x.

Harper, J. F. Plate Dynamics: Caribbean Map Corrections and Hotspot Push. *Geophysical Journal International*, 100(3):423–431, 1990. ISSN 0956-540X. doi:10.1111/j.1365-246X.1990.tb00695.x.

Harrington, L., Zahirovic, S., Salles, T., Braz, C., and Müller, R. D. Tectonic, geodynamic and surface process driving forces of Australia's paleogeography since the Jurassic. In Keep, M. and Moss, S., editors, *The Sedimentary Basins of Western Australia V: Proceedings of the Petroleum Exploration Society of Australia Symposium, Perth, WA, 2019*, page 29, 2019.

Harrison, J. C., St-Onge, M. R., Petrov, O. V., Strelnikov, S. I., Lopatin, B. G., Wilson, F. H., Tella, S., Paul, D., Lynds, T. L., Shokalsky, S. P., Hults, C. K., Bergman, S., Jepsen, H. F.,

and Solli, A. Geological map of the Arctic, 2011. "A" Series Map, 2159A.

Hartley, R. A., Roberts, G. G., White, N., and Richardson, C. Transient convective uplift of an ancient buried landscape. *Nature Geoscience*, 4(8):562–565, 2011. ISSN 1752-0894. doi:10.1038/ngeo1191.

Haug, G. H. and Tiedemann, R. Effect of the formation of the Isthmus of Panama on Atlantic Ocean thermohaline circulation. *Nature*, 393(6686):673–676, 1998. doi:10.1038/31447.

Hayek, J. N., Vilacís, B., Bunge, H.-P., Friedrich, A. M., Carena, S., and Vibe, Y. Continent-scale hiatus maps for the atlantic realm and australia since the upper jurassic and links to mantle flow induced dynamic topography. *Proceedings of the Royal Society A: Mathematical, Physical and Engineering Sciences*, 476(2242):20200390, 2020. doi:10.1098/rspa.2020.0390.

Hayek, J. N., Vilacís, B., Bunge, H.-P., Friedrich, A. M., Carena, S., and Vibe, Y. Correction: Continent-scale hiatus maps for the atlantic realm and australia since the upper jurassic and links to mantle flow-induced dynamic topography. *Proceedings of the Royal Society A: Mathematical, Physical and Engineering Sciences*, 477(2251):20210437, 2021. doi:10.1098/rspa.2021.0437.

Heine, C., Yeo, L. G., and Müller, R. D. Evaluating global paleoshoreline models for the Cretaceous and Cenozoic. *Australian Journal of Earth Sciences*, 62(3):275–287, 2015. doi:10.1080/08120099.2015.1018321.

Heine, C., Müller, R. D., Steinberger, B., and DiCaprio, L. Integrating deep Earth dynamics in paleogeographic reconstructions of Australia. *Tectonophysics*, 483(1-2):135–150, 2010. doi:10.1016/j.tecto.2009.08.028.

Hekinian, R., Bonté, P., P.l, D., P.l, B., C, J., Labeyrie, L., and J.c, D. Volcanics from the Sierra Leone Rise. *Nature (Macmillan Journals), 1979-12 , Vol. 257 , N. 5680 , P. 536-538*, 275, 10 1978. doi:10.1038/275536a0.

Hillis, R. R., Holford, S. P., Green, P. F., Doré, A. G., Gatliff, R. W., Stoker, M. S., Thomson, K., Turner, J. P., Underhill, J. R., and Williams, G. A. Cenozoic exhumation of the southern British Isles. *Geology*, 36(5):371–374, 05 2008. ISSN 0091-7613. doi:10.1130/G24699A.1.

Ho, C. A synthesis of the geologic evolution of Taiwan. *Tectonophysics*, 125(1-3):1–16, 1986. ISSN 0040-1951. doi:10.1016/0040-1951(86)90004-1.

Hodges, K. 3.08 - geochronology and thermochronology in orogenic systems. In Holland, H. D. and Turekian, K. K., editors, *Treatise on Geochemistry*, pages 263–292. Pergamon, Oxford, UK, 2003. ISBN 978-0-08-043751-4. doi:10.1016/B0-08-043751-6/03024-3.

Hoernle, K., Timm, C., Hauff, F., Tappenden, V., Werner, R., Jolis, E., Mortimer, N., Weaver, S., Riefstahl, F., and Gohl, K. Late Cretaceous (99-69 Ma) basaltic intraplate volcanism on and around Zealandia: Tracing upper mantle geodynamics from Hikurangi Plateau collision to Gondwana breakup and beyond. *Earth and Planetary Science Letters*, 529:115864, 2020. doi:10.1016/j.epsl.2019.115864.

Hoggard, M. J., White, N., and Al-Attar, D. Global dynamic topography observations reveal limited influence of large-scale mantle flow. *Nature Geoscience*, 9(6):456–463, 2016. doi:10.1038/ngeo2709.

Hoggard, M. J., Winterbourne, J., Czarnota, K., and White, N. Oceanic residual depth mea-

surements, the plate cooling model, and global dynamic topography. *Journal of Geophysical Research: Solid Earth*, 122(3):2328–2372, 2017. doi:10.1002/2016JB013457.

Hoggard, M. J., Austerman, J., Randel, C., and Stephenson, S. Observational estimates of dynamic topography through space and time. In Marquardt, H., Ballmer, M. adn Cottaar, S., and Konter, J., editors, *Mantle convection and surface expressions*, pages 371–411. American Geophysical Union (AGU), Washington DC, USA, 2021. ISBN 9781119528609. doi:10.1002/9781119528609.ch15. Chapter 15.

Höink, T. and Lenardic, A. Three-dimensional mantle convection simulations with a low-viscosity asthenosphere and the relationship between heat flow and the horizontal length scale of convection. *Geophysical Research Letters*, 35(10):L10304, 2008. doi:10.1029/2008GL033854.

Höink, T. and Lenardic, A. Long wavelength convection, poiseuille-couette flow in the low-viscosity asthenosphere and the strength of plate margins. *Geophysical Journal International*, 180(1):23–33, 2010. doi:10.1111/j.1365-246X.2009.04404.x.

Höink, T., Jellinek, A. M., and Lenardic, A. Viscous coupling at the lithosphere-asthenosphere boundary. *Geochemistry, Geophysics, Geosystems*, 12(10):Q0AK02, 2011. doi:10.1029/2011GC003698.

Höink, T., Lenardic, A., and Richards, M. Depth-dependent viscosity and mantle stress amplification: Implications for the role of the asthenosphere in maintaining plate tectonics. *Geophysical Journal International*, 191(1):30–41, 2012. doi:10.1111/j.1365-246X.2012.05621.x.

Holdt, M. C., White, N. J., Stephenson, S. N., and Conway-Jones, B. W. Densely sampled global dynamic topographic observations and their significance. *Journal of Geophysical Research: Solid Earth*, 127(7):e2022JB024391, 2022. doi:10.1029/2022JB024391.

Hopper, J. R., Funck, T., Stoker, M. S., Árting, U. E., Péron-Pinvidic, G., Doornenbal, J. C., and Gaina, C., editors. *Tectonostratigraphic atlas of the North-East Atlantic region*. The Geological Survey of Denmark and Greenland, Copenhagen, Denmark, 09 2014a. ISBN 9788778713780. doi:10.22008/FK2/ZZQRQ1/R6C6IW.

Hopper, J. R., Funck, T., Stoker, M. S., Árting, U. E., Péron-Pinvidic, G., Doornenbal, J. C., Gaina, C., and Contributors, N.-T. NAG-TEC ArcGIS Project, 2014b.

Horbach, A. *Theory and application of the adjoint method in geodynamics and an extended review of analytical solution methods to the Stokes equation*. PhD thesis, Ludwig-Maximilians-Universität München, July 2020. URL `http://nbn-resolving.de/urn:nbn:de:bvb:19-278281`.

Horbach, A., Bunge, H.-P., and Oeser, J. The adjoint method in geodynamics: Derivation from a general operator formulation and application to the initial condition problem in a high resolution mantle circulation model. *GEM-International Journal on Geomathematics*, 5(2):163–194, 2014. doi:10.1007/s13137-014-0061-5.

Horton, B. K. Sedimentary record of andean mountain building. *Earth-Science Reviews*, 178:279–309, 2018. ISSN 0012-8252. doi:10.1016/j.earscirev.2017.11.025.

Hosseini, K., Sigloch, K., Tsekhmistrenko, M., Zaheri, A., Nissen-Meyer, T., and Igel, H. Global mantle structure from multifrequency tomography using P, PP and P-diffracted waves. *Geophysical Journal International*, 220(1):96–141, 2020. doi:10.1093/gji/ggz394.

Houseman, G. The dependence of convection planform on mode of heating. *Nature*, 332(6162): 346–349, 1988. doi:10.1038/332346a0.

Huang, X., Betzler, C., Wu, S., Bernhardt, A., Eagles, G., Han, X., and Hovland, M. First documentation of seismic stratigraphy and depositional signatures of Zhongsha atoll (Macclesfield Bank), South China Sea. *Marine and Petroleum Geology*, 117:104349, 2020. ISSN 0264-8172. doi:10.1016/j.marpetgeo.2020.104349.

Hwang, J. H., Leonov, Y., Li, T., Petrov, O., and Tomurtogoo, O. Atlas of geological maps of central Asia and adjacent regions. Geological Publishing House, 2008. scale 1:2.5 M, 9 sheets, Beijing, China.

Iaffaldano, G., Hawkins, R., Bodin, T., and Sambridge, M. REDBACK: Open-source software for efficient noise-reduction in plate kinematic reconstructions. *Geochemistry, Geophysics, Geosystems*, 15(4):1663–1670, 2014. ISSN 1525-2027. doi:10.1002/2014GC005309.

Iaffaldano, G., Davies, D. R., and Demets, C. Indian Ocean floor deformation induced by the Reunion plume rather than the Tibetan Plateau. *Nature Geoscience*, 11(5):362–366, 2018. ISSN 17520908. doi:10.1038/s41561-018-0110-z.

Iaffaldano, G. Has the Tibetan Plateau risen in the Early/Mid-Miocene? Constraints from plate-motion reconstructions and seismicity of the Indian Ocean lithosphere. *Geophysical Journal International*, 225(2):1349–1358, 2021. ISSN 1365246X. doi:10.1093/gji/ggab027.

Iaffaldano, G. and Bunge, H.-P. Rapid plate motion variations through geological time: Observations serving geodynamic interpretation. *Annual Review of Earth and Planetary Sciences*, 43:571–592, 2015. doi:10.1146/annurev-earth-060614-105117.

Iaffaldano, G. and Bunge, H. Relating rapid plate-motion variations to plate-boundary forces in global coupled models of the mantle/lithosphere system: Effects of topography and friction. *Tectonophysics*, 474(1-2):393–404, sep 2009. ISSN 00401951. doi:10.1016/j.tecto.2008.10.035.

Iaffaldano, G., Husson, L., and Bunge, H.-P. Monsoon speeds up Indian plate motion. *Earth and Planetary Science Letters*, 304(3-4):503–510, 2011. doi:10.1016/j.epsl.2011.02.026.

Iaffaldano, G., Bodin, T., and Sambridge, M. Reconstructing plate-motion changes in the presence of finite-rotations noise. *Nature Communications*, 3(May):1048, 2012. ISSN 2041-1723. doi:10.1038/ncomms2051.

Iaffaldano, G., Bunge, H.-P., and Dixon, T. H. Feedback between mountain belt growth and plate convergence. *Geology*, 34:893–896, 2006. doi:10.1130/G22661.1.

Ingle, J.C., J. Subsidence of the Japan Sea: Stratigraphic evidence from ODP sites and onshore sections. In Tamaki, K., Suyehiro, K., Allan, J., McWilliams, M., and et al., editors, *Proccedings ODP, Scientific Results*, volume 127/128 Pt. 2, page 1197–1218, 1992. doi:10.2973/odp.proc.sr.127128-2.132.1992.

Instituto Geológico, Minero y Metalúrgico (INGEMMET). GEOCATMIN: Geología nacional millón 1:1.000.000, Perú, 2016, 2016. Lima, Peru, `http://catalogo.geoidep.gob.pe:8080/metadatos/srv/api/records/0ebbba1d-a562-4d09-9dae-c7845e28102a`.

Ismail-Zadeh, A., Schubert, G., Tsepelev, I., and Korotkii, A. Inverse problem of thermal convection: Numerical approach and application to mantle plume restoration. *Physics of the Earth and Planetary Interiors*, 145(1-4):99–114, 2004. doi:10.1016/j.pepi.2004.03.006.

Jaireth, S., McKay, A., and Lambert, I. Association of large sandstone uranium deposits with hydrocarbons. *AUSGEO news*, 89:1–6, 2008.

Japsen, P. Sonic velocity of chalk, sandstone and marine shale controlled by effective stress: Velocity-depth anomalies as a proxy for vertical movements. *Gondwana Research*, 53:145–158, 2018. doi:10.1016/j.gr.2017.04.013.

Japsen, P. and Chalmers, J. A. Neogene uplift and tectonics around the North Atlantic: overview. *Global and Planetary Change*, 24(3-4):165–173, 2000. ISSN 0921-8181. doi:10.1016/S0921-8181(00)00006-0.

Japsen, P., Green, P. F., and Chalmers, J. A. Separation of palaeogene and neogene uplift on nuussuaq, west greenland. *Journal of the Geological Society*, 162(2):299–314, 2005. ISSN 0016-7649. doi:10.1144/0016-764904-038.

Japsen, P., Bonow, J. M., Green, P. F., Cobbold, P. R., Chiossi, D., Lilletveit, R., Magnavita, L. P., and Pedreira, A. Episodic burial and exhumation in NE Brazil after opening of the South Atlantic. *Bulletin*, 124(5-6):800–816, 2012. doi:10.1130/B30515.1.

Jelsma, H., Barnett, W., Richards, S., and Lister, G. Tectonic setting of kimberlites. *Lithos*, 112:155–165, 2009. ISSN 00244937. doi:10.1016/j.lithos.2009.06.030. Proceedings of the 9th International Kimberlite Conference.

Jiaodong, Z., Xuanhua, C., Qiuli, L., Chengzhai, L., Bing, L., Jie, L., Gang, L., and Fenglou, R. Mesozoic "Red Beds" and its evolution in the Hefei Basin. *Acta Geologica Sinica - English Edition*, 86(5):1060–1076, 2012. doi:10.1111/j.1755-6724.2012.00731.x.

Jones, A. G., Afonso, J. C., and Fullea, J. Geochemical and geophysical constrains on the dynamic topography of the Southern African Plateau. *Geochemistry, Geophysics, Geosystems*, 18(10):3556–3575, 2017. doi:10.1002/2017GC006908.

Jorge, G., Montes Ramírez, N., Almanza Meléndez, M., Alcárcel Gutiérrez, F., Madrid Montoya, C., and Diederix, H. Geological map of colombia 2015. *Journal of International Geosciences*, 40(3):201–212, sep 2015. ISSN 07053797, 25861298. doi:10.18814/epiiugs/2017/v40i3/017023. `http://www.episodes.org/articleDetail.do?p=1894`.

Kano, K., Uto, K., and Ohguchi, T. Stratigraphic review of Eocene to Oligocene successions along the eastern Japan Sea: Implication for early opening of the Japan Sea. *Journal of Asian Earth Sciences*, 30(1):20–32, 2007. ISSN 1367-9120. doi:10.1016/j.jseaes.2006.07.003.

Karato, S. Rheology of the earth's mantle: A historical review. *Gondwana Research*, 18:17–45, 2010. doi:10.1038/nature07138.

Karato, S.-i. and Wu, P. Rheology of the upper mantle: A synthesis. *Science*, 260(May): 771–778, 1993. ISSN 0036-8075. doi:10.1126/science.260.5109.771.

Kendall, J.-M. and Lithgow-Bertelloni, C. Why is africa rifting? *Geological Society, London, Special Publications*, 420(1):11–30, 2016. ISSN 0305-8719. doi:10.1144/SP420.17.

Kennett, B. L. N., Widiyantoro, S., and van der Hilst, R. D. Joint seismic tomography for bulk sound and shear wave speed in the earth's mantle. *Journal of Geophysical Research: Solid Earth*, 103(B6):12469–12493, 1998. doi:10.1029/98JB00150.

King, L. C. Pediplanation and isostasy: An example from South Africa. *Quarterly Journal of*

the Geological Society, 111(1-4):353–359, 1955. doi:10.1144/GSL.JGS.1955.111.01-04.18.

Kirillova, G. L. Late Mesozoic–Cenozoic sedimentary basins of active continental margin of Southeast Russia: paleogeography, tectonics, and coal–oil–gas presence. *Marine and Petroleum Geology*, 20(3):385–397, 2003. ISSN 0264-8172. doi:10.1016/S0264-8172(03)00046-1. Paleogeographic reconstruction and hydrocarbon basins: Atlantic, Caribbean, South America, Middle East, Russian Far East, Arctic.

Koelemeijer, P., Ritsema, J., Deuss, A., and van Heijst, H. J. SP12RTS: A degree-12 model of shear- and compressional-wave velocity for Earth's mantle. *Geophys. J. Int.*, 204(2):1024–1039, 12 2016. ISSN 0956-540X. doi:10.1093/gji/ggv481.

Kohl, N. and Rüde, U. Textbook efficiency: Massively parallel matrix-free multigrid for the stokes system. *SIAM Journal on Scientific Computing*, 44(2):C124–C155, 2022. doi:10.1137/20M1376005.

Kohn, M. J., editor. *Paleoaltimetry: Geochemical and thermodynamic approaches*, volume 66 of *Reviews in Mineralogy and Geochemistry*. De Gruyter, Virgina, USA, 2007. doi:10.1515/9781501508608.

Kohn, M. J., editor. *Paleoaltimetry: Geochemical and thermodynamic approaches*, volume 66 of *Reviews in Mineralogy and Geochemistry*. De Gruyter, 2018.

Kollenz, S., Glasmacher, U. A., Rossello, E. A., Stockli, D. F., Schad, S., and Pereyra, R. E. Thermochronological constraints on the cambrian to recent geological evolution of the argentina passive continental margin. *Tectonophysics*, 716:182–203, 2017. ISSN 0040-1951. doi:https://doi.org/10.1016/j.tecto.2016.11.019.

Krob, F. C., Glasmacher, U. A., Karl, M., Perner, M., Hackspacher, P. C., and Stockli, D. F. Multi-chronometer thermochronological modelling of the late neoproterozoic to recent t-t-evolution of the se coastal region of brazil. *Journal of South American Earth Sciences*, 92: 77–94, 2019. ISSN 0895-9811. doi:10.1016/j.jsames.2019.02.012.

Krob, F. C., Eldracher, D. P., Glasmacher, U. A., Husch, S., Salomon, E., Hackspacher, P. C., and Titus, N. P. Late Neoproterozoic-to-recent long-term t–T-evolution of the Kaoko and Damara belts in NW Namibia. *International Journal of Earth Sciences*, 109(2):537–567, 2020a. doi:10.1016/j.gr.2020.02.010.

Krob, F. C., Glasmacher, U. A., Bunge, H.-P., Friedrich, A. M., and Hackspacher, P. C. Application of stratigraphic frameworks and thermochronological data on the Mesozoic SW Gondwana intraplate environment to retrieve the Paraná-Etendeka plume movement. *Gondwana Research*, 84:81–110, aug 2020b. ISSN 1342937X. doi:10.1016/j.gr.2020.02.010.

Lanari, R., Faccenna, C., Natali, C., Şengül Uluocak, E., Fellin, M. G., Becker, T. W., Göğüş, O. H., Youbi, N., Clementucci, R., and Conticelli, S. The Atlas of Morocco: A Plume-Assisted Orogeny. *Geochemistry, Geophysics, Geosystems*, 24(6):e2022GC010843, 2023. doi:10.1029/2022GC010843.

Lenardic, A., Seales, J., Moore, W., and Weller, M. Convective and tectonic plate velocities in a mixed heating mantle. *Geochemistry, Geophysics, Geosystems*, 22(2):e2020GC009278, 2020. doi:10.1029/2020GC009278.

Levander, A., Schmandt, B., Miller, M. S., Liu, K., Karlstrom, K. E., Crow, R. S., Lee, C. T. A., and Humphreys, E. D. Continuing Colorado plateau uplift by delamination-style convective

lithospheric downwelling. *Nature*, 472(7344):461–U540, Apr 28 2011. ISSN 0028-0836. doi:10.1038/nature10001.

Levorsen, A. I. Studies in paleogeology. *AAPG Bulletin*, 17(9):1107–1132, 1933. doi:10.1306/3D932BA2-16B1-11D7-8645000102C1865D.

Li, Y., He, D., Chen, L., Mei, Q., Li, C., and Zhang, L. Cretaceous sedimentary basins in Sichuan, SW China: Restoration of tectonic and depositional environments. *Cretaceous Research*, 57:50–65, 2016. ISSN 0195-6671. doi:10.1016/j.cretres.2015.07.013.

Lin, A. T., Watts, A. B., and Hesselbo, S. P. Cenozoic stratigraphy and subsidence history of the South China Sea margin in the Taiwan region. *Basin Research*, 15(4):453–478, 2003. doi:doi.org/10.1046/j.1365-2117.2003.00215.x.

Lin, A. T., Yang, C.-C., Wang, M.-H., and Wu, J.-C. Oligocene-Miocene sequence stratigraphy in the northern margin of the South China Sea: An example from Taiwan. *Journal of Asian Earth Sciences*, 213:104765, 2021. ISSN 1367-9120. doi:10.1016/j.jseaes.2021.104765.

Lin, Y.-A., Colli, L., and Wu, J. NW Pacific-Panthalassa intra-oceanic subduction during Mesozoic times from mantle convection and geoid models. *Geochemistry, Geophysics, Geosystems*, 23(11):e2022GC010514, 2022. doi:10.1029/2022GC010514.

Lindquist, S. J. The North Sakhalin Neogene total petroleum system of Eastern Russia. Open-File Report 99-50-O, USGS, 2000. 18 pp.

Lithgow-Bertelloni, C. and Richards, M. A. The dynamics of Cenozoic and Mesozoic plate motions. *Reviews of Geophysics*, 36(1):27–78, 1998. doi:10.1029/97RG02282.

Liu, L., Spasojević, S., and Gurnis, M. Reconstructing Farallon plate subduction beneath North America back to the Late Cretaceous. *Science*, 322(5903):934–938, 2008. doi:10.1126/science.1162921.

Loureiro, J., Pérez Cerdán, F., Spoturno, J., Faraone, M., Guerrero, S., and Sánchez Bettucci, L. Versión digital y actualización del mapa geológico del Uruguay de DINAMIGE a escala 1:500.000. In *VIII Congreso Uruguayo de Geología 2016*, 2016. MIEM, Ministerio de Industria, Energia y Minería. Montevideo, Uruguay.

Lovell, B. Comment on Green, P., I. Duddy, I., and P. Japsen, P., 2022. Episodic kilometre-scale burial and exhumation and the importance of missing section. *Earth-Science Reviews*, 238: 104354, 2023. ISSN 0012-8252. doi:10.1016/j.earscirev.2023.104354.

Lu, C., Forte, A. M., Simmons, N. A., Grand, S. P., Kajan, M., Lai, H., and Garnero, E. The sensitivity of joint inversions of seismic and geodynamic data to mantle viscosity. *Geochemistry, Geophysics, Geosystems*, 21(4):e2019GC008648, 2020. doi:10.1029/2019GC008648.

Lucas, S. G., Emry, R. J., Chkhikvadze, V., Bayshashov, B., Tyutkova, L. A., Tleuberdina, P. A., and Zhamangara, A. Upper Cretaceous–Cenozoic lacustrine deposits of the Zaysan Basin, Eastern Kazakhstan. In *Lake basins through space and time*, pages 335–340. American Association of Petroleum Geologists, 01 2000. ISBN 9781629810713. doi:10.1306/St46706C29.

MacGregor, D. S. Late Cretaceous–Cenozoic sediment and turbidite reservoir supply to South Atlantic margins. *Geological Society, London, Special Publications*, 369(1):109–128, 2013. doi:10.1144/SP369.7.

Maher, S. M., Wessel, P., Müller, R. D., Williams, S. E., and Harada, Y. Absolute plate motion

of Africa around Hawaii-Emperor bend time. *Geophysical Journal International*, 201(3): 1743–1764, 2015. ISSN 0956-540X. doi:10.1093/gji/ggv104.

Maia, M., Sichel, S., Briais, A., Brunelli, D., Ligi, M., Ferreira, N., Campos, T., Mougel, B., Brehme, I., Hemond, C., Motoki, A., Moura, D., Scalabrin, C., Pessanha, I., Alves, E., Neto, A., and Oliveira, P. Extreme mantle uplift and exhumation along a transpressive transform fault. *Nature Geoscience*, 9, 07 2016. doi:10.1038/ngeo2759.

Marlow, M. S., Exon, N. F., Ryan, H. F., and Dadisman, S. V. Offshore structure and stratigraphy of New Ireland Basin in Northern Papua New Guinea. In Marlow, M. S. and Dadisman, S. V., editors, *Geology and offshore resources of Pacific island arcs: New Ireland and Manus region, Papua New Guinea*, Earth Science Series, pages 137–155. ARRAY(0x55691b5e1350), Houston, Texas, 1988.

Maslin, M. A., Haug, G. H., Sarnthein, M., and Tiedemann, R. The progressive intensification of northern hemisphere glaciation as seen from the North Pacific. *Geologische Rundschau*, 85(3):452–465, 1996. doi:10.1007/BF02369002.

Matthews, K. J., Hale, A. J., Gurnis, M., Müller, R. D., and DiCaprio, L. Dynamic subsidence of Eastern Australia during the Cretaceous. *Gondwana Research*, 19(2):372–383, 2011. doi:10.1016/j.gr.2010.06.006.

Matthews, K. J., Maloney, K. T., Zahirovic, S., Williams, S. E., Seton, M., and Müller, R. D. Global plate boundary evolution and kinematics since the late paleozoic. *Global and Planetary Change*, 146:226–250, 2016. ISSN 0921-8181. doi:10.1016/j.gloplacha.2016.10.002.

McAlpine, K. D. Mesozoic stratigraphy, sedimentary evolution, and petroleum potential of the Jeanne d'Arc Basin, Grands Banks of Newfoundland, 1990. Online resource, `https://www.osti.gov/etdeweb/biblio/6040642`.

McKenzie, D. Surface deformation, gravity anomalies and convection. *Geophysical Journal International*, 48(2):211–238, 02 1977. doi:10.1111/j.1365-246X.1977.tb01297.x.

McKenzie, D., Watts, A., Parsons, B., and Roufosse, M. Planform of mantle convection beneath the pacific ocean. *Nature*, 288(5790):442–446, 1980. doi:10.1038/288442a0.

McNamara, A. K. A review of large low shear velocity provinces and ultra low velocity zones. *Tectonophysics*, 760:199–220, 2019. doi:10.1016/j.tecto.2018.04.015.

McNamara, A. K. and Zhong, S. Degree-one mantle convection: Dependence on internal heating and temperature-dependent rheology. *Geophysical Research Letters*, 32(1):L01301, 2005a. doi:10.1029/2004GL021082.

McNamara, A. K. and Zhong, S. Degree-one mantle convection: Dependence on internal heating and temperature-dependent rheology. *Geophysical Research Letters*, 32(1):L01301, 2005b. doi:10.1029/2004GL021082.

Meco, J., Scaillet, S., Guillou, H., Lomoschitz, A., Carracedo, J. C., Ballester, J., Betancort, J.-F., and Cilleros, A. Evidence for long-term uplift on the Canary Islands from emergent Mio-Pliocene littoral deposits. *Global and Planetary Change*, 57(3-4):222–234, 2007. ISSN 0921-8181. doi:10.1016/j.gloplacha.2006.11.040.

Meinhold, G. Rutile and its applications in earth sciences. *Earth–Science Reviews*, 102(1-2): 1–28, 2010. ISSN 0012–8252. doi:10.1016/j.earscirev.2010.06.001.

Meng, Q.-R., Hu, J.-M., Jin, J.-Q., Zhang, Y., and Xu, D.-F. Tectonics of the late Mesozoic wide extensional basin system in the China–Mongolia border region. *Basin Research*, 15(3): 397–415, 2003. doi:10.1046/j.1365-2117.2003.00209.x.

Menning, M. and Hendrich, a. Stratigraphic table of Germany 2016 (STG2016). German Research Centre for Geosciences, 2016. Postdam, Germany.

Merdith, A. S., Williams, S. E., Collins, A. S., Tetley, M. G., Mulder, J. A., Blades, M. L., Young, A., Armistead, S. E., Cannon, J., Zahirovic, S., and Müller, R. D. Extending full–plate tectonic models into deep time: Linking the Neoproterozoic and the Phanerozoic. *Earth-Science Reviews*, 214:103477, 2021. ISSN 0012–8252. doi:10.1016/j.earscirev.2020.103477.

Merkouriev, S. and DeMets, C. High-resolution Neogene reconstructions of Eurasia-North America Plate motion. *Geophysical Journal International*, 198(1):366–384, JUL 2014. ISSN 0956-540X. doi:10.1093/gji/ggu142.

Miall, A. D. The valuation of unconformities. *Earth-Science Reviews*, 163:22–71, 2016. doi:10.1016/j.earscirev.2016.09.011.

Milani, E. J., Melo, J. H. G., Souza, P. A., Fernandes, L. A., and França, A. B. Bacia do Paraná. *Boletim de Geociencias - Petrobras*, 15(2):265–287, 2007.

Miller, K. G., Browning, J. V., Schmelz, W. J., Kopp, R. E., Mountain, G. S., and Wright, J. D. Cenozoic sea-level and cryospheric evolution from deep-sea geochemical and continental margin records. *Science Advances*, 6(20):eaaz1346, 2020. doi:10.1126/sciadv.aaz1346.

Ministerio de Agricultura y Ganadería (MAGAP). Mapa hidrogeológico de Ecuador, 2005. Quito, Ecuador, `http://sni.gob.ec/coberturas`.

Mitrovica, J. X., Beaumont, C., and Jarvis, G. T. Tilting of continental interiors by the dynamical effects of subduction. *Tectonics*, 8(5):1079–1094, 1989. doi:10.1029/TC008i005p01079.

Mitrovica, J. X. Haskell [1935] revisited. *Journal of Geophysical Research: Solid Earth*, 101 (B1):555–569, 1996. doi:10.1029/95JB03208.

Mohr, M., Rüde, U., Wohlmuth, B., and Bunge, H.-P. Challenges for mantle convection simulations at the exa-scale: Numerics, algorithmics and software. In Neittaanmäki, P. and Rantalainen, M.-L., editors, *Impact of Scientific Computing on Science and Society*, volume 58 of *Computational Methods in Applied Sciences*, pages 75–92. Springer International Publishing, 2023. doi:10.1007/978-3-031-29082-4_4.

Molnar, P., England, P. C., and Jones, C. H. Mantle dynamics, isostasy, and the support of high terrain. *Journal of Geophysical Research: Solid Earth*, 120(3):1932–1957, 2015. doi:10.1002/2014JB011724.

Morgan, J. P. and Smith, W. H. F. Flattening of the sea-floor depth-age curve as a response to asthenospheric flow. *Nature*, 359(8):524–527, 1992a. doi:10.1038/359524a0.

Morgan, J. P. and Smith, W. H. Flattening of the sea-floor depth-age curve as a response to asthenospheric flow. *Nature*, 359(6395):524–527, 1992b. doi:10.1038/359524a0.

Morgan, J. P., Morgan, W. J., Zhang, Y.-S., and Smith, W. H. F. Observational hints for a plume-fed, suboceanic asthenosphere and its role in mantle convection. *Journal of Geophysical Research: Solid Earth*, 100(B7):12753–12767, 1995a. doi:10.1029/95JB00041.

Morgan, J. P., Morgan, W. J., Zhang, Y.-S., and Smith, W. H. F. Observational hints for a plume-

fed, suboceanic asthenosphere and its role in mantle convection. *Journal of Geophysical Research: Solid Earth*, 100(B7):12753–12767, 1995b. doi:10.1029/95JB00041.

Morgan, W. J. Gravity anomalies and convection currents: 1. a sphere and cylinder sinking beneath the surface of a viscous fluid. *Journal of Geophysical Research (1896-1977)*, 70 (24):6175–6187, 1965. doi:10.1029/JZ070i024p06175.

Moucha, R., Forte, A. M., Mitrovica, J. X., Rowley, D. B., Quéré, S., Simmons, N. A., and Grand, S. P. Dynamic topography and long-term sea-level variations: There is no such thing as a stable continental platform. *Earth and Planetary Science Letters*, 271(1):101–108, 2008a. doi:10.1016/j.epsl.2008.03.056.

Moucha, R., Forte, A. M., Mitrovica, J. X., Rowley, D. B., Quéré, S., Simmons, N. A., and Grand, S. P. Dynamic topography and long-term sea-level variations: There is no such thing as a stable continental platform. *Earth and Planetary Science Letters*, 271(1):101–108, jul 2008b. ISSN 0012-821X. doi:10.1016/j.epsl.2008.03.056.

Mpodozis, C., Arriagada, C., Basso, M., Roperch, P., Cobbold, P., and Reich, M. Late mesozoic to paleogene stratigraphy of the Salar de Atacama Basin, Antofagasta, Northern Chile: Implications for the tectonic evolution of the Central Andes. *Tectonophysics*, 399, 2005.

Müller, D., Royer, J.-Y., Cande, S., Roest, W., and Maschenkov, S. New constraints on the late cretaceous/tertiary plate tectonic evolution of the caribbean. *Sedimentary Basins of the World*, 4:33–59, 12 1999. doi:10.1016/S1874-5997(99)80036-7.

Müller, R. D., Flament, N., Cannon, J., Tetley, M. G., Williams, S. E., Cao, X., Bodur, O. F., Zahirovic, S., , and Merdith, A. A tectonic-rules-based mantle reference frame since 1 billion years ago — implications for supercontinent cycles and plate–mantle system evolution. *Solid Earth*, 13:1127–1159, 2022. doi:10.5194/se-13-1127-2022.

Müller, R. D., Royer, J.-Y., and Lawver, L. A. Revised plate motions relative to the hotspots from combined Atlantic and Indian Ocean hotspot tracks. *Geology*, 21(3):275–278, 03 1993. ISSN 0091-7613. doi:10.1130/0091-7613(1993)021<0275:RPMRTT>2.3.CO;2.

Müller, R. D., Sdrolias, M., Gaina, C., Steinberger, B., and Heine, C. Long-term sea-level fluctuations driven by ocean basin dynamics. *Science*, 319(5868):1357–1362, mar 2008. doi:10.1126/science.1151540.

Müller, R. D., Seton, M., Zahirovic, S., Williams, S. E., Matthews, K. J., Wright, N. M., Shephard, G. E., Maloney, K. T., Barnett-Moore, N., Hosseinpour, M., Bower, D. J., and Cannon, J. Ocean basin evolution and global-scale plate reorganization events since Pangea breakup. *Annual Review of Earth and Planetary Sciences*, 44(1):107–138, jun 2016. ISSN 0084-6597. doi:10.1146/annurev-earth-060115-012211.

Müller, R. D., Hassan, R., Gurnis, M., Flament, N., and Williams, S. E. Dynamic topography of passive continental margins and their hinterlands since the Cretaceous. *Gondwana Research*, 53:225–251, jan 2018. ISSN 1342-937X. doi:10.1016/j.gr.2017.04.028.

Müller, R. D., Zahirovic, S., Williams, S. E., Cannon, J., Seton, M., Bower, D. J., Tetley, M. G., Heine, C., Le Breton, E., Liu, S., Russell, S. H. J., Yang, T., Leonard, J., and Gurnis, M. A global plate model including lithospheric deformation along major rifts and orogens since the triassic. *Tectonics*, 38(6):1884–1907, 2019. doi:10.1029/2018TC005462.

Müller, R. D., Cannon, J., Qin, X., Watson, R. J., Gurnis, M., Williams, S., Pfaffelmoser,

T., Seton, M., Russell, S. H. J., and Zahirovic, S. Gplates: Building a virtual earth through deep time. *Geochemistry, Geophysics, Geosystems*, 19(7):2243–2261, 2018a. doi:10.1029/2018GC007584.

Müller, R., Hassan, R., Gurnis, M., Flament, N., and Williams, S. Dynamic topography of passive continental margins and their hinterlands since the Cretaceous. *Gondwana Research*, 53:225–251, 2018b. ISSN 1342-937X. doi:10.1016/j.gr.2017.04.028. Rifting to passive margins.

Natarov, S. and Conrad, C. The role of Poiseuille flow in creating depth-variation of asthenospheric shear. *Geophysical Journal International*, 190:1297–1310, 09 2012. doi:10.1111/j.1365-246X.2012.05562.x.

Nelson, P. L. and Grand, S. P. Lower-mantle plume beneath the Yellowstone hotspot revealed by core waves. *Nature Geoscience*, 11(4):280–284, 2018. doi:10.1038/s41561-018-0075-y.

New Zealand Geological Survey. North Island and South Island. Department of Scientific and Industrial Research, 1972. scale 1:1 M, 1st edition.

Nicolas, M. Phanerozoic stratigraphic correlation chart for Manitoba. Online resource, 2020. Open File OF2020-7, 2 p. `https://www.manitoba.ca/iem/info/libmin/OF2020-7.pdf`.

Nyblade, A. A. and Robinson, S. W. The African Superswell. *Geophysical Research Letters*, 21(9):765–768, 1994. doi:10.1029/94GL00631.

Ocean Drilling Program (ODP). Ocean Drilling Program, 1985–2004. Legs 100–210, Sites 625–1277, `https://iodp.tamu.edu/scienceops/maps.html`.

Ogg, J. G. Chapter 5 - geomagnetic polarity time scale. In Gradstein, F. M., Ogg, J. G., Schmitz, M. D., and Ogg, G. M., editors, *The geologic time scale*, pages 85–113. Elsevier, Boston, USA, 2012. ISBN 978-0-444-59425-9. doi:10.1016/B978-0-444-59425-9.00005-6.

Ogg, J. G., Ogg, G. M., and Gradstein, F. M. 1-introduction. In Ogg, J. G., Ogg, G. M., and Gradstein, F. M., editors, *A concise geologic time scale*, pages 1–8. Elsevier, 2016. ISBN 978-0-444-63771-0. doi:10.1016/B978-0-444-59467-9.00001-7.

O'Neill, C., Müller, R. D., and Steinberger, B. On the uncertainties in hot spot reconstructions and the significance of moving hot spot reference frames. *Geochemistry, Geophysics, Geosystems*, 6(4):Q04003, 2005. ISSN 1525–2027. doi:10.1029/2004GC000784.

Orts, S. and Ramos, V. A. Evidence of Middle to Late Cretaceous compressive deformation in the high Andes of Mendoza, Argentina. *Abstracts with programs, Backbone of the Americas, Patagonia to Alaska, Mendoza, GSA Special Meetings-AGA Publicaciones Especiales*, 5:65, 2006.

Oyarzun, R., Doblas, M., López-Ruiz, J., and María Cebrá, J. Opening of the central Atlantic and asymmetric mantle upwelling phenomena: Implications for long-lived magmatism in western North Africa and Europe. *Geology*, 25(8):727–730, 08 1997. ISSN 0091-7613. doi:10.1130/0091-7613(1997)025<0727:OOTCAA>2.3.CO;2.

Pail, R., Goiginger, H., Schuh, W.-D., Höck, E., Brockmann, J. M., Fecher, T., Gruber, T., Mayer-Gürr, T., Kusche, J., Jäggi, A., and Rieser, D. Combined satellite gravity field model goco01s derived from goce and grace. *Geophysical Research Letters*, 37(20):L20314, 2010. doi:10.1029/2010GL044906.

Panggabean, H. and Heryanto, R. An appraisal for the petroleum source rocks on oil seep and rock samples of the Tertiary Seblat and Lemau Formations, Bengkulu Basin. *Jurnal Geologi Indonesia*, 4(1):43–55, 2009. doi:10.17014/ijog.vol4no1.20095.

Parnell-Turner, R., White, N., Henstock, T., Murton, B., Maclennan, J., and Jones, S. M. A continuous 55-million-year record of transient mantle plume activity beneath Iceland. *Nature Geoscience*, 7(12):914, 2014. doi:10.1038/ngeo2281.

Partridge, T. C. and Maud, R. R. Geomorphic evolution of Southern Africa since the Mesozoic. *South African Journal of Geology*, 90(2):179–208, 06 1987. ISSN 1012-0750. doi:10520/AJA10120750_958.

Paton, D. A., van der Spuy, D., di Primio, R., and Horsfield, B. Tectonically induced adjustment of passive-margin accommodation space; influence on the hydrocarbon potential of the Orange Basin, South Africa. *American Association of Petroleum Geologists Bulletin*, 92(5): 589–609, 2008. ISSN 01491423. doi:10.1306/12280707023.

Paulson, A. and Richards, M. A. On the resolution of radial viscosity structure in modelling long-wavelength postglacial rebound data. *Geophysical Journal International*, 179(3):1516–1526, 2009. doi:10.1111/j.1365-246X.2009.04362.x.

Pekeris, C. L. Thermal convection in the interior of the earth. *Geophysical Journal International*, 3:343–367, dec 1935. ISSN 0956540X, 1365246X. doi:10.1111/j.1365-246X.1935.tb01742.x.

Petersen, S. V. and Schrag, D. P. Antarctic ice growth before and after the Eocene-Oligocene transition: New estimates from clumped isotope paleothermometry. *Paleoceanography*, 30 (10):1305–1317, 2015. doi:10.1002/2014PA002769.

Petit, C. and Déverchère, J. Structure and evolution of the Baikal rift: A synthesis. *Geochemistry, Geophysics, Geosystems*, 7(11):Q11016, 2006. doi:10.1029/2006GC001265.

Pitman, W., Talwani, M., and Heirtzler, J. Age of the north atlantic ocean from magnetic anomalies. *Earth and Planetary Science Letters*, 11(1):195–200, 1971. ISSN 0012-821X. doi:10.1016/0012-821X(71)90163-4.

Poore, H. R., White, N., and Jones, S. M. A neogene chronology of iceland plume activity from v-shaped ridges. *Earth and Planetary Science Letters*, 283(1-4):1–13, 2009. ISSN 0012-821X. doi:10.1016/j.epsl.2009.02.028.

Prasad, B. and Pundir, B. S. Gondwana biostratigraphy and geology of West Bengal Basin, and its correlation with adjoining Gondwana basins of India and western Bangladesh. *Journal of Earth System Science*, 129(22):1–45, 2019. doi:10.1007/s12040-019-1287-2.

Pubellier, M. and Morley, C. The basins of Sundaland (SE Asia): Evolution and boundary conditions. *Marine and Petroleum Geology*, 58:555–578, 2014. doi:10.1016/j.marpetgeo.2013.11.019.

Qi, J. and Yang, Q. Cenozoic structural deformation and dynamic processes of the Bohai Bay Basin province, China. *Marine and Petroleum Geology*, 27(4):757–771, 2010. ISSN 0264-8172. doi:10.1016/j.marpetgeo.2009.08.012.

Rabbani, A. R. Geochemistry of crude oil samples from the Iranian sector of the Persian Gulf. *Journal of Petroleum Geology*, 31(3):303–316, 2008. doi:10.1111/j.1747-5457.2008.00422.x.

Rahimpour-Bonab, H., Shariatinia, Z., and Siemann, M. G. Role of rifting in evaporite deposition in the Great Kavir Basin, central Iran. *Geological Society, London, Special Publications*, 285(1):69–85, 2007. doi:10.1144/SP285.5.

Rainbird, R. H. and Ernst, R. E. The sedimentary record of mantle-plume uplift. In Ernst, R. E. and Buchan, K. L., editors, *Mantle plumes: their identification through time*, volume 352, pages 227–246. Geological Society of America; 1999, 2001. doi:10.1130/0-8137-2352-3.227.

Ravenna, M., Lebedev, S., Fullea, J., and Adam, J. M.-C. Shear-wave velocity structure of southern Africa's lithosphere: Variations in the thickness and composition of cratons and their effect on topography. *Geochemistry, Geophysics, Geosystems*, 19(5):1499–1518, 2018. doi:10.1029/2017GC007399.

Raymond, O. L., Gallagher, R., Shaw, R., Yeates, A. N., Doutch, H. F., Palfreyman, W. D., Blake, D. H., and Highet, L. Surface geology of Australia 1:2.5 million scale dataset 2012 edition, 2012. Commonwealth of Australia (Geoscience Australia).

Reali, R., Van Orman, J. A., Pigott, J. S., Jackson, J. M., Boioli, F., Carrez, P., and Cordier, P. The role of diffusion-driven pure climb creep on the rheology of bridgmanite under lower mantle conditions. *Scientific Reports*, 9(1):2053, 2019. ISSN 2045–2322. doi:10.1038/s41598-018-38449-8.

Reiners, P. W. and Brandon, M. T. Using thermochronology to understand orogenic erosion. *Annual Review of Earth and Planetary Sciences*, 34(1):419–466, 2006. doi:10.1146/annurev.earth.34.031405.125202.

Renne, P. R., Ernesto, M., Pacca, I. G., Coe, R. S., Glen, J. M., Prévot, M., and Perrin, M. The age of Paraná flood volcanism, rifting of Gondwanaland, and the Jurassic-Cretaceous boundary. *Science*, 258(5084):975–979, 1992. doi:10.1126/science.258.5084.975.

Ricard, Y., Fleitout, L., and Froidevaux, C. Geoid heights and lithospheric stresses for a dynamic Earth. *Annales Geophysicae*, 2(3):267–286, 1984. ISSN 0755–0685.

Richards, M. A. and Engebretson, D. C. Large-scale mantle convection and the history of subduction. *Nature*, 355(6359):437–440, 1992a. doi:10.1038/355437a0.

Richards, M. A. and Engebretson, D. C. Large-scale mantle convection and the history of subduction. *Nature*, 355(6359):437–440, 1992b. doi:10.1038/355437a0.

Richards, M. A. and Hager, B. H. Geoid anomalies in a dynamic Earth. *Journal of Geophysical Research: Solid Earth*, 89(B7):5987–6002, 1984. doi:10.1029/JB089iB07p05987.

Richards, M. A. and Lenardic, A. The cathles parameter (ct): A geodynamic definition of the asthenosphere and implications for the nature of plate tectonics. *Geochemistry, Geophysics, Geosystems*, 19(12):4858–4875, 2018. doi:10.1029/2018GC007664.

Richards, M. A., Yang, W.-S., Baumgardner, J. R., and Bunge, H.-P. Role of a low-viscosity zone in stabilizing plate tectonics: Implications for comparative terrestrial planetology. *Geochemistry, Geophysics, Geosystems*, 2(8):2000GC000115, aug 2001. ISSN 15252027. doi:10.1029/2000GC000115.

Rickers, F., Fichtner, A., and Trampert, J. The Iceland-Jan Mayen plume system and its impact on mantle dynamics in the North Atlantic region: Evidence from full-waveform inversion. *Earth and Planetary Science Letters*, 367:39–51, 2013. ISSN 0012-821X.

doi:10.1016/j.epsl.2013.02.022.

Rigg, J. W. D. and Hall, R. Structural and stratigraphic evolution of the Savu Basin, Indonesia. *Geological Society, London, Special Publications*, 355(1):225–240, 2011. doi:10.1144/SP355.11.

Riis, F. Quantification of cenozoic vertical movements of scandinavia by correlation of morphological surfaces with offshore data. *Global and Planetary Change*, 12(1):331–357, 1996. ISSN 0921-8181. doi:10.1016/0921-8181(95)00027-5.

Ritsema, J., Deuss, A., van Heijst, H. J., and Woodhouse, J. H. S40RTS: A degree-40 shear-velocity model for the mantle from new Rayleigh wave dispersion, teleseismic traveltime and normal-mode splitting function measurements. *Geophysical Journal International*, 184(3): 1223–1236, mar 2011. ISSN 0956-540X. doi:10.1111/j.1365-246X.2010.04884.x.

Roberts, G. G. and White, N. Estimating uplift rate histories from river profiles using African examples. *Journal of Geophysical Research: Solid Earth*, 115(B2):B02406, 2010. doi:10.1029/2009JB006692.

Rohde, J. K., van den Bogaard, P., Hoernle, K., Hauff, F., and Werner, R. Evidence for an age progression along the Tristan-Gough volcanic track from new 40Ar/39Ar ages on phenocryst phases. *Tectonophysics*, 604:60–71, 2013. ISSN 00401951. doi:10.1016/j.tecto.2012.08.026.

Rosleff-Soerensen, B., Reuning, L., Back, S., and Kukla, P. A. The response of a basin-scale Miocene barrier reef system to long-term, strong subsidence on a passive continental margin, Barcoo Sub-basin, Australian North West Shelf. *Basin Research*, 28(1):103–123, 2016. ISSN 13652117. doi:10.1111/bre.12100.

Rotzien, J. R., Lowe, D. R., King, P. R., and Browne, G. H. Stratigraphic architecture and evolution of a deep-water slope channel-levee and overbank apron: The Upper Miocene Upper Mount Messenger Formation, Taranaki Basin. *Marine and Petroleum Geology*, 52:22–41, 2014. ISSN 0264-8172. doi:10.1016/j.marpetgeo.2014.01.006.

Rowley, D. B. Earth's constant mean elevation: Implication for long-term sea level controlled by oceanic lithosphere dynamics in a Pitman world. *The Journal of Geology*, 125(2):141–153, 2017. doi:10.1086/690197.

Russell, M. and Gurnis, M. The planform of epeirogeny: Vertical motions of Australia during the Cretaceous. *Basin Research*, 6(2-3):63–76, 1994. ISSN 13652117. doi:10.1111/j.1365-2117.1994.tb00076.x.

Sadler, P. M. Sediment accumulation rates and the completeness of stratigraphic sections. *The Journal of Geology*, 89(5):569–584, 1981. doi:10.1086/628623.

Said, A., Moder, C., Clark, S., and Abdelmalak, M. M. Sedimentary budgets of the tanzania coastal basin and implications for uplift history of the east african rift system. *Journal of African Earth Sciences*, 111:288 – 295, 2015a. ISSN 1464-343X. doi:10.1016/j.jafrearsci.2015.08.012.

Said, A., Moder, C., Clark, S., and Ghorbal, B. Cretaceous-cenozoic sedimentary budgets of the southern mozambique basin: Implications for uplift history of the south african plateau. *Journal of African Earth Sciences*, 109:1 – 10, 2015b. ISSN 1464-343X. doi:10.1016/j.jafrearsci.2015.05.007.

Samuel, S. P. *Depositional history of Paleocene sediments in the offshore Canterbury Basin,*

New Zealand. PhD thesis, Te Herenga Waka-Victoria University of Wellington, 2010. Unpublished MSc.

Sandiford, M. The tilting continent: A new constraint on the dynamic topographic field from Australia. *Earth and Planetary Science Letters*, 261(1-2):152–163, 2007. ISSN 0012821X. doi:10.1016/j.epsl.2007.06.023.

Saskatchewan Ministry of Energy and Resources. Saskatchewan Stratigraphic Correlation Chart (revised 2022). Online resource, 2022. `https://pubsaskdev.blob.core.windows.net/pubsask-prod/93751/Strat%252BChart%252BFeb_2022.pdf`.

Saunders, A. D., Jones, S. M., Morgan, L. A., Pierce, K. L., Widdowson, M., and Xu, Y. G. Regional uplift associated with continental large igneous provinces: The roles of mantle plumes and the lithosphere. *Chemical Geology*, 241(3-4):282–318, 2007a. doi:10.1016/j.chemgeo.2007.01.017.

Saunders, A., Jones, S., Morgan, L., Pierce, K., Widdowson, M., and Xu, Y. Regional uplift associated with continental large igneous provinces: The roles of mantle plumes and the lithosphere. *Chemical Geology*, 241(3):282–318, 2007b. ISSN 0009-2541. doi:10.1016/j.chemgeo.2007.01.017.

Savva, D., Pubellier, M., Franke, D., Chamot-Rooke, N., Meresse, F., Steuer, S., and Auxietre, J. Different expressions of rifting on the South China Sea margins. *Marine and Petroleum Geology*, 58:579–598, 2014. ISSN 0264-8172. doi:10.1016/j.marpetgeo.2014.05.023. Evolution, Structure, and Sedimentary Record of the South China Sea and Adjacent Basins.

Schaeffer, A. J. and Lebedev, S. Global shear speed structure of the upper mantle and transition zone. *Geophysical Journal International*, 194(1):417–449, 04 2013a. ISSN 0956-540X. doi:10.1093/gji/ggt095.

Schaeffer, A. J. and Lebedev, S. Global shear speed structure of the upper mantle and transition zone. *Geophysical Journal International*, 194(1):417–449, 2013b. doi:10.1093/gji/ggt095.

Schaeffer, A. J., Lebedev, S., and Becker, T. W. Azimuthal seismic anisotropy in the Earth's upper mantle and the thickness of tectonic plates. *Geophysical Journal International*, 207 (2):901–933, 2016. ISSN 1365246X. doi:10.1093/gji/ggw309.

Schilling, J.-G., Hanan, B. B., McCully, B., Kingsley, R. H., and Fontignie, D. Influence of the sierra leone mantle plume on the equatorial mid-atlantic ridge: A nd-sr-pb isotopic study. *Journal of Geophysical Research: Solid Earth*, 99(B6):12005–12028, 1994. doi:10.1029/94JB00337.

Schott, B. and Schmeling, H. Delamination and detachment of a lithospheric root. *Tectonophysics*, 296(3-4):225–247, NOV 10 1998. ISSN 0040-1951. doi:10.1016/S0040-1951(98)00154-1.

Schuberth, B. S. A., Bunge, H.-P., and Ritsema, J. Tomographic filtering of high-resolution mantle circulation models: Can seismic heterogeneity be explained by temperature alone? *Geochemistry, Geophysics, Geosystems*, 10(5):Q05W03, 2009. ISSN 1525-2027. doi:10.1029/2009GC002401.

Sehrt, M., Glasmacher, U. A., Stockli, D. F., Jabour, H., and Kluth, O. The southern moroccan passive continental margin: An example of differentiated long-term landscape evolution in gondwana. *Gondwana Research*, 53:129–144, 2018. ISSN 1342-937X.

doi:10.1016/j.gr.2017.03.013.

Sempere, T., Herail, G., Oller, J., and Bonhonmme, M. G. Late Oligecene early Miocene major tectonic crisis and related basins in Bolivia. *Geology*, 18:946–949, 1990. ISSN 0091-7613. doi:10.1130/0091-7613(1990)018<0946:LOEMMT>2.3.CO;2.

Sempere, T., Marshall, L. G., Rivano, S., and Godoy, E. Late Oligocene early Miocene compresional tectosedimentary episode and associated land-mammal faunas in the Andes of central Chile and Adjacent Argentina (32-37 S). *Tectonophysics*, 229:251–264, 1994.

Sempere, T., Folguera, A., and Gerbault, M. New insights into Andean evolution: An introduction to contributions from the 6th ISAG symposium (Barcelona, 2005). *Tectonophysics, in the press*, 2008a. doi:10.1016/j.tecto.2008.03.011.

Sempere, T., Folguera, A., and Gerbault, M. New insights into Andean evolution: An introduction to contributions from the 6th ISAG symposium (Barcelona, 2005). *Tectonophysics*, 459 (1-4):1–13, NOV 1 2008b. ISSN 0040-1951. doi:10.1016/j.tecto.2008.03.011.

Semple, A. G. and Lenardic, A. Plug flow in the Earth's asthenosphere. *Earth and Planetary Science Letters*, 496:29–36, 2018a. ISSN 0012821X. doi:10.1016/j.epsl.2018.05.030.

Semple, A. G. and Lenardic, A. Plug flow in the Earth's asthenosphere. *Earth and Planetary Science Letters*, 496:29–36, 2018b. ISSN 0012821X. doi:10.1016/j.epsl.2018.05.030.

Sepehr, M. and Cosgrove, J. Structural framework of the Zagros Fold–Thrust Belt, Iran. *Marine and Petroleum Geology*, 21(7):829–843, 2004. ISSN 0264-8172. doi:10.1016/j.marpetgeo.2003.07.006. Oil and Gas in Compressional Belts.

Serviço Geológico do BrasilSGB. Carta geológica do Brasil ao milionésimo, 2010. Brasília, Brazil, `http://geosgb.cprm.gov.br/geosgb/downloads.html`.

Servicio Geológico Minero Argentino (SEGEMAR). Mapa geológico de Argentina, 2017. San Martín, Argentina, `https://sigam.segemar.gov.ar/geonetwork39/srv/eng/catalog.search#/metadata/9987cbd01e1bca5a6979257c7618524b5d8c5ce0`.

Servicio Nacional de Geología y Minería (SERNAGEOMIN). Mapa geológico de Chile: Versión digital, 2003. Santiago, Chile, `http://portalgeominbeta.sernageomin.cl/`.

Seton, M., Müller, D. R., Zahirovic, S., Gaina, C., Torsvik, T., Shephard, G., Talsma, A., Gurnis, M., Turner, M., Maus, S., and Chandler, M. Global continental and ocean basin reconstructions since 200Ma. *Earth-Science Reviews*, 113(3-4):212–270, 2012. ISSN 0012-8252. doi:10.1016/j.earscirev.2012.03.002.

Seton, M., Müller, R. D., Zahirovic, S., Williams, S., Wright, N. M., Cannon, J., Whittaker, J. M., Matthews, K. J., and McGirr, R. A global data set of present-day oceanic crustal age and seafloor spreading parameters. *Geochemistry, Geophysics, Geosystems*, 21(10): e2020GC009214, 2020. doi:10.1029/2020GC009214.

Shephard, G. E., Bunge, H.-P., Schuberth, B. S., Müller, R. D., Talsma, A., Moder, C., and Landgrebe, T. Testing absolute plate reference frames and the implications for the generation of geodynamic mantle heterogeneity structure. *Earth and Planetary Science Letters*, 317: 204–217, 2012. doi:10.1016/j.epsl.2011.11.027.

Shi, J., Jin, Z., Fan, T., Liu, Q., Zhang, F., and Fan, X. Sequence development, depositional filling evolution, and prospect forecast in northern Aryskum Depression of South

Turgay Basin, Kazakstan. *Energy Exploration & Exploitation*, 34(4):621–642, 2016. doi:10.1177/0144598716650067.

Simmons, N. A., Myers, S. C., Morency, C., Chiang, A., and Knapp, D. R. SPiRaL: A multiresolution global tomography model of seismic wave speeds and radial anisotropy variations in the crust and mantle. *Geophys. J. Int.*, 227(2):1366–1391, July 2021. ISSN 1365-246X. doi:10.1093/gji/ggab277.

Simmons, N. A., Forte, A. M., and Grand, S. P. Joint seismic, geodynamic and mineral physical constraints on three-dimensional mantle heterogeneity: Implications for the relative importance of thermal versus compositional heterogeneity. *Geophysical Journal International*, 177 (3):1284–1304, 2009a. ISSN 0956540X. doi:10.1111/j.1365-246X.2009.04133.x.

Simmons, N. A., Forte, A. M., and Grand, S. P. Joint seismic, geodynamic and mineral physical constraints on three-dimensional mantle heterogeneity: Implications for the relative importance of thermal versus compositional heterogeneity. *Geophysical Journal International*, 177 (3):1284–1304, 2009b. doi:10.1111/j.1365-246X.2009.04133.x.

Sissingh, W. Kineamtic sequence stratigraphy of the European Cenozoic Rift system and Alpine Foreland Basin: Correlation with Mediterranean and Atlantic plate-boundary events. *Netherlands Journal of Geosciences*, 85(2):77–129, 2006. doi:10.1017/S0016774600077921.

Sleep, N. H., Ebinger, C. J., and Kendall, J.-M. Deflection of mantle plume material by cratonic keels. In *The Early Earth: Physical, Chemical and Biological Development*. Geological Society of London, 01 2002. ISBN 9781862391093. doi:10.1144/GSL.SP.2002.199.01.08.

Sloss, L. L. Sequences in the cratonic interior of North America. *Geological Society of America Bulletin*, 74(2):93–114, 1963.

Sloss, L. L. Tectonic episodes of cratons: Conflicting North American concepts. *Terra Nova*, 4 (3):320–328, 1992. doi:10.1111/j.1365-3121.1992.tb00821.x.

Sloss, L. Synchrony of phanerozoic sedimentary-tectonic events of the north american craton and the russian platform. In *24th International Geological Congress, Montreal*, volume 6, pages 24–32, 1972.

Smith-Rouch, L. S. *Oligocene–Miocene Maykop/Diatom total petroleum system of the South Caspian Basin Province, Azerbaijan, Iran, and Turkmenistan*, volume 2201-I. U.S. Geological Survey Bulletin, Reston, Virginia, 2006. `https://pubs.usgs.gov/bul/2201/I/`.

Song, Y., Stepashko, A., Liu, K., He, Q., Shen, C., Shi, B., and Ren, J. Post-rift tectonic history of the Songliao Basin, NE China: Cooling events and post-rift unconformities driven by orogenic pulses from plate boundaries. *Journal of Geophysical Research: Solid Earth*, 123(3):2363–2395, 2018. doi:10.1002/2017JB014741.

Spasojevic, S., Liu, L., and Gurnis, M. Adjoint models of mantle convection with seismic, plate motion, and stratigraphic constraints: North America since the Late Cretaceous. *Geochemistry, Geophysics, Geosystems*, 10(5):Q05W02, 2009. doi:10.1029/2008GC002345.

Spasojevic, S., Gurnis, M., and Sutherland, R. Inferring mantle properties with an evolving dynamic model of the Antarctica-New Zealand region from the Late Cretaceous. *Journal of Geophysical Research: Solid Earth*, 115(B5):B05402, 2010. doi:10.1029/2009JB006612.

Spice, H. E., Fitton, J. G., and Kirstein, L. A. Temperature fluctuation of the Iceland mantle plume through time. *Geochemistry, Geophysics, Geosystems*, 17(2):243–254, 2016.

doi:10.1002/2015GC006059.

Stacey, F. D. and Davis, P. M. *Physics of the Earth*. Cambridge University Press, New York, USA, 2008. doi:10.1017/CBO9780511812910.

Stanca, R. M., McCarthy, D. J., Paton, D. A., Hodgson, D. M., and Mortimer, E. J. The tectono-stratigraphic architecture of the Falkland Plateau basin; implications for the evolution of the Falkland Islands Microplate. *Gondwana Research*, 105:320–342, 2022. ISSN 1342-937X. doi:10.1016/j.gr.2021.09.014.

Stanley, J. R., Flowers, R. M., and Bell, D. R. Erosion patterns and mantle sources of topographic change across the southern African Plateau derived from the shallow and deep records of kimberlites. *Geochemistry, Geophysics, Geosystems*, 16(9):3235–3256, 2015. ISSN 15252027. doi:10.1002/2015GC005969.

Steinberger, B. Effects of latent heat release at phase boundaries on flow in the Earth's mantle, phase boundary topography and dynamic topography at the Earth's surface. *Physics of the Earth and Planetary Interiors*, 164(1-2):2–20, 2007. doi:10.1016/j.pepi.2007.04.021.

Steinberger, B. and O'Connell, R. J. Changes of the Earth's rotation axis owing to advection of mantle density heterogeneities. *Nature*, 387(6629):169–173, 1997. doi:10.1038/387169a0.

Steinberger, B. and Torsvik, T. H. Absolute plate motions and true polar wander in the absence of hotspot tracks. *Nature*, 452:620–623, 2008. doi:10.1038/nature06824.

Steinberger, B., Schmeling, H., and Marquart, G. Large-scale lithospheric stress field and topography induced by global mantle circulation. *Earth and Planetary Science Letters*, 186 (1):75–91, 2001. ISSN 0012821X. doi:10.1016/S0012-821X(01)00229-1.

Steinmann, G., Lisson, C. I., Sieberg, A., and Stappenbeck, R. *Geologie von Peru*. Carl Winters Universitätsbuchhandlung, Heidelberg, 1929.

Steno, N. *De solido intra solidum naturaliter contento dissertationis prodromus*. PhD thesis, Florence, Maar, 1669. Thesis translated by Winter, John Garrett, in 1916, available at `https://archive.org/details/cu31924012131458/page/n39/mode/2up`.

Stephenson, S. N., Hoggard, M. J., Holdt, M. C., and White, N. Continental residual topography extracted from global analysis of crustal structure. *Journal of Geophysical Research: Solid Earth*, 129(4):e2023JB026735, 2024. doi:https://doi.org/10.1029/2023JB026735. e2023JB026735 2023JB026735.

Stille, H. Die Begriffe Orogenese und Epirogenese. *Zeitschrift der Deutschen Geologischen Gesellschaft*, 71:164–208, 1919.

Stille, H. Kanon der strandverschienbungen in grundfragen der vergleichenden tektonik. *Verlag Gebrüder Bornträger, Berlin*, page 443 pp, 1924a.

Stille, H. Grundfragen der Vergleichenden Tektonik. *Gebrüder Borntraeger*, 71:1–443, 1924b. doi:10.1017/S0016756818000560.

Stoker, M. S. and Shannon, P. M. Neogene evolution of the NW European Atlantic margin: Results from the STRATAGEM project. *Marine and Petroleum Geology*, 22(9–10):965–968, 2005. ISSN 0264-8172. doi:10.1016/j.marpetgeo.2005.04.006.

Storey, B. C. The role of mantle plumes in continental breakup: Case histories from Gondwanaland. *Nature*, 377:301–308, 1995. ISSN 0028-0836. doi:10.1038/377301a0.

Storey, M., Mahoney, J. J., Saunders, A. D., Duncan, R. A., Kelley, S. P., and Coffin, M. F. Timing of hot spot-related volcanism and the breakup of Madagascar and India. *Science*, 267 (5199):852–855, 1995. ISSN 00368075. doi:10.1126/science.267.5199.852.

Stotz, I. L., Iaffaldano, G., and Davies, D. R. Late miocene pacific plate kinematic change explained with coupled global models of mantle and lithosphere dynamics. *Geophysical Research Letters*, 44(14):7177–7186, 2017. doi:10.1002/2017GL073920.

Stotz, I. L., Iaffaldano, G., and Davies, D. R. Pressure-driven Poiseuille flow: A major component of the torque-balance governing pacific plate motion. *Geophysical Research Letters*, 45 (1):117–125, 2018. doi:10.1002/2017GL075697.

Stotz, I. L., Tassara, A., and Iaffaldano, G. Pressure-driven Poiseuille flow inherited from Mesozoic mantle circulation led to the Eocene separation of Australia and Antarctica. *Journal of Geophysical Research: Solid Earth*, 126(4):e2020JB019945, 2021a. doi:10.1029/2020JB019945.

Stotz, I. L., Vilacís, B., Hayek, J. N., Bunge, H.-P., and Friedrich, A. M. Yellowstone plume drives neogene north american plate motion change. *Geophysical Research Letters*, 48(18): e2021GL095079, 2021b. doi:10.1029/2021GL095079.

Stotz, I. L., Vilacís, B., Hayek, J. N., Carena, S., and Bunge, H.-P. Plume driven plate motion changes: New insights from the south atlantic realm. *Journal of South American Earth Sciences*, 124:104257, 2023. ISSN 0895-9811. doi:10.1016/j.jsames.2023.104257.

Stotz, I. L., Carena, S., Vilacís, B., Hayek, J. N., and Bunge, H.-P. Kerguelen plume drives the Eocene directional change in Australia plate motion. *Lithosphere*, 2024(3):13, 2024. doi:10.2113/2024/lithosphere_2023_289.

Strogen, D. P., Seebeck, H., Nicol, A., and King, P. R. Two-phase Cretaceous–Paleocene rifting in the Taranaki Basin region, New Zealand; implications for Gondwana break-up. *Journal of the Geological Society*, 174(5):929–946, 2017. doi:10.1144/jgs2016-160.

Suess, E. *Das Antlitz der Erde: Erster Band*. F. Tempsky, Prag und Wien, and G. Freytag, Leipzig, 1883.

Suo, Y., Li, S., Cao, X., Wang, X., Somerville, I., Wang, G., Wang, P., and Liu, B. Mesozoic-Cenozoic basin inversion and geodynamics in East China: A review. *Earth-Science Reviews*, 210:103357, 2020. ISSN 0012-8252. doi:10.1016/j.earscirev.2020.103357.

Sutherland, R., Spasojevic, S., and Gurnis, M. Mantle upwelling after Gondwana subduction death explains anomalous topography and subsidence histories of eastern New Zealand and west Antarctica. *Geology*, 38(2):155–158, 2010. ISSN 00917613. doi:10.1130/G30613.1.

Tackley, P. J. Effects of strongly variable viscosity on three-dimensional compressible convection in planetary mantles. *Journal of Geophysical Research: Solid Earth*, 101(B2):3311–3332, FEB 10 1996. ISSN 2169-9313. doi:10.1029/95JB03211.

Taira, A., Okada, H., Whitaker, J. H., and Smith, A. J. The Shimanto Belt of Japan: Cretaceous-Lower Miocene active-margin sedimentation. *Geological Society, London, Special Publications*, 10(1):5–26, 1982. doi:10.1144/GSL.SP.1982.010.01.01.

Takano, O. Intermittent formation, sedimentation and deformation history of Cenozoic forearc basins along the Northwestern Pacific margins as an indicator of tectonic scenarios. In Itoh, Y., Takano, O., Takashima, R., Nishi, H., and Yoshida, T., editors, *Dynamics*

of arc migration and amalgamation, chapter 1, pages 1–24. IntechOpen, Rijeka, 2017. doi:10.5772/intechopen.68290.

Takashima, R., Nishi, H., and Yoshida, T. Stratigraphic and petrological insights into the Late Jurassic-Early Cretaceous tectonic framework of the Northwest Pacific margin. In Itoh, Y., Takano, O., Takashima, R., Nishi, H., and Yoshida, T., editors, *Dynamics of arc migration and amalgamation*, chapter 3, pages 45–66. IntechOpen, Rijeka, 2017. doi:10.5772/intechopen.68289.

Tasistro-Hart, A. R. and Macdonald, F. A. Phanerozoic flooding of North America and the Great Unconformity. *Proceedings of the National Academy of Sciences*, 120(37):e2309084120, 2023. doi:10.1073/pnas.2309084120.

Tate, R., Tan, D., Ng, T., and (compilers). Geological map of peninsular Malaysia, 2008. scale 1:1 M, Geological Society of Malaysia.

Teng, S., Wang, Y., Tang, C., Huang, C., Huang, T., Yu, M., and Ke, A. Tectonic aspects of the Paleogene depositional basin of northern Taiwan. *Proceedings of the Geological Society of China*, 34:313–336, 1991.

The Geotraverse Project. World Data Center for Solid Earth Physics. Geophysical Center of the Russian Academy of Sciences, 2001–2016. Online resource, Last accessed 09.12.2022.

Tingdong, L. Geological map of Asia and Europe. Geological Publishing House, 1997. scale 1:5 M, 9 sheets, Beijing, China.

Tinker, J., de Wit, M., and Brown, R. Mesozoic exhumation of the southern Cape, South Africa, quantified using apatite fission track thermochronology. *Tectonophysics*, 455(1-4): 77–93, 2008. doi:10.1016/j.tecto.2007.10.009.

Torsvik, T. H., Tucker, R. D., Ashwal, L. D., Eide, E. A., Rakotosolofo, N. A., and de Wit, M. J. Late Cretaceous magmatism in Madagascar: Palaeomagnetic evidence for a stationary Marion hotspot. *Earth and Planetary Science Letters*, 164(1-2):221–232, 1998. ISSN 0012821X. doi:10.1016/S0012-821X(98)00206-4.

Torsvik, T. H., Müller, R. D., Van der Voo, R., Steinberger, B., and Gaina, C. Global plate motion frames: Toward a unified model. *Reviews of Geophysics*, 46(3):RG3004, 2008. doi:10.1029/2007RG000227.

Torsvik, T. H., Van der Voo, R., Preeden, U., Mac Niocaill, C., Steinberger, B., Doubrovine, P. V., van Hinsbergen, D. J., Domeier, M., Gaina, C., Tohver, E., Meert, J. G., McCausland, P. J., and Cocks, L. R. M. Phanerozoic polar wander, palaeogeography and dynamics. *Earth-Science Reviews*, 114(3):325–368, 2012. ISSN 0012-8252. doi:10.1016/j.earscirev.2012.06.007.

Travis, B., Weinstein, S., and Olson, P. Three-dimensional convection planforms with internal heat generation. *Geophysical Research Letters*, 17(3):243–246, 1990. doi:10.1029/GL017i003p00243.

Troll, V. R. and Carracedo, J. C. Chapter 1 - The Canary Islands: An introduction. In Troll, V. R. and Carracedo, J. C., editors, *The geology of the Canary Islands*, pages 1–41. Elsevier, 2016. ISBN 978-0-12-809663-5. doi:10.1016/B978-0-12-809663-5.00001-3.

Turcotte, D. L. and Oxburgh, E. R. Finite amplitude convective cells and continental drift. *Journal of Fluid Mechanics*, 28(1):29–42, 1967. doi:10.1017/S0022112067001880.

Ulmishek, G. F. *Petroleum geology and resources of the Middle Caspian Basin, former Soviet Union*, volume 2201-A. U.S. Geological Survey Bulletin, Denver, Colorado, 2001a. doi:10.3133/b2201A. https://pubs.usgs.gov/bul/2201/A/.

Ulmishek, G. F. *Petroleum geology and resources of the North Caspian Basin, Kazakhstan and Russia*, volume 2201-B. U.S. Geological Survey Bulletin, Denver, Colorado, 2001b. doi:10.3133/b2201B. https://pubs.usgs.gov/bul/2201/B/.

Ulmishek, G. F. *Petroleum geology and resources of the North Ustyurt Basin, Kazakhstan and Uzbekistan*, volume 2201-D. U.S. Geological Survey Bulletin, Denver, Colorado, 2001c. doi:10.3133/b2201D. https://pubs.usgs.gov/bul/2201/D/.

Ulmishek, G. F. *Petroleum geology and resources of the Amu-Darya basin, Turkmenistan, Uzbekistan, Afghanistan, and Iran*, volume 2201-H. U.S. Geological Survey Bulletin, Reston, Virginia, 2004. doi:10.3133/b2201H. https://pubs.usgs.gov/bul/2201/H/.

Uruski, C., Baillie, P., and Stagpoole, V. Development of the Taranaki Basin and comparisons with the Gippsland Basin: Implications for deepwater exploration. *The APPEA Journal*, 43 (1):185–196, 2003. doi:10.1071/AJ02009.

Vail, P. R., Mitchum Jr, R. M., and Thompson III, S. Seismic stratigraphy and global changes of sea level: Part 4. Global cycles of relative changes of sea level: Section 2. Application of seismic reflection configuration to stratigraphic interpretation. In *Seismic Stratigraphy: Applications to Hydrocarbon Exploration*, pages 83–97. American Association of Petroleum Geologists, Memoir no. 26, 1977.

Valdiya, K. S. *Tertiary Basins: Along coasts and Offshore*, pages 675–706. Springer International Publishing, Cham, 2016. doi:10.1007/978-3-319-25029-8_20.

van Herwaarden, D. P., Boehm, C., Afanasiev, M., Thrastarson, S., Krischer, L., Trampert, J., and Fichtner, A. Accelerated full-waveform inversion using dynamic mini-batches. *Geophysical Journal International*, 221(2):1427–1438, 2020. doi:10.1093/gji/ggaa079.

van Hinsbergen, D., Steinberger, B., Doubrovine, P., and Gassmöller, R. Acceleration and deceleration of India-Asia convergence since the Cretaceous: Roles of mantle plumes and continental collision. *Journal of Geophysical Research: Solid Earth*, 116, 06 2011. doi:10.1029/2010JB008051.

Van Hinsbergen, D. J., Steinberger, B., Doubrovine, P. V., and Gassmöller, R. Acceleration and deceleration of India-Asia convergence since the Cretaceous: Roles of mantle plumes and continental collision. *Journal of Geophysical Research: Solid Earth*, 116(B6):B06101, 2011. ISSN 21699356. doi:10.1029/2010JB008051.

Vibe, Y., Friedrich, A. M., Bunge, H.-P., and Clark, S. R. Correlations of oceanic spreading rates and hiatus surface area in the North Atlantic realm. *Lithosphere*, 10(5):677–684, aug 2018. ISSN 1941-8264. doi:10.1130/L736.1.

Vibe, Y., Bunge, H.-P., and Clark, S. R. Anomalous subsidence history of the West Siberian Basin as an indicator for episodes of mantle induced dynamic topography. *Gondwana Research*, 53:99–109, 01 2018a. ISSN 1342-937X. doi:10.1016/j.gr.2017.03.011. Rifting to Passive Margins.

Vilacís, B., Hayek, J. N., Stotz, I. L., Bunge, H.-P., Friedrich, A. M., Carena, S., and Clark, S. Evidence for active upper mantle flow in the atlantic and indo-australian realms since

the upper jurassic from hiatus maps and spreading rate changes. *Proceedings of the Royal Society A: Mathematical, Physical and Engineering Sciences*, 478(2262):20210764, 2022. doi:10.1098/rspa.2021.0764.

Vilacís, B., Brown, H., Bunge, H.-P., Carena, S., Hayek, J. N., Stotz, I. L., Wang, R. Z., and Friedrich, A. M. Dynamic topography and the planform of mantle convection since the Jurassic inferred from Global Continental Hiatus Maps. *Proceedings of the Royal Society A: Mathematical, Physical and Engineering Sciences*, 480(2302):20240311, 2024. doi:10.1098/rspa.2024.0311. Special feature: Foundations of Operational Geodynamics.

Vilacís, B., Carena, S., Hayek, J. N., Robl, G., Friedrich, A. M., Bunge, H.-P., and Ma, J. Manual vs digital hiatus extraction: A case study for China. *Jounal of Structural Geology*, In prep. Special feature: Observation, quantification and simulation of rock deformation and mountain building processes.

von Eynatten, H., Kley, J., Dunkl, I., Hoffmann, V.-E., and Simon, A. Late cretaceous to paleogene exhumation in central europe – localized inversion vs. large-scale domal uplift. *Solid Earth*, 12(4):935–958, 2021. doi:10.5194/se-12-935-2021.

Vynnytska, L. and Bunge, H.-P. Restoring past mantle convection structure through fluid dynamic inverse theory: Regularisation through surface velocity boundary conditions. *GEM-International Journal on Geomathematics*, 6(1):83–100, 2015. doi:10.1007/s13137-014-0060-6.

Wagner, R. Tabela Stratigraficzna Polska Pozakarpacka. Panstwowy Instytut Geologiezny (Polish Geological Insitute), 2008.

Wang, B., Doust, H., and Liu, J. Geology and petroleum systems of the East China Sea Basin. *Energies*, 12(21):4088, 2019. ISSN 1996-1073. doi:10.3390/en12214088.

Wang, P., Li, Q., and Li, C.-F. Chapter 5 - Basins and stratigraphy. In Wang, P., Li, Q., and Li, C.-F., editors, *Geology of the China Seas*, volume 6 of *Developments in Marine Geology*, pages 341–468. Elsevier, 2014. doi:10.1016/B978-0-444-59388-7.00005-6.

Wang, R., Shi, W., Xie, X., Zhang, X., Wang, L., Manger, W., and Busbey, A. B. Coupling of strike-slip faulting and lacustrine basin evolution: sequence stratigraphy, structure, and sedimentation in the North Yellow Sea Basin (West Bay Basin offshore North Korea), eastern China. *Marine and Petroleum Geology*, 120:104548, 2020. ISSN 0264-8172. doi:10.1016/j.marpetgeo.2020.104548.

Warners-Ruckstuhl, K. N., Meijer, P. T., Govers, R., and Wortel, M. J. A lithosphere-dynamics constraint on mantle flow: Analysis of the Eurasian plate. *Geophysical Research Letters*, 37 (18):L18308, 2010. ISSN 00948276. doi:10.1029/2010GL044431.

Warners-Ruckstuhl, K. N., Govers, R., and Wortel, R. Lithosphere-mantle coupling and the dynamics of the Eurasian Plate. *Geophysical Journal International*, 189(3):1253–1276, 2012. ISSN 0956540X. doi:10.1111/j.1365-246X.2012.05427.x.

Warners-Ruckstuhl, K. N., Govers, R., and Wortel, R. Tethyan collision forces and the stress field of the Eurasian Plate. *Geophysical Journal International*, 195(1):1–15, 2013. ISSN 0956540X. doi:10.1093/gji/ggt219.

Waters, C., Gillespie, M. R., Smith, K., Auton, C., Floyd, J., Leslie, A., Millward, D., Mitchell, W., McMillan, A., Stone, P., Barron, A., Dean, M., Hopson, P., Krabbendam, M., Browne,

M., Stephenson, D., Akhurst, M., and Barnes, R. P. *Stratigraphical chart of the United Kingdom: Northern Britain*. British Geological Survey, Nottingham, UK, 2007a. ISBN 978-0-7518-3562-5. 1 poster.

Waters, C., Smith, K., Hopson, P. M., Willson, D., Bridge, D., Carney, J., Cooper, A., Crofts, R., A., E. R., Mathers, S. J., Moorlock, B., Scrivener, R., McMillan, A., Ambrose, K., Barclay, W., and Barron, A. *Stratigraphical chart of the United Kingdom: Southern Britain*. British Geological Survey, Nottingham, UK, 2007b. ISBN 978-0-7518-3561-8. 1 poster.

Weinstein, S. A. and Christensen, U. Convection planforms in a fluid with a temperature-dependent viscosity beneath a stress-free upper boundary. *Geophysical Research Letters*, 18 (11):2035–2038, 1991. doi:10.1029/91GL02663.

Weismüller, J., Gmeiner, B., Ghelichkhan, S., Huber, M., John, L., Wohlmuth, B., Rüde, U., and Bunge, H.-P. Fast asthenosphere motion in high-resolution global mantle flow models. *Geophysical Research Letters*, 42(18):7429–7435, 2015. doi:10.1002/2015GL063727.

Westaway, R. Forces associated with mantle plumes. *Earth and Planetary Science Letters*, 119 (3):331–348, 1993a. ISSN 0012821X. doi:10.1016/0012-821X(93)90142-V.

Westaway, R. Forces associated with mantle plumes. *Earth and Planetary Science Letters*, 119 (3):331–348, 1993b. ISSN 0012821X. doi:10.1016/0012-821X(93)90142-V.

Wheeler, H. E. Time-stratigraphy. *AAPG Bulletin*, 42(5):1047–1063, 05 1958a. ISSN 0149-1423. doi:10.1306/0BDA5AF2-16BD-11D7-8645000102C1865D.

Wheeler, H. E. Time-stratigraphy. *AAPG Bulletin*, 42(5):1047–1063, 1958b. doi:10.1306/0BDA5AF2-16BD-11D7-8645000102C1865D.

Wheeler, H. E. Baselevel, lithosphere surface, and time-stratigraphy. *GSA Bulletin*, 75(7):599–610, 07 1964. ISSN 0016-7606. doi:10.1130/0016-7606(1964)75[599:BLSAT]2.0.CO;2.

White, N. and Lovell, B. Measuring the pulse of a plume with the sedimentary record. *Nature*, 387(6636):888–891, 1997. doi:10.1038/43151.

Whittaker, J., Müller, R., Sdrolias, M., and Heine, C. Sunda-java trench kinematics, slab window formation and overriding plate deformation since the Cretaceous. *Earth and Planetary Science Letters*, 255(3-4):445–457, 2007. doi:10.1016/j.epsl.2006.12.031.

Wieczorek, M. A. and Meschede, M. Shtools: Tools for working with spherical harmonics. *Geochemistry, Geophysics, Geosystems*, 19(8):2574–2592, 2018. doi:10.1029/2018GC007529.

Wiens, D. A. and Stein, S. Implications of oceanic intraplate seismicity for plate stresses, driving forces and rheology. *Tectonophysics*, 116(1–2):143–162, 1985. ISSN 00401951. doi:10.1016/0040-1951(85)90227-6.

Winterbourne, J., Crosby, A., and White, N. Depth, age and dynamic topography of oceanic lithosphere beneath heavily sedimented Atlantic margins. *Earth and Planetary Science Letters*, 287(1):137–151, 2009a. ISSN 0012-821X. doi:10.1016/j.epsl.2009.08.019.

Winterbourne, J., Crosby, A., and White, N. Depth, age and dynamic topography of oceanic lithosphere beneath heavily sedimented Atlantic margins. *Earth and Planetary Science Letters*, 287(1):137–151, 2009b. ISSN 0012-821X. doi:10.1016/j.epsl.2009.08.019.

Wong, T. E. The Paleocene-Eocene succession in the Guianan Basin. *Bulletin de la Société*

belge de Géologie, 103(3-4):281–291, 1994.

Wu, J., Suppe, J., Lu, R., and Kanda, R. Philippine sea and East Asian plate tectonics since 52 Ma constrained by new subducted slab reconstruction methods. *Journal of Geophysical Research: Solid Earth*, 121(6):4670–4741, 2016. doi:10.1002/2016JB012923.

Xi, D., Wan, X., Li, G., and Li, G. Cretaceous integrative stratigraphy and timescale of China. *Science China Earth Sciences*, 62(1):256–286, 2019. doi:10.1007/s11430-017-9262-y.

Yamamoto, M., Morgan, J. P., and Morgan, W. J. Global plume-fed asthenosphere flow-I: Motivation and model development. In Foulger, G. R. and Jurdy, D. M., editors, *Plates, plumes and planetary processes*, volume 430, pages 165–188. Geological Society of America, Boulder, Colorado, USA, 2007a. doi:10.1130/2007.2430(09).

Yamamoto, M., Morgan, J. P., and Morgan, W. J. Global plume-fed asthenosphere flow-II: Application to the geochemical segmentation of mid-ocean ridges. In Foulger, G. R. and Jurdy, D. M., editors, *Plates, plumes and planetary processes*, volume 430, pages 189–208. Geological Society of America, Boulder, Colorado, USA, 2007b. doi:10.1130/2007.2430(10).

Yan, Y., Xia, B., Lin, G., Carter, A., Hu, X., Cui, X., Liu, B., Yan, P., and Song, Z. Geochemical and Nd isotope composition of detrital sediments on the north margin of the South China Sea: Provenance and tectonic implications. *Sedimentology*, 54(1):1–17, 2007. doi:10.1111/j.1365-3091.2006.00816.x.

Yang, C. S., Li, S. Z., Li, G., Yang, C. Q., Yang, Y. Q., Dai, L. M., Suo, Y. H., Li, Q., and Jiang, Y. B. Tectonic units and proto-basin of the East China Sea Shelf Basin: Correlation to Mesozoic subduction of the Palaeo-Pacific Plate. *Geological Journal*, 51(S1):149–161, 2016. doi:https://doi.org/10.1002/gj.2776.

Yang, F., Hu, P., Zhou, X., Zhang, R., Peng, Y., Li, X., and Qiu, D. The Late Jurassic to Early Cretaceous strike-slip faults in the Subei-South Yellow Sea Basin, Eastern China: Constraints from seismic data. *Tectonics*, 39(10):e2020TC006091, 2020. doi:10.1029/2020TC006091.

Zheng, H. Birth of the Yangtze River: Age and tectonic-geomorphic implications. *National Science Review*, 2(4):438–453, 10 2015. ISSN 2095-5138. doi:10.1093/nsr/nwv063.

Zhong, S., McNamara, A., Tan, E., Moresi, L., and Gurnis, M. A benchmark study on mantle convection in a 3-D spherical shell using CitcomS. *Geochemistry, Geophysics, Geosystems*, 9(10):Q10017, 2008. doi:10.1029/2008GC002048.

Zhou, X., Jiang, Z., Atuquaye Quaye, J., Duan, Y., Hu, C., Liu, C., and Han, C. Ichnology and sedimentology of the trace fossil-bearing fluvial red beds from the lowermost member of the Paleocene Funing Formation in the Jinhu Depression, Subei Basin, East China. *Marine and Petroleum Geology*, 99:393–415, 2019. ISSN 0264-8172. doi:10.1016/j.marpetgeo.2018.10.032.

Zhu, J.-C., Meng, Q.-R., Feng, Y.-L., Yuan, H.-Q., Wu, F.-C., Wu, H.-B., Wu, G.-L., and Zhu, R.-X. Decoding stratigraphic evolution of the Hailar Basin: Implications for the late Mesozoic tectonics of NE China. *Geological Journal*, 55(3):1750–1762, 2020a. doi:10.1002/gj.3563.

Zhu, X., Shen, C., Zhou, R., Xu, J., Zhao, J.-x., Wang, L., and Ge, X. Paleogene sediment provenance and paleogeographic reconstruction of the South Yellow Sea Basin, East China: Constraints from detrital zircon UPb geochronology and heavy mineral as-

semblages. *Palaeogeography, Palaeoclimatology, Palaeoecology*, 553:109776, 2020b. doi:10.1016/j.palaeo.2020.109776.

Ziegler, P. A., Cloetingh, S., and van Wees, J.-D. Dynamics of intra-plate compressional deformation: The alpine foreland and other examples. *Tectonophysics*, 252(1):7 – 59, 1995. ISSN 0040-1951. doi:https://doi.org/10.1016/0040-1951(95)00102-6.